Universidad de Valladolid

ESCUELA DE INGENIERÍAS INDUSTRIALES

DEPARTAMENTO DE INGENERÍA DE SISTEMAS Y AUTOMÁTICA

TESIS DOCTORAL:

MODELLING, SIMULATION AND ADVANCED CONTROL OF SMALL-SCALE REVERSE OSMOSIS DESALINATION PLANTS

Presentada por Luis Gómez Palacín para optar al grado de doctor por la Universidad de Valladolid

Dirigida por:
César de Prada Moraga
y Fernando Tadeo Rico

Universidad de Valladolid

SCHOOL OF INDUSTRIAL ENGINEERING

DEPARTMENT OF SYSTEMS ENGINEERING AND
AUTOMATIC CONTROL

PHD THESIS:

MODELLING, SIMULATION AND ADVANCED CONTROL OF SMALL-SCALE REVERSE OSMOSIS DESALINATION PLANTS

A Thesis submitted by Luis Gómez Palacín for the degree
of Doctor of Philosophy in the University of Valladolid

Supervised by:
César de Prada Moraga
& Fernando Tadeo Rico

To Patricia

Summary

Over the last few decades, desalination has become an effective technique to produce drinkable water, from sea and brackish water, in regions where the fresh water availability is insufficient to fulfil the water demand. From the nineties onwards, Reverse Osmosis (RO) has become the most popular technology for desalination. This is because the RO desalination plants require less energy, investment cost and maintenance than other alternative desalination processes. Around 50% of the plants operating, and most plants under construction, are based on RO technology.

This thesis is focused on the modelling, simulation and advanced control of one particular type of RO desalination plants: small-scale plants situated in remote areas. Typically, these plants are powered by renewable energies (such as solar panels and wind turbines) and provide drinkable water for small villages and settlements. They are very popular in arid or semi arid regions, where there is an important availability of solar radiation and wind, such as the Maghreb and the South of Europe. The correct operation of these plants fulfils the water demand and optimizes the use of the renewable energy. Besides, the advanced control deals with other issues, such as the minimization of the consumption of chemicals, the minimization of the volume of stored water, the scheduling of the stops and cleaning of the plant, the design of fault detection tools, etc.

The first part of this thesis deals with the modelling of RO desalination plants. In line with this thesis, a dynamic simulation library was developed for RO desalination plants. This library is based on first principles, physical and chemical equations and correlations from the literature. It can be used for different purposes, such as the comparison of control strategies, optimization of variables, testing, capacity design, parameter estimation, data reconciliation, etc. Some of the

components of the library were validated using an RO pilot plant.

The second part of this thesis deals with the advanced control of RO desalination plants, powered by renewable energy. The advanced control was done using the developed simulation library, and it covers several issues, such as the model-based predictive control, the integration of process design and control, the economic optimization of the energy consumption and the cleaning scheduling, etc.

The third and last part of this thesis deals with the multi-scale modelling of the RO membranes, which are the core of the RO desalination plants. In particular, the dynamic development of the salt gradient, which takes place in the boundary layer close to the membrane surface, was modelled. This modelling approach presents several improvements over other modelling strategies.

Contents

Acknowledgements

I would like to express my appreciation to the following people, who have helped me during the years of my PhD candidature.

To my advisor, Professor César de Prada. For his kind help, wise advice and attentive supervision. For his nice patience and warm friendship. And for the beautiful opportunity he gave me.
To Professor Fernando Tadeo, for his useful help, feedback and nice comments.
To my colleagues from the OPEN-GAIN project and SETA company, especially to Hamza Elfil and Amenallah Guizani, for their cordial welcome, feedback and comments. To Johanna and Syafiie, for their kind help.
To my colleagues from the University of Manchester (UK), especially to Constantinos Theodoropoulos, for his warm welcome. To Weiguo Xie for his kind help and feedback. To my friends, Michael, Anestis, Yannis, and many others.
To my colleagues from the department of Systems Engineering and Automatic Control of the University of Valladolid (Spain), Felipe, Miguel Ángel, Gloria, María Jesús, Jesús María, Rubén, Mar, Daniel S., María, Daniel N., Diego N., Santi, Teresa, Smaranda, Elena, Meriem, and many others.
To my colleagues from the CTA (Valladolid, Spain). To my friends, Alejandro, Alexander, Beatriz, Jacobo, Diego, Marina, Luis Mañanes, Almudena, Transi, Richard, Silvia, Raúl, Mónica, María H., María M., María Ángeles, Rogelio, Rebeca, Cristina, and many others, for the wonderful moments we shared.
To my colleagues from the Technical University of Dortmund (Germany), especially to Professor Sebastian Engell, for his warm welcome.

To my colleagues from the Engineering Department of ABB (Bangalore, India), especially to Subbaiah Senthilmurugan and Srinivas Mekapati, for their friendly welcome.
To my colleagues from the Federal University of Santa Catarina (Florianopolis, Brazil), especially to Daniel Pagano and Agustinho Plucenio, for their kind welcome. To my friends, André, Gabi, Renzo, Liliana, Teresa, Omar, Cindy, Yesid, Luis E., Clemens, Karina, Miriam, Vanessa, Mauricio, Rodrigo, and many others, for the beautiful moments we shared.
To my colleagues from the CERN-ICE (Geneva, Switzerland), especially to Enrique Blanco, Benjamin Bradu and Philippe Gayet, for their cordial welcome. To my friends, Silvia, Borja, Adrien, Theodora, Maria, Jerónimo, William, Philippe, David, Tiago, Marc, Alexey, Maxime, Jeremy, Jacques, Jean-Michel, Daniel, Alejandro, Marcin, Camille, Efthymia, Nabil, and many others.
To my colleagues from the CAFE project, especially to Antonio A. Alonso and Luis Taboada, for their kind advice.
To my colleagues from the ISA (Spain), for their useful advice.
To my colleagues from the EA (Spain), for their kind advice.
To Alan Hynds, for his entertaining English lessons and his nice help.
To all the friends I made during these years, for the nice memories.
To my parents and my brother.
To my travelling companion, friend and partner, Patricia.

Chapter 1

Introduction

First part of this chapter gives general ideas about the desalination process. Section 1.1 briefly describes the world situation and the most important technologies for desalination. Since Reverse Osmosis (RO) has become the most popular technology, and it is the technology used in this thesis, it is described in greater detail.

Second part of this chapter deals with the backdrop of this thesis. Section 1.2 summarizes the state of the art of RO desalination plants, from three different points of view: 1) control; 2) mathematical modelling; and 3) simulation tools. The framework, objectives and main contributions of the thesis are summarized, respectively, in sections 1.4, 1.3 and 1.5. Finally, the organization of the thesis is shown in section 1.6.

1.1 Desalination

1.1.1 World Situation

During the last few decades, the increase in water consumption and the decrease in rainfall, have led to a lack of fresh water in several countries. Figure 1.1 shows a typical development of the annual precipitation over the last century (source: the International Desalination Association, IDA). Figure 1.1 corresponds to the city of Perth (Australia), but similar plots can be shown for other places around the world. As can be seen, the average total precipitation is decreasing, the gap between periodic droughts is becoming shorter and the max-

imum peaks are falling. Predictions for the following years are even worse.

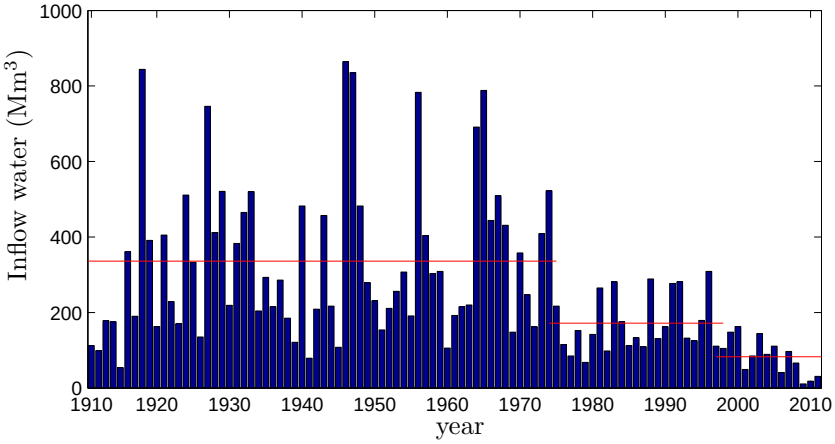

Figure 1.1: Annual inflow to Perth (Australia) dams over the last century (Mm^3). Red lines mean, respectively, the average annual inflow for the periods (1910-1975), (1976-1996) and (1997-2010). Adapted from the IDA.

Living in a world of water, the lack of drinkable water seems ironic. The truth is that 97.5% of the world's water is salty and not potable. Besides, most of the fresh water (2.5% of the total world water) is in a solid state (68.9%) or is groundwater (30.8%). Only 0.3% (of the 2.5%) is stored in lakes and rivers and is available for human consumption. In fact, more than 1.1 billion people are living in regions of scarcity and have problems to obtain drinkable water. The estimations for the future are more dramatic. By 2025, 1.8 billion people will be living in high scarcity regions (source: the Spanish Association of Desalination, AEDyR).

The direct consumption of potable water (domestic use, bathing, feeding) is about 150-250 L/(day·person). However, to produce most of the foodstuffs and daily articles, we consume a huge quantity of potable water. Table 1.1 summaries the water requirements for different common articles (source: the Association of Environmental Science, COAMBCV).

Taking this into account, the real water consumption is really around 2-5 m^3/(day·person), or 750 - 2 000 m^3/(year·person). Regions

Article	Water requirement
1 cup of coffee:	140 L
1 kg paper:	200 L
1 kg potatoes:	1 000 L
12 eggs:	1 500 L
1 T-shirt:	4 000 L
1 kg meat:	50 000 L

Table 1.1: Water consumption for different daily articles and foodstuffs.

with less than 1 700 m^3/(year·person) are considered to have hydraulic stress, and regions with less than 1 000 m^3/(year·person) are considered to have hydraulic scarcity. Figure 1.2 shows the estimation for 2015 of world water availability.

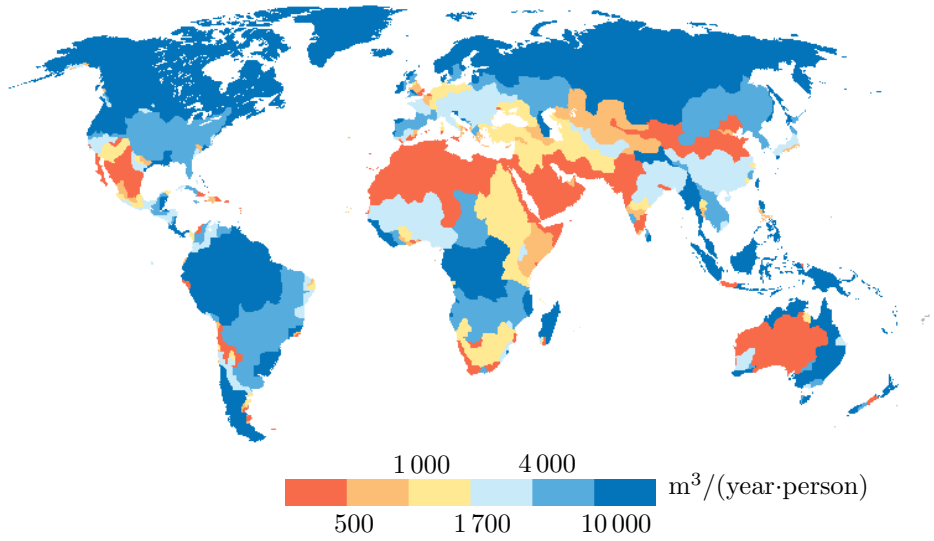

Figure 1.2: Estimation of the world water situation in 2015. Adapted from the IDA.

Hydraulic scarcity regions are found all around the world. Several countries of Africa, Asia, Australia, the Middle East, southern Europe and North America suffer the lack of fresh water. Hydraulic scarcity

is even found in regions that, a priori, are considered to have an excess of water, such as the Central Europe, the United Kingdom and several regions of South America.

To combat this lack of drinkable water, over the last few decades, desalination has become an effective solution. Desalination is a process that produces drinkable water, removing most of the salt from of a water stream (sea or brackish). Feed water is divided into two streams: 1) the desalted and drinkable water flow; and 2) the reject flow (or brine), which contains most of the salt. This is illustrated in figure 1.3.

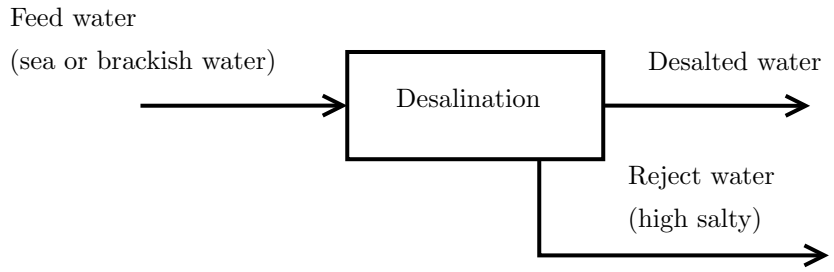

Figure 1.3: Desalination process.

Nowadays, the total amount of drinkable water which is produced from desalination exceeds 80 Mm^3/day, and the estimation for 2015 goes beyond 120 Mm^3/day. This means that a huge effort in development, research, building of new plants and improvement of the technology, will be carried out over the following years.

In fact, current desalination technology is pretty advanced. The cost of drinkable water obtained from desalination is decreasing every year. Nowadays, the cost of desalted water produced in large-scale desalination plants is lower than 0.50 €/m^3. This is several orders of magnitude lower than for other basic foodstuffs. The power consumption for desalination (around 3.3 kWh/m^3) is close to the thermodynamic limit (around 1.0 kWh/m^3). One of the most important milestones in desalination was the use of energy recovery systems during the nineties, which involved the drastic minimization of the power consumption. Thanks to the continuous research in desalination technology, a better ratio between power consumption and cost is expected for the near future.

Year	Technology	Power (kWh/m^3)	Cost (€/m^3)
1970	MSF	22	2.10
1975	MSF	21	2.04
1980	VC	18	1.82
1985	VC	15	1.12
1990	RO	8.5	0.87
1995	RO	5.8	0.73
2000	RO	4.0	0.51
2005	RO	3.5	0.48
2010	RO	3.3	0.47

Table 1.2: Evolution of the desalination technology over the last 40 years. Adapted from the IDA.

Table 1.2 summarizes the evolution of the desalination process over the last few decades. Multi-stage Flash (MSF), Vapour Compression (VC), and other technologies, were widely utilized in the past. However, from the nineties onwards, RO has become by far the most popular technology. RO desalination plants require less energy, investment cost and maintenance than other alternative desalination processes. Only in the Middle East, where robustness is considered more important than energy efficiency, is MSF technology still extensively used.

Desalted water production (Mm^3/day)		
Year:	2010	2015
Saudi Arabia	11.5	16.4
EAU	8.4	11.4
USA	7.9	10.6
Spain	3.8	5.0
Kuwait	3.2	4.3
Algeria	2.6	4.5
China	2.2	5.3
Australia	1.4	3.5

Table 1.3: Countries with more desalted water production. Adapted from the IDA.

Table 1.3 summarizes the countries with the greatest desalination capacity, and an increasing estimation for 2015. Most of the countries belong to the Middle East or to the Mediterranean. The USA, China and Australia complete this table. Besides, in the following years, an important increase in the desalination capacity of the following countries is expected: Bahrain, Qatar, Oman (in the Middle East), Israel, Malta, Cyprus, Morocco, Egypt, Tunisia (in the Mediterranean), India, Pakistan (in Asia), Mexico (in North America), Namibia (in Africa), and many others.

Table 1.4 shows the distribution of the desalination capacity by regions. Notice that close to 50% of the world desalination capacity belongs to the Middle East. This makes sense, since the Middle East is a region with a high hydraulic scarcity but with great energy reserves (more than 60% of the world petroleum reserves are in the Middle East).

Region	Ratio
Middle East:	48 %
North America:	15 %
Asia:	14 %
Europe:	12 %
Africa:	6 %
Australia:	2 %
Rest:	3 %

Table 1.4: Desalted water production by regions. Adapted from the IDA.

1.1.2 Desalination Technologies

There are several desalination technologies and several ways to classify them (see, for example, El-Dessouky and Ettouney (2002)). From the driven-force point of view, the desalination techniques can be divided into two important groups: power-driven processes and heat-driven processes, as can be seen below:

- Power-driven processes:
  - Reverse Osmosis (RO).

  - Electrodialysis Reversal (EDR).
  - Mechanical Vapour Compression (MVC).
- Heat-driven processes:
  - Multi-stage Flash (MSF).
  - Multiple Effect Distillation (MED).
  - Thermal Vapour Compression (TVC).
  - Membrane Distillation (MD).
  - Humidification-Dehumidification (HD).
- Others:
  - Freezing.
  - Ion Exchange.

As commented previously, MSF, MED, MVC and TVC were widely used in the past. Nowadays, they are still used in regions with low fuel prices or when a heat source is available. From the nineties onwards, RO has become the most popular desalination technology (especially for large-scale seawater desalination plants), with the exception of the Middle East, where MSF is the preferred technology. EDR is very common for medium-scale desalination plants, for brackish and surface water, with a high concentration of particulates and a low concentration of salt. MD and HD are nowadays used only for small-scale desalination plants powered by solar radiation. Freezing has a very high energy efficiency ratio, but involves important problems for the manipulation of the ice and it is used very little. Finally, Ion Exchange produces very high-quality water, but it is only used for industrial applications, not for drinkable water.

Freezing and Ion Exchange are outside the topic of this thesis. The rest of the technologies are briefly described below. Finally, an RO desalination plant is described in section 1.1.3.

1.1.2.1 Multi-stage Flash (MSF)

Nowadays, MSF is the most popular technology in the Middle East, where around 50% of the world's desalted water is produced. Most

of the biggest desalination plants in the world[1], are based on MSF technology and situated in the Middle East. Figure 1.4 shows the main elements of an MSF unit.

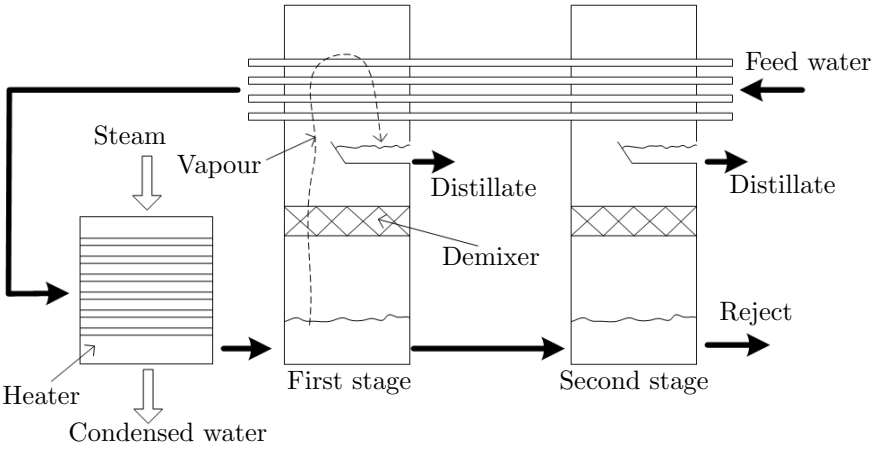

Figure 1.4: MSF diagram.

Feed water (typically seawater) is pumped through the tubes of the heater, which is fed externally with steam. The temperature of the feed water is increased until close to boiling point, but avoiding the evaporation in this element. The temperature reached is called the "Top Brine Temperature" (TBT), and typically takes values between 90 and 115 ºC. Next, the feed flow is carried to the first stage, where part of the stream is evaporated by the effect of flashing. The vacuum is obtained using a condenser, whose cold stream is its own feed water, before being carried to the heater. So, two effects are obtained: the vacuum for flashing, and the preheating of the feed flow. This preheating decreases the consumption of external steam. Next, the feed flow is carried to the following stage, where the process is repeated. Feed water is able to boil in each stage, through the increase of the vacuum in each successive stage. In order to avoid the transport of liquid drops with the evaporated flow, each stage has a demixer. Figure 1.4 shows a two-stage MSF system, but MSF systems typically

[1]The Shuaiba III (Saudi Arabia) is the largest desalination plant in the world, producing about 880 000 m^3/day. While the Ras Al Khair (Saudi Arabia) desalination plant, which currently is under construction, will produce about 1 025 000 m^3/day.

consist of 15-25 stages, and they can consist of up to 40 stages. The evaporated flow in each stage corresponds to the desalted water flow, and the drain flow of the last stage corresponds to the reject flow.

Since the evaporation takes places without any hot surface, calcium scaling is minimized (but not avoided). Corrosion and calcium scaling take place in the heater pipes, which is the most common problem in MSF plants. Otherwise, MSF is a robust and easily operated system, but with a high energy consumption ratio. See El-Dessouky et al. (1999), Cheremisinoff (2002) and Gebel and Yuce (2008) for an in-depth description of the MSF technology, Peñate and García-Rodríguez (2012) and Ghaffour et al. (2013) for a perspective on its use, Kahraman and Cengel (2005) and Al-Weshahi et al. (2013) for the energy consumption analysis, Ali et al. (1999) and Lior (2012) for an in-depth description of the control strategy, and Al-Sahlawi (1999) and Borsani and Rebagliati (2005) for an economic comparison with other technologies.

1.1.2.2 Multiple Effect Distillation (MED)

MED desalination plants were very popular in the sixties, until it was made obsolete by other technologies. Figure 1.5 shows the most important components of a MED unit.

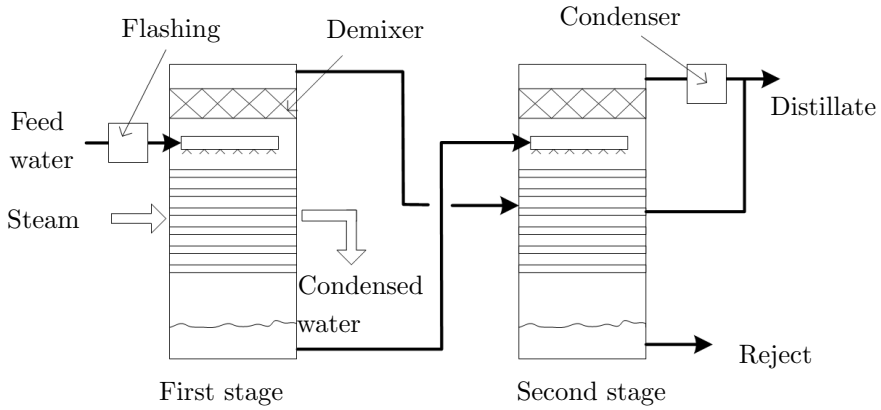

Figure 1.5: MED diagram.

Feed water (typically seawater) is pumped to the top of the first stage. It is distributed by dripping drops over the area of the stage.

Next, feed water comes into contact with the hot surface of a rack of tubes. These tubes are fed with external steam. Part of the feed water is evaporated. The feed water is divided into two streams: 1) a liquid brine stream; and 2) a vapour stream. The brine flow is pumped to the top of the second stage, and the process is repeated. The steam in the tubes of the second stage is the vapour stream obtained in the first stage. In order to obtain a difference in temperature, the pressure of the second stage is decreased by flashing. Figure 1.5 shows a two-stage MED system, but MED systems typically consist of up to 12 stages.

The major drawbacks of MED plants are the corrosion and calcium scaling, which take place in the tubes of the heaters. The corrosion and scaling are higher in MED plants than in MSF ones, because in MED plants, the evaporation takes places over the surface of the tubes. Several types of salt can create scale in the tubes, but the most important ones are calcium carbonate ($CaCO_3$), gypsum plaster ($CaSO_4 \cdot 0.5H_2O$), and magnesium hydroxide ($Mg(OH)_2$). Between 90 and 95 °C, the predominant type is $CaCO_3$ and between 95 and 105 °C it is $Mg(OH)_2$. Due to the scaling, the efficiency of the MED plants decreases considerably. See Al-Ahmad and Aleem (1993) for an in-depth description of the scaling process, Gebel and Yuce (2008) for an in-depth description of the MED technology, and Ophir and Lokiec (2005) and Sayyaadi and Saffari (2010) for an economic overview.

1.1.2.3 Vapour Compression (VC)

VC is another desalination technique more popular in the past. It is based on MED technology, and both technologies are sometimes coupled in the same plant. The evaporation in each stage is obtained thanks to vacuum pumps (MVC) or by heating (TVC). See El-Dessouky et al. (2000) and Liang et al. (2013) for a more detailed description of a VC system, and Wu and Zhang (2003) and Sharafa et al. (2011) for a hybrid desalination plant MED-VC.

1.1.2.4 Electrodialysis Reversal (EDR)

EDR is a desalination technique useful for removing charged particles from the feed water. For brackish water with low salinity (less than 3 000 ppm), EDR presents a better energy consumption ratio than

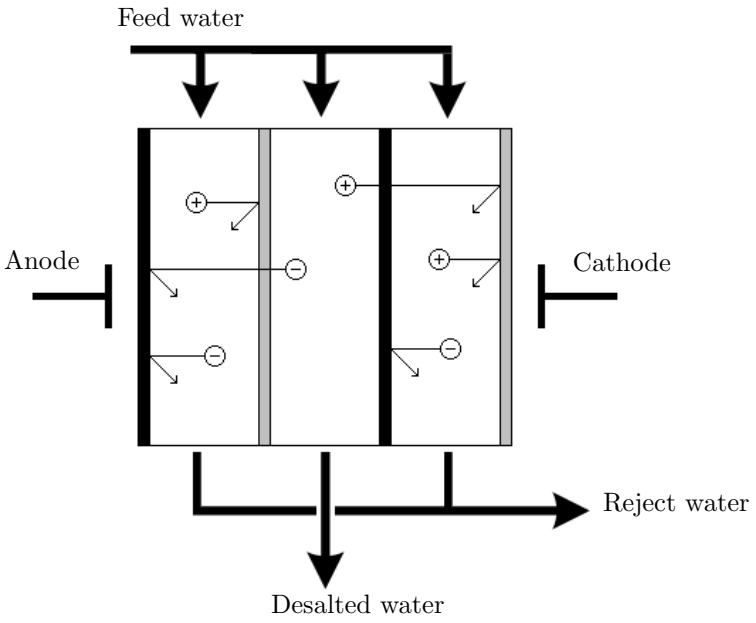

Figure 1.6: EDR diagram.

RO. Typically, it is used as a secondary stage in a desalination plant or in a water purification plant.

Figure 1.6 illustrates the EDR process. Thanks to a high electric field, ions are forced to cross a semipermeable membrane, and are removed from the feed flow. There are two types of membrane: 1) anion-exchange membranes, which block the pass of cations; and 2) cation-exchange membranes, which block the pass of anions. The membranes are placed alternately in an EDR module: anion-exchange membrane – cation-exchange membrane – anion-exchange membrane – cation-exchange membrane etc. Due to the high electric field, anions (such as chloride ion, Cl^-) flow in the direction of the anode and pass through the anion-exchange membranes, but are rejected by the cation-exchange membranes. In the same way, cations (such as sodium ion, Na^+) flow in the direction of the cathode and pass through the cation-exchange membranes, but are rejected by the anion-exchange membranes. At the end of the EDR unit, the feed flow has been divided into two streams: a desalted stream free of ions, and a brine stream.

The unwanted deposition of charged colloidal components can be

partially removed from the surface of the membranes by reversing the electric field. Besides, a manual cleaning should be done periodically.

Figure 1.7: EDR system. Water purification plant of Abrera (Spain), property of the company ATLL.

(a) EDR modules. (b) EDR module without case.

Figure 1.8: EDR modules. Water purification plant of Abrera (Spain), property of the company ATLL.

Figure 1.7 shows the EDR system of the water purification plant of Abrera[2] (Spain). This EDR system is used for the elimination of colloidal components, which give colour and smell to the drinkable water. It is used as a second stage of the purification plant. The first stage is based on conventional purification techniques (coagulation and flocculation) for physical water treatment.

Figure 1.8 shows several EDR modules. The left hand picture shows two EDR modules with the connection for the brine stream and desalted stream, and the right hand picture shows an EDR module without case, where the multiple membranes can be seen. See, for example, Allison (1995), Chao and Liang (2008), Strathmann (2010) and Tanaka (2012) for an in-depth description of EDR technology, and Peñate et al. (2013) for the description of an EDR plant powered by renewable energy. In addition, the application of EDR in the water purification plant of Abrera can be seen in Valero and Arbos (2010).

1.1.2.5 Membrane Distillation (MD)

MD is an emerging desalination technology used in small-scale desalination plants. It is based on a hydrophobic membrane. Vapour water molecules can cross the membrane, but liquid water molecules are rejected. Vapour is produced by an external energy source, typically solar radiation. Since the operation temperature is low (around 80 °C), conventional flat collectors can be used as the energy supply system. The most important advantage of MD technology is that chemicals are not needed for the pretreatment. See Lagana et al. (2000) and El-Bourawi et al. (2006) for an in-depth description of MD desalination plants, Chang et al. (2012) and Ho et al. (2013) for the MD modelling, and Alklaibi and Lior (2005) and Peñate and García-Rodríguez (2012) for a perspective on its use.

1.1.2.6 Humidification-Dehumidification (HD)

As in the case of MD, HD is another emerging desalination technology, but currently used only for small-scale desalination plants. Feed water is heated by an external energy source, typically solar radia-

[2]The EDR system of the water purification plant of Abrera (Spain) is the biggest in the world, with a production of 200 000 m^3/day.

tion. Then, it is distributed in drops and put in contact with a dry air stream in a humidification chamber. Part of the water evaporates and is transferred to the air stream, which increases its humidity. Next, humidified air is pumped to a condenser chamber, where the evaporated water is collected. However, the system must be large in size due to the low efficiency of the condensation. See Bourouni et al. (2001), Parekha et al. (2004) and Narayan et al. (2013) for a more detailed description of HD technology, and Farid et al. (2003) for the HD modelling.

1.1.2.7 Reverse Osmosis

RO is a separation process that uses high pressure to force water molecules through a semi permeable membrane, which retains the salt particles on one side. The pressure required depends mainly on the salt concentration of the feed flow. Typical values for the operating pressure are over 40 bar for brackish water and over 80 bar for seawater (see Wong et al. (2012)). This pressure is supplied by high-pressure pumps of positive-displacement or (more commonly) centrifugal type.

(a) Spiral wound. (b) Hollow fibre.

Figure 1.9: RO modules cutaways, from the company DOW. IDA 2011 World Congress, Australia.

The flow and characteristics of the desalted water (called "permeate") depend on several factors, such as the salt concentration,

operating pressure, temperature, membrane permeability, membrane surface, etc. To produce a high desalted water volume, the membranes are packed in different configurations. Table 1.5 shows the most typical packing configurations for RO membranes. By far the most popular packing configuration is the spiral wound. However, the use of hollow fine-fibre modules is increasing, due to their high density ratio. Figure 1.9 shows two cross-sections for a spiral wound and a hollow fibre RO module, from the company DOW.

Type	Packing density (m^2/m^3)
Concentric tubular	100
Hollow fibre	200
Plate and frame	300
Spiral wound	600
Hollow fine-fibre	3 000

Table 1.5: Packing density of membrane modules. Adapted from Sheikholeslami (2007).

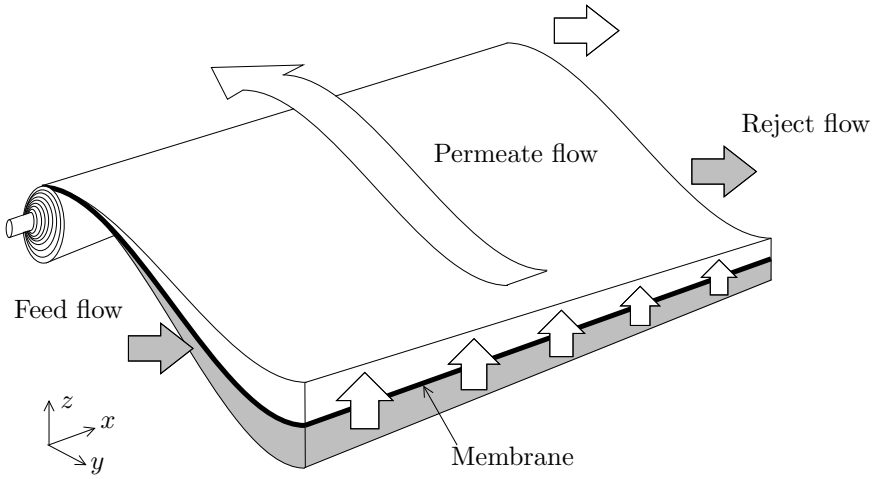

Figure 1.10: Diagram of a spiral-wound RO module.

In a spiral wound RO module, the feed stream flows parallel to the membrane. The permeate flow crosses the membrane perpendicular

to the feed flow. Next, the permeate flows to an inner tube (see figure 1.9.a), where the desalted water is collected. Figure 1.10 illustrates an RO module.

Some of the most important RO module manufactures are DOW, TORAY and Hydranautics. There are several types of RO membranes (for seawater, brackish water, high rejection, high recovery, low flux, etc.), and the choice of the correct membrane depends mainly on characteristics of the feed water.

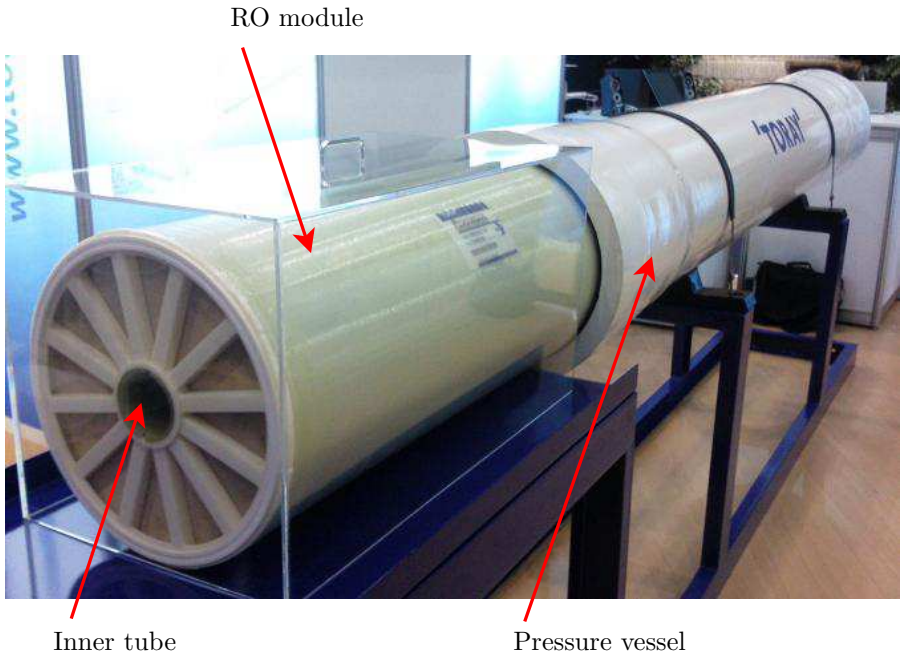

Figure 1.11: Pressure vessel from the company TORAY. IDA 2011 World Congress, Australia.

The size of the RO modules is normalized, with a width of 4, 8 and 16 inches, and a length of one meter. The most popular RO modules are 8-in wide, but the current trend is to operate with wider RO modules in the following years. RO modules are placed in series in chambers called "pressure vessels", which are designed to support the high pressure required for desalination.

The number of RO modules in one pressure vessel can vary from 1 to 14, but typically takes a value around 7. An RO pressure vessel has one input (the feed flow), and two outputs (the permeate and the reject

flow). Figure 1.11 shows a pressure vessel from the company TORAY. The pressure vessels are connected in parallel, forming a rack or train of pressure vessels, as can be seen in figure 1.12. Each high-pressure pump supplies the required pressure energy to one pressure vessel rack.

Figure 1.12: Racks of RO pressure vessels. Desalination plant of Barcelona-Llobregat (Spain), property of the company ATLL.

1.1.3 RO Desalination Plants

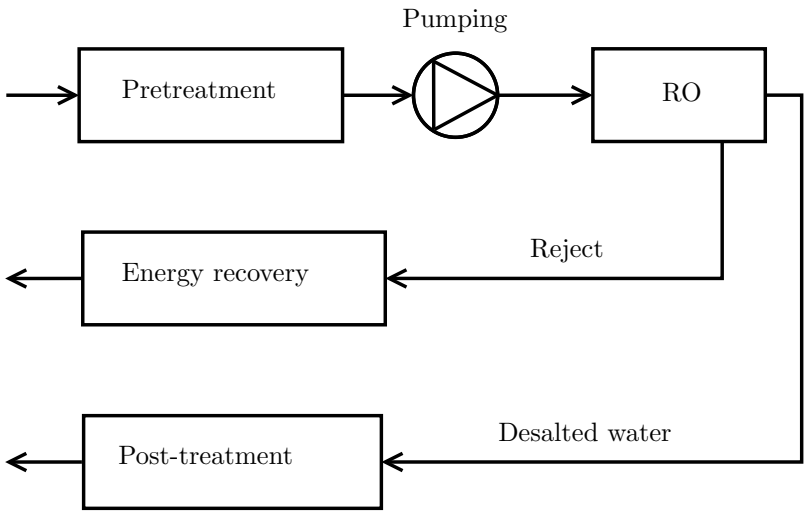

Figure 1.13: RO desalination diagram.

An RO desalination plant has the following stages or sections: 1) the pretreatment of the feed flow; 2) the pumping system with the high-pressure pumps; 3) the RO pressure vessel racks; 4) the post-treatment of the desalted flow before being consumed; and 5) the energy recovery of the reject flow before being removed; as is illustrated in figure 1.13.

Figure 1.14 shows a picture of the desalination plant of Barcelona-Llobregat (Spain), where the RO pressure vessel racks, the high-pressure pumps, the energy recovery system and the connections pipes between the different sections can be seen.

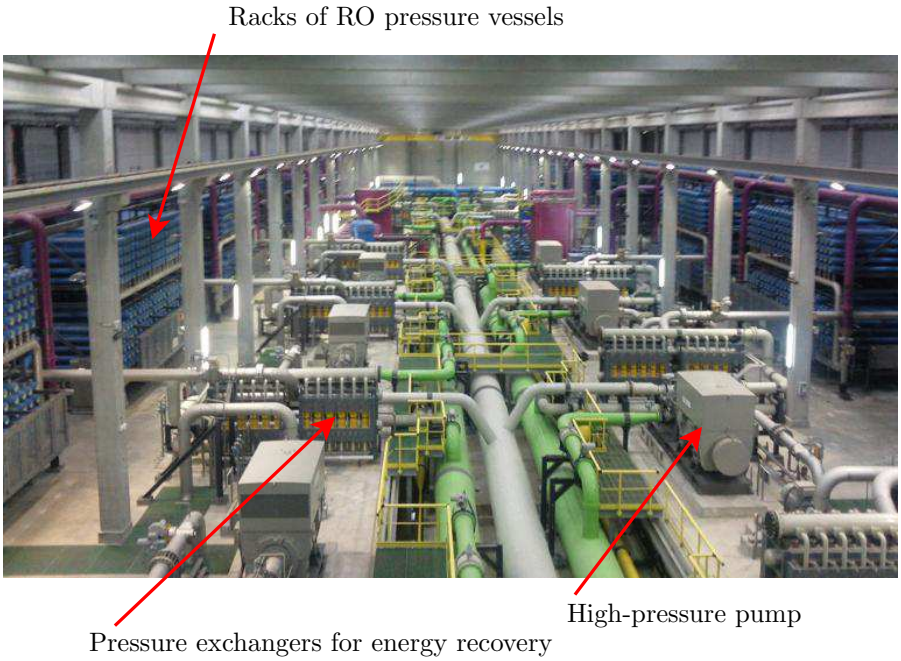

Figure 1.14: Seawater desalination plant of Barcelona-Llobregat (Spain), property of the company ATLL.

1.1.3.1 Pretreatment

Due to the extremely narrow pores of the RO membranes, they are very easily blocked. In addition, RO membranes are very sensitive to pH, acids and chemicals. In order to increase the life of the membranes and avoid membrane damage, the feed water should be pretreated before being pumped to the RO pressure vessels. See, for instance

Gray (2010), Grady et al. (2011), and Palacín et al. (2010a). The pretreatment can consist of several of the following stages:

Figure 1.15: Decantation tanks. Water purification plant of Abrera (Spain), property of the company ATLL.

First of all, a correct water intake (through submerged breakwaters and deep canalizations) avoids the arrival of foam, oil and other pollutants to the desalination plant. Traditional physical methods for the removal of the suspended solids and organic particles are very common after the water intake. The coagulation - flocculation - decantation system is successfully used to remove the larger particles. Coagulation means the formation and growth of colloidals, and it is favoured by the addition of chemical components (such as aluminium sulfate ($Al_2(SO_4)_3{\cdot}6H_2O$), iron(III) sulfate ($Fe_2(SO_4)_3$), iron(III) chloride ($FeCl_3$), aluminium oxide (Al_2O_3), etc.).

Flocculation means the aggregation of the colloidals until becoming suspended particles, in the form of floc or flakes. This is favoured by the addition of different polyelectrolytes and flocculants (such as calcium hydroxide, aluminium sulfate, sodium silicate, etc.). Finally, decantation means the precipitation of the suspended particles. This is favoured by the low velocity of the water, when the feed flows through big decantation tanks and lamellar decanters. Figure 1.15 shows the

Figure 1.16: Tanks for the addition of chemicals. Desalination plant of Barcelona-Llobregat (Spain), property of the company ATLL.

decantation tanks of the water purification plant of Abrera. The precipitation of solids on the RO membrane surfaces can be avoided by the addition of antiscaling and the correct pH adjustment. Figure 1.16 shows the tanks for the addition of chemicals in the desalination plant of Barcelona-Llobregat.

The biggest particulates (larger than 10 μm) are typically removed using sand filters. Sand filters are tanks (open or pressurized) with a sand bed. Feed water flows through the sand, which captures the suspended amounts from the water. When the sand filter is saturated, a cleaning should be done. This consists of several stages, but mainly, the sand bed is shaken by an inverse flow (air or water) at high velocity. The saturation of the sand filter can easily be detected by the measurement of the pressure drop between the inlet and outlet of the filter. Figure 1.17 shows the pressurized sand filters of the desalination plant of Barcelona-Llobregat.

Smaller particulates can be removed from the water by different grades of filtration: microfiltration (MF), ultrafiltration (UF), and

Figure 1.17: Pressurized sand filters. Desalination plant of Barcelona-Llobregat (Spain), property of the company ATLL.

Type	Porous size	Operation pressure	Component eliminated
MF	0.1-10 μm	0.5-2 bar	Bacteria and particulates
UF	10-200 nm	2-5 bar	Viruses and macromolecules
NF	1-20 nm	5-10 bar	Ions and small molecules

Table 1.6: Filtration processes. Adapted from IDA.

nanofiltration (NF), as summarized in table 1.6. Although the cost of UF and NF is still high, it is expected that in the next few years, the chemical additions will be replaced by these filtration techniques.

1.1.3.2 Pumping

Around 75% of the energy consumption of most desalination plants is due to the pumping system. This consists of high-pressure pumps, which increase the pressure of the feed flow over the osmotic pressure (to over 80 bar for seawater).

Each pump supplies pressure to one RO pressure vessel rack. Depending on the water demand, some high-pressure pump - RO pressure vessel rack modules can be connected or disconnected. High-pressure

pumps are typically of centrifugal type (for seawater), or positive-displacement type (for sea and brackish water). Figure 1.18 shows a cutaway of a five-stage pump, from the company KSB.

Figure 1.18: High-pressure multistage pump from the company KSB. IDA 2011 World Congress, Australia.

1.1.3.3 Post-Treatment

The recommended salt content of the drinkable water is around 200-400 ppm. Since an RO system produces permeate water with a salinity lower than 50 ppm, it should be remineralized before being consumed. Besides the health issue, remineralization decreases the high corrosion potential of the desalted water. The controlled remineralization can be done by several mechanisms, as follows: 1) blending with the correct volume of pretreated water; 2) percolation by calcite limestone; 3) percolation by dolomite limestone; 4) addition of sodium carbonate and carbon dioxide; 5) addition of calcium chloride and sodium bicarbonate; etc.

In addition, the post-treatment process consists of the pH adjustment (by the addition of acids or basis) and disinfection. Typical methods for disinfection are: 1) the addition of chemicals (such as chlorine dioxide or ammonia); 2) the addition of biocides; 3) disinfection by ozonification; 4) disinfection by ultraviolet light; etc. Figure

Figure 1.19: Ultraviolet disinfection chambers. Water purification plant of Sant Joan Despí (Spain), property of the company Agbar.

1.19 shows the ultraviolet disinfection chambers of the water purification plant of Sant Joan Despí (Spain).

1.1.3.4 Energy Recovery

The pressure of the permeate flow is around atmospheric pressure. However, the pressure of the reject flow is very high, close to the pressure supplied by the high-pressure pump. (The pressure drop between the inlet of the RO pressure vessel and the reject output is less than 1 bar.) Small-scale RO desalination plants have a valve that strangulates the reject flow before it is carried to the drain. In the case of medium and big-scale desalination plants, it is possible to recover part of the pressure energy of the reject flow. The most important energy recovery systems are: 1) turbines; 2) pressure exchangers; and 3) retarded osmosis.

Turbines were the first attempt to recover the pressure energy of the reject. The reject flow is carried to the turbine and pushes the turbine's blades. The rotor of the turbine is connected to the rotor of the high-pressure pump of the RO system. The most popular types of turbine are Francis (currently obsolete) and Pelton, with a recovery efficiency of 40% and 70% respectively. An in-depth description of turbines can be seen in Woodcock and White (1981) and Wilson et al. (1987); while an economic comparison between turbines and other energy recovery systems can be seen in Peñate and García-Rodríguez (2011) and Lemes et al. (2013).

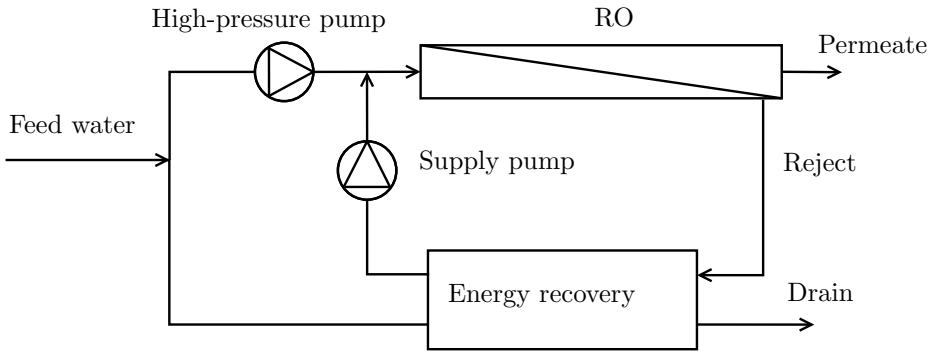

Figure 1.20: Pressure exchanger diagram.

Pressure exchanger devices (also called "isobaric chambers") put into contact the reject flow with part of the feed water (see Mei et al. (2012)). Each stream in one extreme of a conduction. Reject flow pushes the feed water, supplying pressure energy. The efficiency of the pressure exchanger system is over 90%. Figure 1.20 illustrates an RO desalination system with a pressure exchanger device.

Figure 1.21: Rack of pressure exchangers, from the company ERI (type PX). Desalination plant of Barcelona-Llobregat (Spain), property of the company ATLL.

After the pretreatment system, the feed flow is divided into two streams (approximately of the same value). The first stream is pumped by the high-pressure pump to the required operating pressure. The second stream is pumped to the pressure exchanger device, where its pressure is increased. Next, a supply pump is required to supply the rest of the pressure energy, up to the required operating pressure. The energy consumption of the supply pump is several times lower than the high-pressure pump. By using a pressure exchanger device, an RO desalination module almost duplicates its water production capacity. See section 2.1.3 at page 62 for an in-depth description of the pressure exchanger devices.

By far the most popular pressure exchanger device is called PX, and belongs to the company ERI. A rack of PXs can be seen in figure 1.21. It consists of a mobile chamber with different holes. Reject and feed flow come into contact through these holes. The rotation of the chamber is done automatically by the pressure difference between the streams. The rotation causes the water to go in and out of the holes. An in-depth description of the PX exchangers can be seen in Stover (2007) and Cameron and Clemente (2008), while a real application of the PX technology can be seen in Stover and Martin (2009).

Other popular pressure exchanger devices are called DWEER (Dual Work Exchanger Energy Recovery), from the company Flowserve; and SalTec, from the company KSB. Unlike PX, DWEER and SalTec consist of two fixed chambers, connected by a set of variables, while a physical separator is located between the reject flow and the feed flow.

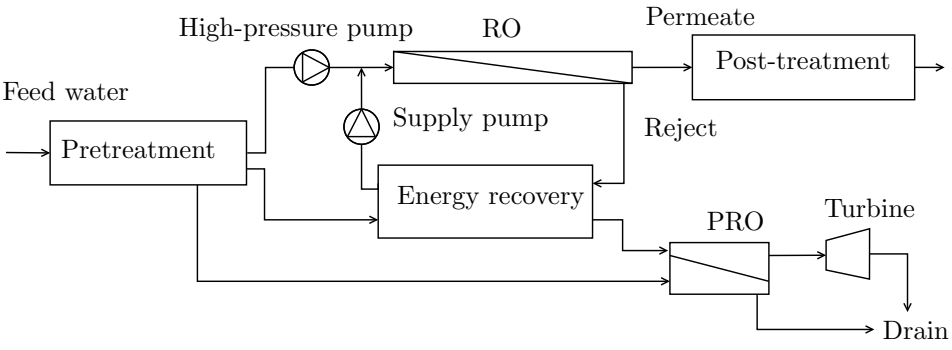

Figure 1.22: PRO diagram.

Pressure Retarded Osmosis (PRO) is a recent technology for en-

ergy recovery. It is based not on the high pressure of the reject, but on its high salt concentration. It can be used as a second stage of the energy recovery system. Figure 1.22 illustrates an RO desalination plant with PRO. The reject flow is placed in contact with the pretreated water flow through a semi permeable membrane. The different salt concentration on both sides of the membrane causes the osmosis effect and the pressure increase of the reject flow. Then, part of the pressure energy of the reject can be recovered thanks to a second pressure exchanger or a Pelton turbine. The use of PRO is still fairly unusual. See, for example, Achilli et al. (2009), Thorsen and Holt (2009), Kim et al. (2012b) Klaysom et al. (2013) and Kim and Elimelech (2013) for an in-depth description of this technology.

1.1.4 Boron Concentration Limits

As commented previously, the salt content of the desalted water produced in the RO systems is too low to be consumed directly by humans, and a controlled remineralization is required. However, this is not the case with boron. The legislation about the boron concentration in the drinkable water depends on the country[3], but typically a concentration of less than 0.5-1.0 ppm is required[4]. This is around the same concentration obtained with an RO system, and often a simple RO system is not enough to fulfil the boron requirement. In order to deal with this, several strategies can be followed. See Kim et al. (2012a) and Jin et al. (2012) for an in-depth description of the boron removal form water.

Typically, the desalted water obtained in the RO system (called "first stage") is refiltered in a second RO system (called "second stage"), as is illustrated in figure 1.23. The second stage RO filtration consists of the same elements as in the first stage: pumps and racks of RO pressure vessels, etc. Since the feed flow of the second stage is in fact desalted water, the operating pressure supplied by the pumps

[3]In fact, in some countries (such as many of the Maghreb), the boron concentration is not mentioned in the legislation.

[4]In some countries, such as Israel, where the water network for human consumption and for irrigation is the same, the removal of Boron is critical. Boron reacts during the germination of the plants, and prevents their correct growth. See Tripler et al. (2007), Yermiyahu et al. (2008) for a more detailed description.

is only a few bars. The energy consumption of the second stage RO system is around 25% of the energy consumption of the first stage.

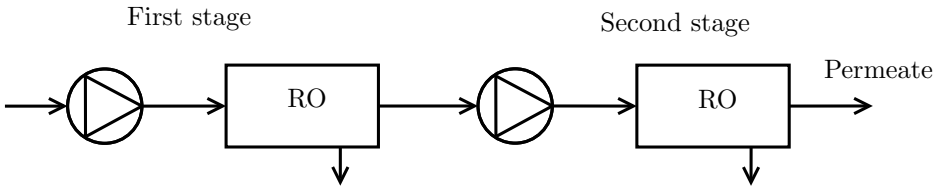

Figure 1.23: Boron removal with two RO filtration stages.

Depending on the boron elimination ratio in the first stage, not all the permeate flow of the first stage should be refiltered. Part of the permeate of the first stage can be by-passed by the second stage, as can be seen in figure 1.24. By optimizing the by-passed permeate flow, an important decrease in the energy consumption in the second stage can be obtained.

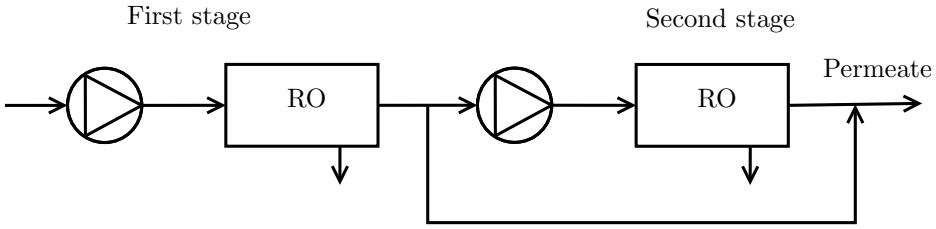

Figure 1.24: By-pass of the permeate.

The number of boron particulates that crosses the membrane depends on the position along the pressure vessel. Better boron removal is obtained in the RO modules close to the feed water input, where the feed flow concentration is lower. Pressure vessels with two permeate flows (one close to the feed water input, and other close to the brine output) make it possible to automatically divide the permeate flow into two permeate flows, one with low boron concentration, which fulfils the boron concentration constraints, and a second with high boron concentration, which should be refiltered in a second stage. The ratio between both permeate flows is controlled by manipulating two valves in the permeate lines, as is illustrated in figure 1.25.

In addition, the use of specific RO membranes with high boron

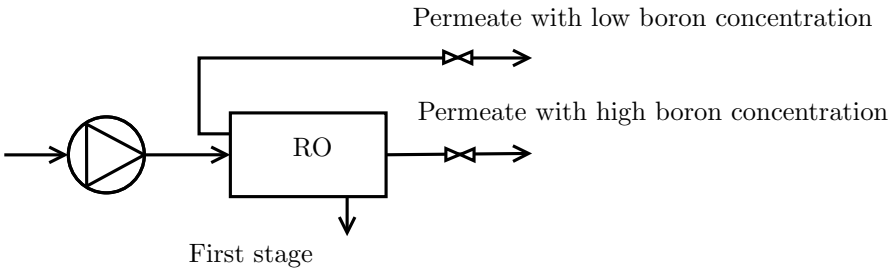

Figure 1.25: One stage filtration with two permeate outlets.

rejection, in several cases, allows avoiding the use of the second RO stage.

The future of the boron legislation is not clear. A current discussion about this is taking place. Some experts consider the legislation concerning the boron concentration is too strict. By increasing the boron requirement only up to 2.0 ppm, the second stage RO system could be removed in several desalination plants, obtaining an important pumping consumption saving. See Chung et al. (2012) and Peñate and García-Rodríguez (2012) for an in-depth description of the trend in RO desalination plants.

1.1.5 Scaling and Fouling

There are many effects that can causes the degrading and fouling of the RO membranes. Prevention and the correct pretreatment of the feed water before it arrives at the RO pressure vessels is the best barrier. Fouling can never be completely avoided, but its nature and type altered, and the cleaning made easier. Fouling, and its prevention, depends on several factors, such as the feed water characteristics, temperature, flux through the RO membranes, pH, etc. Once the fouling has taken place, an early detection and correct cleaning can solve the problem. A variation in more than 10% of some variables of the system (operating pressure, permeate salinity, permeate flow, pressure drop, etc.) is a good signal that fouling is taking place. The Silt Density Index (SDI) is a very popular index for the measurement of the fouling potential. The SDI depends on the water turbidity and particle concentration, but there is no direct correlation between them. The cleaning protocol depends on the fouling, and typically includes

several stages, in which different chemical components are pumped through the pressure vessels. The most common causes for membrane degrading are described below, and their consequences in the permeate characteristic (quality, pressure and flow), are summarized in table 1.7. See Mariall et al. (1999), Lim and Bai (2003), and Sheikholeslami (2007) for an in-depth description of the fouling types and cleaning.

Scaling means the precipitation of carbonates and sulfates due to supersaturation of the water. The most common scaling chemical species are calcium carbonate ($CaCO_3$), calcium sulfate ($CaSO_4$), barium sulfate ($BaSO_4$) and strontium sulfate ($SrSO_4$); and rarely calcium fluoride (CaF_2) and silicon dioxide (SiO_2), which is the most complicated to remove. The correct pH adjustment is the easiest way to avoid scaling, carrying the feed water under saturation. The Langelier Saturation Index (LSI) is a very useful index to determine the scaling potential of the feed water.

For highly salty water (over 10^4 ppm), the Stiff & Davis Stability Index (S&DSI) is more exact. There are several other indexes, such as the Ryznar Stability Index (RSI), the Puckorius Scaling Index (PSI), the Calcium Saturation Index (CSI), etc., which calculate the scaling potential more accurately. However, the LSI is still the most popular index. See Sheikholeslami (2007) and Gebel and Yuce (2008) for an in-depth description of the scaling effect. In addition, see Elfil and Roques (2004) for a more detailed description of the calcium carbonate equilibrium, which is divided into three zones: aggressive (or corrosive), scaling and metastable zones; see Elfil and Hannachi (2006) for a correction of the LSI, taking into account the metastable zone; finally, see Wang et al. (2013) for a summary of the chemical treatment of RO membranes.

The growth of microorganisms in the membranes, which is called "biofouling", can take place if the substrate concentration in the feed water is large enough. Microorganisms can block or break the membranes. In addition, it can also cause the presence of pathogens in the permeate water.

The precipitation of metal oxides and hydroxides can cause important fouling of the membranes. The most common metals are iron, aluminium, manganese, nickel, copper, etc. Metals can be present in the feed water, or they can come from pipe corrosion (e.g. iron) or from the coagulation and flocculation stages (e.g. aluminium). Other

common fouling components are colloidal particles, oils, small solids, organic particles, etc. (See Boo et al. (2012) and Zuo and Wang (2013).)

Type of fouling	Consequences in the permeate		
	Salt	Pressure	Flow
Scaling	Increase ($< 20\%$)	Increase ($< 50\%$)	Decrease $< 10\%$)
Oxides and hydroxides	Fast increase ($> 2\times$)	Fast increase ($> 2\times$)	Fast decrease (>50%)
Colloidal	Slow increase ($> 2\times$)	Slow decrease ($> 2\times$)	Slow decrease ($> 50\%$)
Biofouling	Increase ($> 2\times$)	Increase ($> 2\times$)	Decrease ($> 50\%$)
Porous obstruction	Increase ($< 10\%$)	Fast increase ($< 50\%$)	Fast decrease $< 20\%$)

Table 1.7: Fouling types and consequences in the permeate. Adapted from Sheikholeslami (2007).

Chemical cleaning is done once the fouling has being detected. Since chemical cleaning is very aggressive to the RO membranes and means an important extra expense, it should be minimized. More than one - two chemical cleanings per year means than the pretreatment is wrong and the plant is being badly operated.

There are other types of cleaning that are done periodically with clean water. Since they are done without chemicals, the membranes do not suffer. Flushing involves the pumping of feed water through the pressure vessels, with a very high flow. It is done periodically each several hours for a few minutes, and favours the eliminations of solids. Each several days, a washing of the membranes is done. This involves a more exhaustive cleaning, where clean water is pumped, in the reverse and inverse directions, through the pressure vessels. It favours the removal of precipitations and scaling. Finally, when a rack of pressure vessels is to be shut off over a long period (several days), the pressure vessels should be filled with clean water, with a low concentration of antiscaling agents.

1.1.6 Vocabulary

This section summarizes the most common vocabulary used in desalination. See Cheremisinoff (2002), Gebel and Yuce (2008) and Hernández-Suárez (2010) for a detailed summary of the equations and correlations used for the design of desalination plants.

TDS: This is the acronym of Total Dissolved Solids, and measures the salt content of the water. It embraces all the anions present in the water, such as chloride (Cl^-), sodium (Na^+), sulfate (SO_4^{2-}), magnesium (Mg^{2+}), calcium (Ca^{2+}), potassium (K^+), bicarbonate (HCO_3^-), and many others. Its units are ppm or g/m^3. Although it is only an approximation, the most common way to measure the TDS is by the measurement of conductivity (S). The relation between TDS and conductivity is typically calculated by a polynomial function, as in equation (1.1):

$$\text{TDS} = a_0 + a_1 \cdot S + a_2 \cdot S^2 + a_3 \cdot S^3 + ... \tag{1.1}$$

where S is the conductivity (μS/cm), and the parameters a_0, a_1, a_2, a_3... depend on the characteristics of the water. See Cheremisinoff (2002) for some values for these parameters.

A simpler function, proposed by Hernández-Suárez (2010), can be seen in equation (1.2):

$$\begin{array}{lcl} \text{if TDS} < 5\,000 & \rightarrow & 0.64 \cdot S \\ \text{if TDS} \geq 5\,000 & \rightarrow & 0.80 \cdot S \end{array} \tag{1.2}$$

Salt Rejection: This is the ratio between the salinity of the water produced versus the salinity of the feed water, as follows:

$$\text{Salt Rejection} = \frac{\text{TDS of the feed - TDS of the permeate}}{\text{TDS of the feed}} \cdot 100 \tag{1.3}$$

Water Recovery: This is the ratio between the produced water flow and the feed water flow, as follows:

$$\text{Water Recovery} = \frac{\text{Permeate flow}}{\text{Feed flow}} \cdot 100 \tag{1.4}$$

SEC: This is the acronym for the Specific Energy Consumption. It measures the ratio between the energy consumption and the produced water flow. It is a useful index to compare different desalination technologies and plants:

$$\text{SEC} = \frac{\text{Energy}}{\text{Permeate flow}} \ (\text{kWh/m}^3) \tag{1.5}$$

Fresh Water: The salt concentration for drinkable water should be lower than 500 ppm.

Brackish Water: The chemical species and concentration depend strongly on the place, and even on the season. Water is considered brackish when its salinity is between 500 and 30 000 ppm. At 20°C, the osmotic pressure of brackish water varies between 0.4 bar (for 500 ppm) and 25 bar (for 30 000 ppm).

Seawater: The salinity of seawater depends on the ocean or sea. Table 1.8 summarizes the salinity characteristics of different oceans and seas. π_{20} is an estimation of the osmotic pressure at 20 °C, for each sample. The real operating pressure of a desalination plant, which is supplied by the high-pressure pump, is higher than this value, due to the increment of salt along the length of the pressure vessels and on the RO membrane surface.

Sea/Ocean	TDS	Cl^-	Na^+	SO_4^{2-}	Mg^{2+}	π_{20} (bar)
Red Sea	55 800	46%	31%	8%	4%	43
Persian Gulf	47 000	52%	26%	7%	4%	36
Atlantic Ocean	37 800	54%	30%	8%	3%	29
Mediterranean Sea	36 800	56%	30%	7%	4%	29
Pacific Ocean	35 900	52%	34%	11%	2%	28

Table 1.8: Salinity characteristics of seawater. Adapted from Karajeh and BenJemaa (2011).

1.1.7 Energy Consumption

As commented previously, the energy consumption of desalination plants has suffered an important decrease in the last few decades (from

22 kWh/m^3 in 1970 to the current 3.3 kWh/m^3). The main factors that have contributed to this reduction are: 1) the improvement in the energy recovery system; 2) the improvement in pumping efficiency; and 3) the improvement in membrane technology. Table 1.9 summarizes the main contributions for the energy consumption of a typical seawater reverse osmosis (SWRO) desalination plant. Around 75% of the energy consumption is due to the pumping of the first and second stages. Notice this table does not include the energy consumption due to the pumping of the feed water from the well/sea to the plant, nor the pumping of the reject stream from the plant to the drain[5].

Section	Energy consumption
Pumping for RO of 1st stage	60%
Pumping for RO of 2nd stage	16%
Pretreatment	9%
Pumping of clean water	7%
Energy losses and security	5%
Chemical addition (dosification)	0.5%
Pumping of mud	0.5%
Lighting and others	2%
Total	3.3 kWh/m^3

Table 1.9: Energy consumption of a large-scale RO desalination plant by sections. Adapted from Karajeh and BenJemaa (2011).

Typically, large-scale desalination plants are connected to a high-voltage electricity network, which supplies the main part of its energy consumption. In the case of the Middle-East, fossil fuels and nuclear energy are very popular (see Aljohani (2004) and Misra and Kupitz (2004)). Renewable energies are still used relatively little due to the high cost in comparison with conventional sources of energy. It is mainly limited to small-scale desalination plants, located in areas without a reliable electricity grid. Australia is an important exception, where the biggest seawater desalination plants are powered by

[5]The pumping energy consumption depends on the relative position relative between the desalination plant and the feed water source. For a desalination plant located next to the sea, the energy consumption takes values around 0.6 kWh/m3.

renewable energies[6] In addition, it is an emerging technology, and the prediction for the following years is for an increase in its application. See García-Rodríguez (2002) and Mathioulakis et al. (2007) for an in-depth description of desalination plants coupled with renewable energy consumption for desalination plants. Table 1.10 compares the cost of different desalination plants with a conventional SWRO plant. The source is the PRODES project (Promotion of Renewable Energy for Water Production through Desalination). An in-depth description of this project can be seen in Tzen and Papapetrou (2012).

Technology	Feed water	Cost (€/m^3)
Conventional RO	Seawater	<0.50
RO + Wind turbines	Seawater	1.40
RO + PV panels	Seawater	12.20
RO + PV panels	Brackish	8.30
EDR + PV panels	Brackish	8.50
MED + Solar radiation	Seawater	1.60
MED + Biomass	Seawater	5.10

Table 1.10: Desalination cost using renewable energy. Adapted from PRODES.

There are two ways to couple renewable energy and desalination: 1) use the renewable energy as a source of heat; and 2) use the renewable energy to produce electrical energy, consequently consumed by the plant. Besides, any source of heat may be used to produce electricity through a thermal engine. The use of renewable energy as a source of heat is linked with the heat-powered processes, such as MSF, MED, TCV, HD and MD; and the use of renewable energy as a source of electrical energy is linked with the power-driven processes, such as EDR and RO. In the case of MCV, renewable energy can be used in both ways.

[6]The biggest desalination plants in Australia are the Wonthaggi desalination plant (with a production of 400 000 m^3/day), the Kurnell desalination plant (with a production of 250 000 m^3/day), the Perth seawater desalination plant (with a production of 130 000 m^3/day), and the Gold Coast desalination plant (with a production of 120 000 m^3/day).

Solar radiation is the most used renewable energy. It can be used as a heat source, thanks to different engines such as solar ponds, flat plates, evacuated tubes, concentrating collectors, etc; and as a method to produce electricity, thanks to thermal engines or photovoltaic panels (PV). Wind velocity is another of the most popular renewable energies to produce electricity, thanks to wind turbines or wind generators. Besides, other renewable energy sources which can be used for desalination are biomass, geothermal heat, wave power, etc.

1.1.8 Environmental Impact

Typically, SWRO plants drain the reject flow to the sea. The most important sources of environmental degradation, caused by a desalination plant, are the reject flow with a high salt content and the pollution during the chemical cleaning. Even though chemical cleaning is only done every so often, the drain-off of chemicals should be carefully studied. Since the chemical components of the reject flow are the same as those of the feed water, it is not considered as a pollutant. However, its high salinity may cause negative effects in the local environment, specially to the flora and fauna at the bottom of the sea (called "benthos"). The higher density of the reject flow causes its accumulation in the seabed, if there is a poor blend with the fresh water. Besides, the increase in salt causes greater light reflection and the consequent lack of light.

Some of the living beings most affected by an increase in salinity are: the posidonia (such as the *p. oceanica*, also called "Neptune grass") and the cymodocea (such as the *c. nodosa*, also called "little Neptune grass"). They are different types of sea grass, which generate underwater grasslands. Their presence is fundamental, because they are the base of different marine ecosystems (thanks to their high production of oxygen). Other living beings affected by the salinity increase are different types of seaweed, bivalves, etc.

Some of the solutions for the environmental degradation due to the drain of the reject flow are: 1) the drain of the brine through a net of drains (instead of one single drain); 2) the drain of the brine in a breaker region (where there is a very well blend); and 3) the drain of the brine in a current degraded region (such as a port). It is very common that an SWRO plant is built close to a sewage treatment

plant. The reject flow from the desalination plant is blended with the low-salty treated-water flow from the sewage treatment plant, and the total salinity is kept within the legal limits.

1.2 State of the Art

1.2.1 Modelling of RO Desalination Plants

The study, design, control and optimal operation of RO plants require adequate models. These can vary very much in complexity and size according with the intended application.

For instance, the advanced control and optimization techniques (see section 1.2.3) may require simplified models of the desalination system. The computational time of the models sometimes is as important as their accuracy. In this case, a simplified modelling, consisting of a limited number of equations, is preferred; such as the mathematical modelling proposed by Alatiqi et al. (1999), Al-Bastaki and Abbas (1999), Gambier and Badreddin (2003, 2004), Baker (2004) and Alvisi et al. (2007), which are based on mass balances; Selvaraj et al. (1995) and Abbas and Al-Bastaki (2005), which are based on neural networks; Robertson et al. (1996), Assef et al. (1997) and Riverol and Pilipovik (2004), which are based on empirical equations and transfer functions; etc.

Other types of models, used often in design, use empirical modelling, based on correlations from experimental data. These models are very powerful to estimate the behaviour of one type and model of membrane (especially the permeate flow), depending on the operating point (pressure and flow) and the characteristics of the feed water (pH, temperature, TDS, turbidity, etc.). However, these models are extrapolated with difficulty.

On the other hand, several authors have proposed mathematical models based on first principles (mass, momentum and energy balances) and physical and chemical equations. These models have a set of parameters which may be fit in order to characterize each specific system. These models are easily extrapolated to several systems and cover a broad type of RO membranes, however their accuracy is lower.

The work developed by Taniguchi (1978) is one of the first works dealing with the characterization of RO modules. It presents exper-

imental equations for the characterization of different types of RO spiral-wound modules. An initial mathematical model for RO modules is presented by Chiolle et al. (1978), which is valid for high-rejection efficiency and is based on Darcy's law. This model is the starting point for the following works, as commented below. For instance, the extension proposed by Kamalesh et al. (1982) is valid for low flux; the modification proposed by Gupta (1985) is valid for high flux; while Slater et al. (1985) studies the influence of the feed concentration. Finally, Palanki and Gupta (1987) improved the model taking into account multiple solutes.

Initially, the profile of the pressure drop is rejected, as seen in the modelling proposed by Evangelista (1986). This assumption is studied by Schock and Miquel (1987), who propose equations for the calculation of the pressure drop, and by Evangelista and Jonsson (1988a,b), who take into account a variable pressure drop depending on the feed flow.

Other effects that have been studied for different authors are: the interactions between the solutes (Dickson et al. (1992)), the presence of organic components (Williams et al. (1999)), the influence of pH (Prats et al. (2000)), the influence of temperature (Goosen et al. (2002)), and the increase of salt close to the RO membrane surface (Sablani et al. (2001) and Kim and Hoek (2005)).

The modelling of the RO desalination plant is extended to MD and HD desalination plants, respectively by Schofield et al. (1987) and Hickey and Gooding (1994); while Sagiv and Semiat (2005) analyse the influence of the cleaning on the RO membrane. Besides, the work developed by Vrouwenvelder et al. (2009) deals with the influence of fouling in the membrane.

The modelling of the fouling of the membranes, has been studied mainly from the point of view of the scaling, as seen in the works developed by Oh et al. (2009), Al-Amoudi (2010), Mi and Elimelech (2010a), Mizrahi et al. (2012), Kostoglou and Karabelas (2013b), Qureshi et al. (2013), and Weinrich et al. (2013). In addition, Mariall et al. (1999) present the modelling of the fouling due to inorganic components, and Lim and Bai (2003), Mi and Elimelech (2010b) and Xu et al. (2010) due to organic components; while Bacchin et al. (2011) analyse the fouling due to colloidal particles. Finally, Sarkar and De (2012) present the modelling of the blocking of the pores.

Although most of the previous mathematical models are implicit, the problem of the numerical integration of the mathematical system is not studied in-depth until the works developed by Senthilmurugan et al. (2005), Song and Ma (2005), Senthilmurugan and Gupta (2006) and Zhou et al. (2006), who propose numerical algorithms for the integration of non-linear models (based on the models proposed by Evangelista and Jonsson (1988a,b)). The time-dependent system is solved by Kouhikamali (2010), Hou et al. (2012), and Thu et al. (2013); while Kostoglou and Karabelas (2013a) solve the numerical problem assuming a steady state. Finally, Marcovecchio et al. (2010) and Nakayama and Sano (2013) show the numerical integration of the modelling of a hollow-fibre RO system.

Nowadays, the computational fluid dynamics (CFD) techniques have been thoroughly applied in desalination plants, as seen in the works developed by Li et al. (2012), Shakaib et al. (2012), Al-Sharif et al. (2013), and Ghadiri et al. (2013).

There are several ways to calculate the mass transport through the membrane: the model used by Vonk and Smit (1983) is based on the capillary flow; the model used by Palanki and Gupta (1987) is based on solution diffusion; the model used by Soltanieh and Sahebdelfar (2001) is based on equilibrium adsorption; etc. However, most of the works use equations based on the Kedem-Katchalsky model (KK), proposed by Kedem and Katchalsky (1958, 1961), and on the Spiegler-Kedem model (SK), proposed by Spiegler and Kedem (1966). Both models assume linear dependence between the mass transport and the pressure difference, and are valid for non-charged membranes (most of the membranes used in desalination are of non-charged type). Since KK and SK models are the most popular models for the design of RO membranes, several authors have proposed different extensions to these models. For example, the works developed by Sapienza et al. (1990), Marinas and Selleck (1992), Soltanieh and Sahebdelfar (2001) and Zhao et al. (2012), extend the KK and SK models to several solutes; while Mistry et al. (2013) study the behaviour of electrolyte solutions. The work presented by Kargol (2000) extends the KK model to a non-linear dependence on the pressure difference. The dependence on the temperature of the KK model is studied by Slezak and Turczynski (1986); while Kleinhans (1998) extend the KK model to biological membranes. Finally, Kargol and Kargol (2003) and Koter

(2005, 2006), Zhang et al. (2010) and Wong et al. (2012) propose equations for the calculation of the parameters of these models. On the other hand, in the case of charged membranes, most of the works are based on the Nernst-Planck model, such as the work proposed by Tsuru et al. (1991), Browen et al. (2002), Mohammad and Takriff (2003) and Sagle et al. (2009).

1.2.2 Simulation Tools of RO Desalination Plants

In contrast with the existence of models, there is a lack of dynamic simulation tools for RO plants. Typically, the simulation tools for RO desalination plants are provided by the membrane manufacturers. ROSA, TorayDS, CAROL, and IMSDesign are perhaps the most common software packages for the design of RO plants. However all of them are static and design oriented, not open tools for dynamic simulation. They have been developed by three important membrane manufacturers: DOW, which provides ROSA; TORAY, which provides TorayDS and CAROL; and Hydranautics, which provides IMSDesign. The methodology of these packages is similar. First, the user defines the characteristics of the feed water (quality of the feed water, pH, temperature, TDS, turbidity, etc.) and the required characteristics of the permeate (recovery, maximum TDS and boron concentration, etc.). Next, the software helps the user to choose the best configuration for the plant (such as number of pressure vessels, number of membranes per pressure vessel, possibility of a second pass, pretreatment system, post-treatment system, etc.) and the appropriate model, type and manufacturer of each component. Finally, the optimal solution is chosen by the user by trial and error, taking into account economic factors, the requirements and his/her own practical knowledge. This software is closed, in the sense the user can easily parametrize the elements of the packages, to fit the particular conditions of a simulated plant, but he cannot add new elements with new characteristics.

ROSA, TorayDS, CAROL and IMSDesign are very powerful tools for the design of RO desalination plants, regarding the choice of the elements of the desalination and taking into account the nominal operating point of the plant. However, there are other aspects of the operation that are not cover by these packages. Since these packages

are based on a static operating point, they are not available to study any dynamic effect. Such as the control of the system, how changes in the characteristics of the feed water (such as TDS or temperature) may affect the operation of the system, the comparison between different control strategies, the goodness of the control loops, the tunning of the controllers, the cleaning protocol, the start-up of the system, and a long etcetera. In addition, these packages do not take into account the possible faults that may take place in the plant or the actions to be performed to correct them, such as the growth of microorganisms, the membranes breakage, and the ageing of the elements.

1.2.3 Control of RO Desalination Plants

A large-scale RO desalination plant consists of a set of independent modules, which embrace a high-pressure pump, a rack of RO pressure vessels and an energy recovery system. Depending on the water demand, one or more modules are switched on/off. Typically, these modules are identical, in most of the industrial installations, and work at a constant operating point. The total flow of drinkable water produced by the plant, is the sum of the permeate flow of each module: $n \cdot Q$ where n is the number of operating modules, and Q is the permeate flow produced by one module. So, the total flow produced by the plant is a discrete variable, which only takes on the values multiple to the permeate flow of one module (that is $1 \cdot Q$, $2 \cdot Q$, $3 \cdot Q$, ...). Since the decision to switch on/off one module is carried out with a scale time of several days, the produced water flow of the plant over one day is constant. The differences between the constant produced flow from the plant and the variable water consumption over a day, are buffered thanks to the tanks, reservoirs and water storages facilities of the water supply network.

By the contrary, a small-scale RO desalination plant consists of one single module and is not connected to any water network. The drinkable water is stored in a buffer tank at the end of the producing line, which may causes losses by evaporation, the growth of algae and microorganisms, and the increase of the chemicals consumption.

The control of the system typically uses simple control loops, such as supply pressure to the RO modules or dosification, while the protocols for the start-up, cleaning and security of the plant are done by

a PLC. The setpoint of the controllers are manipulated manually by the operator, who decide the correct operating point based on his/her own knowledge. Nevertheless, there is a big incentive to operate the plant in a different way, looking for the most profitable operating point both, from the point of view of the RO plant itself and considering the whole energy supply system. For this purpose, advanced control systems play an important role.

The number of works dealing with the advanced control of RO desalination plants is low. Some exceptions are summarized below.

The works developed by Robertson et al. (1996) and Abbas (2006) apply linear model-based predictive control (MPC) in a desalination plant. These works use dynamic matrix control (DMC) to minimize the disturbances in a desalination plant. A non-linear MPC, applied to a desalination plant, is developed by McFall et al. (2008) and Bartman et al. (2009a,b). These works successfully apply MPC for monitoring, fault detection and advanced control in a typical RO desalination plant. The work developed by Zafra-Cabeza et al. (2011) uses MPC for the optimization of a desalination plant, from the point of view of risk management (RM). The optimization problem is formulated as a mixed-integer quadratic programming problem (MIQP) and calculates the mitigation actions to minimize costs.

The optimization of the scheduling of the cleaning and replacing of a desalination plant is studied in Hu and Lu (2005), Lu and Hu (2005) and Lu et al. (2006). In these works, a desalination plant is modelled by empirical equations, and the optimization problem is formulated as a mixed-integer non-linear programming problem (MINLP).

Karuppiah et al. (2012) shows the optimal design using an MINLP optimization, taking into account the ageing of the membranes; while Bartman et al. (2010) solve a non-linear dynamic optimization of an RO plant, modelled using first principles. Finally, the optimization developed by Porrazzo et al. (2013) is based on neural networks.

In addition, the optimization problem of desalination plants is studied in Guria et al. (2005), Wilf and Bartels (2005) and Gasmi et al. (2010) (using static optimization) and in Manth et al. (2003), Zhu et al. (2009, 2010), Gu et al. (2013), Bartels and Andes (2013), Bhutani et al. (2013), and Kim et al. (2013) (using dynamic optimization). The calculation of the cost function for RO desalination plants is described in Malek et al. (1996), Uche et al. (2001), Metaiche and

Kettab (2005), Vince et al. (2008), Hernández-Sancho et al. (2011) and Saffarini et al. (2012).

Finally, regarding other desalination technologies, the works developed by Fiorini and Sciubba (2007), Borsani and Rebagliati (2005), Ettouney et al. (1999), Zamen et al. (2009) and Al-Obaidani et al. (2008) calculate, respectively, the cost function for desalination plants based on MED, MSF, VC, HD and MD; while the advanced control is studied, for instance, by Said et al. (2013), Sanaye and Asgari (2013), Mabrouk (2013) and Mabrouk and Fath (2013).

1.3 Objectives of the Thesis

This thesis deals with modelling, dynamic simulation and optimal control of RO plants, trying to contribute to the advance of the knowledge and operation of these plants by focusing in to main topics: dynamic simulation and optimal economic operation.

The first topic develops a dynamic library for the simulation of RO desalination plants. This library considers the dynamic behaviour of the variables of the plant, and deals with the operation and control of the plant. It contains the main components that are present in an RO desalination plant (such as filters, pressure vessels, pumps, membranes, energy recovery devices and pretreatment systems) and it takes into account the typical faults that may take place in a desalination plant (such as scaling, fouling, biofouling, ageing of the elements, and breakage of the membranes). The library is based on mass, momentum and energy balances, physical and chemical equations, and correlations from the literature. Finally, it has been validated using real data, and the parameters of the main components, estimated. The library could be used for different purposes, such as comparison of control strategies, optimization, capacity design, tuning of the controllers, data reconciliation, fault detection, and a long etcetera.

The second objective of the thesis is to improve the operation and control of small-scale desalination plants, based on RO and powered by renewable energy (which are very popular to fulfil drinkable water to small settlements, placed in remote areas). The idea is to couple the energy consumption with the control of the energy production, and manipulate the desalination plant as an active charge, to make easier

the control of the plant, and maximize the consumption of renewable energy. Taking into account the prediction of renewable energy and water demand, it may be possible to adapt the plant to the current state of the system and minimize the operation expenses, while the water demand is fulfilled.

1.4 Framework of the Thesis

The OPEN-GAIN project[7] was part of the Six Framework program of the European Union. It was developed during the period 2007-2011, and its main issue was the development of advanced techniques for the automatic control of small-scale desalination plants, based on RO technology and powered by renewable energies, such as solar panels and wind turbines. The name of this project is an acronym from "**OP**timal **EN**gineering design for dependable water and power **G**eneration in remote **A**reas using renewable energies and **IN**telligent automation". An in-depth description of the project, partners, objectives, publications and milestones, can be consulted in the OPEN-GAIN website[8].

During the execution of this project, the following milestones were achieved: 1) building an RO desalination pilot plant; 2) building an autonomous electricity network, powered by renewable energies; 3) development of a software tool for decision support for the design of desalination plants powered by renewable energies; 4) development of a software tool for the energy management, which deals with different energies sources; 5) development of fault detection software for RO desalination plants; 6) study of field control, supervision, remote monitoring and diagnosis of components; 7) development of a dynamic library for the simulation of RO desalination plants; and 8) study of the advanced control of RO desalination plants. Figure 1.26 shows a picture of the research laboratory of the OPEN-GAIN project, which is placed in the Research and Technology Center of Energy (CRTEn), in Borj Cedria (Tunisia).

Several universities and research centres of the European Union and Mediterranean countries took part in this project. The Process Control and Supervision research group (CSP) of the University of

[7] FP6-2004-INCO-MPC-3, contract number 032535.

[8] `http://www.open-gain.org/`

Figure 1.26: Research laboratory of the OPEN-GAIN project, Borj Cedria, (Tunisia).

Valladolid (UVa) was the leader of the modelling and simulation of the RO system. This thesis summarizes part of this work.

1.5 Contribution of the Thesis

To the best of the author's knowledge, this thesis presents several contributions on the modelling, simulation and optimal operation of RO desalination plants, as follows:

1. The development of a dynamic simulation library for RO desalination plants. This library is called ROSIM (**R**everse **O**smosis **Sim**ulation Library) and covers several aspects not taken into account by the commercial libraries for RO desalination plants.

   The ROSIM library is focused on the dynamic development of the system. In particular, the ROSIM library deals with the following issues: testing the field control (pressure, flow, level and concentration controllers), validating a control strategy (emptiness of tanks, fulfilling of the water demand, etc.), operation

during the cleanings, breakage of the membranes, fouling and scaling of the RO membranes, biofouling, ageing of the RO membranes, etc.

The ROSIM library does not deal with the issues of the commercial libraries. ROSIM and the commercial libraries do not compete with each other, they are complementary.

2. The optimal operation of an RO desalination plant, powered by renewable energy, on a short and long-term scale, coupling the energy consumption with the control of the energy production. The key idea is to manipulate the desalination plant as an active charge, taking into account the prediction of renewable energy and water demand, as well as integrating in the problem the scheduling of the cleaning of the RO plant and the economy of the operation.

3. The integrated process and control design of an RO desalination plant, powered by renewable energy.

4. A new multi-scale modelling of the salt gradient that takes places on the boundary layer of RO membranes, which presents several advantages versus other modelling approaches.

1.6 Organization of the Thesis

This thesis is organized as follows:

Chapter 1: First section of this chapter describes the desalination process: the world situation, the evolution of desalination in the last few decades, the different desalination techniques, the main sections of a desalination plant, the environmental impact, etc. Next, section 1.2 summarizes the state of the art of the modelling and control of desalination plants. Finally, sections 1.3 - 1.6 show the objectives of the thesis and its main contributions and organization.

Chapter 2: This chapter deals with the modelling of desalination plants. First, section 2.1 summarizes the mathematical equations which model the most important components of a desalination plant, such as filters, membranes, pumps, energy recovery

system, etc. The modelling is based on first principles, physical and chemical equations and correlations from the literature. Next, section 2.2 describes the simulation library for RO desalination plants (called ROSIM), arising with this thesis. Finally, section 2.3 shows several experiments using the ROSIM library, such as the development of the operation in a desalination plant, when biofouling takes place, or the development of the operation depending on the ageing of the components.

Chapter 3: This chapter is focused on the validation of the ROSIM library. First, section 3.1 describes an RO pilot plant, which is used for testing and validation. Then, section 3.3 shows the validation of the ROSIM library, using experimental data from the pilot plant.

Chapter 4: This chapter is dedicated to the application of advanced control and economic optimization to RO plants. In particular, section 4.1 shows the predictive control of a desalination plant, which deals with the economic optimization of the plant; section 4.2 shows the integrated process and control design of a desalination plant; while section 4.3 shows the optimization of the scheduling operation.

Chapter 5: This chapter deals with a new multi-scale modelling of the salty gradient that takes place on the boundary layer of the RO membranes.

Chapter 6: This chapter summarizes the conclusion, future work and the publications arising from the thesis.

Appendix A: This appendix is an extended abstract in Spanish of the thesis. It summarizes the objectives, contribution and organization of the thesis.

Appendix B: This appendix gives a summary of the ROSIM library, developed in EcosimPro.

The thesis finishes with the list of symbols, acronyms, webpages, figures, tables and bibliography.

Chapter 2

Modelling and Simulation

This chapter deals with the simulation library arising from the thesis. This library is focused on the dynamic simulation of RO desalination plants and includes the typical components presented in these plants. It is called ROSIM, which is the acronym of **R**everse **O**smosis **SIM**ulation library. Section 2.1 describes the mathematical modelling of the main components of an RO desalination plant (such as RO membranes, filters and energy recovery system), which is in the core of the components of the ROSIM library. This modelling is based on first principles and physical and chemical equations.

The ROSIM library was developed in the simulation environment EcosimPro. EcosimPro provides an object-oriented and non-causal approach and is capable of processing complex systems, represented by differential algebraic equations (DAE) and discrete events. Section 2.2 gives general ideas about EcosimPro, summarizes the purpose and methodology of the ROSIM library and described briefly the components included in the library. Finally, section 2.3 shows several simulations using this library and the main effects that take place in an RO desalination plant.

2.1 Mathematical Modelling

The mathematical modelling shown in this section is based on first principles (mass, momentum and energy balances), physical and chemical equations and correlations from the literature, and it is represented by differential algebraic equations (DEA). In the case of the RO mod-

ules, it follows the Kedem-Katchalsky (KK) and the Spiegler-Kedem (SK) models. It was presented in Syafiie et al. (2008a,b, 2009, 2010) and Palacín et al. (2012a,b).

2.1.1 RO Modules

Figure 2.1 shows two RO spiral-wound modules from the company CSM. A spiral-wound module consists of a square-shaped spacer and membrane, which is rolled up with a high packing capacity. The feed flow is pumped in the axial direction of the RO module. White the permeate flow crosses the membrane perpendicular to the feed flow, goes from the membrane to the inner tube with a spiral trajectory, and goes out of the RO module in the axial direction, as is represented in figure 2.2.

Figure 2.1: RO modules from the company CSM. IDA 2011 World Congress, Australia.

The characteristics of the feed water (such as pressure and salt concentration) depend on the position on the RO module. With the goal of modelling the system, the RO module is discretized in the axial

(x) and the radial (y) directions. Figure 2.3 shows the two-dimension discretization of the RO module.

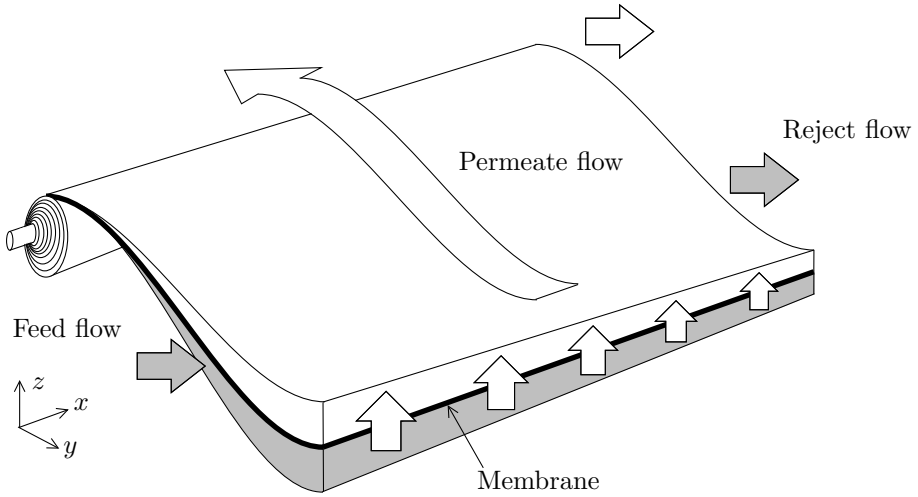

Figure 2.2: Diagram of a spiral-wound RO module.

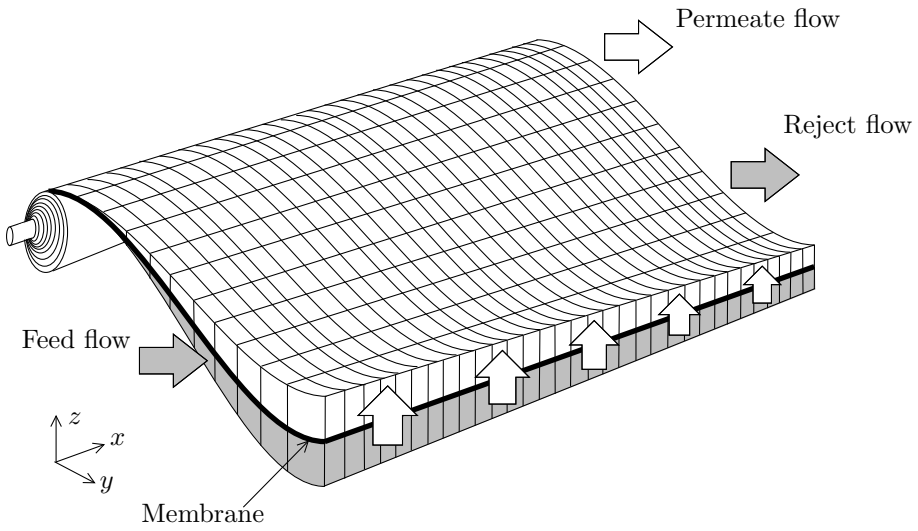

Figure 2.3: Two-dimension discretization of the RO module.

Figure 2.4 shows one element of the previous discretization. The element has been turned 90 degrees with respect to the diagram of

figure 2.3. The feed flow goes from the bottom to the top of the diagram, and the permeate flow crosses the membrane from the left to the right of the diagram. J_w is the water flux that crosses the membrane and Q_f is the flow of the feed stream.

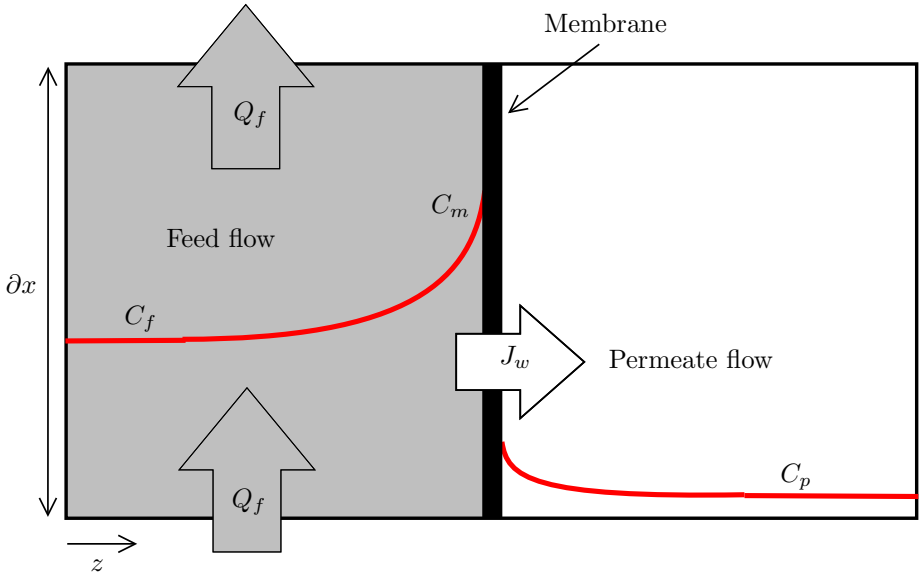

Figure 2.4: Element of the two-dimension discretization. The red line is the profile of the salt concentration.

The red line represents the profile of the salt concentration. C_f is the salt concentration of the bulk of the feed stream, C_m is the salt concentration on the membrane surface, and C_p is the salt concentration of the bulk of the permeate stream. Salt molecules are transported by the permeate flow until the membrane. The majority are rejected by the membrane itself and the accumulation of salt occurs. The increase of the salt concentration close to the membrane surface is called "concentration polarization" and it is measured by the polarization module (ϕ), which depends on C_f, C_m and C_p, as seen in following equation:

$$\phi = \frac{C_m - C_p}{C_f - C_p} \tag{2.1}$$

The KK model calculates the permeate flux as follows:

$$J_w = A_w \cdot (\Delta P - \sigma \cdot \Delta\pi) \tag{2.2}$$

where A_w is the water permeability of the membrane, σ is the reflection coefficient and measures the rejection of the salt molecules by the membrane (close to 1), ΔP is the pressure difference between the feed side and the permeate side, and $\Delta\pi$ is the osmotic pressure difference across the membrane.

The osmotic pressure can be calculated using the Morse equation:

$$\pi = i \cdot R \cdot T \cdot \frac{C}{PM} \tag{2.3}$$

where i is the van't Hoff coefficient, which depends on the increase of molecules when the salt is dissolved in water (2 for sodium chloride), R is the gas constant, T is the temperature, PM is the molar weight and C is the salt concentration.

Typically, these variables are embraced in one single factor (a_1), as follows:

$$\pi = a_1 \cdot C \tag{2.4}$$

Replacing the osmotic pressure in the equation (2.2) gives:

$$J_w = A_w \cdot (\Delta P - \sigma \cdot a_1 \cdot (C_m - C_p)) \tag{2.5}$$

Since C_m cannot be measured and C_f is easily measured, it is more convenient to calculate the permeate flux as a function of this second variable, as follows:

$$J_w = A_w \cdot (\Delta P - \sigma \cdot a_1 \cdot \phi \cdot (C_f - C_p)) \tag{2.6}$$

Two parameters of the equation (2.6) are unknown: σ and ϕ. The SK model calculates σ as follows:

$$\sigma = \frac{R_m}{1 - F + F \cdot R_m} \tag{2.7}$$

where R_m is the salt rejection on the membrane surface and F is a dimensionless factor depending on the water and salt permeability.

R_m can be calculated as follows:

$$R_m = \frac{C_m - C_p}{C_m} \tag{2.8}$$

While F can be calculated as follows:

$$F = \exp\left(\frac{J_w \cdot (1-\sigma)}{B_s}\right) \tag{2.9}$$

where B_s is the salt permeability of the membrane.

Finally, the SK model calculates the polarization module as follows:

$$\phi = \exp\left(\frac{J_w}{k_m}\right) \tag{2.10}$$

where k_m is the mass transfer coefficient.

The different authors propose empirical expressions for the calculation of k_m (for instance, see Evangelista (1986), Song and Ma (2005), Kargol and Kargol (2003), and Koter (2005)). Most of the equations follow the form:

$$k_m = a_2 \cdot Q_f^{a_3} \tag{2.11}$$

where a_2 and a_3 are proportional factors that depend on each system.

Since the mathematical system formed by equations (2.7-2.10) has several algebraic loops, the integration of the equations is difficult to solve and should be done numerically.

The pressure drop of the feed side is neglected in the radial direction (y), while a dependence with the velocity in the axial direction (x) is assumed, as seen below:

$$\frac{\partial P_f}{\partial y} = 0 \tag{2.12}$$

$$\frac{\partial P_f}{\partial x} = a_f \cdot \mu \cdot u_f^{b_f} \tag{2.13}$$

where P_f is the pressure of the feed side, u_f is the water velocity of the feed stream, and a_f and b_f are proportional factors that depend on each system.

On the contrary, the pressure drop on the permeate side is neglected in the axial direction (x), while a dependence with the velocity in the radial direction (y) is assumed, as seen below:

$$\frac{\partial P_p}{\partial x} = 0 \tag{2.14}$$

$$\frac{\partial P_p}{\partial y} = a_p \cdot \mu \cdot u_p^{b_p} \tag{2.15}$$

where P_p is the pressure of the permeate side, u_p is the water velocity of the permeate stream, and a_p and b_p are proportional factors that depend on each system.

The values of a_f, a_p, b_f and b_p depend on each system. For instance, see the works developed by Schock and Miquel (1987), Boudinar et al. (1992), Schwinge et al. (2004) and Senthilmurugan et al. (2005), which propose several values for these parameters, depending on the characteristics of the RO modules.

The profile of the u_f and u_p may be easily calculated thanks to a mass balance of the water, as represented in figure 2.5. Equation (2.16) shows the mass balance at the feed side, and equation (2.17) shows the mass balance at the permeate side.

$$h_f \cdot \frac{\partial u_f}{\partial x} = -J_w \tag{2.16}$$

$$h_p \cdot \frac{\partial u_p}{\partial y} = +J_w \tag{2.17}$$

where h_f and h_p are, respectively, the size of the feed spacer and the permeate spacer, as seen in figure 2.5.

Finally, the profile of the salt concentration may be calculated by the mass balance of the salt. Equation (2.18) shows the mass balance at the feed side, and equation (2.19) shows the mass balance at the permeate side.

$$\frac{\partial C_f}{\partial t} = \frac{\partial (u_f \cdot C_f)}{\partial x} - \frac{J_s}{h_f} \tag{2.18}$$

$$\frac{\partial C_p}{\partial t} = \frac{\partial (u_p \cdot C_p)}{\partial y} + \frac{J_s}{h_p} \tag{2.19}$$

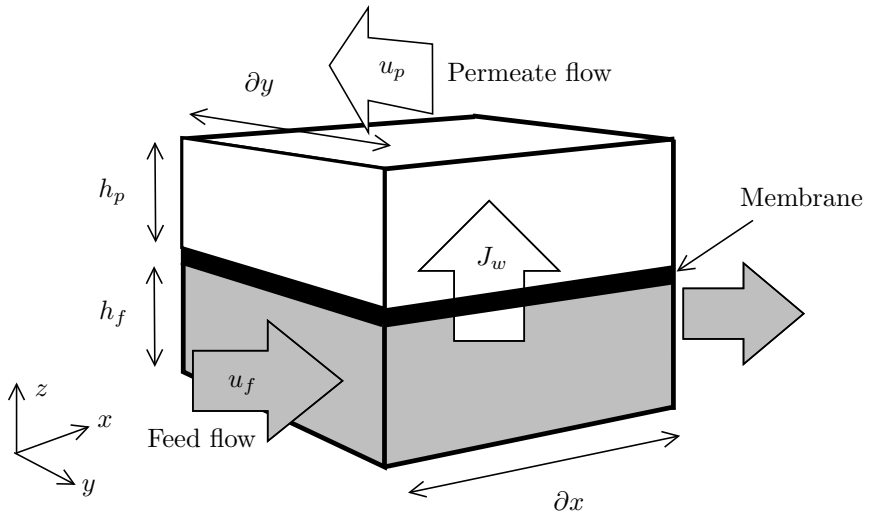

Figure 2.5: Mass balance in one element of the discretization.

where J_s is the salt flux that crosses the membrane.

The KK model proposes the following expression for the calculation of J_s:

$$J_s = B_s \cdot (C_f - C_p) \tag{2.20}$$

The mathematical system formed by equations (2.6-2.20) has as many variables as equations and, a priori, it may be solved. However, the relation between ϕ, C_m, J_w and J_s is not explicit, and will cause several algebraic loops. The mathematical integration of the system is not easy, and may cause problems for the convergence of the numerical integration. These algebraic loops may be broken adding the discretization in the direction perpendicular to the feed flow (z). Figure 2.6 shows the elements of the three-dimension discretization of the RO module: axial (x), radial (y) and perpendicular to the feed flow (z).

In the feed side, no flow in the radial direction is assumed, while the variance of mass flow in the axial direction corresponds to the increase of mass flow in the z direction. So, the mass balance for the feed side is:

$$\frac{\partial u_f(x,y,z)}{\partial x} = -\frac{\partial u_f(x,y,z)}{\partial z} \tag{2.21}$$

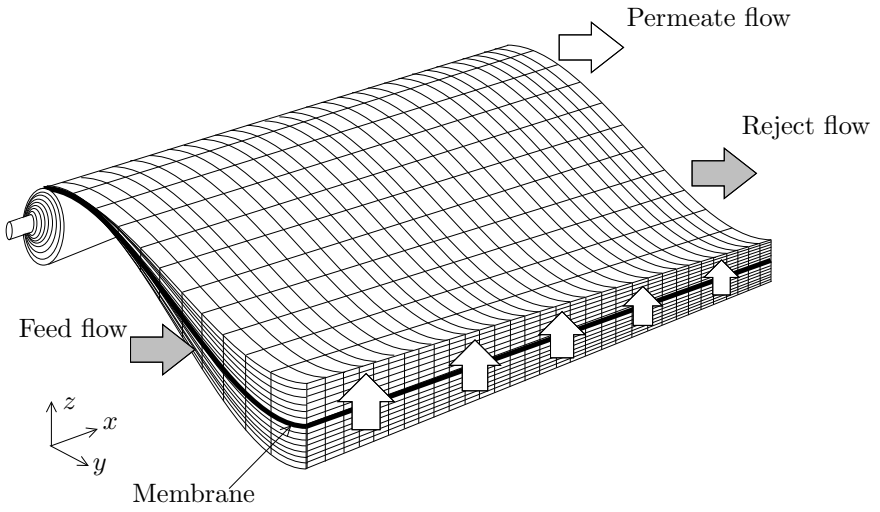

Figure 2.6: Three-dimension discretization of the RO module.

$$\text{with } u_f(z = h_f) = J_w(x, y) \tag{2.22}$$

On the contrary, in the permeate side, no flow in the axial direction is assumed, and the increase of mass flow in the radial direction corresponds to the permeate flow that crosses the membrane, in each element of the discretization. The mass balance for the permeate side is:

$$\frac{\partial u_p(x, y, z)}{\partial y} = +\frac{\partial u_p(x, y, z)}{\partial z} \tag{2.23}$$

The salt mass balance for the feed side is shown in equation (2.24). Term [1] is the dynamic variation of salt in each element of the discretization. Term [2] corresponds to the input/output flow of salt, due to the feed water flow, while term [3] corresponds to the input/output mass flow of salt, due to the permeate flow.

$$\underbrace{\frac{\partial C_f(x, y, z)}{\partial t}}_{[1]} = \underbrace{\frac{\partial (u_f(x, y, z) \cdot C_f(x, y, z))}{\partial x}}_{[2]} - \underbrace{\frac{\partial (u_f(x, y, z) \cdot C_f(x, y, z))}{\partial z}}_{[3]} \tag{2.24}$$

$$\text{with } C_f(z = h_f) = C_m(x, y) \tag{2.25}$$

Finally, the salt mass balance for the permeate side is shown in equation (2.26). Term [1] is the dynamic variation of salt in each element of the discretization. Term [2] corresponds to the input/output mass flow of salt, due to the permeate flow that crosses the membrane, while term [3] corresponds to the input/output mass flow of salt, due to the permeate flow that goes to the inner tube of the RO module.

$$\underbrace{\frac{\partial C_p(x,y,z)}{\partial t}}_{[1]} = \underbrace{\frac{\partial (u_p(x,y,z) \cdot C_p(x,y,z))}{\partial y}}_{[2]} - \underbrace{\frac{\partial (u_f(x,y,z) \cdot C_p(x,y,z))}{\partial z}}_{[3]} \tag{2.26}$$

$$\text{with} = \begin{cases} u_p(z = h_f) = J_w(x, y) \\ C_p(z = h_f) \cdot u_p(z = h_f) = J_s(x, y) \end{cases} \tag{2.27}$$

2.1.2 Ageing of the RO Membranes

The life time of an RO module is about 3-5 years. On the one hand, the water permeability (A_w) decreases over time, and a higher operating pressure is needed to keep the initial permeate flow. For instance, figure 2.7 shows a typical behaviour of the operating pressure over 5 years. Notice that after 1550 days, the required operating pressure has exceeded the maximum allowable pressure for the plant, which in the example case is 55 bar.

On the other hand, the salt permeability (B_s) increases over time, and more salt particles are able to cross the membrane. Figure 2.8 shows a typical evolution of the salt concentration in the permeate flow. Notice that after 1350 days, the salt concentration has exceeded the maximum allowable salt concentration, which in the example case is 300 ppm.

Hu and Lu (2005) propose the following modelling for the ageing of the RO modules. The water permeability (A_w) is divided into three factors, as can be seen below:

$$A_w = A_{w0} \cdot A_{wi} \cdot A_{wr} \tag{2.28}$$

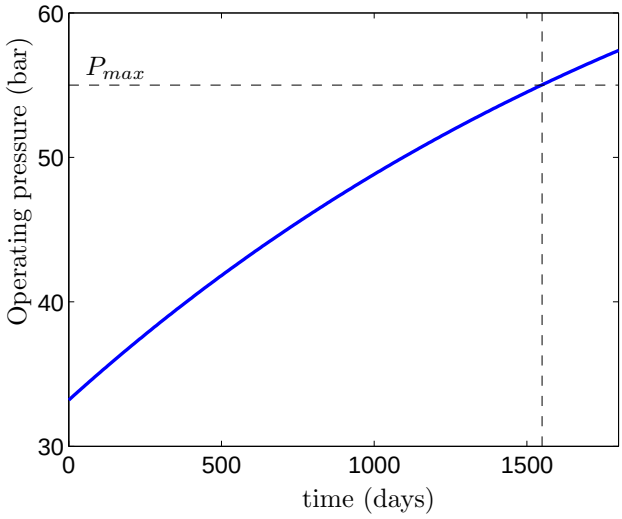

Figure 2.7: Typical behaviour of the operating pressure supplied by the high pressure pump. The maximum allowable operating pressure (P_{max}) is exceeded after 1550 days.

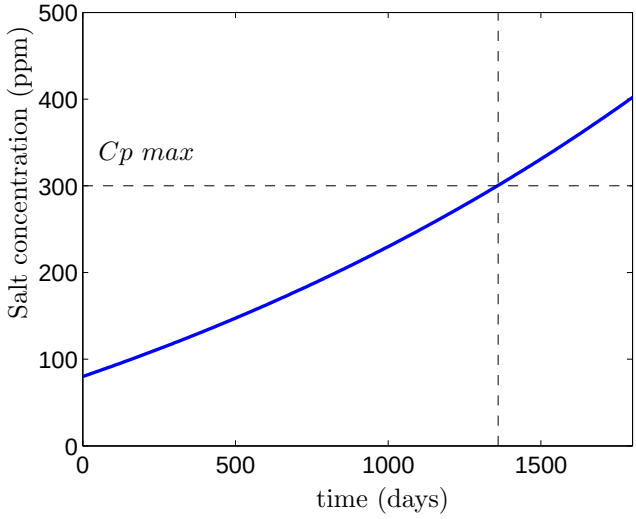

Figure 2.8: Typical behaviour of the salt concentration of the permeate flow (C_p). The maximum salt concentration for drinkable water ($C_{p\ max}$) is exceeded after 1350 days.

where A_{w0} is the initial water permeability at the beginning of the operation, A_{wi} embraces the irreversible ageing of the membrane, which can be reset only by the replacement of the RO module, and A_{wr} embraces the reversible fouling, which can be eliminated by chemical cleanings. Both factors can be calculated as follows:

$$A_{wi} = 1 - \Psi_A \cdot (t - t_{RP}) \tag{2.29}$$

$$A_{wr} = \exp\left(-\frac{t - t_{CL}}{\Gamma_A}\right) \tag{2.30}$$

where Ψ_A and Γ_A are empirical factors that depend on the characteristics of each desalination plant (see Lu et al. (2006) to obtain some typical values), $t - t_{RP}$ is the time delay from the last replacement, and $t - t_{CL}$ is the time delay from the last chemical cleaning. A_{w0} has the units of A_w, while A_{wi} and A_{wr} are dimensionless. Initially, the value of A_{wi} and A_{wr} is 1, and decreases with time. A_{wi} is reset after one replacement, and A_{wr} is reset after one replacement or one chemical cleaning.

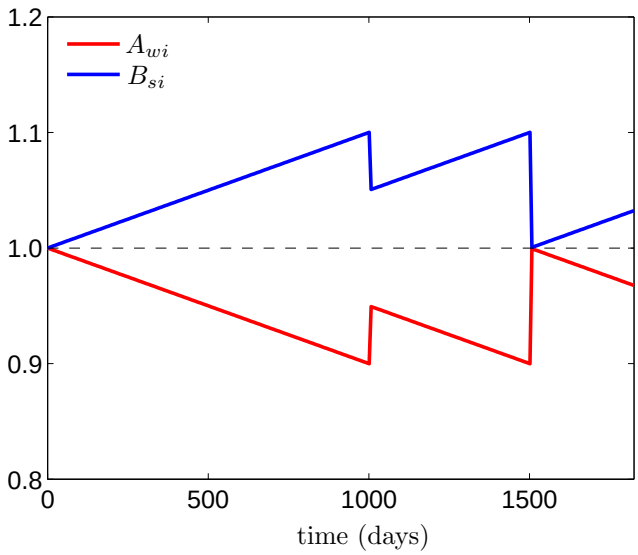

Figure 2.9: Behaviour of the irreversible factor for the water and salt permeability, with partial replacement at 1 000 days, and full replacement of the modules at 1 500 days.

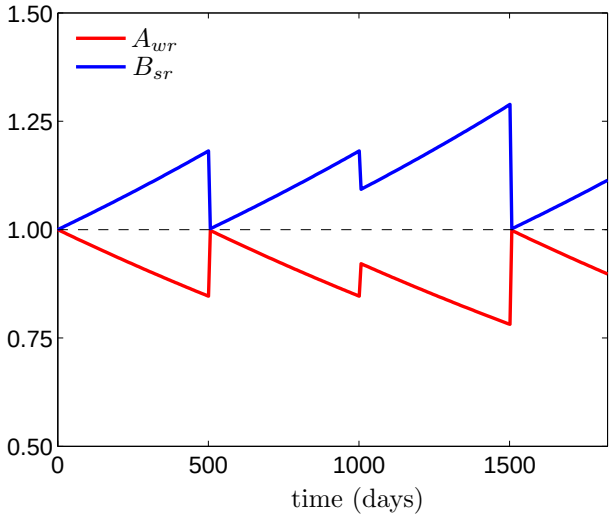

Figure 2.10: Reversible factor for the water and salt permeability, with chemical cleaning at 500 days, partial replacement at 1 000 days, and full replacement of the modules at 1 500 days.

Similar equations can be formulated for the salt permeability:

$$B_s = B_{s0} \cdot B_{si} \cdot B_{sr} \tag{2.31}$$

$$B_{si} = 1 + \Psi_B \cdot (t - t_{RP}) \tag{2.32}$$

$$B_{sr} = \exp\left(+\frac{t - t_{CL}}{\Gamma_B}\right) \tag{2.33}$$

where B_{s0} has the units of B_s and is the initial salt permeability at the beginning of the operation. B_{si} is the irreversible ageing of the salt permeability and is dimensionless. B_{sr} embraces the reversible fouling of the salt permeability and is dimensionless. Initially, the value of B_{si} and B_{sr} is 1, and increases with time. B_{si} is reset after one replacement, and B_r is reset after one replacement or one chemical cleaning.

Figures 2.9 and 2.10 show the evolution of A_i, B_i (figure 2.9), A_r and B_r (figure 2.10), during an operation time of 5 years. A chemical cleaning is done at 500 days, a replacement of 50% of the membrane

modules is done at 1 000 days, and a replacement of 100% of the membrane modules is done at 1 500 days. The cleaning and the two replacements correspond to the steps on the different curves.

Finally, the total water and salt permeabilities are plotted, respectively, in figures 2.11 and 2.12.

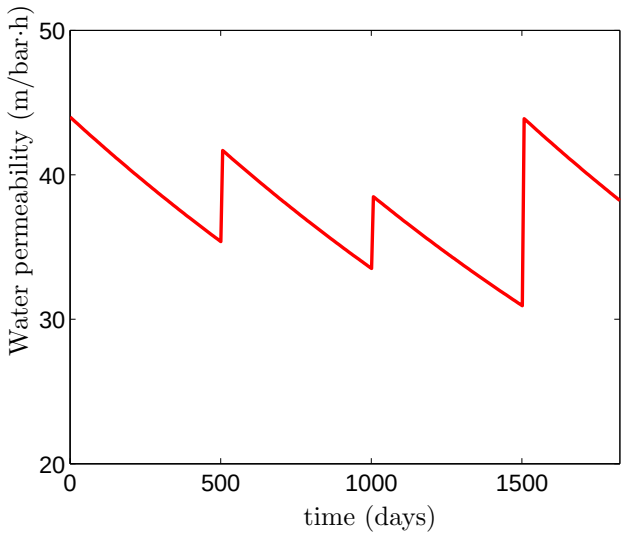

Figure 2.11: Behaviour of the water permeability (A_w) over 5 years, with a chemical cleaning at 500 days, partial replacement at 1 000 days, and full replacement of the modules at 1 500 days.

On the first approximation, we can work with an average value of the fouling parameters ($\Psi_A, \Gamma_A, \Psi_B, \Gamma_B$) for each pressure vessel. In this case, in order to model the partial replacement of the RO modules of each pressure vessel, equations (2.29-2.33) can be written as follows:

$$A_{wi} = 1 - \Psi_A \cdot t + x_A \tag{2.34}$$

$$B_{si} = 1 + \Psi_B \cdot t - x_B \tag{2.35}$$

$$A_{wr} = y_A \cdot \exp\left(-\frac{t - t_{CL}}{\Gamma_A}\right) \tag{2.36}$$

$$B_{sr} = y_B \cdot \exp\left(+\frac{t - t_{CL}}{\Gamma_B}\right) \tag{2.37}$$

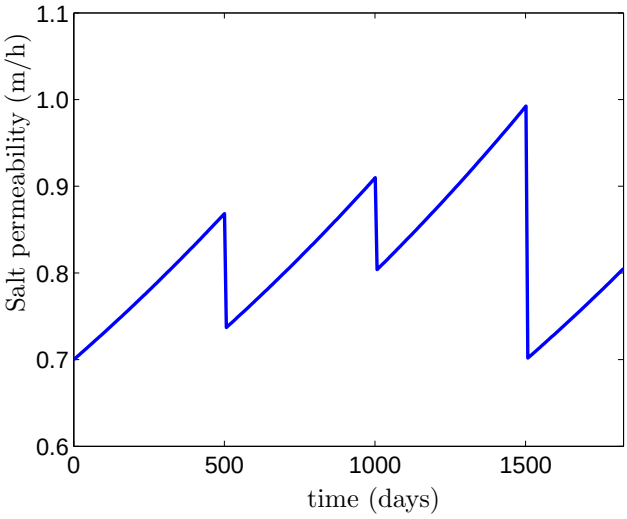

Figure 2.12: Behaviour of the salt permeability (B_s) over 5 years, with a chemical cleaning at 500 days, partial replacement at 1 000 days, and full replacement of the modules at 1 500 days.

where x_A, x_B, y_A and y_B are internal parameters of the modelling, which are calculated as follows:

$$x_A = \begin{cases} t = 0 & \to 0 \\ t = t_{RP} & \to x_A + r \cdot (1 - A_i) \end{cases} \tag{2.38}$$

$$x_B = \begin{cases} t = 0 & \to 0 \\ t = t_{RP} & \to x_B + r \cdot (B_i - 1) \end{cases} \tag{2.39}$$

$$y_A = \begin{cases} t = 0 & \to 1 \\ t = t_{RP} & \to (1 - r) \cdot y_A + r \cdot \exp\left(\dfrac{t - t_{CL}}{\Gamma_A}\right) \\ t = t_{CL} & \to 1 \end{cases} \tag{2.40}$$

$$y_B = \begin{cases} t = 0 & \to 1 \\ t = t_{RP} & \to (1 - r) \cdot y_B + r \cdot \exp\left(-\dfrac{t - t_{CL}}{\Gamma_B}\right) \\ t = t_{CL} & \to 1 \end{cases} \tag{2.41}$$

where r is the percentage of RO modules replaced.

Since the ageing parameters depend on several factors, such as the salt concentration, operating pressure, flux, etc., and these variables vary along the length of the RO module, a better approximation requires working with different parameters for each RO module. Initially, we can assume a linear dependence in the axial direction (x), as follows:

$$\begin{aligned} \Psi_A(x) &= a_{\Psi_A} + b_{\Psi_A} \cdot x \\ \Psi_B(x) &= a_{\Psi_B} + b_{\Psi_B} \cdot x \\ \Gamma_A(x) &= a_{\Gamma_A} + b_{\Gamma_A} \cdot x \\ \Gamma_B(x) &= a_{\Gamma_B} + b_{\Gamma_B} \cdot x \end{aligned} \tag{2.42}$$

where the parameters $a_{\Psi_A}, b_{\Psi_A}, a_{\Psi_B}...$ should be calculated for each desalination plant.

2.1.3 Pressure Exchanger Devices

Figure 2.13 shows a diagram of a pressure exchanger device. The brine stream means the reject flow from the RO pressure vessels, and the feed stream means feed water pumped from the pretreatment system.

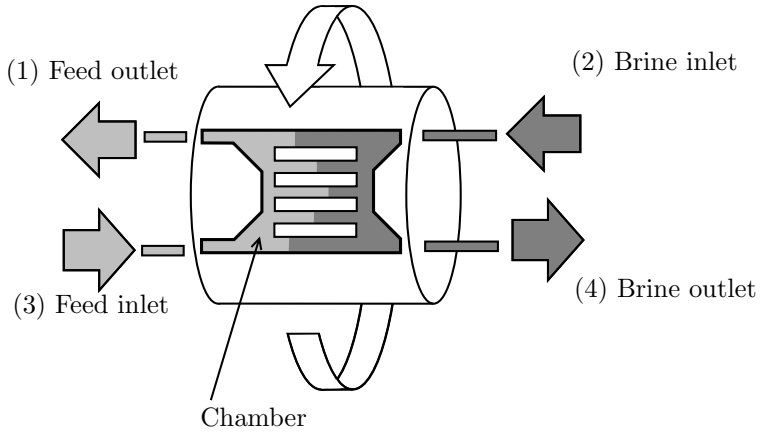

Figure 2.13: Diagram of a pressure exchanger.

– The point 1 is the output of the feed flow. At this point, this stream has a high pressure and a low concentration of salt.

- The point 2 is the input of the reject flow. At this point, this stream has a high pressure and a high concentration of salt.
- The point 3 is the input of the feed flow. At this point, this stream has a low pressure and a low concentration of salt.
- The point 4 is the output of the reject flow. At this point, this stream has a low pressure and a high concentration of salt.

At point 2, the brine flow pushes the water inside the chamber space and transfers part of its pressure energy. The water inside the chamber space goes out of the exchanger at point 1. Before the brine flow arrives at point 1, the chamber has rotated 180 degrees. At point 3, it is the feed flow that pushes the water inside the chamber. The brine flow goes out of the chamber at point 4. The rotation of the chamber is caused automatically by the pressure difference between points 2 - 3.

Figure 2.14 shows a cutaway of a pressure exchanger. This pressure exchanger is of PX type, from the company ERI.

Figure 2.14: Pressure exchanger cutaway from the company ERI. IDA 2011 World Congress, Australia.

The total flow that enters the chamber is equal to the total flow that goes out of the chamber.

$$Q_3 + Q_2 = Q_1 + Q_4 \tag{2.43}$$

However, the feed flow that enters the chamber (point 3) is different from the feed flow that goes out of the chamber (point 1); and the brine flow that enters (point 2) is different from the brine flow that goes out (point 4). This difference is called "lubrication flow" (q_{lub}). The following equations show the relationships between these streams:

$$Q_1 = Q_3 - q_{lub} \tag{2.44}$$

$$Q_4 = Q_2 + q_{lub} \tag{2.45}$$

where Q_1, Q_2, Q_3 and Q_4 are, respectively, the volumetric flow at the points 1, 2, 3 and 4.

The input flows can be calculated as a function of the pressure difference at each side of the pressure exchangers, as shown in equations (2.46-2.47).

$$Q_2 = k_2 \cdot (P_2 - P_1)^{n_2} \tag{2.46}$$

$$Q_3 = k_3 \cdot (P_3 - P_4)^{n_3} \tag{2.47}$$

where P_1, P_2, P_3 and P_4 are, respectively, the pressure at the points 1, 2, 3 and 4.

Finally, assuming that the lubrication flow depends on the input flow and pressure, it can be calculated by an empirical equation, as follows:

$$\begin{aligned} q_{lub} = \quad & a_0 + a_{21} \cdot P_2 + a_{22} \cdot P_2^2 + ... + a_{31} \cdot P_3 + a_{32} \cdot P_3^2 + ... \\ & + b_{21} \cdot Q_2 + b_{22} \cdot Q_2^2 + ... + b_{31} \cdot Q_3 + b_{32} \cdot Q_3^2 + ... \end{aligned} \tag{2.48}$$

where a_i and b_i are proportional parameters.

Since there is no physical separation between the currents, a partial blend of the currents occurs. This means that the salt concentration of the feed is higher at point 1 than at point 3. The mixture of the currents may be measured with the mixture module (mix), as follows:

$$mix = \frac{C_1 - C_3}{C_2 - C_3} \tag{2.49}$$

where C_1, C_2 and C_3 are, respectively, the salt concentration at points 1, 2 and 3.

From equation (2.49), the salt concentration of the feed outlet (C_1) may be calculated as:

$$C_1 = mix \cdot (C_2 - C_3) + C_3 \tag{2.50}$$

Assuming a dependence of the mixture module with the lubrication flow, the mixture module may be calculated using an empirical equation as follows:

$$mix = a_{q0} + a_{q1} \cdot q_{lub} + a_{q2} \cdot q_{lub}^2 + ... \tag{2.51}$$

where a_{qi} are proportional parameters.

Finally, the salt concentration of the brine outlet (C_4) may be calculated from a mass balance of the salt:

$$C_4 = \frac{C_2 \cdot Q_2 + C_3 \cdot Q_3 - C_1 \cdot Q_1}{Q_4} \tag{2.52}$$

2.1.4 Sand Filters

A sand filter consists of a tank (open or pressurized) with a sand bed. Feed water flows through the sand, which captures the larger suspended solids (larger than 10 μm). Figure 2.15 symbolizes a sand filter with square-shaped base and vertical flow. The feed water is carried to the sand filter at the top, and clean water is carried out of the sand filter at the bottom. Q is the feed flow and X_1 and X_2 are, respectively, the concentration of suspended solids of the inlet and outlet feed.

Assuming a constant distribution of suspended solids in the radial direction (axis x and y), equation (2.53) shows the mass balance for the suspended solids.

$$\underbrace{A \cdot \varepsilon \cdot \frac{\partial X}{\partial t}}_{[1]} = \underbrace{Q \frac{\partial X}{\partial z}}_{[2]} - \underbrace{A \cdot \varepsilon \cdot J_X}_{[3]} \tag{2.53}$$

where A is the cross section area of the tank, ε is the porosity of the sand bed, and J_X is the mass flow of solids that are captured by the sand per water volume (kg/(m^3·s)).

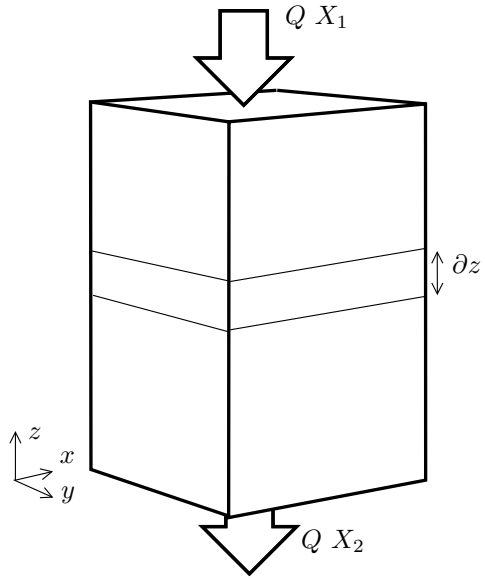

Figure 2.15: Diagram of a sand filter.

Therm [1] of the equation (2.53) corresponds to the dynamical variation on the solids concentration, in each element of the discretization. Term [2] means the input/output mass flow of solids, of each element, due to the feed water flow. And term [3] corresponds to the solids that are captured by the sand in each element.

J_X varies with the height of the sand, and may be calculated as follows:

$$J_X(z) = k_1 \cdot (X_{bed\ maximum} - X_{bed}) \cdot X^{n_1} \tag{2.54}$$

where k_1 and n_1 are coefficients that depend on each system, $X_{bed\ maximum}$ is the maximum quantity of solids that can be adsorbed by the sand, and X_{bed} is the current quantity of solids captured by the sand.

X_{bed} varies along the z direction, and it can be calculated by a mass balance:

$$\frac{\partial X_{bed}}{\partial t} = \frac{\varepsilon}{1-\varepsilon} \cdot J_X \tag{2.55}$$

During the cleaning of the sand filter, the captured solids are removed from the sand. During the cleaning, the removing of the solids

may be calculated by an empirical equation, as follows:

$$J_X(z) = -k_2 \cdot X_{bed}^{n_2} \tag{2.56}$$

where k_2 and n_2 are empirical parameters, and depend on the cleaning efficiency.

The pressure drop of the stream is neglected in the perpendicular direction (x, y), while a dependence with the velocity in the axial direction (z) is assumed, as seen below:

$$\frac{\partial P}{\partial x} = \frac{\partial P}{\partial y} = 0 \tag{2.57}$$

$$\frac{\partial P}{\partial z} = a \cdot \mu \cdot u^b \tag{2.58}$$

where u is the velocity of the feed water flow, a is the flow resistance, and b is a proportional factor that depends on each system.

The velocity depends on the cross section, as follows:

$$u = \frac{Q}{A \cdot \varepsilon} \tag{2.59}$$

And the flow resistance depends on the quantity of captured solids by the sand, and may be calculated by an empirical equation as follows:

$$a = \frac{a_1}{a_2 - X_{bed}} \tag{2.60}$$

where a_1 and a_2 are proportional factors that depend on each system.

2.1.5 Filters

Figure 2.16 shows a cartridge filter. The particular filter in the picture removes suspended solids larger than 5 μm from the feed water. The left hand picture shows the filter connected to the desalination system, and the right hand picture shows the internal module. When the filtration module is saturated (as the one in the picture), it should be changed for a new one. The saturation of the cartridge filter may be detected by a high pressure drop (more than 0.5-1.0 bar) on both sides of the filter.

(a) Cartridge filter connected to the desalination system.

(b) Internal filtration module.

Figure 2.16: Cartridge filter.

The pressure drop along the inlet and outlet of the filter may be calculated as a function of the solids captured by the filter itself, as follows:

$$\Delta P = k_1 \cdot Q^{n_1} \cdot (1 + k_2 \cdot m_X^{n_2}) \tag{2.61}$$

where ΔP is the pressure drop, Q is the feed flow through the filter, m_X is the mass of solids captured by the filter, and k_1, k_2, n_1 and n_2 are constants that depend on the system.

The increase of solids captured by the filter can be calculated as follows:

$$m'_X = -k_3 \cdot Q \cdot X_{inlet} \cdot \sigma \tag{2.62}$$

where X_{inlet} is the concentration of suspended solids at the inlet of the filter, σ is the reflection coefficient and measures the efficiency of the filter, and k_3 is a proportional factor.

Moreover, some authors have proposed different theoretical equations for the modelling of the filtration (see, for instance, Sondhi and Bhave (2001) and Li (2007)), as follows:

$$J = \frac{\varepsilon^3}{(1-\varepsilon)^2} \cdot \frac{\Delta P \cdot h_1^n}{h_2 \cdot \mu \cdot k} \tag{2.63}$$

where J is the water flow, ε is the porosity, h_1 is the pore size, h_2 is the membrane thickness, μ is the viscosity, and n and k are empirical constants that represent the effects that shape and aggregate style of particles have on the resistance of the filter.

2.2 The ROSIM Library

The ROSIM library was developed in the simulation environment EcosimPro. EcosimPro is a powerful modelling and dynamic simulation software, which provides an object-oriented and non-causal approach[1]. The mathematical modelling is represented by DAE (implicit or explicit) and discrete events, and then encapsulated in reusable components. The user builds his/her own model by connecting to each other these components. The global mathematical system, which is formed by the interconnection of the individual models, should be solved as a whole. EcosimPro has symbolic methods, which manipulates the mathematical system and looks for the optimal path and steps, which should be followed to solve the system. Depending on the system, it may be necessary to break algebraic loops or solve high index problems. Finally, the integration of the mathematical system is solved using advanced numerical solvers, such as the Fortran methods DASSL, DASSLX, DASPG and DASPK. See Urquía and Dormido (2003) and Martín-Villalba et al. (2008) for an in-depth description of the methodology of object-oriented environments. For very complex systems, the simulation may be distributed on several computers (see Alves et al. (2005, 2008) for an in-depth description of distributed simulation using EcosimPro).

Other advantages of the environment EcosimPro are the connection with external tools (such as MATLAB, C++ and Java methods,

[1]See Vázquez et al. (2010) for an in-depth description of the use of this simulation environment.

data bases, etc.), and its libraries and tools for optimization (see Navia et al. (2012) and Sarabia et al. (2012)), advanced control (see Sarabia et al. (2006, 2009) and Prada et al. (2011, 2012)) and process simulation (see Merino (2008), Salazar et al. (2012), and Acebes et al. (2013)).

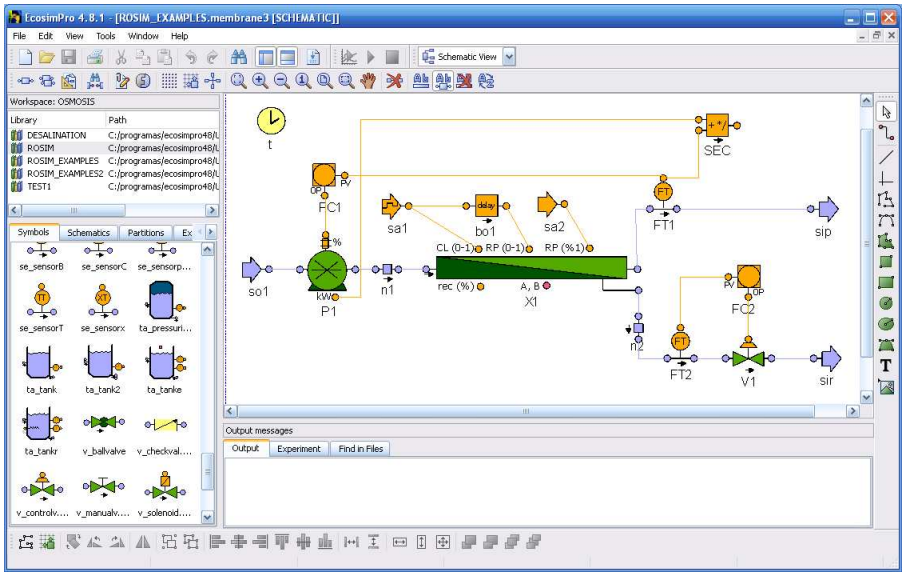

Figure 2.17: View of EcosimPro.

The ROSIM library is focused in the dynamic simulation of RO desalination plants. It has the typical components that can be found in an RO desalination plant, such as RO pressure vessels, pumps, filters, energy recovery systems, the addition of chemicals, tanks, valves, pipes, etc. The user can easily build his/her own simulated plant by dragging and dropping elements of the ROSIM library onto the canvas. Then, the components are connected to each other, imitating the connections in a real plant. Finally, each component may be parametrized to fit it to the particular conditions of the simulated plant. In addition, the ROSIM library has analogue components (such as transmitters, controllers, operational blocks, etc.) that can be used for the design of the control and supervision systems. This library was presented in Palacín et al. (2008a), and upgraded in Palacín et al. (2009c, 2011b). Figure 2.17 shows a view of the graphical interface of EcosimPro and the ROSIM library.

2.2.1 Overview

The ROSIM library uses water as the working fluid. The user may set the quality of the feed water of the simulated plant. The variables that can be characterized by the user are shown below:

- Salt concentration.
- Boron concentration.
- Suspended particles of different sizes.
- Temperature.
- pH.
- Presence of microorganisms.
- Substrate that serves as nourishment for the microorganisms.

New chemical species can easily be added, thanks to the enumerate-type variables of the EcosimPro language.

The following effects are taken into account in the ROSIM library:

- The scaling and fouling of the different components of the desalination plant.
- The biofouling and growth of microorganisms.
- The breakage of the membranes and filters.
- The ageing of the different components.
- The reverse flow in pipes.
- The emptiness and overflow of tanks.

On the contrary, the following effects were neglected.

- The effect of the sound velocity in pipes.
- The two-phase flow.
- The heat losses by radiation.

- The behaviour of real gases.
- The water hammer in pipes.

The first four effects are neglected because they take place outside the typical operation range of a desalination plant. The last effect is neglected because it takes place with an extremely fast time constant. If these effects were simulated, the integration of the mathematical equations would be too slow. In any case, EcosimPro has specific libraries for the simulation of these effects, such as the FLUIDAPRO library, which may be easily interconnected to the ROSIM library.

2.2.2 Types of Ports

The components of the ROSIM library uses three different ports: 1) '`p_1`' is an analogue port, which operates with a scalar variable; 2) '`p_n`' is an analogue port, which operates with an analogue vector; and 3) '`p_osm`' is a hydraulic port, which imitates the hydraulic connections on a real desalination plant.

The variables concerning the '`p_osm`' port are shown below:

- P: Pressure (bar).
- Q: Volumetric flow (m^3/h). The flow may be positive or negative. Positive flow means that the direction of flow is direct, from the input to the output. Negative flow indicates that the direction of flow is in reverse, from the output to the input.
- C: Salt concentration (ppm).
- B: Boron concentration (ppm).
- T: Temperature (ºC).
- pH: pH (-).
- x[mix]: Concentration of the different compounds that may be found in the stream (ppm). 'mix' is an enumeration that includes the following species:
  - X: Microorganisms

- S: Substrate that serves as nourishment for the microorganisms.
- $p0$: Suspended particles larger than 10 μm.
- $p1$: Suspended particles of between 1 - 10 μm.
- $p2$: Suspended particles of between 0.1 - 1 μm.
- $p3$: Suspended particles of between 10^{-2} - 0.1 μm.
- $p4$: Suspended particles of between 10^{-3} - 10^{-2} μm.

2.2.3 Types of Components

The components of the ROSIM library can be divided into two groups: 1) analogue components; and 2) hydraulic components.

2.2.3.1 Analogue Components

The analogue components correspond to blocks that operate analogue signals, such as transmitters, controllers and operational blocks. In general, they are used to configure the control system.

There are two types of analogue components: 1) components that operate with scalars, which use the port '`p_1`'; 2) components that operate with vectors, which use the port '`p_n`'; and 3) components that operate with scalars and vectors, which use both types of ports. For an easy component identification, the symbols of the analogue components that operate with scalars are orange, while the components that operate with vectors are purple.

Whenever several analogue components are connected (either scalar or vector type), the calculation of the variables of each component is done sequentially. Each block calculates the variables of their output ports depending on the value of the variables of the input ports.

2.2.3.2 Hydraulic Components

The hydraulic components correspond to components that operate with hydraulic flows. In general, they correspond to the typical elements that can be found in a desalination plant, such as RO pressure vessels, pumps, valves, tanks, etc. The hydraulic components operate with the '`p_osm`' port.

Although all the hydraulic components may be connected each other, depending on the components connected, the integration of the mathematical system may be easy, complex, or even not converge. In order to avoid algebraic loops and high index problems, and to make easy the converge of the integration, it is a good practice to divide the hydraulic components in tree types: 1) accumulative components; 2) resistive components; and 3) neutral components.

1) The accumulative components calculate the pressure at the boundaries of a hydraulic line. Basically, they are linked with a mass balance. The pressure (P) is calculated as a function of the mass (m), and the mass is calculated depending on the inlet and outlet flows (Q_i), as seen in equation (2.64). A tank is an example of an accumulative component.

$$\begin{cases} m' = f(Q_1, Q_2, ...) \\ P = g(m) \end{cases} \tag{2.64}$$

2) The resistive components are linked with the energy and momentum balances. These components calculate the flow of a hydraulic line depending on the pressure difference between the input and output ports, as shown in equation (2.65). A valve is an example of a resistive component.

$$Q = f(P_{inlet} - P_{outlet}) \tag{2.65}$$

3) The neutral components calculate neither the pressure nor the flow of the hydraulic line. However, these components may calculate a pressure drop (ΔP), depending on the flow of the stream, as shown in equation (2.66). A filter is an example of a neutral component.

$$\Delta P = P_{inlet} - P_{outlet} = f(Q) \tag{2.66}$$

For easy component identification, the symbols of the accumulative components are shown in blue, the symbols of the resistive components are shown in green, and the symbols of the neutral components are shown in yellow.

To summarize, the pressure is calculated by two accumulative components at the boundaries of the hydraulic line, and the flow is calculated by one resistive component in the middle of the hydraulic line. That is, accumulative and resistive components must be connected alternately. Thus: accumulative component - resistive component - accumulative component - resistive component - etc. Neutral components do not calculate the flow, so it is possible to connect as many as are necessary one after the other, between an accumulative and a resistive component. The rest of the variables (the temperature, pH and concentration of the different compounds) are calculated sequentially, in the direction of flow. Notice that depending on the pressure at the boundaries of the hydraulic line, the flow will be direct or reserve.

For instance, figure 2.18 shows the connection of two open tanks ('A' and 'B') through a ball valve ('V'). The tanks are accumulative-type components and the valve is a resistive-type component. In addition, there are two filters ('X1' and 'X2'), which are neutral-type components.

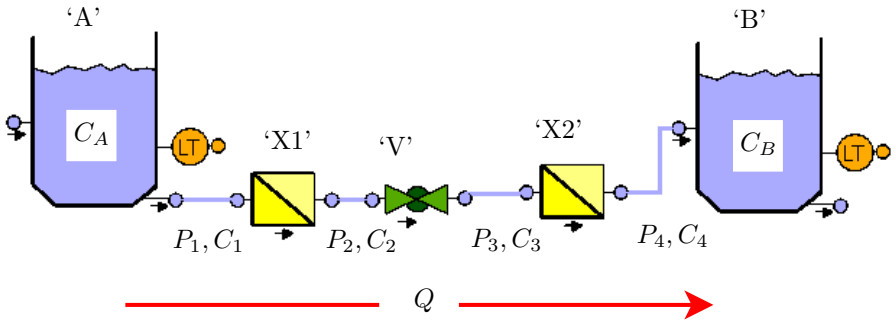

Figure 2.18: Connection of a hydraulic line.

The system consists of the following variables:

– P_1 is the pressure at the output of tank 'A'. It is calculated by this component as a function of the outlet flow:

$$\begin{cases} m_1' = -Q \cdot \rho \\ P_1 = f_1(m_1) \end{cases} \tag{2.67}$$

– P_2 is the pressure at the output of filter 'X1'. This component calculates the pressure drop as a function of the flow.

$$P_2 = P_1 - \text{sign}(Q) \cdot \Delta P_{X_1} = P_1 - \text{sign}(Q) \cdot f_2(Q) \tag{2.68}$$

– P_3 is the pressure at the output of valve 'V'. It is calculated by the component 'X2'.

$$P_3 = P_4 + \text{sign}(Q) \cdot \Delta P_{X_2} = P_4 + \text{sign}(Q) \cdot f_3(Q) \tag{2.69}$$

– P_4 is the pressure at the input of tank 'B'. It is calculated by this component as a function of the inlet flow:

$$\begin{cases} m_2' = +Q \cdot \rho \\ P_4 = f_4(m_2) \end{cases} \tag{2.70}$$

– Q is the flow of the hydraulic line. It is calculated by the component 'V', depending on the pressure difference between its input and output.

$$Q = f_5(P_2 - P_3) \tag{2.71}$$

Depending on the sign of the pressure drop, the flow will be direct (from the tank 'A' to the tank 'B', $Q > 0$) or reverse (from the tank 'B' to the tank 'A', $Q < 0$).

– C_A is the solids concentration in the tank 'A'. It is calculated by the component 'A' by a mass balance, as follows:

$$\underbrace{m \cdot C_A'}_{[3]} = -\underbrace{\rho \cdot Q_d \cdot C_A}_{[1]} + \underbrace{\rho \cdot Q_r \cdot C_1}_{[2]} - \underbrace{m' \cdot C_A}_{[3]} \tag{2.72}$$

where Q_d is the direct flow and Q_r is the reverse flow, as follows:

$$\begin{cases} Q_d = \max(Q, 0) \\ Q_r = \max(-Q, 0) \end{cases} \tag{2.73}$$

Therm [1] of the equation (2.72) is the solids mass flow, which goes out of the tank 'A', if the flow is direct. While term [2] is the solids mass flow, which goes into the tank 'A', if the flow is reverse. If the flow is direct, term [2] takes the value zero, while if the flow is reverse, term [1] takes the value zero. Therms [3] embrace the solids accumulation in this tank.

– C_B is the solids concentration in the tank 'B'. It is calculated by the component 'B' by a mass balance, as follows:

$$\underbrace{m \cdot C'_B}_{[3]} = \underbrace{\rho \cdot Q_d \cdot C_2}_{[1]} - \underbrace{\rho \cdot Q_r \cdot C_B}_{[2]} - \underbrace{m' \cdot C_B}_{[3]} \tag{2.74}$$

Therm [1] of the equation (2.74) is the solids mass flow, which goes into the tank 'B', if the flow is direct. While term [2] is the solids mass flow, which goes out of the tank 'B', if the flow is reverse. If the flow is direct, term [2] takes the value zero, while if the flow is reverse, term [1] takes the value zero. Therms [3] embrace the solids accumulation in this tank.

– C_1 is the solids concentration between the tank 'A' and the filter 'X1'. It is calculated sequentially in the direction of the flow. That is, if the flow is direct, C_1 is calculated by the component 'A', as follows:

$$C_1 = C_A \tag{2.75}$$

While if the flow is reverse, C_1 is calculated by the component 'X1', as follows:

$$C_1 = (1 - \xi_1) \cdot C_2 \tag{2.76}$$

where ξ_1 means the efficiency of the filter 'X1'.

– C_2 is the solids concentration between the filter 'X1' and the valve 'V'. If the flow is direct, C_2 is calculated by the component 'X1', as follows:

$$C_2 = (1 - \xi_1) \cdot C_1 \tag{2.77}$$

While if the flow is reverse, C_2 is calculated by the component 'V', as follows:

$$C_2 = C_3 \tag{2.78}$$

– C_3 is the solids concentration between the valve 'V' and the filter 'X2'. If the flow is direct, C_3 is calculated by the component 'V', as follows:

$$C_3 = C_2 \tag{2.79}$$

While if the flow is reverse, C_3 is calculated by the component 'X2', as follows:

$$C_3 = (1 - \xi_2) \cdot C_4 \tag{2.80}$$

where ξ_2 means the efficiency of the filter 'X2'.

– C_4 is the solids concentration between the filter 'X2' and the tank 'B'. If the flow is direct, C_1 is calculated by the component 'X1', as follows:

$$C_4 = (1 - \xi_2) \cdot C_3 \tag{2.81}$$

While if the flow is reverse, C_4 is calculated by the component 'B', as follows:

$$C_4 = C_B \tag{2.82}$$

Since there are as many variables as equations, the system is consistent and easily solved.

2.2.4 List of Components

Figure 2.19 shows the palette of components of the ROSIM library. The name of each component starts with a one- or two-letter code, which is used to codify the component, symbol '_', and the specific component name. This ensures that similar components are grouped in the same area of the library palette.

The components are listed below, while an in-depth description of the ROSIM library can be seen in appendix B at page 233.

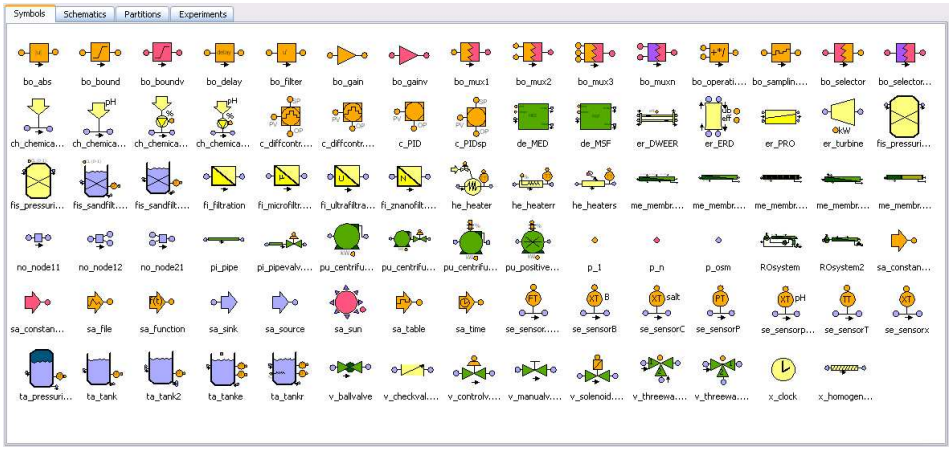

Figure 2.19: Palette of components of the ROSIM library.

- **RO membranes:**
  - **me_membrane:** This component simulates a rack of RO pressure vessels. The user sets the protocol and time instant for cleaning and replacement.
  - **me_membrane_d:** This component simulates a rack of RO pressure vessels. It is similar to "me_membrane", but the mathematical modelling is discretized into two dimensions.
  - **me_membrane_sin:** This component simulates a rack of RO pressure vessels. It is similar to "me_membrane", but the time instant for cleaning and replacement is set by means of an analogue input port.
  - **me_membrane_2m:** This component simulates a rack of RO pressure vessels. It is similar to "me_membrane", but the pressure vessels have two different types of RO modules.
  - **me_membrane_2out:** This component simulates a rack of RO pressure vessels. It is similar to "me_membrane", but this component has two permeate flow outlets: the first permeate outlet has a low concentration of salt and boron, and the second permeate outlet has a high concentration of these species.

- **Pumps:**
  - **pu_centrifugalpump:** This component simulates a centrifugal pump.
  - **pu_centrifugalpumpvalve:** This component simulates a centrifugal pump coupled with a control valve. It has been developed avoiding algebraic loops.
  - **pu_centrifugalpumpvariator:** This component simulates a centrifugal pump, whose velocity is controlled by a speed variator.
  - **pu_positivepump:** This component simulates a positive displacement pump.
- **Energy Recovery Systems:**
  - **er_DWEER:** This component simulates a dual work exchanger energy recovery system.
  - **er_ERD:** This component simulates an energy recovery device.
  - **er_PRO:** This component simulates a pressure retarded osmosis.
  - **er_turbine:** This component simulates a Pelton turbine.
- **Filters:**
  - **fis_pressurizedsandfilter:** This component simulates a pressurized sand filter. The user sets the protocol and time instant for cleaning.
  - **fis_pressurizedsandfilter_sin:** This component simulates a pressurized sand filter. The time instant for cleaning is set by means of an analogue input port.
  - **fis_sandfilter:** This component simulates an open sand filter. The user sets the protocol and time instant for cleaning.
  - **fis_sandfilter_sin:** This component simulates an open sand filter. The time instant for cleaning is set by means of an analogue input port.

  - **fi_filtration:** This component simulates a filter. It removes particles larger than 1 μm.
  - **fi_microfiltration:** This component simulates a microfiltration system. It removes particles larger than 10^{-1} μm.
  - **fi_ultrafiltration:** This component simulates an ultrafiltration system. It removes particles larger than 10^{-2} μm.
  - **fi_znanofiltration:** This component simulates a nanofiltration system. It removes particles larger than 10^{-3} μm.

- **Addition of Chemicals:**
  - **ch_chemical_addition:** This component simulates the addition of a chemical compound. The user defines the chemical species (sodium bisulfite, sodium hypochlorite, antiscalant, etc.) and the flow of the added dose.
  - **ch_chemical_addition_pump:** This component simulates the addition of a chemical compound. It is similar to "ch_chemical_addition", but the added flow is set by means of an analogue input port.
  - **ch_chemical_addition_pH:** This component simulates the addition of an acid or a base. The user defines the pH and the flow of the added dose.
  - **ch_chemical_addition_pH_pump:** This component simulates the addition of an acid or a base. It is similar to "ch_chemical_addition_pH", but the added flow is set by means of an analogue input port.

- **Valves:**
  - **v_ballvalve:** This component simulates an on/off ball valve.
  - **v_checkvalve:** This component simulates a check valve, which prevents reverse flow in a hydraulic line.
  - **v_controlvalve:** This component simulates a control valve.
  - **v_manualvalve:** This component simulates a manual valve.
  - **v_solenoidvalve:** This component simulates an on/off solenoid valve.

  - **v_threewaysvalve12:** This component simulates an L-shaped three-way valve. It has one input and two outputs.
  - **v_threewaysvalve21:** This component simulates an L-shaped three-way valve. It has two inputs and one output.

- **Pipes and Connectors:**
  - **no_node11:** This component simulates a connection between pipes.
  - **no_node12:** This component simulates a T-shaped connection. It has one input and two outputs.
  - **no_node21:** This component simulates a T-shaped connection. It has two inputs and one input.
  - **pi_pipe:** This component simulates a liquid pipe, assuming turbulent flow.
  - **pi_pipevalve:** This component simulates a liquid pipe coupled with a control valve.
  - **x_homogenizer:** This component simulates a homogenizer, by means of a complete mixture volume.

- **Tanks:**
  - **ta_pressurizedtank:** This component simulates a pressurized tank.
  - **ta_tank:** This component simulates an open tank. The mathematical modelling takes into account the emptiness and overflow of the tank.
  - **ta_tanke:** This component simulates an open tank. It is similar to "ta_tank", but this component takes into account the water losses by evaporation.
  - **ta_tankr:** This component simulates an open tank. It is similar to "ta_tank", but this component has a resistor as heater.
  - **ta_tank2:** This component simulates an open tank. It is similar to "ta_tank", but this component has several inputs and outputs.

- **Heat Exchangers:**
  - **he_heater:** This component simulates a liquid-liquid heat exchanger.
  - **he_heaterr:** This component simulates a heater of a liquid current by means of an electrical resistance.
  - **he_heaters:** This component simulates a heater of a liquid current by means of solar radiation.
- **Sensors:**
  - **sa_sensorQ:** This component simulates a massflow sensor.
  - **sa_sensorB:** This component simulates a sensor of the boron concentration.
  - **sa_sensorC:** This component simulates a sensor of the salt concentration.
  - **sa_sensorpH:** This component simulates a pH sensor.
  - **sa_sensorT:** This component simulates a temperature sensor.
  - **sa_sensorx:** This component simulates a sensor of the different chemical species (e.g. particles, microorganisms, etc.).
- **Controllers:**
  - **c_diffcontroller:** This component simulates a controller of incremental type. Each sample time, the controller checks the difference between the setpoint and the control variable. If the difference is higher than a certain gap, the manipulated variable is increased or decreased (depending on the type of the acting) by a value set by the user.
  - **c_diffcontrollersp:** This component simulates a controller of incremental type. It is similar to "c_diffcontroller", but the reference is defined externally.
  - **c_PID:** This component simulates a PID controller.
  - **c_PIDsp:** This component simulates a PID controller. It is similar to "c_PID", but the reference is defined internally.

- **Sources and Sinks:**
  - **sa_constant:** This component sets the value of an analogue variable.
  - **sa_constantv:** This component sets the value of the elements of an analogue vector.
  - **sa_file:** This component establishes the value of an analogue variable using the data in a text file.
  - **sa_function:** This component establishes the value of an analogue variable as a time-dependent function, such as sine, pulse, step, ramp, pulse train, sawtooth, etc.
  - **sa_sink:** This component sets the pressure at the end of a hydraulic line. It also establishes the characteristics of the stream (e.g. salt and boron concentrations, temperature, pH, etc.) in the event of reverse flow.
  - **sa_source:** This component sets the pressure and the characteristics of the stream (e.g. salt and boron concentrations, temperature, pH, etc.) at the start of a hydraulic line.
  - **sa_sun:** This component generates an analogue vector. The first element is the solar radiation and the second element is the ambient temperature.
  - **sa_table:** This component establishes the value of an analogue variable as a table that repeats cyclically.
  - **sa_time:** This component sets the value of an analogue variable as the simulation time value.
- **Analogue Components:**
  - **bo_abs:** This component calculates the absolute value of its input.
  - **bo_bound:** This component limits its input (a scalar) between two values.
  - **bo_boundv:** This component limits its input (a vector) between two values.

  - **bo_delay:** This component delays its input by a given value.
  - **bo_filter:** This component filters its input in accordance with a first order derivate.
  - **bo_gain:** This component multiplies its input (a scalar) by a gain.
  - **bo_gainv:** This component multiplies its input (a vector) by a gain.
  - **bo_mux1:** This component transforms a scalar into a vector of size 1.
  - **bo_mux2:** This component forms a size 2 vector from two scalars.
  - **bo_mux3:** This component forms a size 3 vector from three scalars.
  - **bo_mux3:** This component blends two vectors of n1 and n2 size, respectively, into a single vector of size n1+n2.
  - **bo_operation:** This component performs a simple mathematical operation.
  - **bo_sampling:** This component transforms its input (continuous) into a discontinuous variable.
  - **bo_selector:** This component selects an element of a vector.
  - **bo_selectorv:** This component creates a new vector based on the elements in its input vector.
  - **x_clock:** This component calculates the simulation time in different units. It is useful for plotting.

- **Desalination Systems:**

  - **ROsystem:** This component simulates a desalination system formed by an RO pressure vessel rack, a high-pressure pump with a speed variator, a supply pump, an energy recovery device and a control valve. This is probably one of the most common types of desalination structures.

- **ROsystem2:** This component simulates a desalination system formed by an RO pressure vessel rack, a high-pressure pump with a speed variator and a control valve.
- **de_MED:** This component simulates a multi effect desalination system.
- **de_MSF:** This component simulates a multi-stages flash desalination system.

2.3 Simulation

This section deals with the qualitative analysis of the ROSIM library, and summarizes several experiments which reproduce the typical performance of a desalination plant. In particular, the experiments carried out are: 1) the influence of the quality and temperature of the feed water over the energy consumption and the permeate flow; 2) the behaviour of the cleaning of the desalination plant; 3) the damage to the RO modules due to a wrong pH control; 4) the scaling of carbonates in the RO modules; 5) the presence of microorganisms and their unwanted effects in the permeate flow; and 6) the behaviour of a pressurized sand filter. Notice the quantitative validation of the ROSIM library is carried out in chapter 3.

Figure 2.20 shows the graphical display of a simulated desalination plant, built with the ROSIM library. This simulated plant is used to run the experiments commented on previously. The simulated plant consists of one high-pressure positive-displacement pump, two pressure vessels in parallel (with 4 RO modules each), one pressurized sand filter, one cartridge filter and the addition of chemicals for the pre and post-treatment. In addition, in order to carry out the cleaning of the plant, there are a cleaning tank and a cleaning pump. The blue lines are the hydraulic connections between components (using the port '`p_osm`'), while the orange lines are the analogue connections (using the port '`p_1`') for the control system of the plant. The logic of the control system is embedded in the orange blocks, which simulate a PLC.

The nominal feed flow of the simulated desalination plant is 1 m^3/h, while the nominal water recovery is 60 %. The feed salinity is 15 000 ppm and the initial salt retention of the RO modules is over

99%. The suspended solids concentration of the feed is 10 g/m^3, while the boron concentration is neglected. The volume of the tanks is 2 m^3 and the setpoint of the level controllers is set to 50%. The volume of the pressurized sand filter is 1 m^3 and the porosity of the sand bed is 0.9.

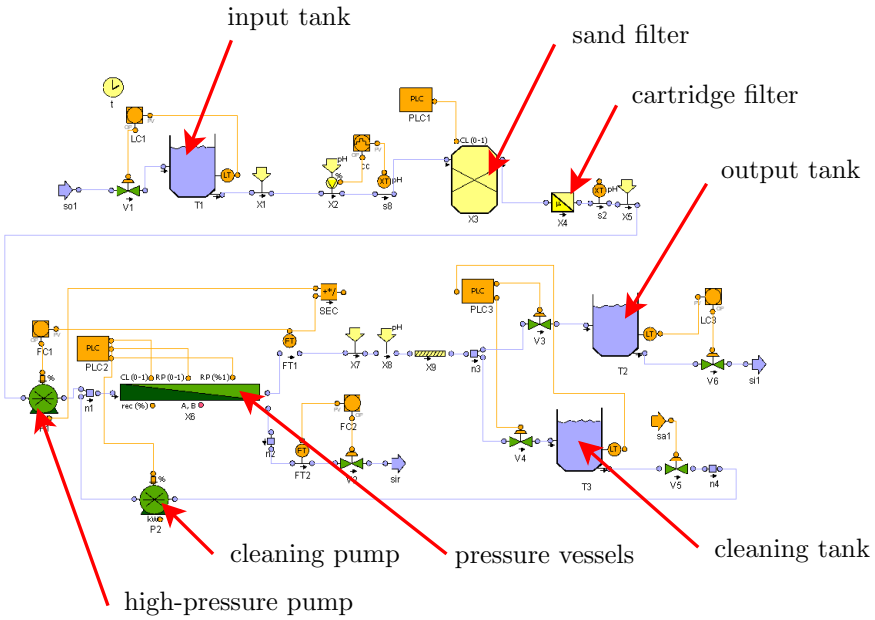

Figure 2.20: Graphic display of the simulated desalination plant used in the qualitative analysis of the ROSIM library.

2.3.1 Influence of the Feed Temperature

The increase of the feed temperature causes the dilatation of the pores of the RO membrane. With a larger size of the pores, more molecules of water and salt are able to cross the membrane. The increase in the temperature has two contrary effects: a higher volume of permeate is produced, but with a lower quality. In general, it is not a good idea to increase the feed temperature.

This experiment consists in simulating a desalination plant over 25 hours, with a variable feed temperature. Figure 2.21 shows the profile of the feed temperature used in this experiment (the input of the simulator). Initially, the feed temperature is set to 25 °C. At time 5 hours, the feed temperature is increased up to 30 °C. At time

14 hours, the feed temperature is set to 20 °C until the end of the experiment.

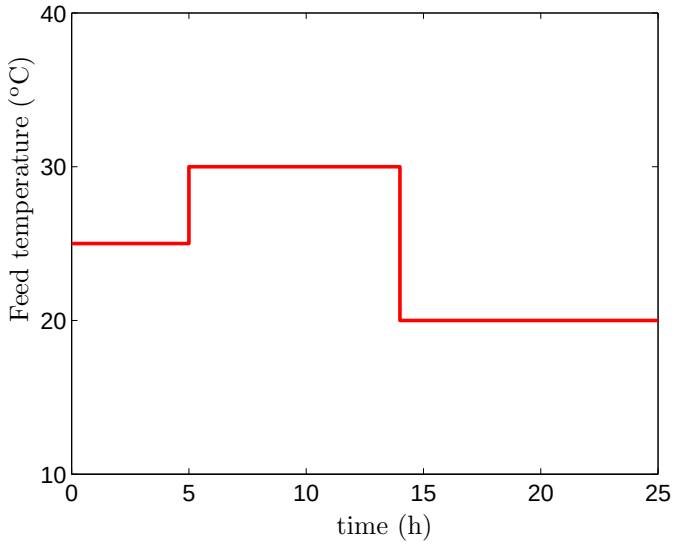

Figure 2.21: Profile of the feed temperature.

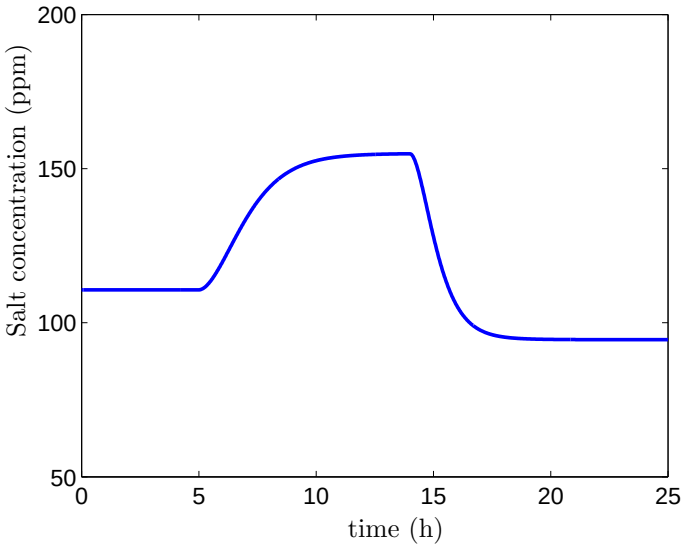

Figure 2.22: Evolution of the salt concentration of the permeate.

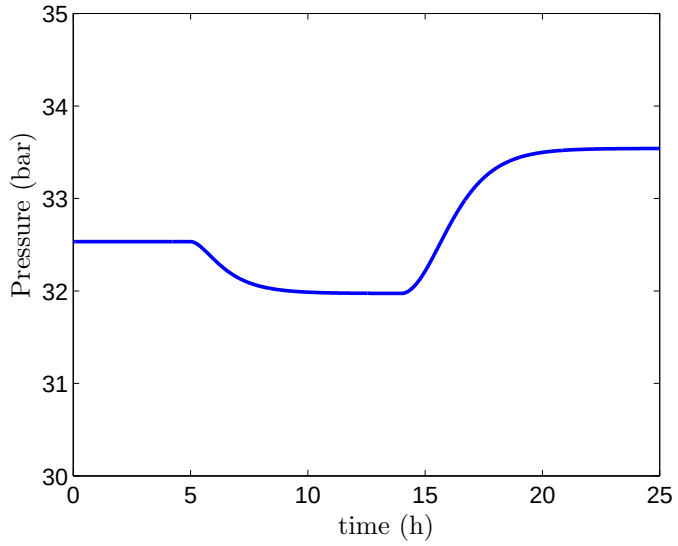

Figure 2.23: Evolution of the operating pressure provided by the high-pressure pump.

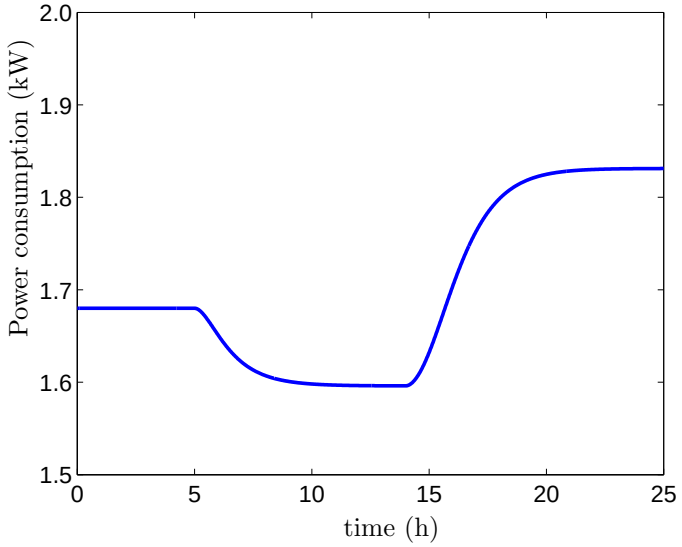

Figure 2.24: Evolution of the power consumption of the desalination plant.

Figures 2.22 and 2.23 show, respectively, the evolution of the salt concentration of the permeate and the operating pressure supplied by the high-pressure pump (the outputs of the simulator).

As commented previously, the salt concentration increases when the feed temperature is higher, as seen in figure 2.22; as well as the permeate flow. Since, in the case of the simulated plant, the permeate flow is controlled by manipulating the speed of the high-pressure pump, the increase of the feed temperature involves a lower requirement of the operating pressure, as seen in figure 2.23. Finally, figure 2.24 shows the behaviour of the power consumption of the simulated plant, which is proportional to the pressure increase supplied by the high-pressure pump.

2.3.2 Influence of the Feed Salt Concentration

The increase of the salt concentration of the feed water always has negative effects. It implies a higher osmotic pressure which should be compensated for the high-pressure pump, a higher energy consumption, a lower volume of permeate with a lower quality, and a shorter life of the RO modules.

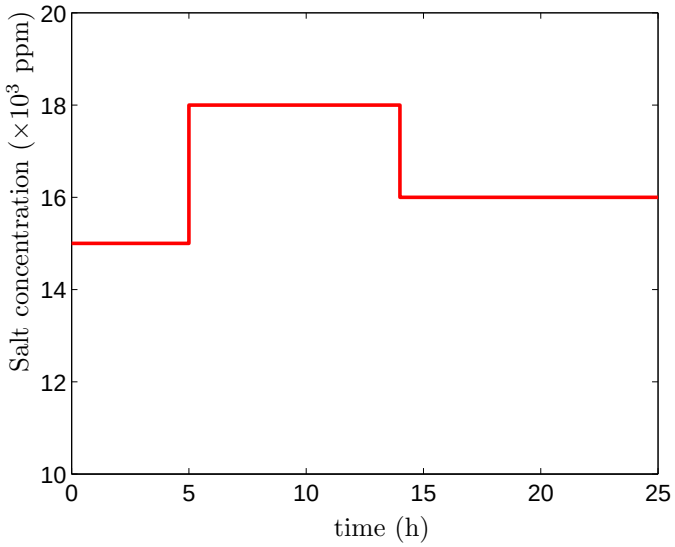

Figure 2.25: Profile of the salt concentration of the feed.

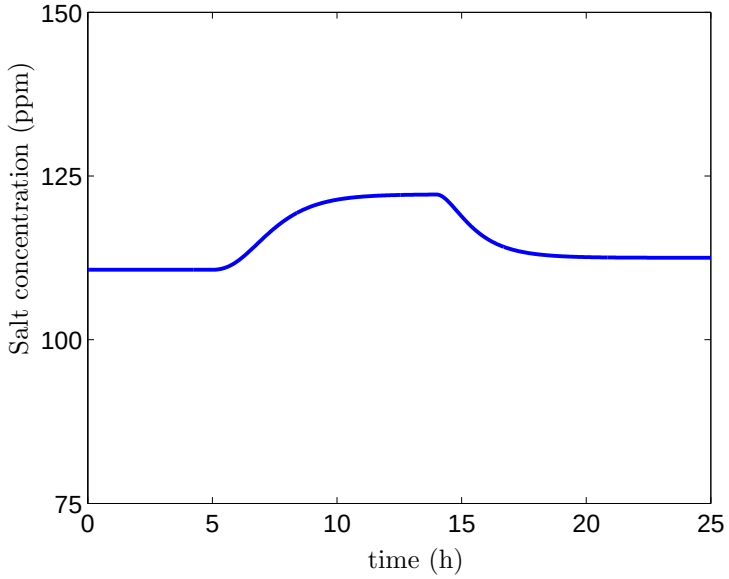

Figure 2.26: Evolution of the salt concentration of the permeate.

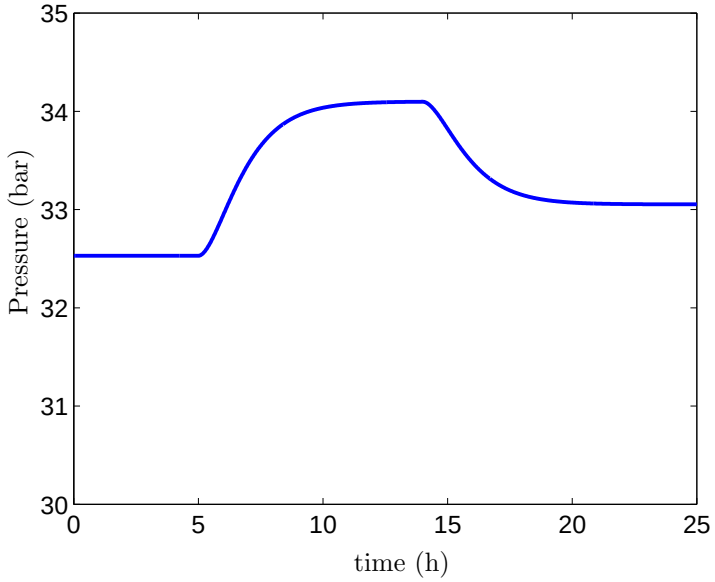

Figure 2.27: Evolution of the operating pressure provided by the high-pressure pump.

This experiment consists in simulating a desalination plant over 25 hours, with a variable salt concentration of the feed. Figure 2.25 shows the profile of the salt concentration of the feed used in this experiment (the input of the simulator). Initially, the salt concentration is set to 15 000 ppm. At time 5 hours, the salt concentration is increased up to 18 000 ppm. At time 14 hours, the feed temperature is set to 16 000 ppm until the end of the experiment.

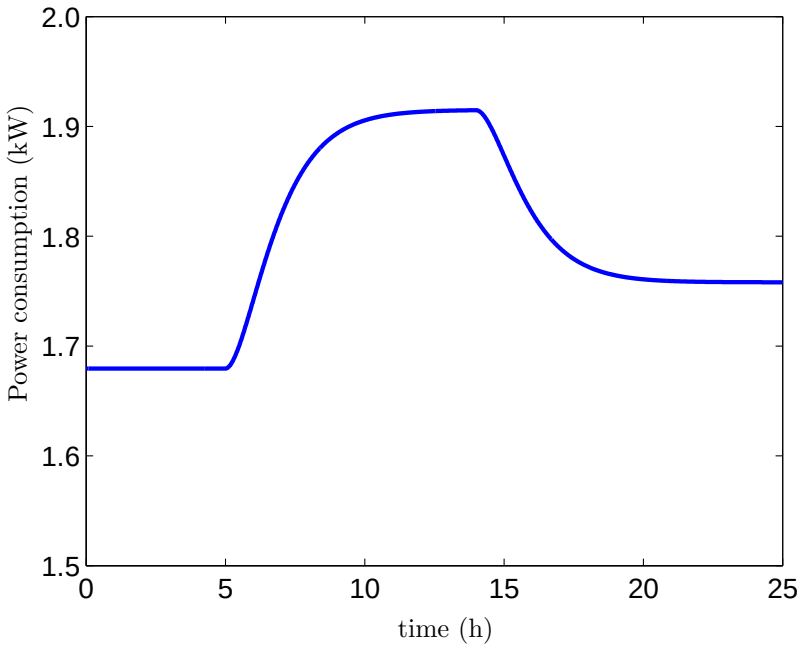

Figure 2.28: Evolution of the power consumption of the desalination plant.

Figures 2.26 and 2.27 show, respectively, the evolution of the salt concentration of the permeate and the pressure increase supplied by the high-pressure pump (the outputs of the simulator). As commented previously, the salt concentration of the permeate and the operating pressure increase when the salt concentration of the feed is higher. Figure 2.28 shows the behaviour of the power consumption of the simulated plant. Since the power consumption is proportional to the operating pressure, figures 2.27 and 2.28 are similar.

2.3.3 Cleaning of a Desalination Plant

This experiment consists in simulating a flushing and washing of the RO modules. As commented in section 1.1.5 at page 30, flushing involves the pumping of feed water through the pressure vessels, with a high flow and a low pressure, and it is used to remove the solids that may have reached to the RO membranes. The flushing is carried out by opening a valve at the outlet of the reject flow. According to the characteristic curve of the high-pressure pump, opening this valve involves changing the operating point from low flow and high pressure, to high flow and low pressure. In this case, the flushing is done at time 10 minutes and lasts 3 minutes.

On the other hand, the washing of the RO modules requires pumping clean water through the pressure vessels. The water used during the washing is provided by a cleaning tank, filled with permeate water. The washing is carried out using a cleaning pump instead of the high-pressure pump. In this case, the washing of the pressure vessels is done at time 30 minutes and last 15 minutes. Figures 2.29 and 2.30 show, respectively, the evolution of the water flow at the inlet of the pressure vessels and the operating pressure.

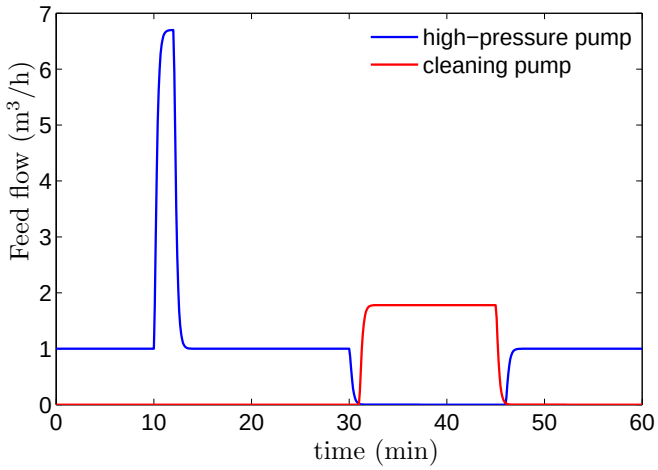

Figure 2.29: Evolution of the feed flow of the pressure vessels. The blue line is the flow through the high-pressure pump, while the red line is the flow through the cleaning pump. There is a flushing at time 10 min, and a washing of the RO membranes at time 30 min.

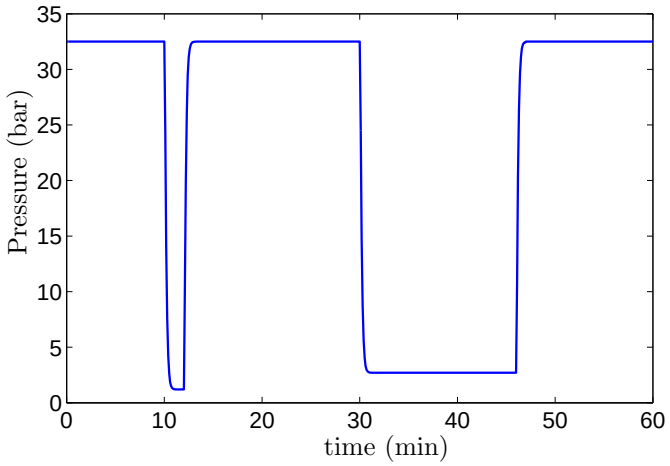

Figure 2.30: Evolution of the operating pressure, provided by the high-pressure pump and the cleaning pump. There is a flushing at time 10 min, and a washing of the RO membranes at time 30 min.

2.3.4 Scaling

This experiment consists in simulating the unwanted effect of the scaling of carbonates in the RO membranes (see section 1.1.5at page 29). The deposition of carbonate molecules over the RO membranes involves mainly two negative effects: 1) The hydraulic permeability of the RO membranes is decreased; and 2) more salt particles are able to cross the RO membranes. So, the required operating pressure, provided by the high-pressure pump, is increased and the quality of the permeate flow gets worse.

Figures 2.31 and 2.32 show, respectively, the evolution of the salt concentration of the permeate and the operating pressure. The blue lines are the normal operation, while the red lines are the profile of the plant when the effect of scaling is taking place. The simulation is run over four days. During the normal operation of the plant, the hydraulic permeability decreases due to the normal fouling of the RO membranes. This fouling is removed thanks to the washing of the RO membranes. During this experiment, three cleanings of the desalination plant are scheduled, at the end of each day, which correspond to the sudden steps in these curves. When the carbonate scaling occurs, the velocity of the fouling is increased, as well as the ratio of the

irreversible fouling (which is not removed by cleaning).

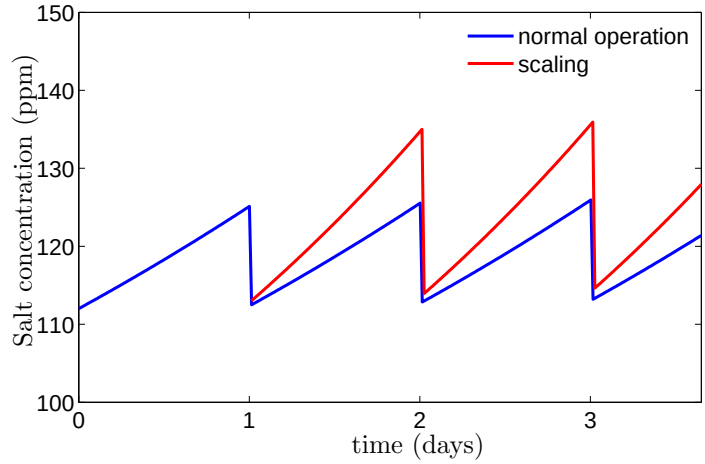

Figure 2.31: Evolution of the salt concentration of the permeate over four days. The blue line corresponds to the normal operation of the plant, while the red line corresponds to the behaviour of the concentration when the effect of scaling is taking place.

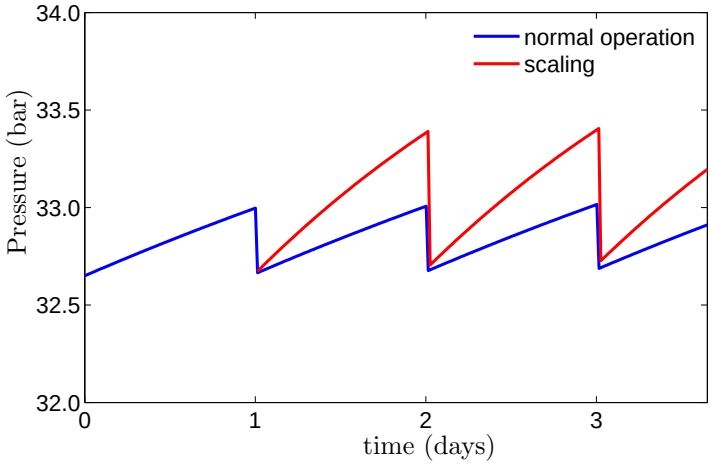

Figure 2.32: Evolution of the operating pressure over four days. The blue line corresponds to the normal operation of the plant, while the red line corresponds to the behaviour of the pressure when the effect of scaling is taking place.

2.3.5 Growth of Microorganisms

This experiment consists in simulating the unwanted effect of the biofouling in the RO membranes. The biofouling has similar effects to the carbonate scaling; however, the loss of permeate quality, and the ratio of irreversible fouling is several times higher.

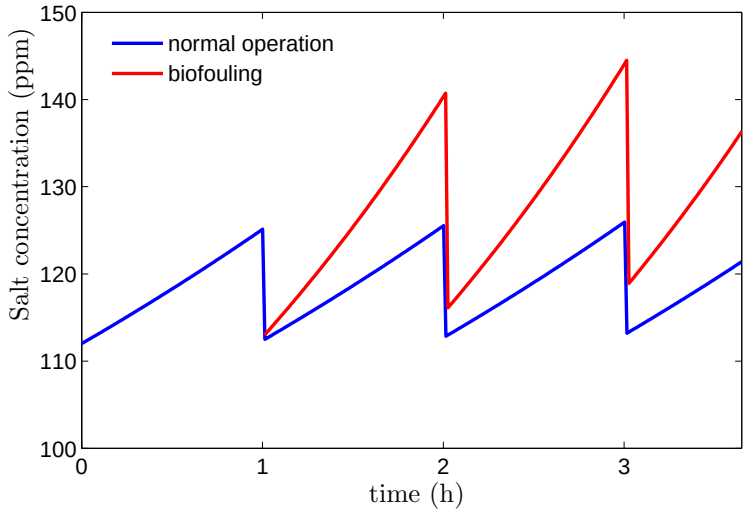

Figure 2.33: Evolution of the salt concentration of the permeate over three days. The blue line corresponds to the normal operation of the plant, while the red line corresponds to the behaviour of the pressure with the growth of microorganisms.

Figures 2.33 and 2.34 show, respectively, the evolution of the salt concentration of the permeate and the operating pressure, provided by the high-pressure pump, over four days. The blue lines are the normal operation of the desalination plant, while the red lines correspond to the profile of these variables with the growth of microorganisms. As in the previous case, there are three cleanings of the desalination plant, scheduled at the end of each day. Notice that the growth of microorganisms involves a faster fouling of the RO membranes and, mainly, a higher ratio of the irreversible fouling, which is not removed by the periodic cleaning of the desalination plants. The elimination of the microorganisms will be done only after a chemical cleaning or the replacement of the RO modules.

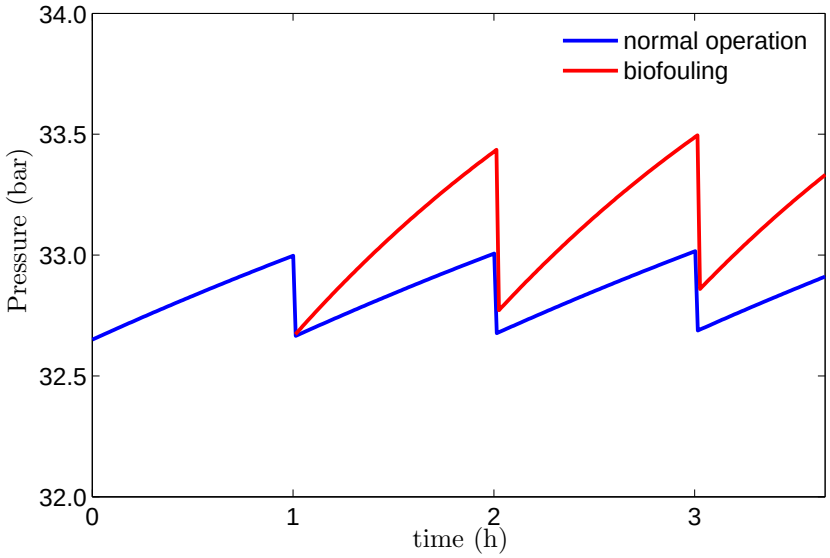

Figure 2.34: Evolution of the operating pressure over three days. The blue line corresponds to the normal operation of the plant, while the red line corresponds to the behaviour of the pressure with the growth of microorganisms.

2.3.6 Damage to the RO Membranes

A wrong pH control at the input of the pressure vessels may involve damage to the RO membranes and the reduction of its service life, and even the formation of small holes in the membranes, which will allow part of the feed water to pass and blend with the permeate flow. The damage to the RO membranes is easily detected thanks to a sudden increase in the salt concentration of the permeate, but mainly, due to a high increase of the permeate pressure. After the damage to the RO membrane, the only solution is the replacement of the damaged modules.

This experiment consists in a simulation of the breaking of the RO modules. Figure 2.35 shows the evolution of the salt concentration of the permeate over one hour, while figure 2.36 shows the profile of the permeate pressure. The breakage of the membrane takes place at time 15 minutes.

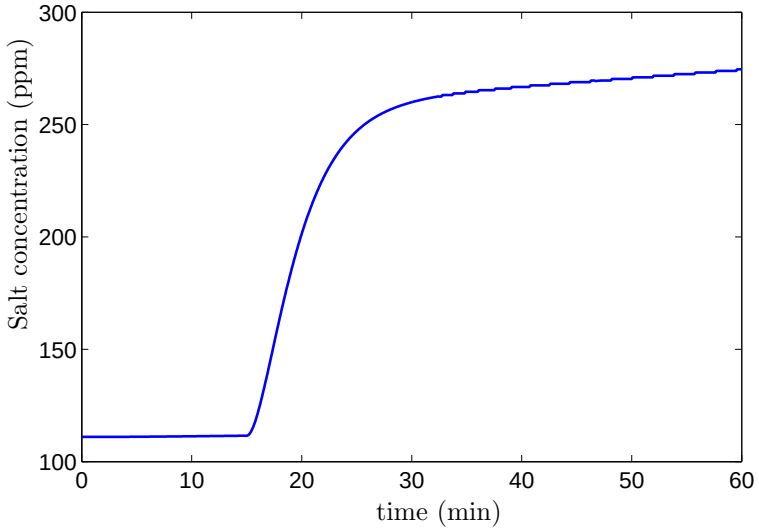

Figure 2.35: Evolution of the salt concentration of the permeate over one hour. After 15 minutes, the breakage of the RO membrane takes place.

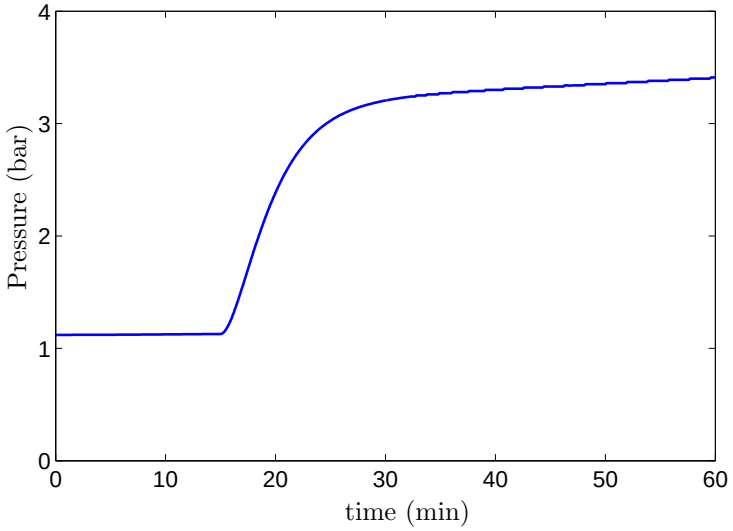

Figure 2.36: Evolution of the pressure of the permeate over one hour. After 15 minutes, the breakage of the RO membrane takes place.

2.3.7 Sand Filter

This experiment consists in simulating the saturation of the sand filter. The suspended solids of the feed water are captured by the sand of the sand filter. As time goes on, more feed water crosses the sand filter and more suspended solids are retained by the sand.

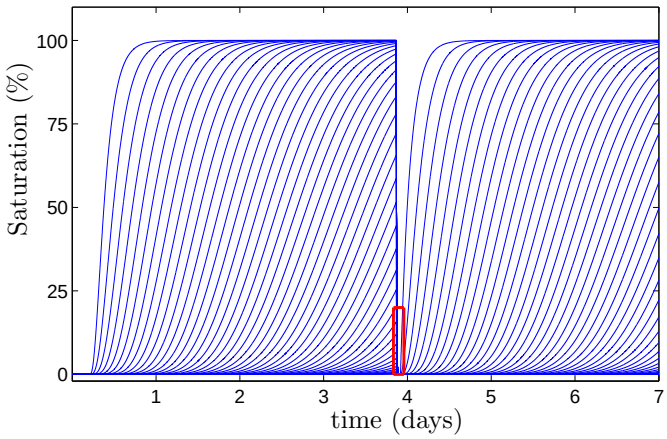

(a) Profile over one week.

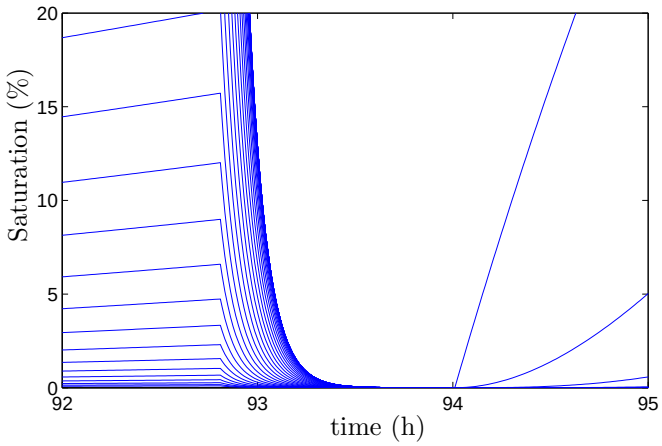

(b) Extension of red square.

Figure 2.37: Saturation of the sand filter over one week. The sand filter is discretized in 50 elements in the flow direction. Each discretization corresponds to one curve. The sand filter is cleaned at the end of the third day. Figure (b) is the extension of the red square of figure (a).

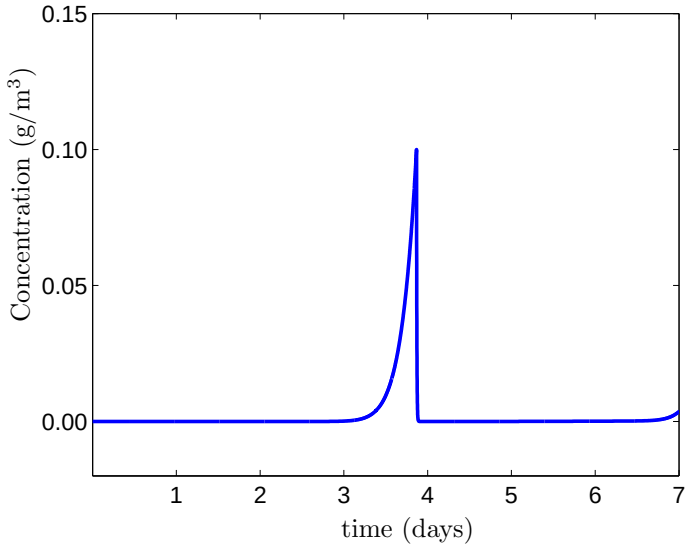

Figure 2.38: Concentration of suspended solids in the outlet of the sand filter. The sand filter is cleaned at the end of the fourth day.

Once the sand is saturated with solids, a cleaning of the filter should be scheduled, which consists in pumping clean water through the filter and shaking the sand by an inverse flow. This experiment is run over one week. Figure 2.38 shows the profile of the concentration of suspended solids at the output of the sand filter. After four days, the sand filter becomes saturated and part of the suspended solids of the feed flow are able to cross the filter. So, at the end of the fourth day, a cleaning of the sand filter is carried out. Figure 2.37 shows the evolution of the saturation of the sand inside the filter. The sand filter is discretized into 50 elements in the axial direction. Each curve of figure 2.37 corresponds to one element of the discretization. The bottom graph of figure 2.37 is the zoom of the red square of the top graph, which consists of the cleaning of the sand filter. The saturation of the element i of the discretization is calculated as follows:

$$\text{Saturation}(i) = \frac{m(i) \cdot n}{m_{max}} \cdot 100 \tag{2.83}$$

where $m(i)$ is the mass of solids captured by the sand of the ith element, n is the number of elements (in the current case, n takes the

value 50), and m_{max} is the maximum quantity of solids that may be captured by the filter (in the current case, m_{max} takes the value 2 kg).

The simulations shown in section 2.3 correspond to several of the effects that have been taking into account for the developing of the ROSIM library. This section describes the qualitative analysis of these effects. In each particular case, the components of the library may be parametrized to fit with each real system. The quantitative validation of the ROSIM library is described in chapter 3.

Chapter 3

Pilot Plant and Model Validation

This chapter deals with the validation of the ROSIM library. The validation is carried out using experimental data from an RO pilot plant. Section 3.1 describes this RO pilot plant, which was built as part of the OPEN-GAIN project. This pilot plant was simulated using the ROSIM library. Section 3.2 describes the parameter estimation of this simulator, and section 3.3 shows the validation of the main components of the simulator.

3.1 RO Pilot Plant

An RO pilot plant was built during the development of the OPEN-GAIN project. The construction of the RO pilot plant was carried out by the specialized company SETA[1], as subcontractor, and it was placed in the Research and Technology Center of Energy[2] (CRTEn). The CRTEn is located close to the village of Borj Cedria, on the Tunisian north cost, 40 km from Tunis.

Figure 3.1 shows a picture of the building where the pilot plant was placed. Besides the pilot plant, this building contains a control room, and several offices, stores and workshops linked to the OPEN-GAIN project.

[1] `http://www.gruposeta.com/`
[2] `http://www.crten.rnrt.tn/`

Figure 3.1: Location of the RO pilot plant.

The characteristics of the RO pilot plant are shown in table 3.1.

Variable	Average value
Feed flow:	0.5-2.5 m^3/h
Recovery:	60 %
Operating pressure:	32 bar
Power consumption:	2.8 kWh/m^3
Feed salinity:	15 200 ppm
Permeate salinity:	240 ppm
Salt Retention:	98 %

Table 3.1: RO pilot plant characteristics.

3.1.1 Description of the RO Pilot Plant

Figure 3.2 shows the flow diagram of the RO pilot plant, which is described below:

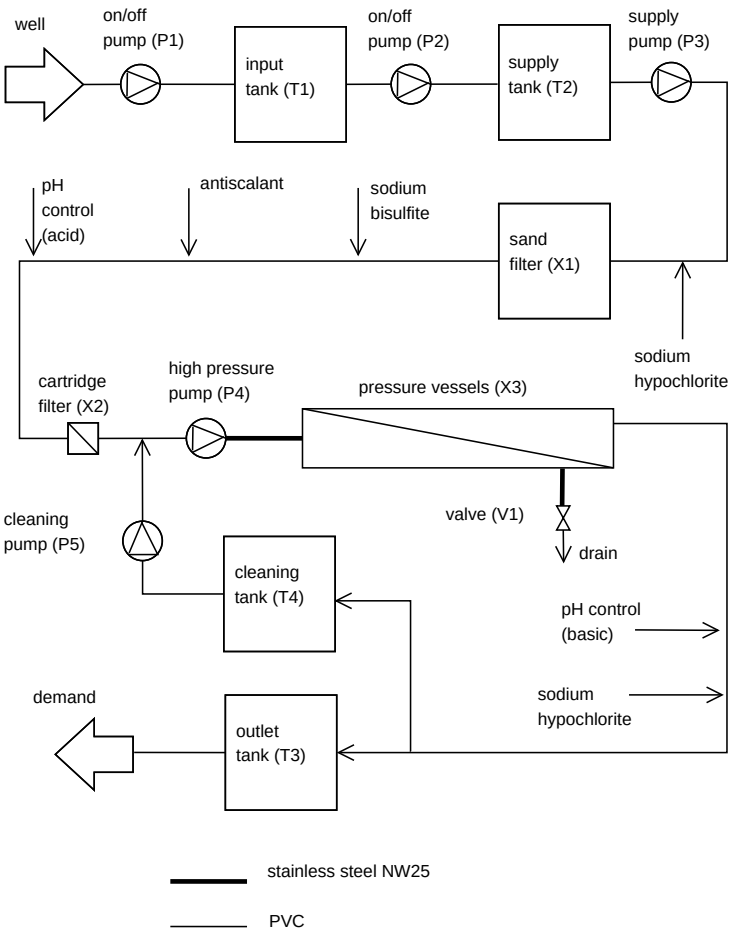

Figure 3.2: Flow diagram of the RO pilot plant.

– First, an on/off pump ('P1') pumps brackish water from a well to an input tank ('T1'), which is located a few tens of meters from the well. From this tank, water is pumped by a second on/off pump ('P2') to a supply tank ('T2').

– Next, a centrifugal pump ('P3') pumps water to a set of filters and chemical additions, as follows:

  – Addition of sodium hypochlorite, which works as a biocide.
  – A sand filter ('X1'), which removes the fine solids from the water.

  - Addition of sodium bisulfite, to remove the sodium hypochlorite excess, which would damage the RO membranes. The maximum sodium hypochlorite in the inlet of the RO membranes should be less than 0.1 ppm.
  - Addition of antiscalant, to avoid scaling on the RO membranes.
  - Control of the pH by the addition of hydrochloric acid. In order to avoid damage to the membranes, the input pH should be limited to between 6.5 - 7.0.
  - A cartridge filter, which removes the dissolved particles larger than 5 μm from the water.

- Then, a high pressure pump with a speed control ('P4') increases the pressure of the stream to a value above the osmotic pressure (over 30 bar) and pumps the water to the pressure vessel ('X3'). The system consists of two parallel pressure vessels, with four RO modules each. The pressurized water is forced to cross the RO membranes. Here, the feed flow is divided into two flows: 1) A reject flow with high pressure and high salinity. 2) A permeate flow with low pressure and low salinity.

- The reject flow is pumped to the drain. At the outlet of the reject flow there is a manual valve, which strangulates the pressurized stream. The pressure of the streams decreases from operating pressure (over 30 bar) to atmospheric pressure.

- The permeate flow is pumped to a set of chemical additions:

  - Addition of sodium hydroxide, to control the pH of the permeate flow.
  - Addition of sodium hypochlorite (until 1 ppm), to remove any bacteriological contamination before consumption. This second sodium hypochlorite addition is several times lower than the addition of hypochlorite at the input of the sand filter since the number of microorganisms in the permeate flow should be negligible.

- Finally, the permeate water is stored in an outlet tank ('T3'), before consumption.

The material of the pipes is PVC, except for two sections: From the high pressure pump to the pressure vessels, and from the pressure vessels to the valve 'V1', where due to the high pressure and salinity of the stream, stainless steel NW25 is required.

The RO pilot plant can be operated in a closed loop, pumping the reject flow and the permeate flow to the supply tank ('T2'), instead of to the drain and to the outlet tank ('T3') respectively. Even when the total water volume is constant, the closed loop operation cannot be done for an unlimited period. The addition of chemicals, such as sodium hydroxide and hydrochloric acid, causes a continuous increase of the salinity of the water. Soon, the required osmotic pressure would be beyond the pressure provided by the high pressure pump.

The RO plant consists of the following elements:

- Eight spiral wound type RO modules from the company Hydranautics (model CPA2-4040).
- Two pressure vessel from the company Hydranautics.
- A high pressure positive displacement pump from the company Grundfos (model BMP 2.2R).
- One centrifugal pump (supply pump 'P3') from the company Grundfos (model CHI 2-60).
- One centrifugal pump (cleaning pump 'P4') from the company Grundfos (model CHI 4-60).
- Two on/off pumps (supply pumps 'P1', 'P2'), provided by CRTEn.
- One sand filter from the company Pevasa, filled with silex sand with a grain size of 0.5-0.7 mm.
- One porous type cartridge filter from the company Pevasa, which rejects particles larger than 5 μm.
- Six dosing pumps from the company Dosim.
- Four PVC tanks of different sizes.

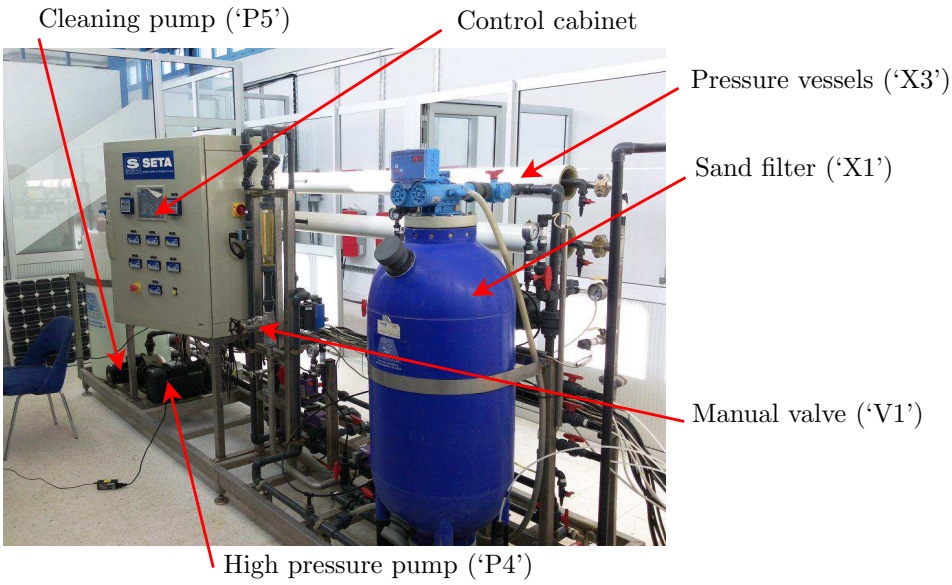

Figure 3.3: RO pilot plant (front view).

Figures 3.3 and 3.4 show two pictures of the RO pilot plant, where the different elements can be seen.

Since the RO plant was developed for testing and validation, it has a high number of sensors (more than for a conventional RO system). In particular, the RO consists of the following sensors:

- One level sensor in each chemical addition tank.
- One level sensor in each storage tank.
- Six pressure sensors along the RO system.
- Two flow sensors (for the feed flow and the permeate flow).
- Two temperature sensors (one in the input of the system and one in the cleaning tank).
- Two pH sensors.
- Two chloride sensors and one redox sensor, to calculate the sodium hypochlorite of the stream along the RO system.

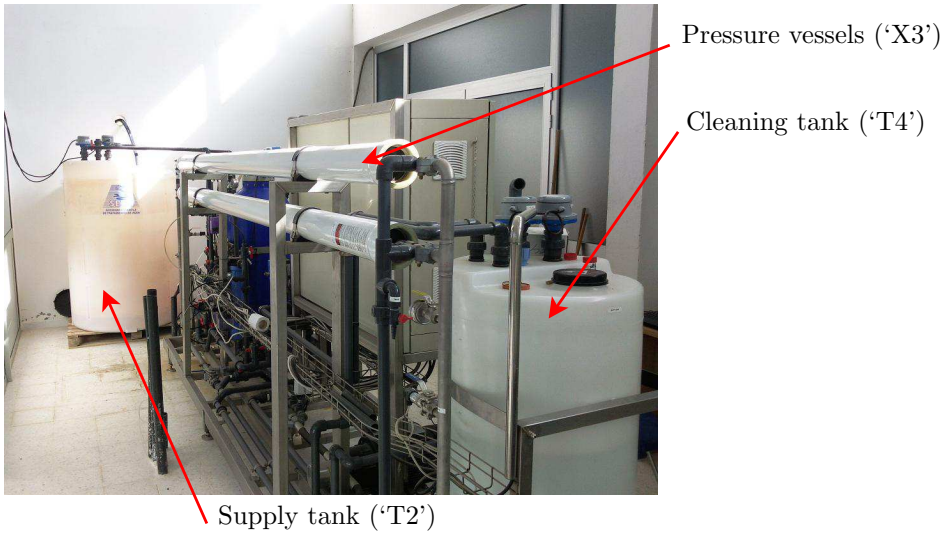

Figure 3.4: RO pilot plant (back view).

– Three conductivity sensors to calculate the salinity of the stream along the RO system.

In order to increase the life of the RO membranes, several types of cleaning should be carried out:

– Flush of the RO membranes. This is done automatically every two hours and lasts three minutes, during which a flush of feed water (with high flow and low pressure) is pumped through the pressure vessel. The flush removes any solids which could have arrived at the RO membranes. The flush is done by the high pressure pump ('P4').

– Wash of the RO membranes. This is done at least once a week, and always when the plant is stopped. It takes 15 minutes, during which a permeate flow is pumped through the RO membranes. The permeate water removes the scaling which can have taken place on the membranes. The conventional cleaning is done by the cleaning pump ('P5'), which pumps permeate water from a cleaning tank ('T4'). When the plant is started up, the permeate flow is automatically pumped to the cleaning tank ('T4') to assure water for future cleaning. Only when this tank is full is the permeate flow pumped to the outlet tank ('T3').

- Chemical cleaning of the RO membranes. This is done only if the fouling of the RO membranes has occurred. The chemical cleaning protocol depends on the type of fouling (biofouling, Iron(III) hydroxide, calcium carbonate, etc.), and consists of different stages, where permeate water is pumped through the pressure vessel, with different chemical additions. Since some of the stages requires hot water, there is an electrical resistance in the cleaning tank.

- Sand filter cleaning. This lasts 30 minutes, during which feed water is pumped backward through the sand filter. The backward flow shakes the sand and removes the attached solids from the sand. The sand filter cleaning should be done at least once a week, but the time instant of the cleaning can be set by the operator.

- Change of the cartridge filter. When the pressure drop along the cartridge filter is higher than 0.8 bar, the cartridge module should be changed for a new one. If the pretreatment is done correctly, the change of the cartridge module need not be done for several months.

3.1.2 Basic Control

Figure 3.5 shows the Process and Instrumentation Diagram of the RO pilot plant, which is described below. The basic control of the plant is carried out by a PLC from OMRON (model CJ1M CPU11), located in the control cabinet (see figure 3.6). This PLC deals with the following issues:

- Start-up and stop of the plant.

- Security logic.

- Control of the touch panel and displays of the different sensors.

- Protocol for the conventional cleaning of the RO membranes.

- Protocol for the cleaning of the sand filter.

- Control loops of the chemical additions.

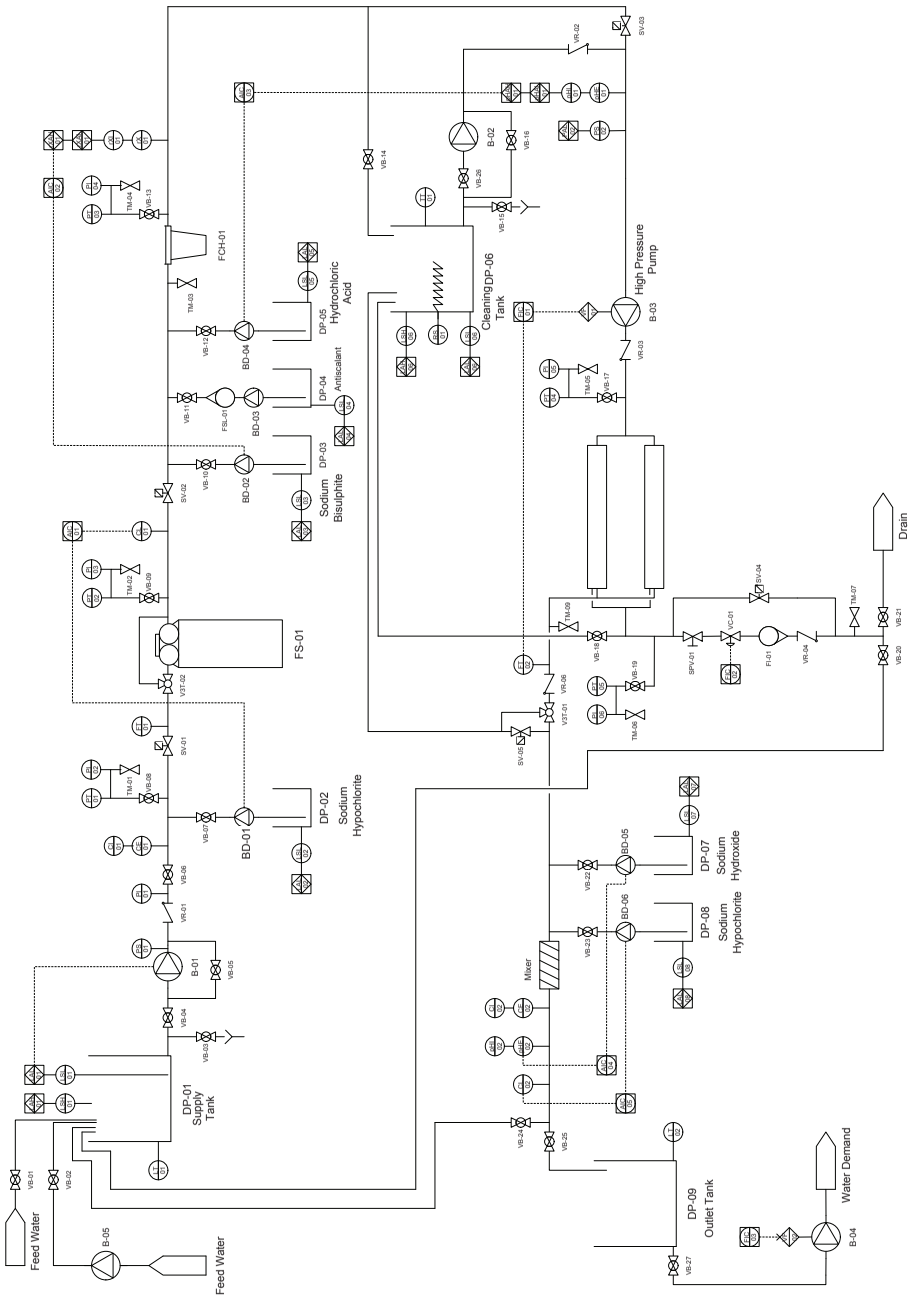

Figure 3.5: Process and instrumentation diagram of the RO pilot plant. Adapted from SETA.

– Control loop of the permeate flow.

– Control of the level of the cleaning tank ('T4').

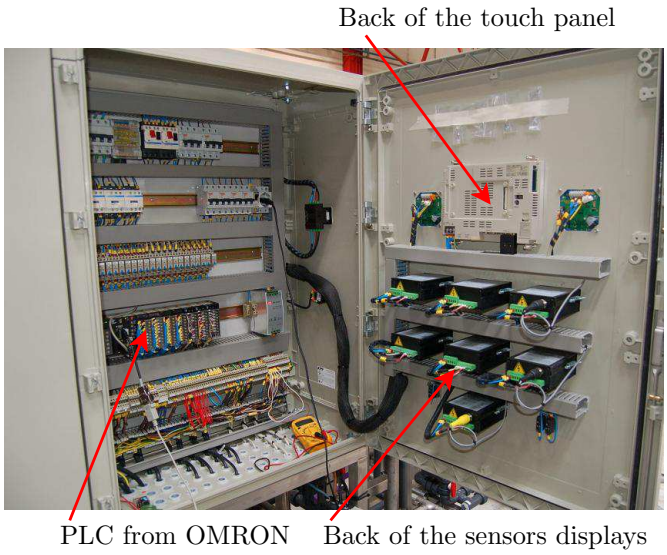

Figure 3.6: Control cabinet of the RO pilot plant.

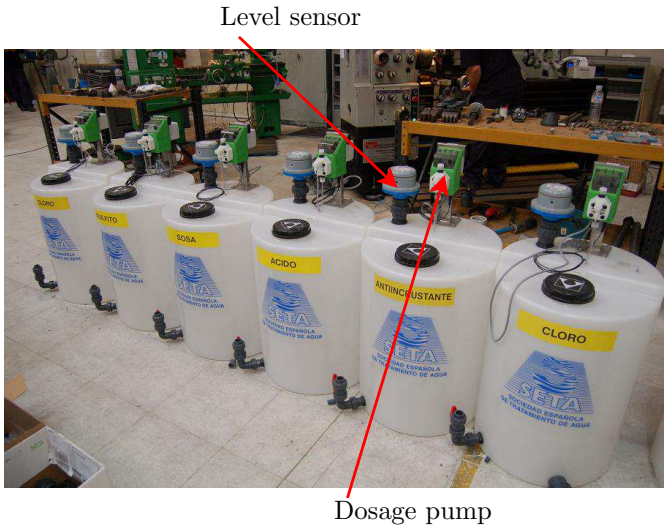

Figure 3.7: Chemical addition tanks.

The chemical additions are carried out by dosing pumps (see figure 3.7), whose flow is proportional to a set of sensors, as follows:

- The sodium hypochlorite dosage at the input of the sand filter is proportional to a chlorine sensor at the outlet of the sand filter.
- The sodium bisulfite dosage is proportional to a redox sensor at the outlet of the cartridge filter.
- The chloride acid dosage is proportional to a pH sensor at the input of the pressure vessels.
- The sodium hypochlorite dosage at the output of the pressure vessels is proportional to a chlorine sensor at the output of the plant.
- The sodium hydroxide dosage is proportional to a pH sensor at the output of the plant.

There is no control loop for the addition of antiscalant, since there is no commercial antiscalant sensor. The antiscalant dosage is calculated off-line, taking into account the characteristics of the feed water.

The permeate and reject flow of the plant are controlled as follows:

- The permeate flow is controlled by the manipulation of the speed of the high pressure pump. The velocity of the pump is calculated by a PID controller located in the PLC.
- The reject flow is controlled manually by the valve V1, at the outlet of the reject flow.

The upper-layer control is carried out by a computer connected to the PLC by an Ethernet bus and using the OPC protocol. It deals with the following issues, which are developed in chapter 4:

- Time instant of the cleaning of the sand filter.
- Time instant of the cleaning of the RO membranes.
- Behaviour of the setpoint of the permeate flow controller.
- Control of the level of the tanks ‘T1’, ‘T2’ and ‘T3’.

– Control of the on/off supply pumps.

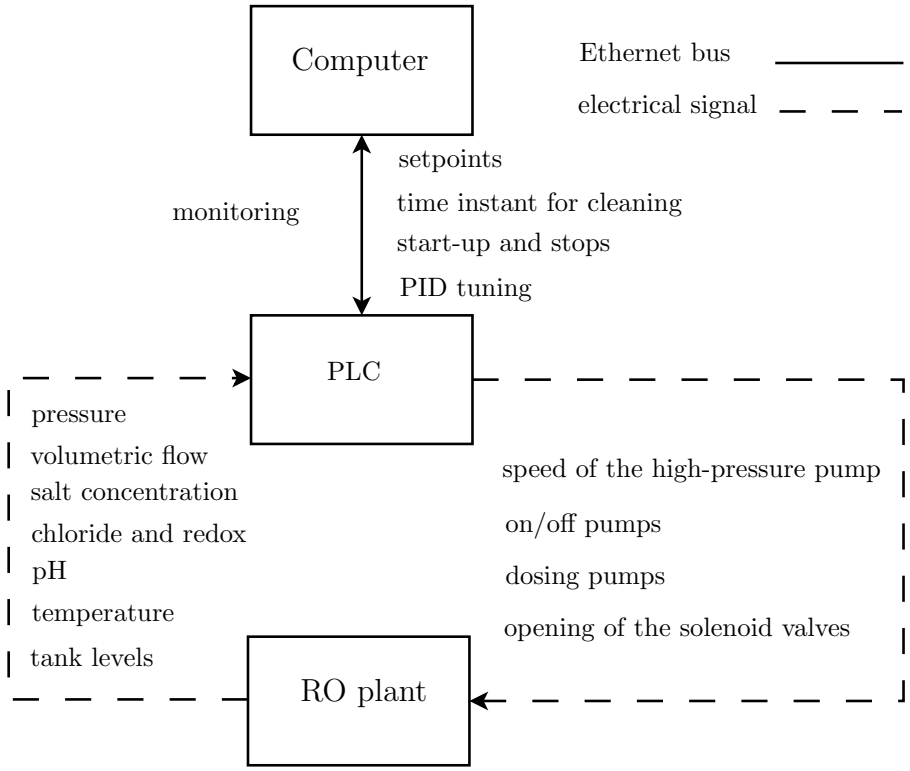

Figure 3.8: Control layers of the RO pilot plant.

Figure 3.8 shows the control layers of the control system of the RO pilot plant. The PLC collects the signals from the plant sensors, and sends them to the computer through the Ethernet bus. The setpoints of the control loops, the time instant for cleaning, start-up and stops, and the PID tuning are all set from the computer and sent to the PLC.

3.1.3 Water Characteristics

The water analyses of the different flows of the RO pilot plant are summarized in table 3.2. Regarding these data, the following considerations were proposed:

Chemical	Feed	Reject	Permeate
Ca^{+} (ppm)	860	2 170	10
Mg^{2+} (ppm)	190	480	3
Na^{+} (ppm)	4 100	11 850	80
K^{+} (ppm)	110	280	6
Fe^{2+} (ppm)	0.5	0.6	–
SO_4^{2-} (ppm)	1 200	3 400	10
HCO_3^{-} (ppm)	540	1 360	10
Cl^{-} (ppm)	7 440	18 900	120
Boron (ppm)	–	–	–
TDS (ppm)	15 200	38 440	240
pH	6.8	7.2	6.3

Table 3.2: Water analysis.

– The concentration of Iron is significant, and the precipitation of Iron(III) hydroxide in the RO membranes could be problematic. In order to avoid this, the Iron(II) is oxidized to Iron(III) in the input tank ('T1') (see figure 3.1). Next, the precipitation of Iron(III) hydroxide would take place in this tank, before the input of the RO plant, avoiding the fouling of the RO membranes. Notice the red colour of tank 'T1' is caused by the precipitation of this component.

– The permeate stream is aggressive, the feed stream is in equilibrium calcium carbonate, and the reject stream is very slightly scaling. The addition of antiscaling should be enough to avoid the precipitation of calcium carbonate and the addition of hydrochloric acid could be stopped. See Elfil and Roques (2004) and Elfil and Hannachi (2006). The extra consumption of acid is common in large-scale desalination plants, where the most important issue is to assure the inhibition of calcium precipitation, even if the consumption of acid is not optimal. On the contrary, for small-scale desalination plants, placed in remote areas with difficult access, the acquisition and transport of chemicals may be a difficult and long procedure, and the minimization of their consumption is one of the main issues.

3.1.4 Energy Supply System

The power required by the RO pilot plant is provided by an autonomous (off-grid) power energy system. It is based on a three-phase AC electric bus. Under optimal conditions, the power is provided by solar panels and a wind turbine. When no renewable energy is available, the system can be operated with a diesel generator. In addition, the system has a set of batteries, whose tasks are: 1) to store energy when an excess of renewable energy is available; and 2) to synchronize the three-phase bus. This synchronization is carried out by three bidirectional commercial inverters, from the company SMA, which are connected between the batteries and the three-phase bus. Finally, the system has a set of inverters, from the same company, to connect the solar panels and the wind turbine with the three-phase bus. See Tadeo et al. (2009) and Salazar et al. (2010b) for a description of this energy supply system, and McGowan et al. (1996), McGowan and Manweli (1998), and Nfah and Ngundam (2008) for the modelling of hybrid power systems.

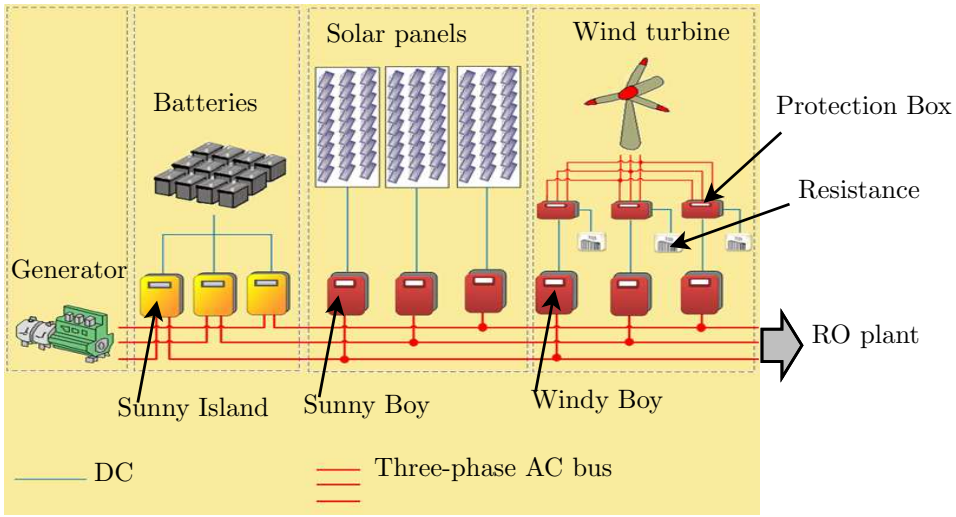

Figure 3.9: Energy supply system. Adapted from Salazar et al. (2010b).

The power energy system consists of the following elements:

– Three sets of solar panels (one for each phase). Each set includes

(a) Diesel generator. (b) Internal detail.

Figure 3.10: Power energy system for the RO pilot plant: Diesel generator.

27 solar modules IS3000P. The maximum power of the solar panels is 135 Wp. See figure 3.11.

- One diesel generator, whose power production is 20 kV·A. (See figure 3.10.)
- One wind turbine Proven 15. The pole is 25 m in height and the maximum power generation, under optimal conditions, is 15 kW. See figure 3.11.
- Twelve batteries PVX2120L (specific for dealing with renewable energies). The maximum stored energy is 30 kWh. See figure 3.12.
- Three SMA Sunny Boy inverters (one for each phase), which transform the DC from the solar panels, to the AC of the bus. See figure 3.12.
- Three SMA Protection Box inverters (one for each phase), which transform the three-phase electric power of the wind turbine, to DC.
- Three SMA Windy Boy inverters (one for each phase), which transform the DC from the SMA Protection Boxes, to the AC of bus.

– Three bidirectional SMA Sunny Island inverters (one for each phase), which connect the sets of batteries to the bus. See figure 3.12.

Figure 3.11: Power energy system for the RO pilot plant: Solar panels and wind turbine.

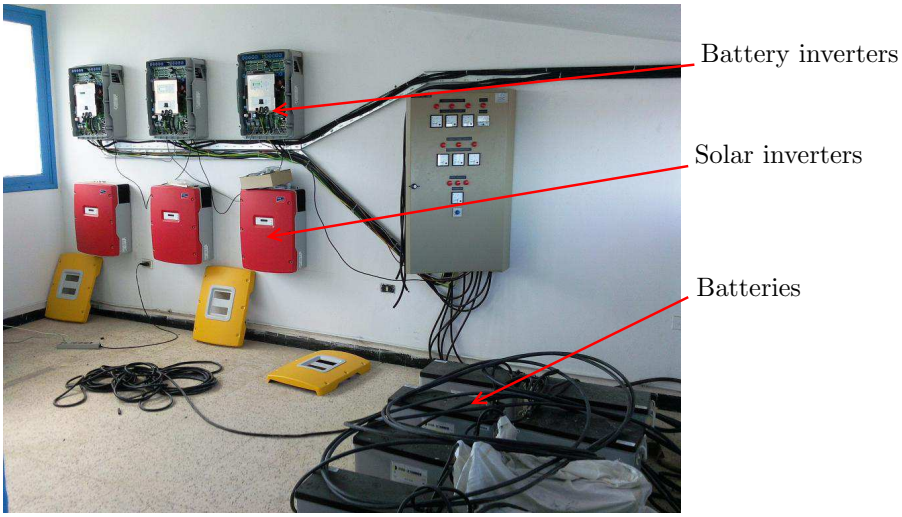

Figure 3.12: Power energy system for the RO pilot plant: Set of batteries, solar power inverters and battery inverters.

Figure 3.9 shows a diagram of the energy supply system. Next, figures 3.11-3.12 show several pictures of the installation of the energy supply system: the solar panels, the wind turbine, the diesel generator, the batteries and a set of inverters.

3.2 Parameter Estimation

The pilot plant was specially designed for testing and experimentation and has a high number of sensors, more than in a typical RO plant. The pressure, volumetric flow and salt concentration may be measured in different points of the plant. As commented previously, the sensors are managed from a PLC, while the data loading is done by a computer connected to the PLC.

Figure 3.13 shows the simulated pilot plant using the ROSIM library. Each component of the real plant (figure 3.5) is linked with one component of the simulator. The blue lines are hydraulic connections (port '`p_osm`' of the ROSIM library) and simulate real connections between components of the plant, while the orange lines are analogue connections (port '`p_1`') and simulate electrical connections of the control system.

The components of the simulator should be parametrized to fit it to the particular conditions of the pilot plant. Some parameters are easily obtained: they may be provided by the manufacturer (such as the characteristic curve of a pump), measured directly from the plant (such as the height and diameter of a tank), or may depend on the environmental conditions (such as the salt concentration and the temperature of the feed flow). Other parameters, however, should be estimated for each particular plant.

The components of the simulator are described below:

- Component 'well' simulates the well and the source of feed water. It is parametrized with the following data:
  - Measured in the plant: Concentration of salt, solids, and suspended particles, pH, temperature.
- Component 'P1' simulates an on/off pump, which carries feed water from the well to the input tank 'T1'. Component 'P2' simulates another on/off pump, which pumps feed water from this

tank to the supply tank 'T2'. Both components are parametrized with the following data:

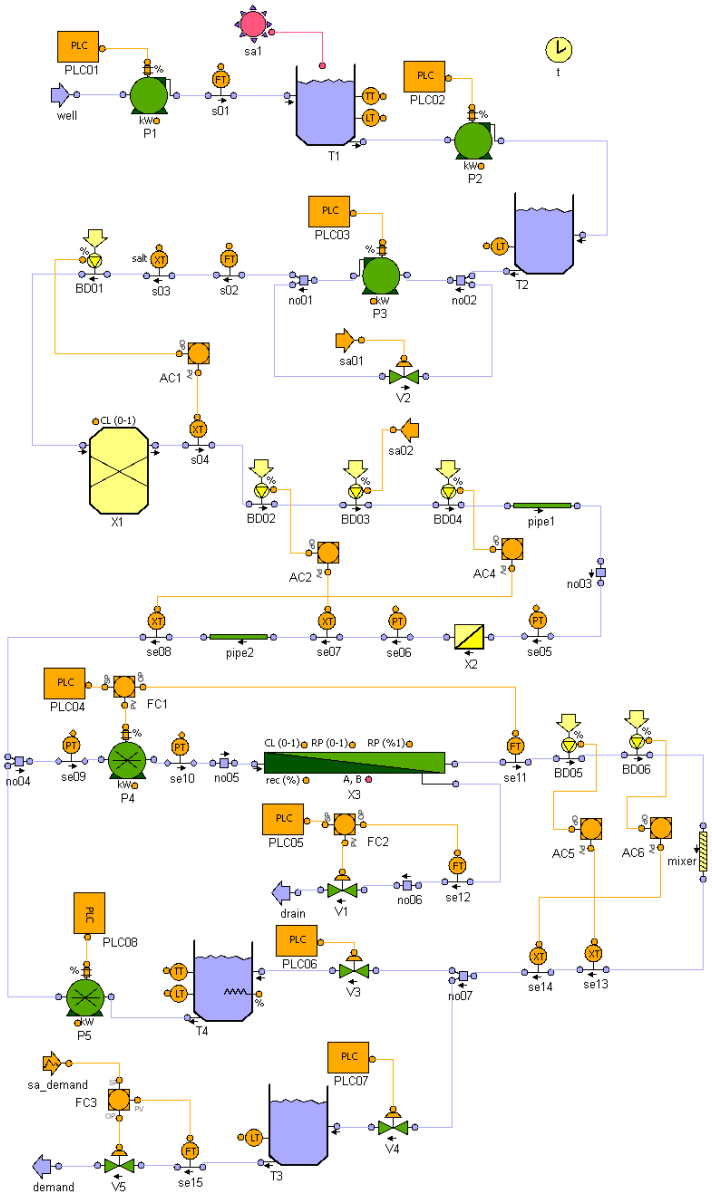

Figure 3.13: Graphic display of the simulated pilot plant using the ROSIM library.

  - Given by the manufacturer: Characteristic curves of the pumps.

- Component ‘T1’ simulates the input tank (see figure 3.1) and ‘T2’ simulates the supply tank (see figure 3.4). These components are parametrized with the following data:
  - Measured in the plant: Area of the base, height of the tanks, height of the input/output connections.
  - Parameters that should be estimated: Evaporation coefficient.
- Component ‘P3’ simulates a centrifugal pump, which carries water from the tank ‘T2’ to the filters. It is parametrized with the following data:
  - Given by the manufacturer: Characteristic curves of the pump.
- Component ‘V2’ simulates a manual ball valve. It is parametrized by the following data:
  - Given by the manufacturer: Characteristic curve of the valve.
  - Parameters that should be estimated: Characteristic valve constant.
- Components ‘BD01’ and ‘AC1’ simulate the addition of sodium hypochlorite. They are parametrized by the following data:
  - Measured in the plant: Volume of the dosage pump, concentration of the dosage, maximum flow of the dosage pump, parameters of the PID tuning.
  - Parameters that should be estimated: Coefficients for the pressure drop.
- Component ‘X1’ simulates a sand filter (see figure 3.3). It is parametrized by the following data:
  - Measured in the plant: Area of the base, height of the tanks, height of the input/output connections, efficiency.

  - Parameters that should be estimated: Coefficients for the pressure drop, porosity, maximum capacity for solids captured, maximum available pressure drop.

- Components 'BD02' and 'AC2' simulate the addition of sodium bisulfite. They are parametrized by the following data:
  - Measured in the plant: Volume of the dosage pump, concentration of the dosage, maximum flow of the dosage pump, parameters of the PID tuning.
  - Parameters that should be estimated: Coefficients for the pressure drop.

- Components 'BD03' simulates the addition of antiscalant. It is parametrized by the following data:
  - Measured in the plant: Volume of the dosage pump, concentration of the dosage, maximum flow of the dosage pump.
  - Parameters that should be estimated: Coefficients for the pressure drop.

- Components 'BD04' and 'AC4' simulate a control of the pH of the stream. They are parametrized by the following data:
  - Measured in the plant: Volume of the dosage pump, concentration of the dosage, maximum flow of the dosage pump, parameters of the PID tuning.
  - Parameters that should be estimated: Coefficients for the pressure drop.

- Components 'pipe1' and 'pipe2' simulate two sections of the pipe. They are parametrized by the following data:
  - Measured in the plant: Diameter of the pipes.
  - Parameters that should be estimated: Coefficients for the pressure drop, equivalent length of the pipe (embracing real length, elbows, joint, etc.).

- Component 'X2' simulates a cartridge filter. It is parametrized by the following data:

  - Measured in the plant: Efficiency.
  - Parameters that should be estimated: Coefficients for the pressure drop, maximum capacity for solids captured, maximum available pressure drop.

- Component 'P4' simulates a high-pressure positive-displacement pump (see figure 3.3). It is parametrized by the following data:
  - Given by the manufacturer: Efficiency of the pump, minimum and maximum speed.
  - Parameters that should be estimated: Curve velocity vs flow.

- Component 'FC1' simulates the speed control of the pump 'P4'. It is parametrized by the following data:
  - Given by the manufacturer: Efficiency of the pump.
  - Measured in the plant: Parameters of the PID tuning.

- Component 'X3' simulates two parallel pressure vessels, with eight RO modules (see figure 3.4). It is parametrized by the following data:
  - Given by the manufacturer: Number of RO modules, area of each module, water recovery, salt rejection, pH limits.
  - Parameters that should be estimated: Water permeability, salt permeability, parameters for the ageing of the membrane, parameters for the calculation of the pressure drop.

- Components 'BD04' and 'AC5' simulate a control of the pH of the stream. They are parametrized by the following data:
  - Measured in the plant: Volume of the dosage pump, concentration of the dosage, maximum flow of the dosage pump, parameters of the PID tuning.
  - Parameters that should be estimated: Coefficients for the pressure drop.

- Components 'BD06' and 'AC6' simulate the addition of sodium hypochlorite. They are parametrized by the following data:

  - Measured in the plant: Volume of the dosage pump, concentration of the dosage, maximum flow of the dosage pump, parameters of the PID tuning.
  - Parameters that should be estimated: Coefficients for the pressure drop.

- Component 'mixer' simulates a homogenizer. It is parametrized by the following data:
  - Measured in the plant: Diameter and length of the homogenizer.
  - Parameters that should be estimated: Coefficients for the pressure drop.

- Component 'T4' simulates the cleaning tank (see figure 3.4). It is parametrized with the following data:
  - Measured in the plant: Area of the base, height of the tank, height of the input/output connections.
  - Parameters that should be estimated: Heat coefficient.

- Component 'P5' simulates a centrifugal pump, which is used for cleaning. It is parametrized with the following data:
  - Given by the manufacturer: Characteristic curves of the pump.

- Component 'T3' simulates the output tank of the desalination plant. It is parametrized with the following data:
  - Measured in the plant: Area of the base, height of the tank, height of the input/output connections.
  - Parameters that should be estimated: Evaporation coefficient.

- Component 'FC3' simulates the water demand of the settlement. It is parametrized by the following data:
  - Fit by the user: Curve of the water demand over time.

- Components ‘V1’ simulate a manual valve, which controls the reject flow (see figure 3.3). It is parametrized by the following data:
  - Given by the manufacturer: Characteristic curve of the valve.
  - Parameters that should be estimated: Characteristic valve constant.
- Components ‘V3’ and ‘V4’ simulate manual ball valves. They are parametrized by the following data:
  - Given by the manufacturer: Characteristic curve of the valve.
  - Parameters that should be estimated: Characteristic valve constant.
- Components ‘V5’ simulate a control valve. It is parametrized by the following data:
  - Given by the manufacturer: Characteristic curve of the valve.
  - Parameters that should be estimated: Characteristic valve constant.
- Components ‘PLC01’, ‘PLC02’, ‘PLC03’, etc. embrace the protocol for cleaning, stops and start-up, which is carried out by the PLC.
- Components ‘s01’, ‘s02’, ‘s03’, etc. simulate different types of sensors and do not need to be parametrized.
- Components ‘no01’, ‘no02’, ‘no03’, etc. simulate connections between pipes and do not need to be parametrized.

Figure 3.14 shows the procedure to calculate the unknown parameters of the simulator.

Where u symbolizes the boundaries of the system, such as the temperature and the salt concentration of the feed flow, and the independent variables, such as the setpoint of the different control loops;

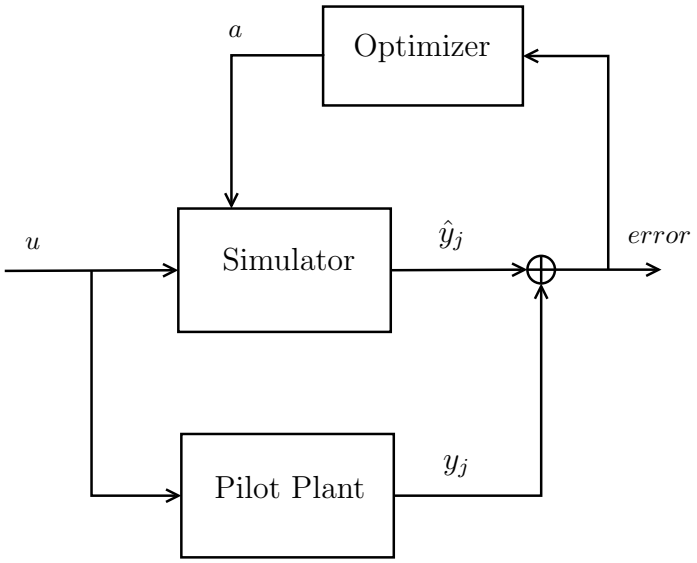

Figure 3.14: Flow diagram of the paramter estimation.

a symbolizes the unknown parameters of the components of the simulator, which are fitted by the optimizer during the parameter estimation; y symbolizes the main variables of the desalination plant that may be measured, and characterize properly the state of the desalination plant, such as the flow, the pressure and the concentration in different points of the pilot plant; $\hat{y}$ symbolizes the same variables, but calculated from the simulator; and *error* is the difference between the measured variables (y) and the calculated variables ($\hat{y}$).

Depending on the evolution of the inputs of the system (the boundaries and the independent variables), the behaviour of y and $\hat{y}$ will vary. The optimizer will adjust the unknown parameters of the simulator (a), trying to equalise the behaviour of $\hat{y}$ with the behaviour of y. In order to achieve a good parameter estimation, the evolution of the boundary variables should be fitted correctly by the user. It should take into account a wide number of states, and embrace the main situations of the plant. On the other hand, if a state is duplicated or prolonged in excess, the working time will be increased without any improvement of the parameter estimation.

The optimizer manipulates the unknown parameters, minimizing an objective function that embraces the errors between y and $\hat{y}$. This

is a dynamic optimization problem as shown in equation (3.1):

$$\min_{a} \text{Objective function} = \sum_{j=1}^{N} \sum_{i=1}^{K} \frac{(y_j(i) - \hat{y}_j(i))^2}{\sigma_j} \tag{3.1}$$

where N is the number of measured variables, K is the number of sample times, and σ_j is the standard deviation of each variable.

Since the error between y and $\hat{y}$ is squared, all the errors are positive. Besides, the error of each variable is divided by its standard deviation, to weight all variables in the addition. The minimization of the objective function may be solved by any non linear optimization algorithm, such as Sequential Quadratic Programming (SQP), which is available in the environment EcosimPro.

3.2.1 RO Membranes and High-Pressure Pump

The parameter estimation of the RO membranes and the high-pressure pump may be calculated independently of the rest of the components, as is described here. As commented on in chapter 2, the KK model calculates the water flux that crosses an RO membrane as follows:

$$J_w = A_w \cdot (\Delta P - \Delta \pi) \tag{3.2}$$

where a value of 1 for the reflection coefficient (σ) has been assumed.

The total permeate flow may be calculated as shown below:

$$Q_p = A \cdot n_m \cdot J_w \tag{3.3}$$

where A is the area of each RO module, and n_m is the number of modules. In the case of the pilot plant, $A = 7.9$ m^2, and $n_m = 8$ RO modules.

This means that if the permeate flow (Q_p) is plotted versus the pressure difference ($\Delta P - \Delta \pi$), the results should be a straight line, whose slope is the water permeability times the total area of the membranes. Figure 3.15 shows experimental data for the permeate flow versus the pressure difference. The different colours correspond to different experiments (with different characteristics of the feed water), while the black lines are the fitting straight lines.

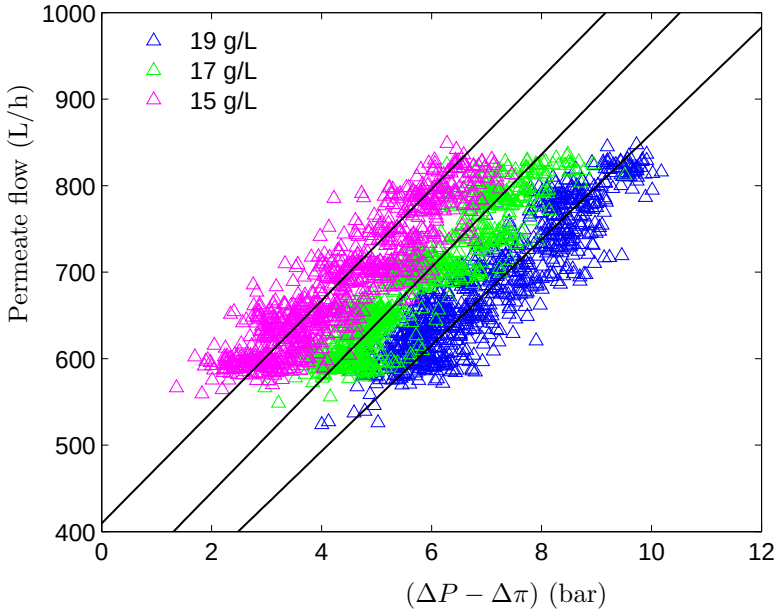

Figure 3.15: Behaviour of the permeate flow versus the pressure difference. Triangles are experimental data from the pilot plant. Magenta, green and blue colours correspond to three different experiments, with different salt concentrations of the feed flow. The black lines are the fitting lines. The slope of these lines are the water permeability of the pilot plant times the total area of the membranes.

From the average slope of the three straight lines, the water permeability results:

$$\text{slope of figure 3.15} = 65.6 \ \ \text{L/(h·bar)} \tag{3.4}$$

$$A_w = 1.04 \ \ \text{L/(m}^2\text{·bar·h)} = 2.89 \cdot 10^{-7} \ \ \text{m/(bar·s)} \tag{3.5}$$

On the other hand, the KK model calculates the salt flux that crosses an RO membrane as follows:

$$J_s = B_s \cdot (C_f - C_p) \tag{3.6}$$

The salt concentration of the permeate flow (C_p) may be calculated

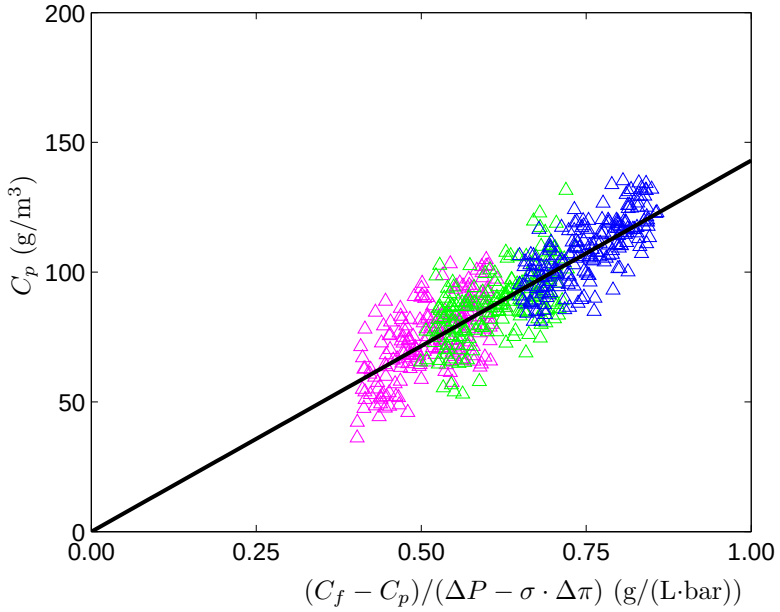

Figure 3.16: Behaviour of the salt concentration of the permeate flow versus the $\frac{C_f - C_p}{\Delta P - \sigma \cdot \Delta\pi}$. Triangles are experimental data from the pilot plant. Magenta, green and blue colours correspond to three different experiments, with different salt concentrations of the feed flow. The black lines are the fitting lines. The slope of these lines are the water permeability of the pilot plant times the total area of the membranes.

dividing equation (3.6) by equation (3.2)[3], whose result is shown in equation (3.7):

$$C_p = \frac{J_s}{J_w} = \frac{B_s}{A_w} \cdot \underbrace{\frac{C_f - C_p}{\Delta P - \sigma \cdot \Delta\pi}}_{[1]} \tag{3.7}$$

By plotting the salt concentration of the permeate versus the term [1] of equation (3.7), the results should be a straight line, whose slope is the salt permeability divided by the water permeability, which was

[3]Notice the units of the salt permeate flux (J_s) are kg/(m^2·s), while the units of the water permeate flux (J_w) are m^3/(m^2·s).

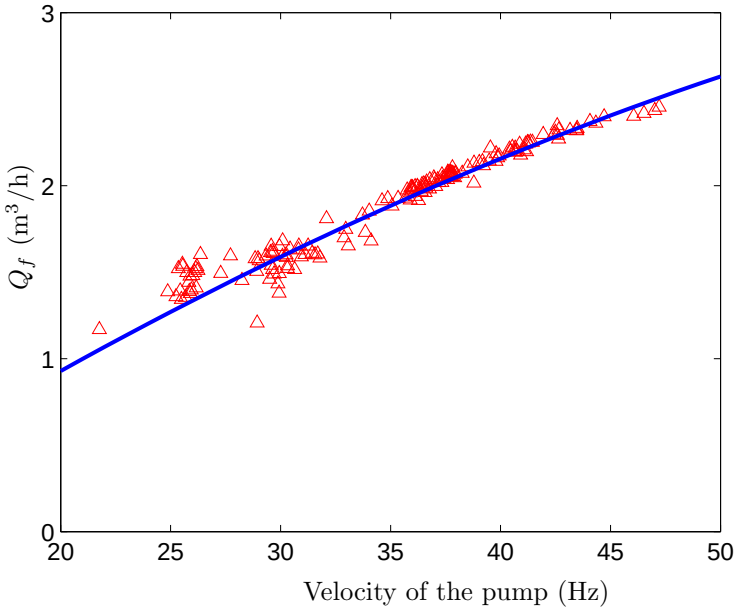

Figure 3.17: Characteristic curve of the high-pressure pump. Red triangles are experimental data from the pilot plant, while the blue line is the fitting polynomial.

calculated previously. Figure 3.16 shows experimental data for the salt concentration of the permeate flow, versus the term [1] from the previous equation, assuming a value of 1 for the reflection coefficient (σ). From this figure and equation (3.5), the salt permeability results:

$$\text{slope of figure } 3.16 = 142 \ \ (\text{L}\cdot\text{bar})/\text{m}^3 = 0.142 \ \ \text{bar} \tag{3.8}$$

$$B_s = 4.10 \cdot 10^{-8} \ \ \text{m/s} \tag{3.9}$$

The high-pressure pump of the pilot plant is a positive displacement pump with a speed control. The relation between the feed flow (Q_f) and the velocity of the pump (u) may be calculated by an empirical equation as follows:

$$Q_f = a_0 + a_1 \cdot u + a_2 \cdot u^2 + ... \tag{3.10}$$

Since the velocity of the pump and the feed flow are measured in the pilot plant, the estimation of the parameters a_0, a_1, a_2... is automatic. Figure 3.17 shows the calculated characteristic curve of the pump. The blue line is the fitting curve (equation (3.10)), while the red triangles are the measured variables. The coefficient of determination of the fitting is > 0.90, while the calculated parameters of the empirical equation are shown below:

$$\begin{cases} a_0 = -668.9 \text{ m}^2/\text{h} \\ a_1 = 89.08 \text{ m}^2/(\text{h}\cdot\text{Hz}) \\ a_2 = -0.462 \text{ m}^2/(\text{h}\cdot\text{Hz}^2) \end{cases} \tag{3.11}$$

3.3 Validation

This section describes three experiments for the validation of the simulator, which was presented in Palacín et al. (2010b,e). The first experiment deals with the validation of the hydraulic (pressure and flow) behaviour of the system. Next, the second experiment deals with the influence of the salt concentration of the feed over the permeate. Finally, the third experiment focuses on the dynamic evolution of salt crossing the membrane.

3.3.1 Pressure and Flow

This experiment consists of the validation of the hydraulic behaviour of the simulator and takes 2 hours. The operating point of the desalination plant is changed by the manipulation of the setpoint of the control loops of the permeate flow and the reject flow. The pressure and flow at different points of the pilot plant are measured and compared with the ones calculated from the simulator. The boundary conditions (u) of the system (the inputs of the simulator) are the profile of the setpoints and the input pressure of the system (figures 3.18 and 3.19).

Figures 3.20-3.24 compare the measured and calculated data. The blue lines are the measured data from the pilot plant, while the red lines are the data provided by the simulator. Figures 3.20 and 3.21 show the behaviour of the pressure, respectively, in the outlet of the

cartridge filter ('X2') and in the outlet of the high-pressure pump. Figures 3.22, 3.23 and 3.24 show the behaviour of the volumetric flow of the feed, permeate and reject respectively. The average error between measured and calculated variables is less than 4%.

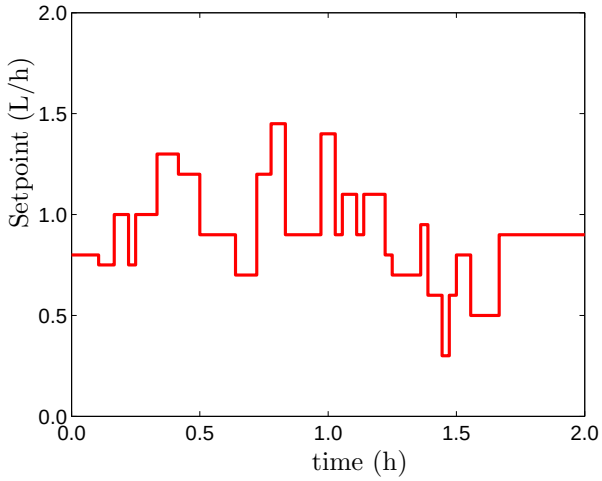

Figure 3.18: Profile of the setpoint of the permeate flow. This variable is an input of the simulator (u).

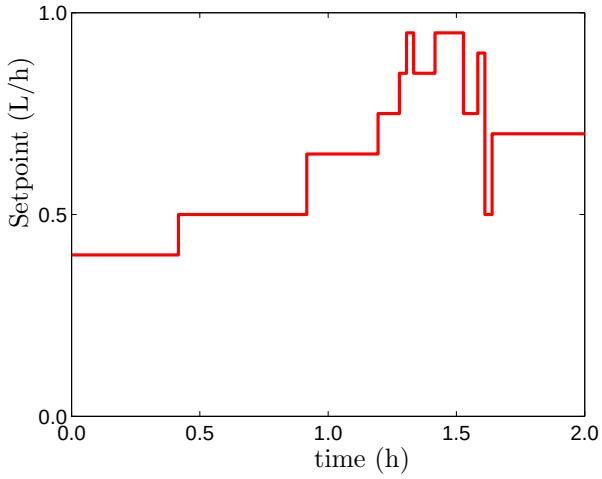

Figure 3.19: Profile of the setpoint of the reject flow. This variable is an input of the simulator (u).

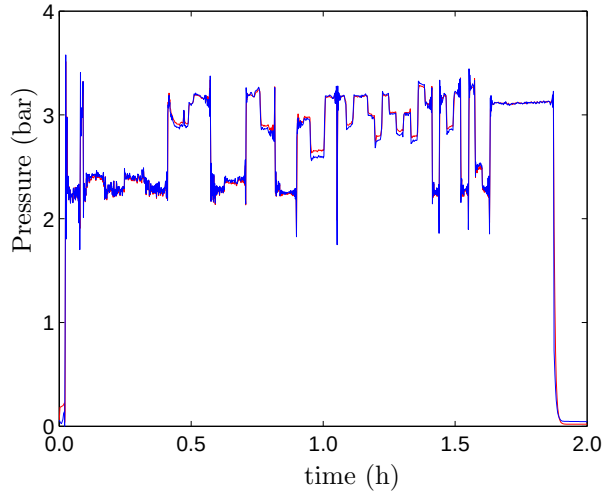

Figure 3.20: Behaviour of the pressure in the outlet of the cartridge filter ('X2'). The blue line is the measured data, from the pilot plant, while the red line is the calculated data from the simulator. 10 minutes before the end, the plant is stopped.

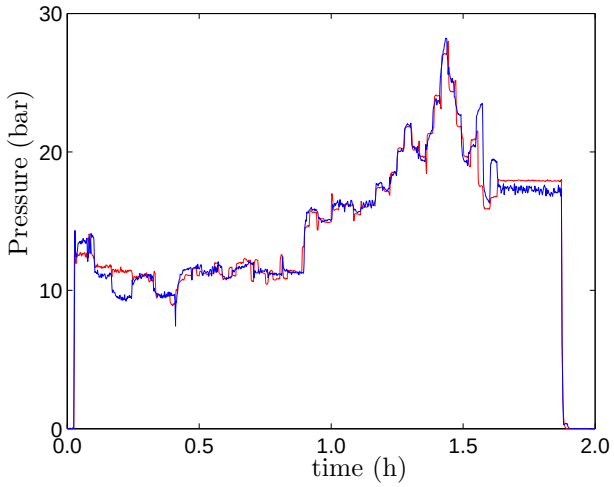

Figure 3.21: Behaviour of the pressure in the outlet of the high-pressure pump ('P4'). The blue line is the measured data from the pilot plant, while the red line is the calculated data from the simulator. 10 minutes before the end, the plant is stopped.

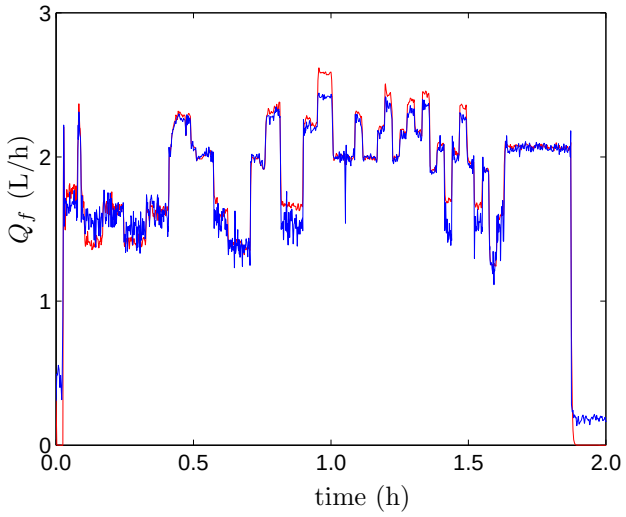

Figure 3.22: Behaviour of the feed flow over 2 hours. The blue line is the experimental data from the pilot plant, while the red line is the calculated data from the simulator.

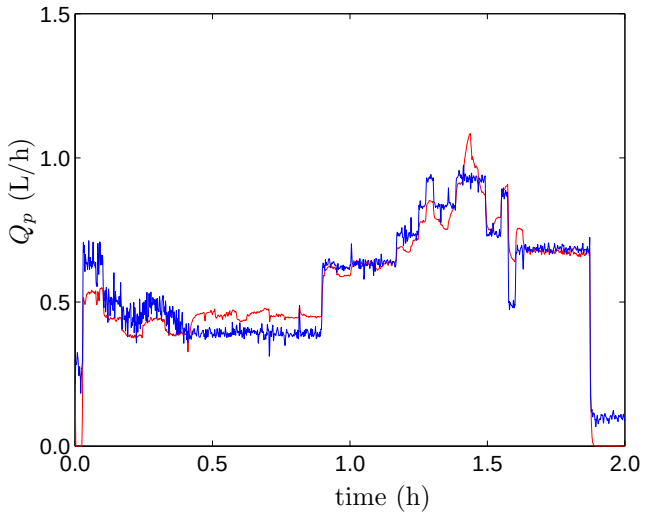

Figure 3.23: Behaviour of the permeate flow over 2 hours. The blue line is the experimental data from the pilot plant, while the red line is the calculated data from the simulator.

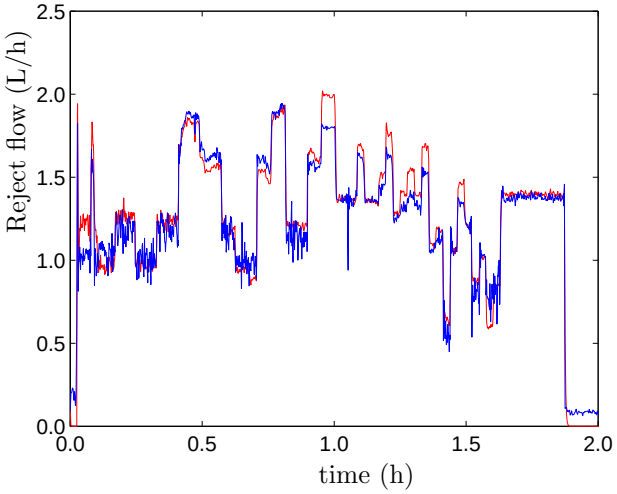

Figure 3.24: Behaviour of the reject flow over 2 hours. The blue line is the experimental data from the pilot plant, while red line is the calculated data from the simulator.

3.3.2 Salt Concentration of the Feed

This experiment consists of the validation of the RO membranes and the influence of the salt concentration of the feed flow. The feed flow and the recovery ratio are changed by manipulating the setpoint of the control loops of the permeate flow and the reject flow. The experiment takes 15 minutes and is repeated three times, with three different salt concentrations of the feed flow: 15, 17 and 19 g/L. The boundary variables (u) of the system (the inputs of the simulator) are the profile of the setpoints (figures 3.25 and 3.26).

Figures 3.25 and 3.26 show the profile of both setpoints which are followed during the experiment, while figures 3.27-3.29 compare the measured and calculated data. The magenta, green and blue lines are the measured water flow crossing the membrane, whose salt concentrations of the feed flow are, respectively, 15, 17 and 19 g/L, and are shown in figures 3.27, 3.28 and 3.29. The black lines correspond to the calculated permeate flow from the simulator. Finally, figure 3.30 shows the calculated behaviour of the velocity of the high-pressure pump, for the three experiments. The average error between measured and calculated variables is less than 2%.

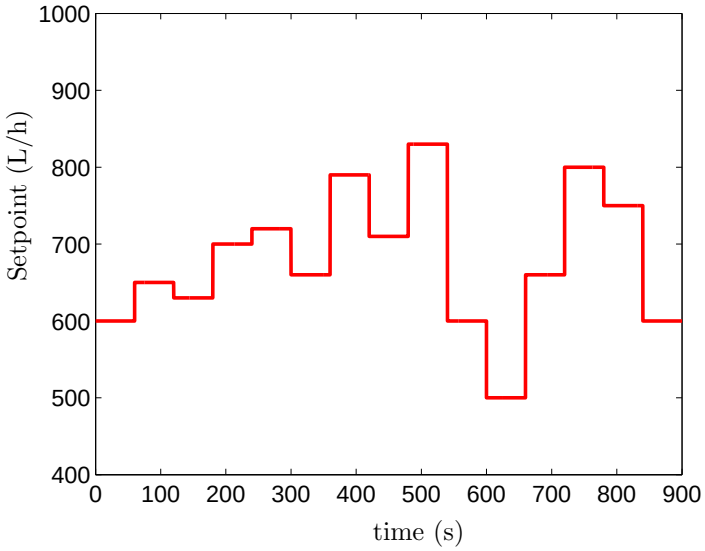

Figure 3.25: Profile of the setpoint of the permeate flow. This variable is an input of the simulator (u).

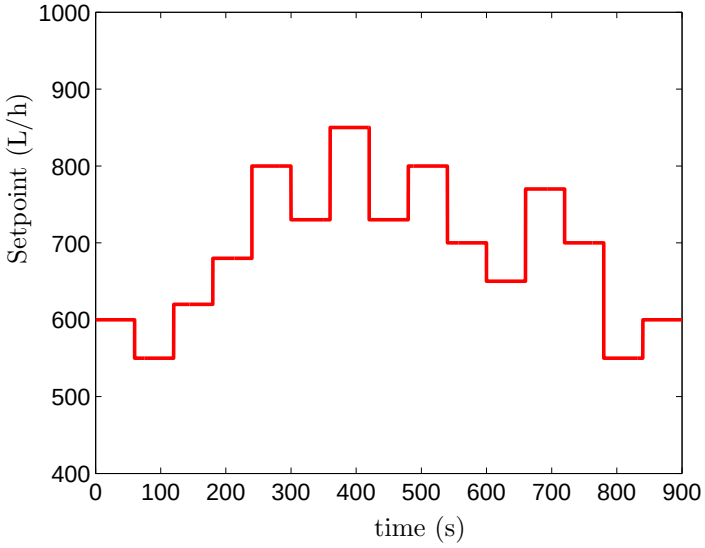

Figure 3.26: Profile of the setpoint of the reject flow. This variable is an input of the simulator (u).

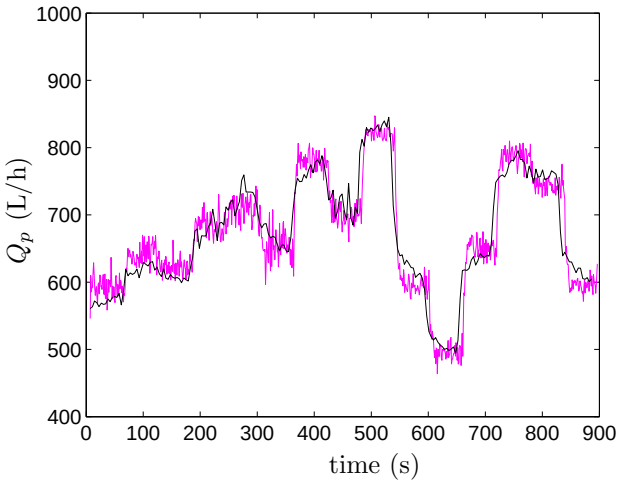

Figure 3.27: Behaviour of the permeate flow over 15 minutes. The magenta line is the measured data from the pilot plant, while the black line is the calculated data from the simulator. The salt concentration of the feed flow is 15 g/L.

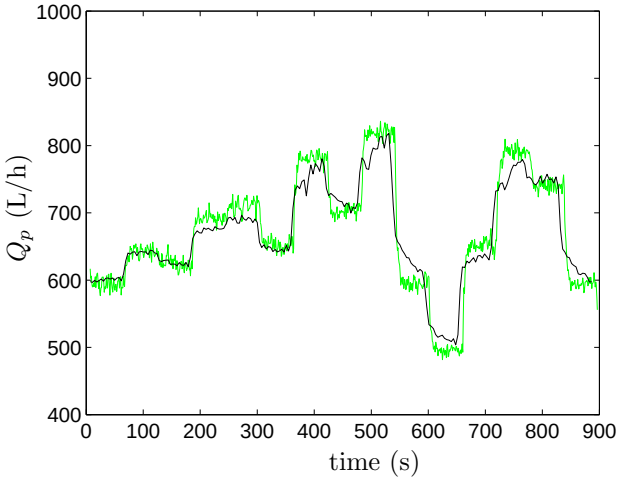

Figure 3.28: Behaviour of the permeate flow over 15 minutes. The green line is the measured data from the pilot plant, while the black line is the calculated data from the simulator. The salt concentration of the feed flow is 17 g/L.

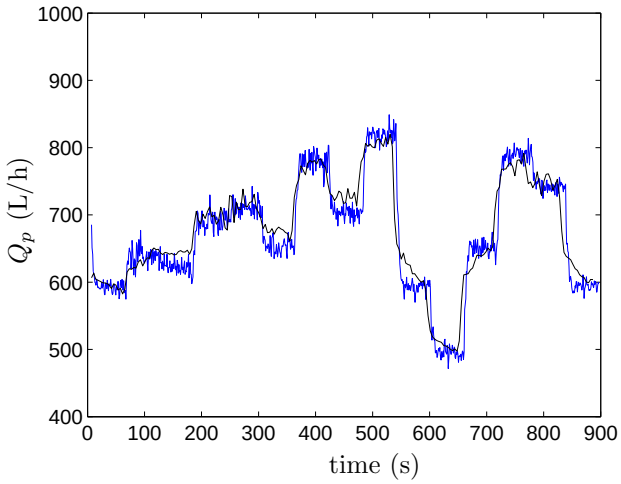

Figure 3.29: Behaviour of the permeate flow over 15 minutes. The blue line is the measured data from the pilot plant, while the black line is the calculated data from the simulator. The salt concentration of the feed flow is 19 g/L.

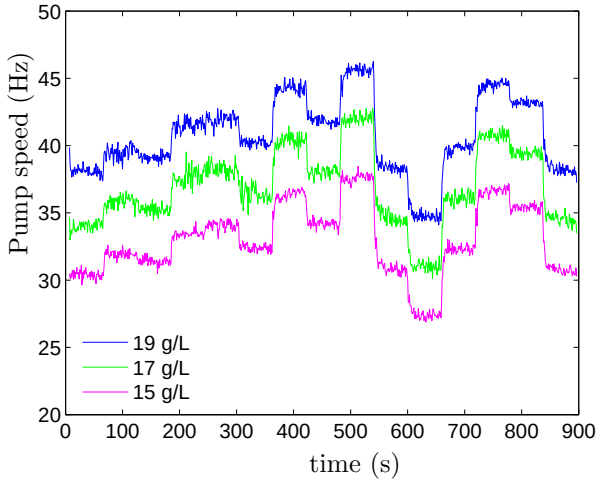

Figure 3.30: Behaviour of the pump speed for the three experiments. The magenta, green and blue lines correspond to the salt concentrations of the feed of 15, 17 and 19 g/L.

3.3.3 Salt Permeability

This experiment consists of the validation of the dynamic behaviour of the salt concentration that crosses the membrane. After a flushing of the membrane, working at a constant operating point, the salt concentration of the permeate is measured and compared with that calculated from the simulator. Although the operating point is constant, the salt concentration takes several minutes to get the steady state. The experiment is repeated three times, with three different salt concentrations of the feed flow: 15, 17 and 19 g/L. The feed flow is kept around 1 500 L/h and the water recovery around 50%. Figures 3.31, 3.32 and 3.33 show, respectively, the behaviour of the permeate concentration for the three experiments.

The magenta, green and blue triangles are, respectively, the measured data for the three experiments, while the black lines are the calculated behaviour of the salt concentration. The profile of the calculated concentration comes from an equation with the form shown in equation (3.12) (see section 2.1.2).

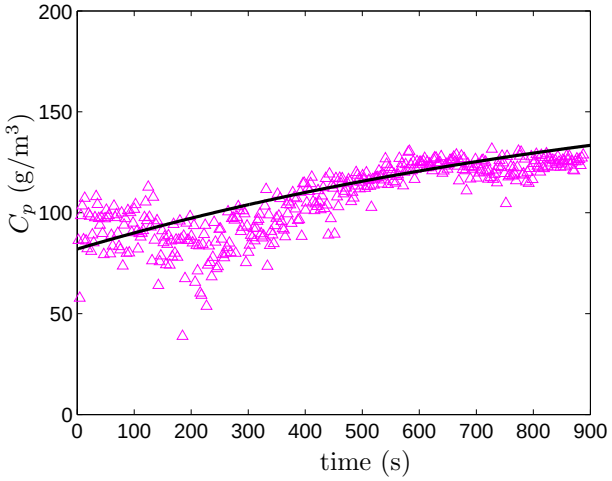

Figure 3.31: Behaviour of the salt concentration permeate flow over 15 minutes. The magenta triangles are the measured data from the pilot plant, while the black line is the calculated data from the simulator. The salt concentration of the feed flow is 15 g/L.

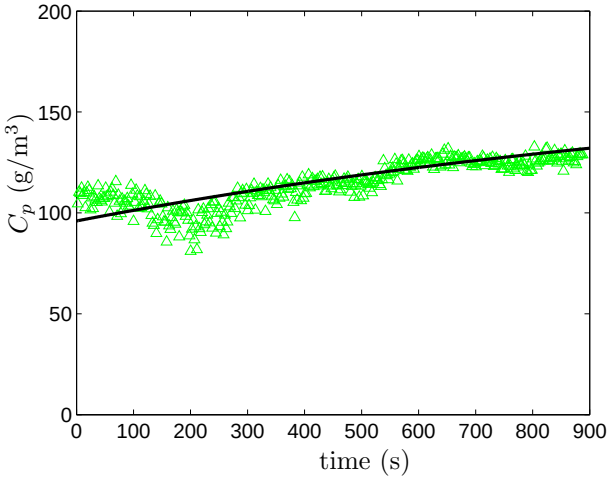

Figure 3.32: Behaviour of the salt concentration permeate flow over 15 minutes. The green triangles are the measured data from the pilot plant, while the black line is the calculated data from the simulator. The salt concentration of the feed flow is 17 g/L.

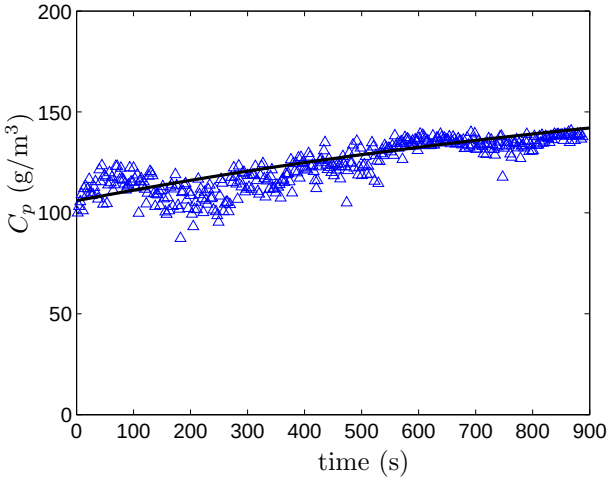

Figure 3.33: Behaviour of the salt concentration permeate flow over 15 minutes. The blue triangles are the measured data from the pilot plant, while the black line is the calculated data from the simulator. The salt concentration of the feed flow is 19 g/L.

$$A_w = A_{w0} \cdot \exp(-\frac{t}{\Gamma}) \tag{3.12}$$

where A_w is the hydraulic permeability, A_{w0} is the initial hydraulic permeability, t is the time from the last flushing or cleaning, and Γ is a parameter that depends on each system. For the pilot plant, the value of Γ was estimated around 1 300 seconds.

The results of the validation are moderate. The inertia and the evolution of the hydraulic variables (pressure and flow) calculated by the simulator follow the same behaviour as the variables measured in the pilot plant. The pipes and valves are characterized correctly with the pressure drop, while the centrifugal pumps are modelled with the characteristic curve, provided by the manufacturer. The positive-displacement high-pressure pump is easily simulated using an empirical equation. The permeate flow that crosses the membrane is correctly calculated depending on the characteristics of the feed water and the operating point (feed flow and water recovery). The behaviour of the salt concentration of the permeate is very noisy, and only an average behaviour can be estimated from the simulator.

Chapter 4

Advanced Control

This chapter deals with the advanced control of small-scale desalination plants, powered by an autonomous power energy system. These desalination plants are very popular for providing drinkable water to small settlements, located in remote regions. The advanced control is studied and tested in the desalination pilot plant described in section 3.1, which represents this kind of desalination plants.

The main objective of the control system is the fulfilment of the water demand of the village. The water demand is not constant, but changes with time. The shape of the water demand is approximately repeated each 24 hours, while its average value depends on the day of the week and the month of the year. Each town has its own characteristic curve of water demand, which depends on such characteristics of the settlement, as the population, the presence and type of industry, and the geographical location. Although the water demand may vary strongly between two different settlements, it can be easily estimated using historical data for the corresponding town.

The second objective of the control system is to optimize the energy consumption of the plant, which is mostly due (above 80%) to the high-pressure pump and the supply pumps. The pilot plant is integrated with an energy supply system, which generates enough energy to power the plant. The energy supply system is autonomous and based on a set of solar panels and a wind turbine. As well as the water demand, the availability of renewable energy (solar radiation and wind velocity) varies during the day. When no renewable energy is available, the energy supply system uses a diesel generator to provide enough energy

to operate the plant. The control system aims to minimize the use of the diesel generator, while still fulfilling the water demand. By manipulating the desalination plant as an active charge and coupling the energy consumption with the control of the energy production, the optimization of the energy consumption may be made easier.

Finally, the control system should deal with the requirement of plant cleaning. In the case of the pilot plant, there are four types of cleaning, as follows: 1) the flushing of the RO membranes is carried out each two hours and lasts three minutes; 2) the washing of the RO membranes is carried out once a day and lasts 15 minutes; 3) the cleaning of the sand filter is carried out once a week and lasts 20 minutes; and 4) the chemical cleaning of the plant, which is done only if the fouling of the RO membranes has occurred (maybe once a year). The advanced control presented in this chapter deals only with the washing of the RO membranes and the cleaning of the sand filter, while the flushing and the chemical cleaning are not considered due to their time scales.

In the case of the pilot plant, the manipulated variables of the control system are: 1) the feed flow, which is controlled by a speed control of the high-pressure pump ('P4' in figure 3.2 at page 105); 2) the reject flow, which is controlled by a control valve at the outlet of the train of pressure vessels ('V1'); 3) the behaviour of the supply pumps ('P1' and 'P2'), which are of on/off type and alternate between on/off switches; and 4) the time instant for the washing of the RO modules ('X3') and the cleaning of the sand filter ('X1').

Consequently, the control system is of hybrid type, considering that it works with both continuous variables (such as the water demand, the availability of renewable energy, the behaviour of the high-pressure pump, and the reject flow) and discrete variables (such as the use of the diesel generator, the cleaning of the plant, and the behaviour of the on/off pumps).

The optimization of the operation has been approached using the advanced control of the pilot plant. The advanced control takes into account the prediction of the variable water demand and the variable availability of renewable energy, and minimizes the use of non-renewable energy, while still fulfilling the water demand and the periodic cleaning. Several advanced control techniques have been studied for the pilot plant. In particular, section 4.1 describes a Model-based

Predictive Control (MPC) of the plant, while section 4.2 proposes the integrated process and control design of the system. Finally, section 4.3 shows the optimization of the scheduling of a desalination plant, on a long-term scale.

4.1 Model-based Predictive Control

The idea behind the MPC is to use the desalination plant as an active charge, and couple the energy consumption and the system operation in the same problem. The control problem is formulated jointly with an economic aim: to fulfil the variable water demand, while minimizing the non-renewable energy consumption. Coupling the energy consumption with the control of the desalination plant, the operation of the system may be improved. Each sample time, the advanced control solves an optimization problem, which minimizes a certain objective function that penalizes the use of diesel. The optimization problem takes into account the prediction of water demand, as well as the prediction of availability of renewable energy (solar radiation and wind velocity), while fulfilling the constraints of the control problem (mainly the fulfilment of the water demand). The MPC of the desalination pilot plant was presented in Palacín et al. (2009d, 2010d, 2011a).

Figure 4.1 shows the structure of the advanced control, where u symbolizes the manipulated variables of the advanced control (such as the feed flow and the operating point), x symbolizes the evolution of the water demand and the availability of renewable energy, $\hat{x}$ symbolizes the prediction of the previous variables, y symbolizes the main variables that characterize the state of the system (such as the level of the tanks and the ratio of coverage), J symbolizes the cost function of the optimization problem, and z symbolizes the parameters (fixed by the user) and the constraints of the optimization problem. Each sample time, depending on the difference between x and $\hat{x}$, the advanced control recalculates the predictions, based on the new measured data.

Section 4.1.1 describes the mathematical formulation of the optimization problem. Then, section 4.1.2 describes the simplified modelling of the desalination system that is used in advanced control. Next, sections 4.1.3, 4.1.4 and 4.1.5 describe, respectively, the predic-

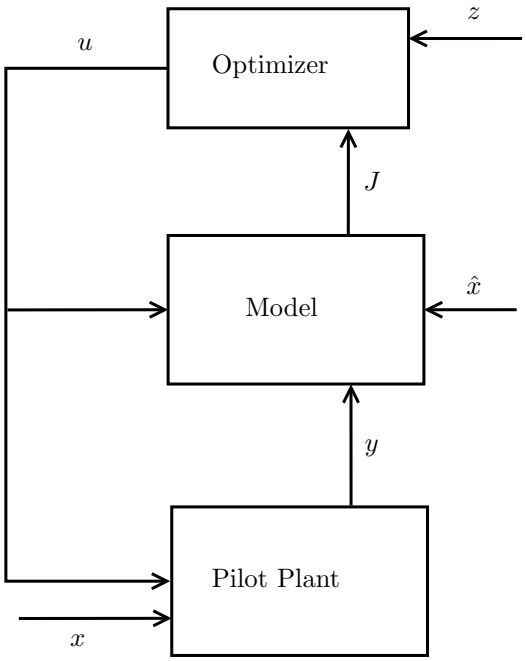

Figure 4.1: Flow diagram of the advanced control.

tions of the water demand, the solar radiation and the wind velocity. Finally, section 4.1.7 shows the behaviour of the desalination pilot plant using predictive control.

4.1.1 Mathematical Formulation

The manipulated variables that can be modified in the control problem are described below. The symbols correspond to the flow diagram of the RO pilot plant, as seen in figures 3.2 and 3.13 at pages 105 and 120, respectively.

- The feed flow (Q_f), which is pumped by the high-pressure pump ('P4').
- The reject flow (Q_p), which is manipulated by a control valve ('V1').
- The on/off signals that active the first supply pumps ('P1'), which pumps brackish water from a well to an input tank ('T1').

– The on/off signals that active the second supply pumps ('P2'), which pumps brackish water from the input tank ('T1') to a supply tank ('T2').

– The on/off signal that activates the cleaning of the system.

The nominal value of the high-pressure pump is 1.5 m^3/h, and thanks to the speed control, the feed flow may be modified by approximately 30% around this value. While the reject flow may be manipulated by the control valve, between 0.5 and 3 m^3/h. The supply pumps ('P1' and 'P2') are on/off centrifugal pumps, which may pump a water flow several times higher than the nominal flow of the high-pressure pump. Thus, these pumps will be switched off most of the time. Finally, in order to increase the life of the membranes, a cleaning of the RO modules should be done once a day.

4.1.1.1 Formulation of the Manipulated Variables

The feed flow and the reject flow are continuous variables, while the profile of the supply pumps and the cleaning of the system are discrete variables. For the optimization problem, the discrete variables should be formulated in the appropriate way, as seen below.

The classical formulation for discrete variables consists in attaching a value (in the case of an on/off pump, 0 or 1) to the variable, every sampling period. For example, the profile of the supply pump 'P1', as seen in figure 4.2, may be formulated as follows:

$$u_{P1} = [0, 0, 0, 0, 1, 1, 1, 1, 0, 0, 1, 1...]_{1\times K} \tag{4.1}$$

where K is the number of sample times, 0 indicates that the pump is stopped, and 1 indicates that the pump is running.

In order to formulate the optimization problem in practical terms, the discrete variables are reformulated using continuous parametrization, as symbolized in figure 4.3 and seen in equation (4.2). (See Sarabia et al. (2009) for an in-depth description of this formulation.)

$$u_{P1} = \begin{bmatrix} t_1 & t_2 & \cdots \\ dt_1 & dt_2 & \cdots \end{bmatrix}_{2\times n} \tag{4.2}$$

where t_i is the time instant for each switch on of the variable, dt_i is the duration of each switch, and n is the number of switches.

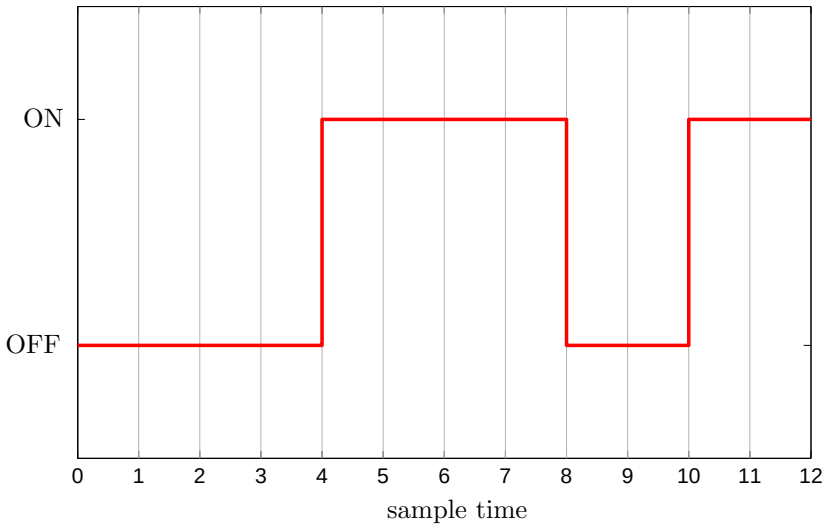

Figure 4.2: Classical formulation of the discrete variables.

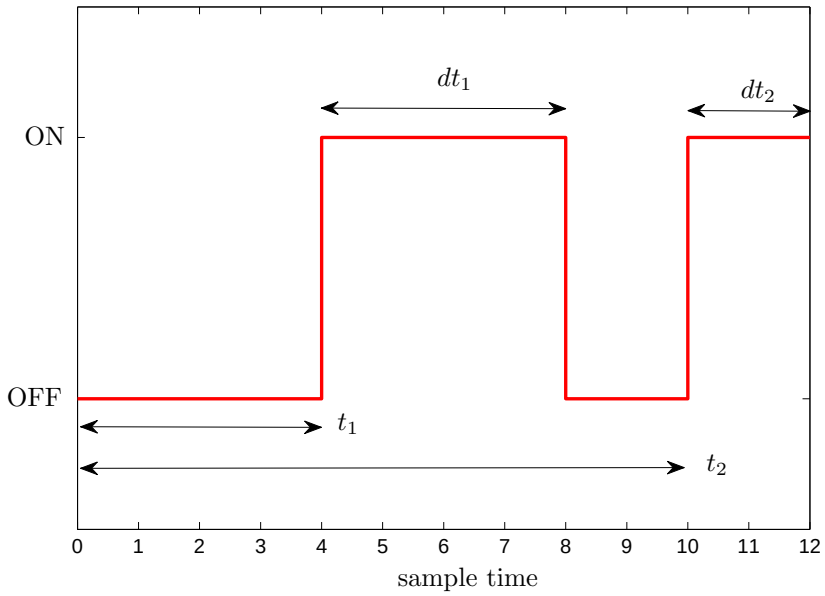

Figure 4.3: Formulation of the discrete variables proposed by Sarabia et al. (2009).

This approach presents two advantages: 1) the number of parameters have been decreased considerably (from K to $2 \cdot n$); and 2) this formulation converts discrete variables into continuous variables (t and dt are continuous variables), which are more easily manipulated.

On the other hand, the continuous variables may be discretized depending on the sample time. For example, the evolution of the flow provided by the high-pressure pump 'P4' over the prediction time (t_H), may be formulated by a vector of N elements, as seen below:

$$u_{P4} = [Q_f(1), Q_f(2), Q_f(3)...]_{1\times N} \tag{4.3}$$

where $Q_f(i)$ is the flow at the ith sample time, N is the number of sample times, and the duration of the sample time is t_H/N.

4.1.1.2 Manipulated Variables

Taking the previous formulation into account, the manipulated variables of the control problem for the RO pilot plant, are:

- The feed flow and the reject flow at each sample time:
  $Q_f(1)$, $Q_f(2)$, $Q_f(3)$, ... $Q_f(N)$.
  $Q_r(1)$, $Q_r(2)$, $Q_r(3)$, ... $Q_r(N)$.
- The time instant for the switches of the supply pumps:
  $t_{P1}(1)$, $t_{P1}(2)$, $t_{P1}(3)$, ... $t_{P1}(n_{P1})$.
  $t_{P2}(1)$, $t_{P2}(2)$, $t_{P2}(3)$, ... $t_{P2}(n_{P2})$.
- The duration of each switch of the supply pumps:
  $dt_{P1}(1)$, $dt_{P1}(2)$, $dt_{P1}(3)$, ... $dt_{P1}(n_{P1})$.
  $dt_{P2}(1)$, $dt_{P2}(2)$, $dt_{P2}(3)$, ... $dt_{P2}(n_{P2})$.
- The time instant for the cleaning of the system:
  $t_{CL}(1)$, $t_{CL}(2)$, $t_{CL}(3)$, ... $t_{CL}(n_{CL})$.

In addition, several parameters of the optimization problem should be fixed by the user, as follows:

- The prediction time: t_H.
- The number of sample times for the continuous variables: N.

- The number of cleanings of the system: n_{CL}.
- The number of switches of the supply pump 'P1': n_{P1}.
- The number of switches of the supply pump 'P2': n_{P2}.

The prediction time and the number of sample times for the continuous variables, should be chosen carefully, to avoid working with a very complex optimization problem (with a high number of manipulated variables), but still having a good representation of the system. In the present case, the optimization problem was solved with the prediction time equals 24 hours and the sample time equals 1 hour. The number of cleanings of the system is actually a constraints of the system, and depends on the characteristics of the feed water. In the present case, the number of cleanings is 1 per day. Finally, the number of switches of the supply pumps is a priori difficult to choose. However, a minimum and maximum numbers of switches may be more easily estimated. In this case, for example, a number of switches between 0-2 switches per day, was assumed. If the number of possibilities is low enough, as in the present case, the optimization problem may be repeated for each scenario.

4.1.1.3 Constraints

The operation of the RO pilot plant involves the requirement of several constraints. The main constraint is to keep the water level in the outlet tank ('T3') higher than a certain value (for example, L_{min}). The water demand takes water from this tank, thus, if the level is kept higher than a minimum value, it is possible to guarantee that the water demand has been fulfilled. In addition, the level of this tank should be kept lower than a certain value (for example, L_{max}), in order to avoid the overflow of the tank. These constraints are summarized below:

$$L_{min} < \text{water level of tank 'T3'} < L_{max} \tag{4.4}$$

Besides, a minimum and maximum level is required for the supply tanks ('T1', 'T2'), to avoid the cavitation of the pumps and the overflow of the tanks, as follows:

$$L_{min} < \text{water level of tanks 'T1'-'T2'} < L_{max} \tag{4.5}$$

Regarding the cleaning of the plant, as commented previously, the washing of the RO membranes should be done at least once a day. This means the time period between two cleanings should be less than 24 hours, as follows:

$$t_{CL}(i) - t_{CL}(i-1) < 24\text{h} \tag{4.6}$$

Finally, there are several constraints concerning the switching on/off of the supply pumps and the high-pressure pump: After a switch on of one supply pump, the next switch off cannot be done until a minimum period has transpired. In the same way, there is a minimum time between a switch off and the next switch on. Regarding the high-pressure pump, the difference between two consecutive increments of the pump speed should be limited by a maximum value so as to guarantee a smooth operation of the system. These constraints are summarized below:

$$\begin{cases} t_{P1}(i) - (t_{P1}(i-1) + d_{P1}(i-1)) > \xi_1 \\ t_{P2}(i) - (t_{P2}(i-1) + d_{P2}(i-1)) > \xi_1 \\ d_{P1}(i) = t_{P1}(i) - t_{P1}(i-1) > \xi_2 \\ d_{P2}(i) = t_{P2}(i) - t_{P2}(i-1) > \xi_2 \\ |Q_f(i) - Q_f(i-1)| < \xi_3 \end{cases} \tag{4.7}$$

where the parameters ξ_1, ξ_2 and ξ_3 represent each constraint.

4.1.1.4 Objective Function

The optimization problem mixes continuous decisions with discrete variables. A priori, a mixed-integer nonlinear programming (MINLP) must be solved. However, following the approach described in Sarabia et al. (2009), the discrete variables have been formulated as continuous variables, and the optimization problem has become a non linear programming (NLP), which may be solved easily. (See, for example, Henderson et al. (1991) and Floudas (1998).)

Mathematically, the optimization problem can be formulated as follows:

$$\begin{cases} \min_u J = \beta_1 \cdot \int_{t=0}^{t_H} E_{nr} \cdot dt + \beta_2 \cdot \Delta u \\ \text{taking into account the constraints (4.4-4.7).} \end{cases} \tag{4.8}$$

where J is the cost function, u symbolizes all the manipulated variables, t_H is the prediction horizon, E_{nr} is the energy for consumption provided by the non-renewable energy sources (such as the diesel generator), and β_i are weight factors to penalize sharp changes in the manipulated variables.

The energy consumption may be calculated, depending on the power consumption of the pumps, as follows:

$$E = \sum_{i=1}^{m} \left(\frac{Q(i) \cdot \Delta P(i)}{\eta(i)} \right) \tag{4.9}$$

where m is the number of pumps, η is the efficiency of each pump and depends on the operating point, as seen below:

$$\eta = a_0 + a_1 \cdot Q_f + a_2 \cdot Q_f^2 + ... \tag{4.10}$$

where the parameters a_0, a_1 and a_2 are empirical factors.

In addition, in order to solve the optimization problem, it is necessary to know several functions, as follows:

- The integration of the equation (4.8) requires a mathematical model of the system. A simplified model of the desalination plant is shown in section 4.1.2.
- The calculation of the constraints (4.4-4.5) requires knowledge of the characteristic curve of the water demand. This is done in section 4.1.3.
- The calculation of the availability of renewable energy requires the prediction of the solar radiation and the wind velocity, which is described in sections 4.1.4 and 4.1.5 respectively.

4.1.2 Simplified Modelling

The MPC of the plant requires the mathematical model of the system to be solved several times per sample time. Taking this into account,

the mathematical model described in chapter 2 is too complex to be used for on-line optimization and there are many details that are not of interest for the economic optimization. This section describes a simplified model of the desalination plant, which is used for advanced control.

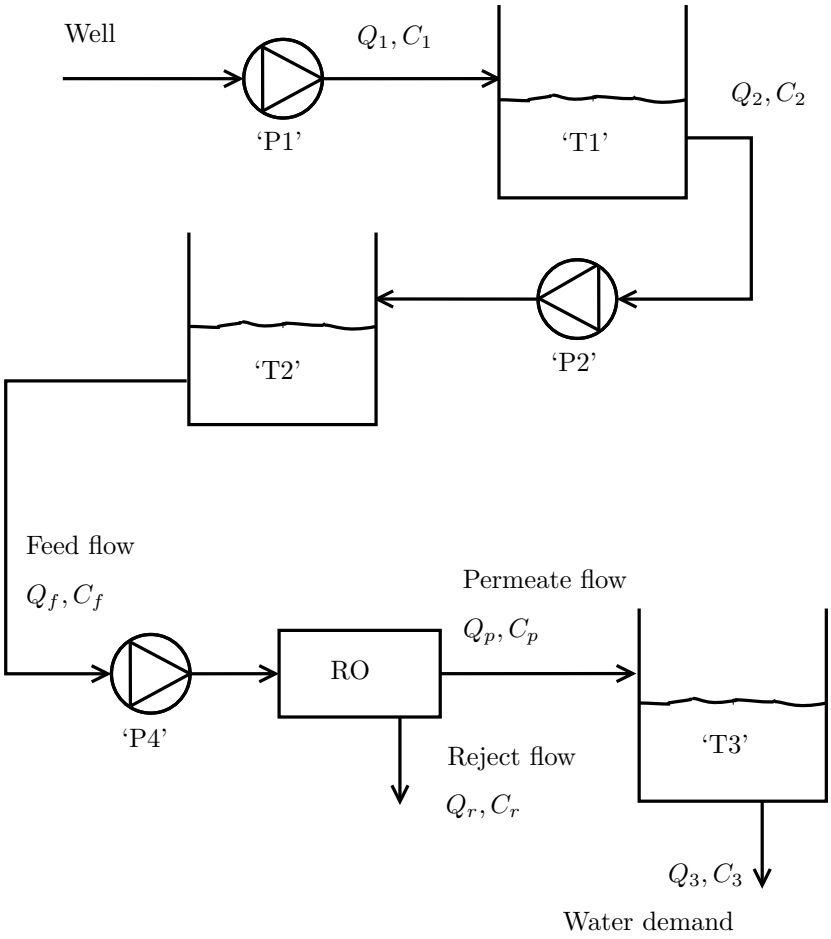

Figure 4.4: Flow diagram of the desalination plant.

Figure 4.4 shows the flow diagram of the pressure vessels, and the main variables of the system. Q_1 and Q_2 are the water flow provided by the supplies pump 'P1' and 'P2', Q_f is the feed water provided by the high-pressure pump 'P4', Q_p is the permeate flow, Q_r is the reject flow and Q_3 is the water demand. C_1 is the salt concentration

at the input of the system, C_2 is the salt concentration at the output of the tank 'T1', C_f is the salt concentration at the output of the tank 'T2', C_p is the salt concentration of the permeate flow, C_r is the salt concentration of the reject flow and C_3 is the salt concentration at the output of the plant.

The permeate flow (Q_p) may be calculated as follows:

$$Q_p = A_w \cdot A \cdot (\Delta P - \Delta\pi) \tag{4.11}$$

where A_w is the water permeability, A is the total area of the RO modules, ΔP is the pressure difference between the pressure supplied by the high-pressure pump and the permeate pressure, and $\Delta\pi$ is the osmotic pressure difference between both sides of the membranes.

The osmotic pressure difference may be calculated as a function of the salt concentration, as follows:

$$\Delta\pi = k \cdot (C_b - C_p) \tag{4.12}$$

where k depends on the temperature, the type of salt, and the van't Hoff and reflection coefficients, and C_b is the average salt concentration of the bulk of the feed flow along the RO modules, which may be calculated as follows:

$$C_b = 0.5 \cdot (C_f + C_r) \tag{4.13}$$

The salt concentration of the permeate (C_p) may be calculated as seen below:

$$C_p = \frac{B_s}{A_w} \cdot \frac{C_b - C_p}{\Delta P - \Delta\pi} \tag{4.14}$$

where B_s is the salt permeability.

The flow (Q_r) and salt concentration (C_r) of the reject streams may be calculated by a mass balance, as follows:

$$C_r = \frac{Q_f \cdot C_f - Q_p \cdot C_p}{Q_r} \tag{4.15}$$

$$Q_r = Q_f - Q_p \tag{4.16}$$

The water recovery (r) is defined as follows:

$$r = \frac{Q_p}{Q_f} \cdot 100 \tag{4.17}$$

The water level of the tanks, may be calculated by a mass balance of the water in each tank, as follows:

$$h_1' = \frac{1}{S_1} \cdot (Q_1 - Q_2) \tag{4.18}$$

$$h_2' = \frac{1}{S_2} \cdot (Q_2 - Q_f) \tag{4.19}$$

$$h_3' = \frac{1}{S_3} \cdot (Q_p - Q_3) \tag{4.20}$$

where h_i is the water level of the tank i, and S_i is the cross section of each tank.

Finally, the salt concentration in each tank, may be calculated by a mass balance of the salt, as seen below:

$$C_2' = \frac{1}{S_1 \cdot h_1} \cdot (Q_1 \cdot C_1 - Q_2 \cdot C_2) - \frac{C_2}{h_1} \cdot h_1' \tag{4.21}$$

$$C_f' = \frac{1}{S_2 \cdot h_2} \cdot (Q_2 \cdot C_2 - Q_f \cdot C_f) - \frac{C_f}{h_2} \cdot h_2' \tag{4.22}$$

$$C_3' = \frac{1}{S_3 \cdot h_3} \cdot (Q_p \cdot C_p - Q_3 \cdot C_3) - \frac{C_3}{h_3} \cdot h_3' \tag{4.23}$$

The mathematical system formed by equations (4.12-4.17) has six independent variables, as follows:

- The salt concentration of the feed flow (C_1), which is a boundary of the system.
- the water demand (Q_3), which is a boundary of the system.
- The water flow provided by the supply pumps (Q_1 and Q_2), which are calculated by the advanced control.
- The feed and permeate flow (Q_f and Q_p), which are calculated by the advanced control.

Instead of (Q_f and Q_p), it is actually possible to solve the optimization problem using other couples of independent variables, such as operating pressure (P) and feed flow (Q_f), water recovery (r) and feed flow (Q_f), etc. In this case, the chosen variables were the feed flow (Q_f) and the permeate flow (Q_p), because allow a easily resolution of the mathematical system and correspond to the controlled variables of the pilot plant.

4.1.3 Prediction of the Water Demand

The nominal value of the water demand depends on the day of the week and the month of the year, but basically, it may be modelled as a periodic curve that is repeated every 24 hours. Each village has its own characteristic curve of water demand, which depends on the population, characteristics of the town, industry, and a long etcetera.

Typically, the water demand curve over 24 hours (Q_{day}) may be modelled by a Fourier series, as follows:

$$Q_{day} = \frac{a_0}{2} + \sum_{i=1}^{n} \left(a_i \cdot \cos(\frac{2\pi}{24} \cdot i \cdot t) + b_i \cdot \sin(\frac{2\pi}{24} \cdot i \cdot t) \right) \tag{4.24}$$

where the parameters a_0, a_i, b_i should be estimated for each village, and t is the time (h).

While the water demand over one year (Q_p) is modelled as in equation (4.25).

$$Q_p = Q_{day} \cdot \Phi_w + b_{year} \tag{4.25}$$

where Φ_w is the ratio of the nominal water demand and the average nominal value of each day of the week (from Monday to Sunday), and b_{year} is a correction factor that represents the variations according to the day of the year.

Since the pilot plant is not connected to any settlement, the water demand was simulated using a control valve in the pilot plant. Figure 4.5 shows the behaviour of the water demand over one week. The top figure corresponds to a summer week, while the bottom figure corresponds to a winter week. The red line is the real water demand, while the blue line is the estimated profile.

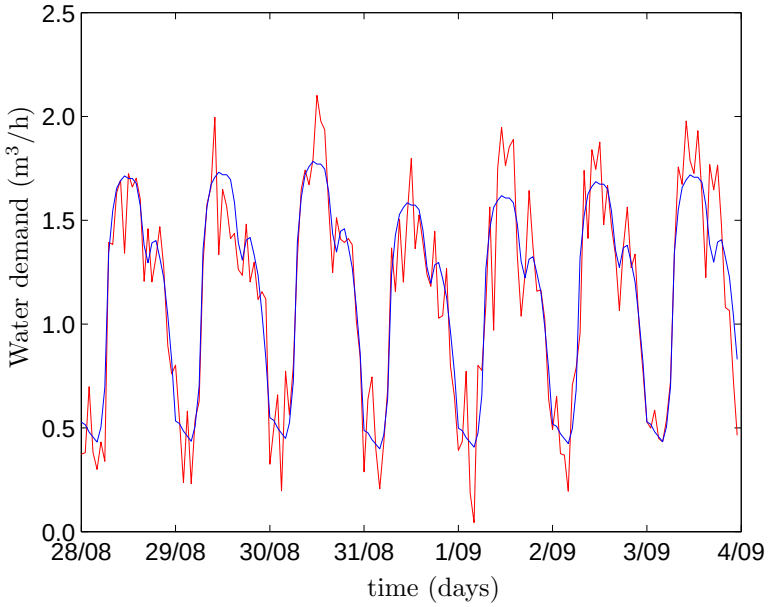

(a) Summer week.

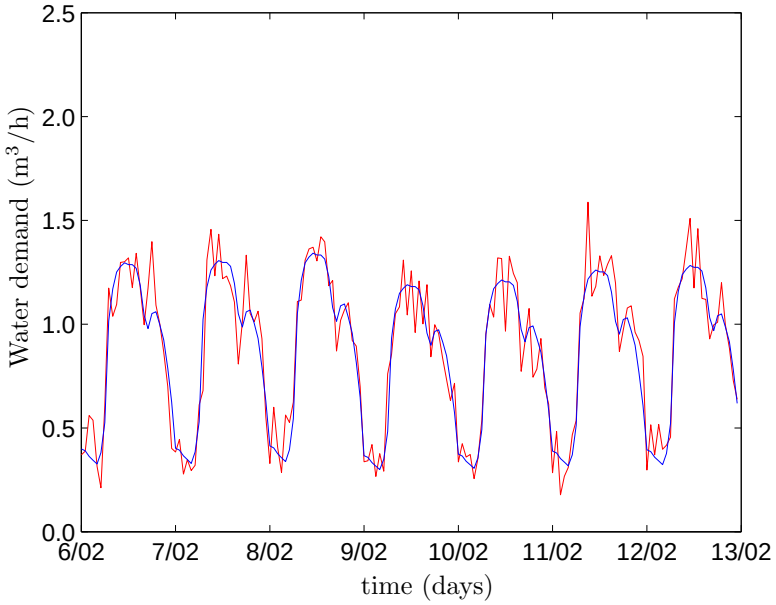

(b) Winter week.

Figure 4.5: Water demand over one week. The red line corresponds to real data, while the blue line corresponds to estimated data.

4.1.4 Prediction of the Solar Radiation

The solar radiation depends on the location, date and degree of coverage. Figure 4.6 shows the behaviour of the solar radiation, over 24 hours of a summer day, in Borj Cedria (Tunisia), which corresponds to the location of the pilot plant. The blue line corresponds to a sunny day, while the red line corresponds to a day partially covered. The difference between the two curves is proportional to the degree of coverage. The solar radiation of a sunny day follows a sinusoidal-shaped curve, with a maximum around noon, and zero value during night. The maximum value and the width of the curve vary along the year. Figure 4.7 shows real data for the solar radiation over one year in the same location.

The solar radiation may be modelled by a sinusoidal distribution (Alvisi et al. (2007)), as follows:

$$I = \frac{\pi}{2 \cdot T_l} \cdot G \cdot \sin(\frac{\pi}{T_l}) \tag{4.26}$$

where I is the solar radiation, T_l is the length of daylight and G is the maximum radiation.

The length of daylight may be calculated by a sinusoidal-shaped equation, as seen below:

$$T_l = a_1 + a_2 \cdot \sin\left(\frac{2\pi}{365} \cdot t + a_3\right) \tag{4.27}$$

where the parameters a_1, a_2, a_3 depend on the location, and t is the time (days).

The maximum radiation, however, depends on the maximum radiation on a sunny day (G_s), as follows:

$$G = (1 - c) \cdot G_s \tag{4.28}$$

where c is the degree of coverage.

As in the case of T_l, the degree of coverage, as well as maximum radiation on a sunny day, may be calculated by a sinusoidal-shaped equation, as seen below, depending on the location and the day of the year.

$$c = b_1 + b_2 \cdot \sin\left(\frac{2\pi}{365} \cdot t + b_3\right) \tag{4.29}$$

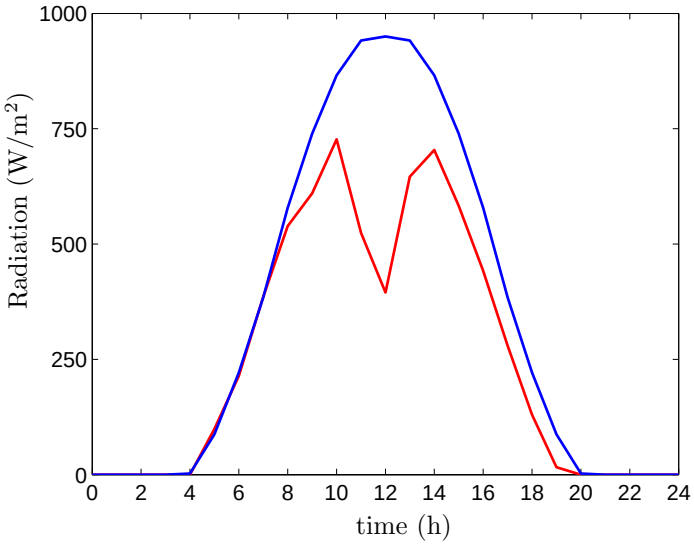

Figure 4.6: Solar radiation over 24 hours in Borj Cedria (Tunisia). The blue line corresponds to a sunny day, while the red line corresponds to a day partially covered.

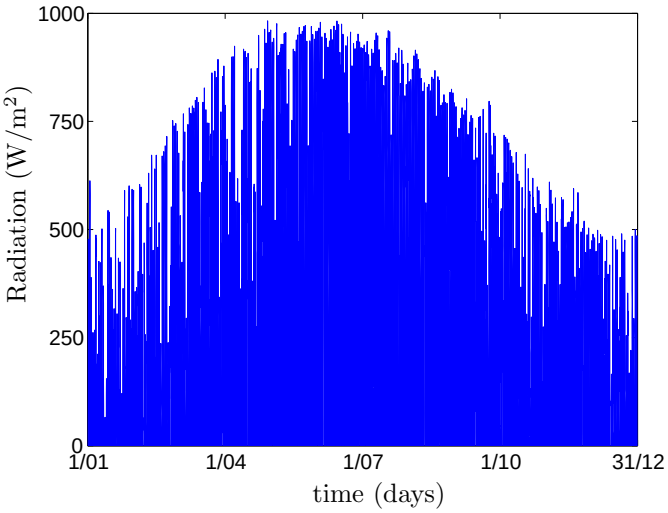

Figure 4.7: Solar radiation over one year in Borj Cedria (Tunisia). The blue line corresponds to a sunny day, while the red line corresponds to a partially covered day.

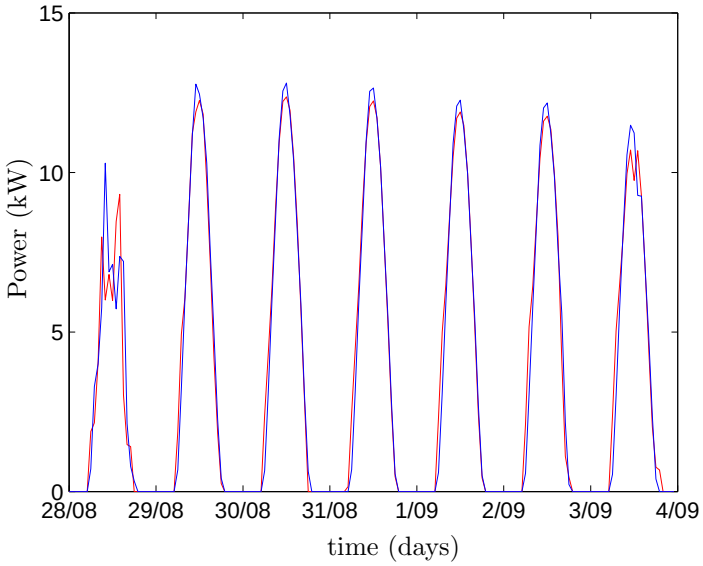

(a) Summer week.

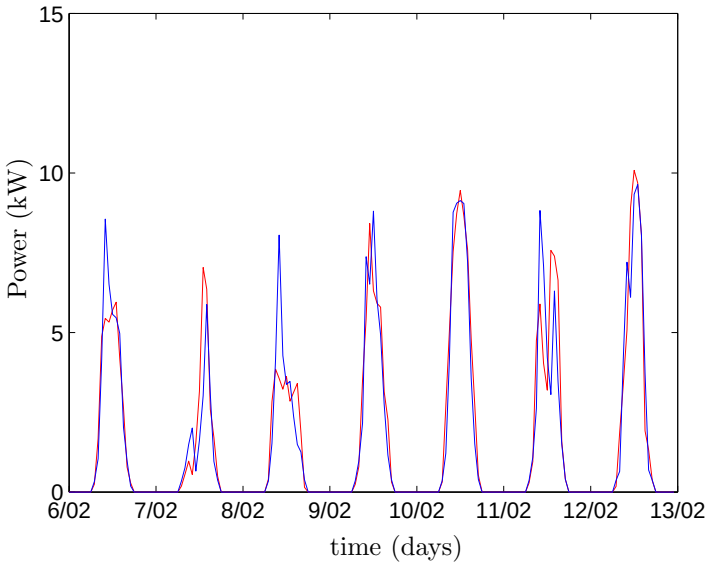

(b) Winter week.

Figure 4.8: Power production from the solar panels in the pilot plant, over one week. The red line corresponds to the real data, while the blue line corresponds to the estimated data.

where the parameters b_1, b_2 and b_3 are empirical factors that depend on the location.

$$G_s = d_1 + d_2 \cdot \sin\left(\frac{2\pi}{365} \cdot t + d_3\right) \tag{4.30}$$

where the parameters d_1, d_2, and d_3 are empirical factors that depend on the location.

Finally, the electrical power (W), produced by the solar panels, depends on the solar radiation and the total area of the solar panels, as follows:

$$W = k \cdot I \cdot A \tag{4.31}$$

where A is the total area of the rack of solar panels, and k is the linear constant for the radiation, which depends on each system, the ageing of the plant, and the atmospheric temperature.

Figure 4.8 shows the electrical power produced in the pilot plant over one week. The red line is the real power production, while the blue line is the estimated one. The top figure corresponds to a summer week, while the bottom figure corresponds to a winter week. Notice that during winter, besides the decrease in the maximum solar radiation, there is an increase in the degree of coverage.

The degree of coverage is recalculated each sample time as a function of the measured radiation (I_{measured}) and the estimated radiation ($I_{\text{estimated}}$), as follows:

$$c = 1 - \frac{I_{\text{estimated}}}{I_{\text{measured}}} \tag{4.32}$$

where $I_{\text{estimated}}$ is calculated from equations (4.26-4.30).

4.1.5 Prediction of the Wind Velocity

In contrast to the solar radiation, the prediction of wind velocity is difficult (see Giebel (2002)). Figure 4.9 shows the wind velocity over one week, in the location of the pilot plant. For long-term scale, the wind velocity cannot be predicted, however, for short-term prediction, the instant wind velocity may be calculated as a function of the measured wind velocity in the previous sample time, as in equation (4.33).

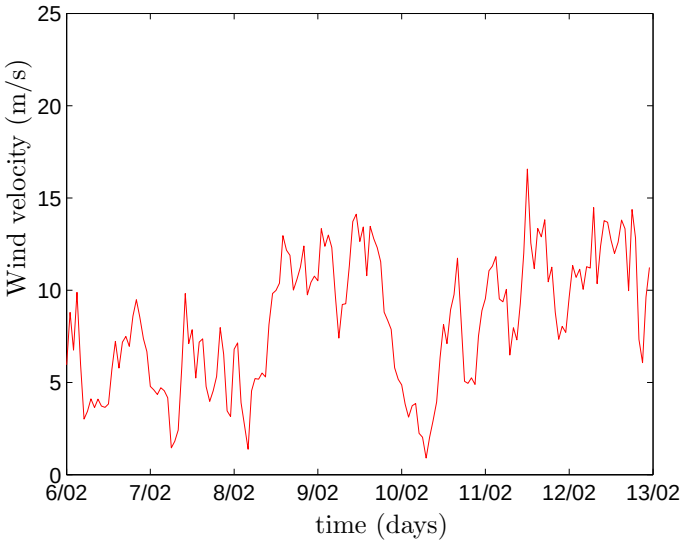

Figure 4.9: Wind velocity in Borj Cedria (Tunisia), over one week.

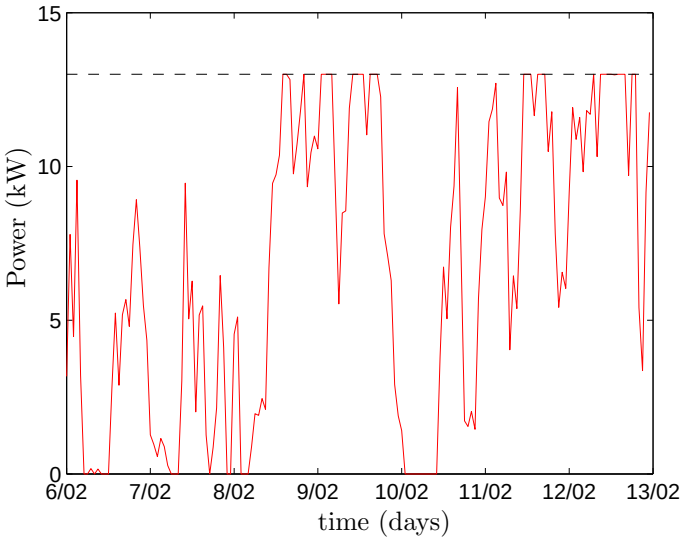

Figure 4.10: Power production from the wind turbine in the pilot plant, over one week. The dotted line corresponds to the maximum power production.

$$\hat{v}_i = (1 - r) \cdot v_{i-1} + r \cdot \hat{v}_{i-1} \tag{4.33}$$

where $\hat{v}_i$ is the estimated wind speed at time i, v_{i-1} is the wind speed measured at the moment before, $\hat{v}_{i-1}$ is the wind speed calculated at the moment before, and r is a parameter that represents the correlation between two consecutive wind speeds.

Basically, the power production provided by a wind turbine may be considered proportional to the wind velocity, with the constraints that a minimum wind velocity (v_{min}) is necessary, and that the production of power is saturated for high wind velocities (beyond v_{max1}). Finally, for very high wind velocity (v_{max2}), the wind turbine should be disconnected to avoid the breakage of the rotor. Equation (4.34) summarizes the profile of a wind turbine.

$$\begin{cases} \text{if } v < v_{min} & \rightarrow W = 0 \\ \text{if } v_{min} < v < v_{max1} & \rightarrow W = k \cdot (v - v_{min}) \\ \text{if } v_{max1} < v < v_{max2} & \rightarrow W = W_{max} \\ \text{if } v > v_{max2} & \rightarrow W = 0 \end{cases} \tag{4.34}$$

where v is the wind velocity, k is a parameter that represents the correlation between the power and the wind velocity, and W_{max} is the maximum power provided by the wind turbine.

Figure 4.10 shows the power production from the pilot plant, over one week. This is due to the wind velocity shown in figure 4.9. Notice the power production is zero for low wind velocity, while it gets saturated when the wind velocity goes beyond v_{max1}.

4.1.6 Implementation

Figure 4.11 shows the implementation of the control system. As commented in chapter 3, the control of the desalination pilot plant is divided in two layers. The lower level is carried out by a PLC from OMRON, and deals with the basic control of the plant and the control loops. The upper layer of the control system is carried out by a computer and is focused in the advanced control described in the present chapter. The connection between the PLC and the computer is done by an Ethernet bus and using the OPC protocol.

The advanced control of the plant was developed in the simulation environment EcosimPro, from the company EA (see section 2.2), which has specific tools for simulation and optimization. The simulation was executed from Matlab, from the company MathWorks, thanks to the corresponding communication toolbox. The connection between the computer and the PLC was done thanks to the OPC toolbox of Matlab and the OPC Server of OMRON (called CX-Server OPC). The execution of the advanced control is done sequentially. Each sample time, the simulator calculates the prediction of water demand and renewable energy. The optimizer calculates the manipulated variables of the plant, minimizing the cost function and fulfilling the constraints. In the next sample time, the advanced control correct the predictions with the new measured data, and recalculate again the manipulated variables.

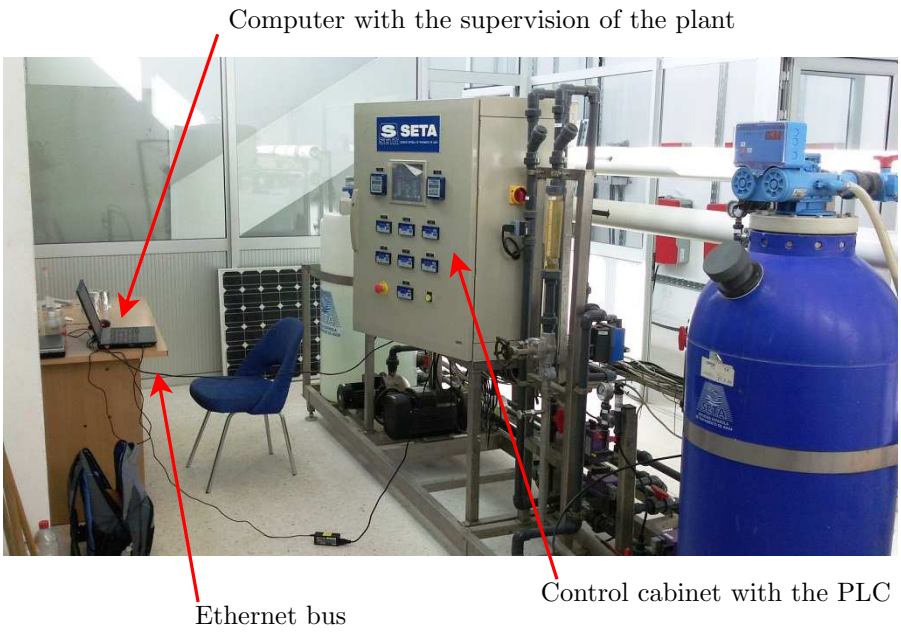

Figure 4.11: Algorithm to coupling both models.

4.1.7 Results

This section shows the behaviour of the RO pilot plant, using the MPC described previously. The control horizon (t_H) is 24 hours; while

the sample time is one hour. The predictions of the water demand, solar radiation and wind velocity are recalculated each hour. The constraints of the optimization problem are summarized below.

Parameters	
$t_H = 24$ h	$N = 24$
$L_{min} = 10$ %	$L_{max} = 90\%$
$\xi_1 = 30$ min	$\xi_2 = 30$ min
$\xi_3 = 0.3$ m^3/h	$\Delta t_{CL} < 24$ h

Table 4.1: Parameters used in the optimization of the operation: equations (4.4-4.8).

Parameters		
a_1 = -0.3824	b_1 = -0.2627	$\Phi_w(1) = 0.993$
a_2 = -0.0916	b_2 = -0.1497	$\Phi_w(2) = 1.010$
a_3 = -0.0059	$b_3 = 0.0203$	$\Phi_w(3) = 1.020$
a_4 = -0.0768	$b_4 = 0.0165$	$\Phi_w(4) = 1.029$
$a_5 = 0.0114$	b_5 = -0.0282	$\Phi_w(5) = 0.06$
$a_6 = 0.0166$	b_6 = -0.0091	$\Phi_w(6) = 0.937$
a_7 = -0.0245	$b_7 = 0.0083$	$\Phi_w(7) = 0.955$
a_8 = -0.0061	b_8 = -0.0107	$a_0 = 0.8745$

Table 4.2: Parameters for the prediction of the water demand: equations (4.24-4.25).

The parameters utilized for the prediction of the water demand, solar radiation and wind velocity are summarized, respectively, in tables 4.2-4.4; while the characteristics and nominal values of the plant simulated may be seen in table 4.5.

Parameters		
$a_1 = 12.0$ h	$a_2 = 3.64$ h	$a_3 = 1.73$
$b_1 = 0.57$	$b_2 = 0.38$	$b_3 = 1.21$
$d_1 = 742$ W/m^2	$d_2 = 211$ W/m^2	$d_3 = 4.64$

Table 4.3: Parameters for the prediction of the solar radiation: equations (4.27-4.30).

Parameters	
$v_{min} = 4$ m/s	$k = 1.63$ kJ/m
$v_{max1} = 12$ m/s	$v_{max2} = 35$ m/s
$W_{max} = 13$ kW	$r = 0.93$

Table 4.4: Parameters for the prediction of the wind velocity: equations (4.33-4.34).

Parameters	
$A_w = 2.89 \cdot 10^{-7}$ m/(bar·s)	$B_s = 4.10 \cdot 10^{-8}$ m/s
$A = 7.90$ m^2/(RO module)	$\Phi = 1.67$
a_0 = -0.20	$a_1 = 1.32$ h/m^3
a_2 = -0.43 (h/m^3)^2	$k = 1.74 \cdot 10^{-3}$ bar/ppm
Nominal values	
$Q_f \sim$ 0.75-2.50 m^3/h	$Q_p \sim$ 0.50-1.25 m^3/h
$C_f \sim$ 15 000 ppm	$C_p \sim$ 200 ppm
$\Delta P \sim$ 28-35 bar	Recovery $\sim$ 60 %
Number of RO modules = 8	Salt retention >99%

Table 4.5: Characteristics of the desalination plant: equations (4.9-4.14).

The advanced control is tested over a summer week (subsection 4.1.7.1) and over a winter week (4.1.7.2), as seen below.

4.1.7.1 Summer Week

Figure 4.12 shows the behaviour of the availability of renewable energy (due to solar radiation and wind velocity). The blue line is the real renewable power provided by the energy supply system, while the red line is the estimated curve. This curve has been recalculated each hour, taking into account the corrections of degree of coverage and wind velocity. Both variables follow a similar profile, which proves the goodness of the energy prediction.

Next, figure 4.13 compares the water demand (blue line) with the water production (that is, the permeate flow) of the pilot plant (red line). The time instants when the permeate flow has the value zero

correspond to the periodical cleaning of the plant. Since the maximum water demand takes place approximately when more renewable energy is available, the operation of the plant may be easily optimized.

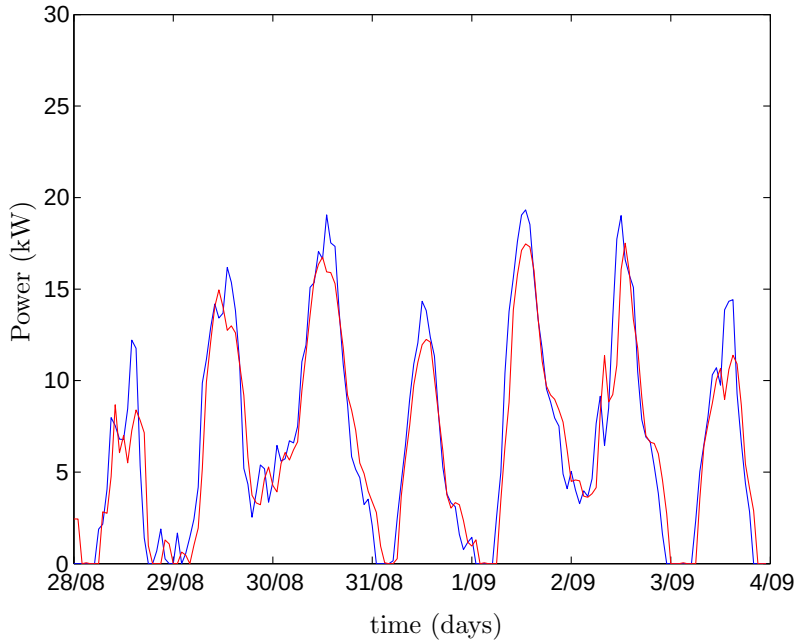

Figure 4.12: Behaviour of the renewable power provided by the energy supply system, over one summer week. The blue line is the real curve, while the red line is the estimated curve (recalculated each hour).

Figure 4.14 shows the evolution of the renewable power provided by the energy supply system (blue line) and the profile of the power consumed by the desalination plant (red line). When the renewable energy curve is lower than the consumption curve, the energy difference is provided by the diesel generator, which is precisely what the control system aims to minimize. The total energy provided by the diesel generator over one week corresponds to the blue-coloured areas.

The sudden peaks of the red curve correspond to the periodical cleaning of the system. The time instants of the cleaning is calculated by the control system when using advanced control, and is fixed when the plant is operated without advanced control. During the cleaning, the water production is zero, but not the power consumption of the

plant, because several pumps are still operating.

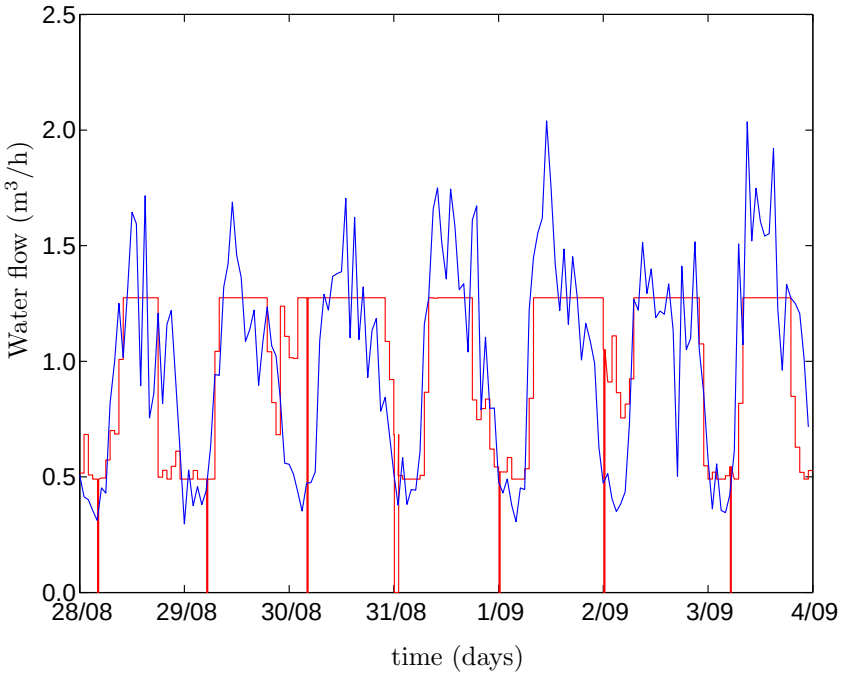

Figure 4.13: Evolution of the water demand and the permeate flow of the pilot plant, over one summer week. The blue line is the water demand, while the red line is the permeate flow. The permeate flow has the value zero when the cleaning of the system is in progress.

The upper graph of figure 4.14 corresponds to the profile of the pilot plant, using the advanced control, while the lower graph corresponds to the evolution of the pilot plant working at a constant operating point (without any action from the control system). It is easily seen that the use of non-renewable energy (blue area) decreases with the use of the MPC. In the current case, the decrease in the use of the diesel generator is over 30%.

Figure 4.15 shows the water level in the tank at the outlet of the production line ('T3'), with and without advanced control. The blue line corresponds to the evolution of the water level with advanced control, while the red line corresponds to the evolution of the water level without advanced control (with a constant operating point).

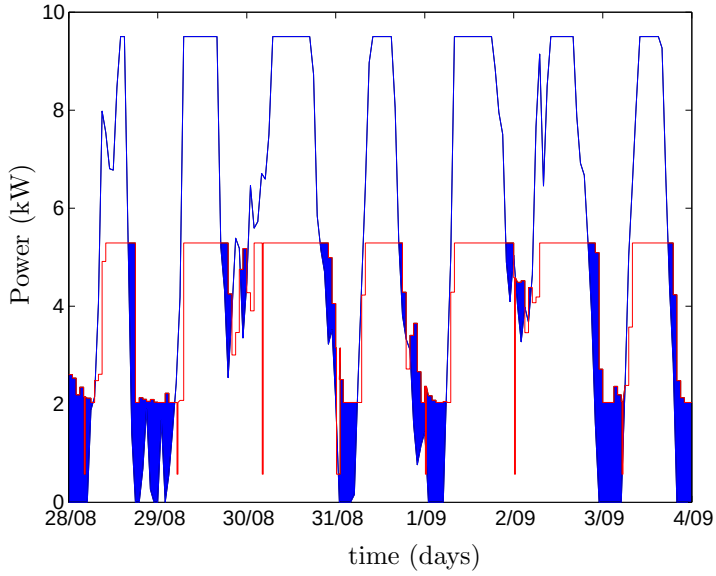

(a) With advanced control.

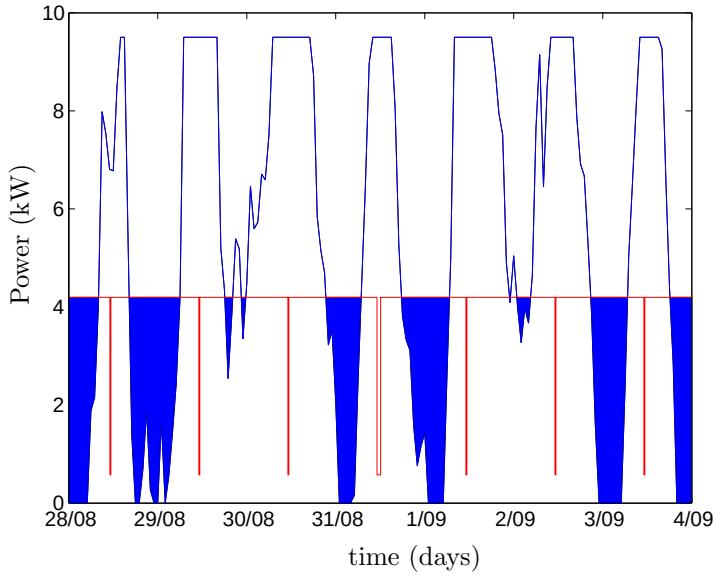

(b) Without advanced control.

Figure 4.14: The blue line is the availability of renewable power over one week, while the red line is the power consumption by the desalination plant. The blue area corresponds to the total non-renewable energy consumption.

The level is kept between the constraints (dotted lines) using the advanced control; while without advanced control the level water goes sometimes over 100 % (the water overflows the tank) or takes the value zero (the tank gets empty and the water demand is not fulfilled).

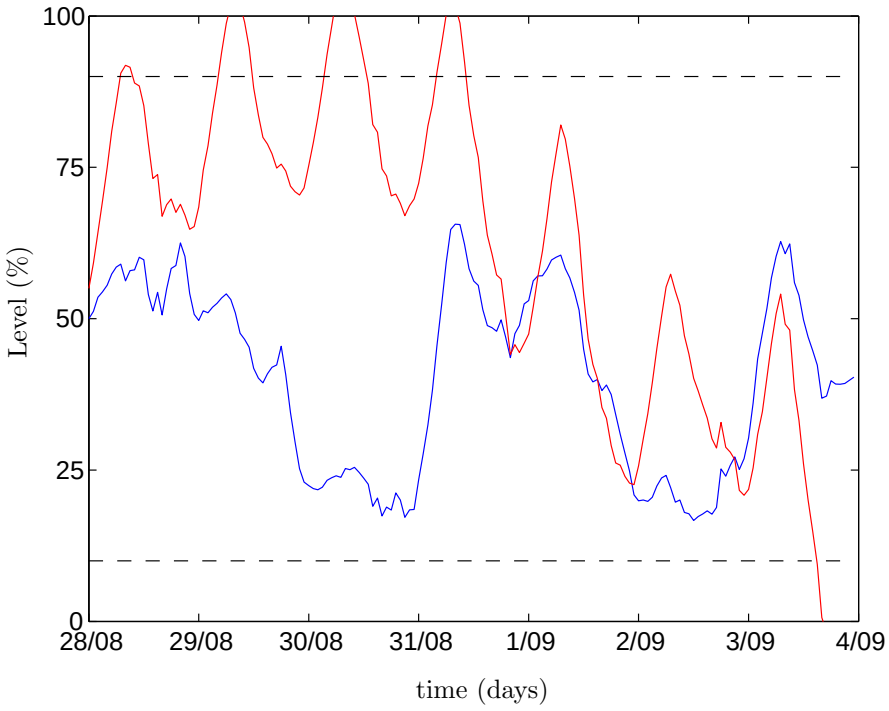

Figure 4.15: Evolution of the water level in the tank at the outlet of the production line ('T3') over one week. The blue line is the level profile with advanced control, while the red line is the level profile without advanced control.

4.1.7.2 Winter Week

Similar curves are obtained for the winter week. Typically, for a winter week, a lower availability of renewable energy is expected, but also a lower water demand.

First, figure 4.16 shows the evolution of the availability of renewable energy. The blue line is the real renewable power, while the red line is the estimated curve, which is recalculated each hour. Next,

figure 4.17 compares the water demand (blue line) with the permeate flow (red line), and shows the time instants when the cleaning of the desalination plant are scheduled, which correspond to the time instant the red line takes the value zero.

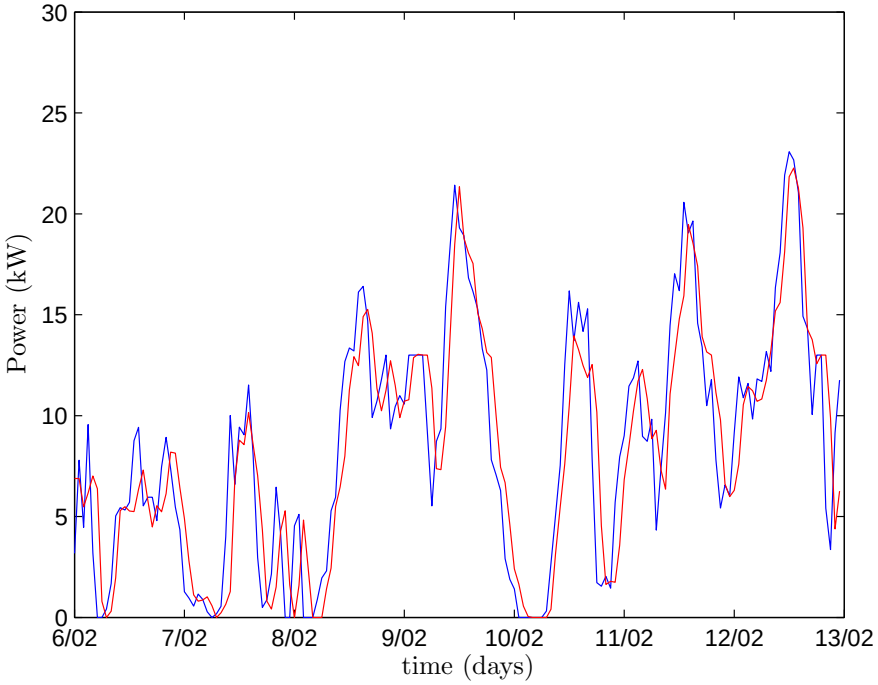

Figure 4.16: Behaviour of renewable power provided by the energy supply system over one winter week. The blue line corresponds to the real curve, while the red line corresponds to the estimated curve.

Figure 4.18 shows the evolution of the renewable power provided by the energy supply system (blue line) and the profile of the power consumed by the desalination plant (red line). The power provided by the diesel generator may be calculated as the addition of the blue-coloured areas. The upper graph corresponds to the evolution of the desalination plant using the proposed advanced control, while the lower graph is done without any advanced control. It is easily seen that the diesel requirement is minimized using advanced control. In the current case, the decrease in the use of the diesel generator is over 40%.

Finally, figure 4.19 shows the water level in the tank at the outlet of the production line ('T3'). The blue line is the water level with advanced control, while the red line is the water level without advanced control. Notice that, without advanced control, the water level goes to zero over several days, which means the water demand is not fulfilled during this period.

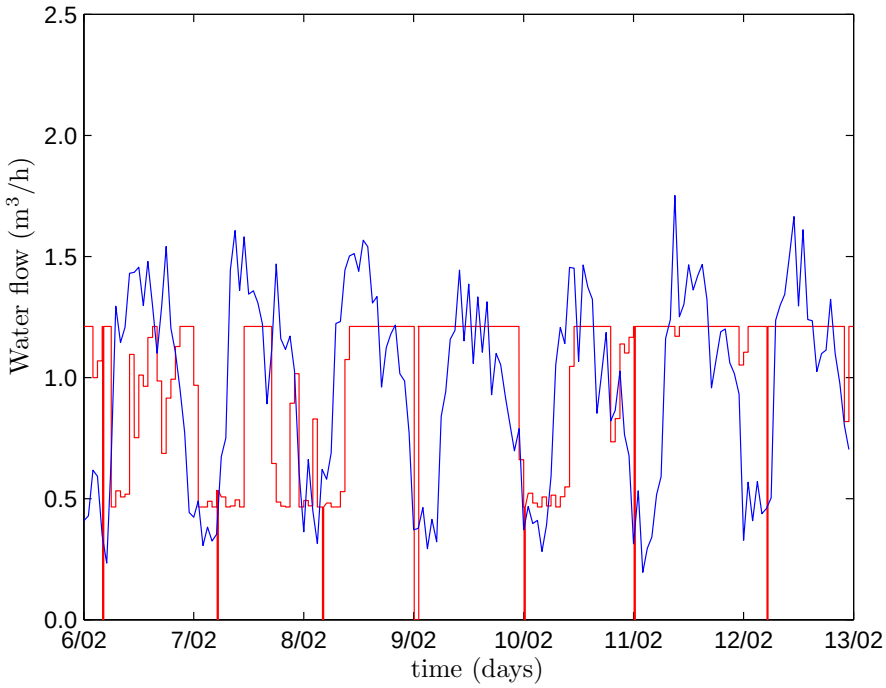

Figure 4.17: Evolution of the water demand and permeate flow from the pilot plant over one week. The blue line is the water demand, while the red line is the permeate flow. The permeate flow has the value zero when the cleaning of the system is in progress.

The results of the advanced control show the operation of the pilot plant may be optimized, taking into account the prediction of water demand and renewable energy. The advanced control minimizes the use of non-renewable energy, while still fulfilling the water demand and the cleaning requirements.

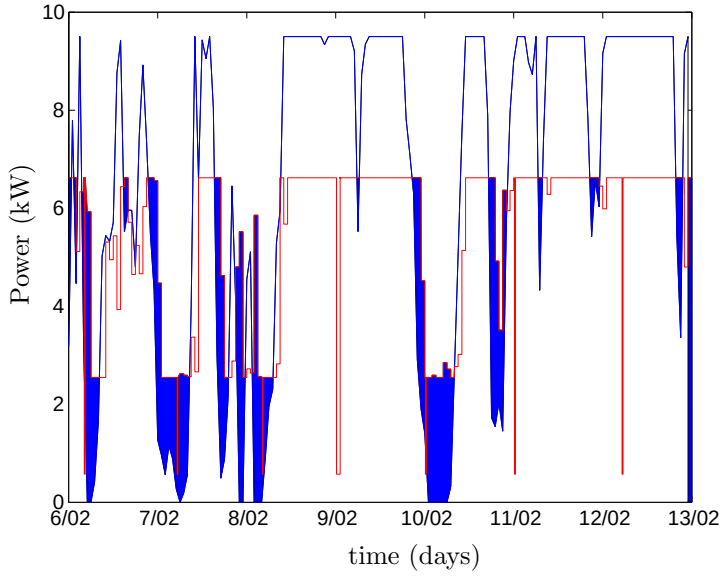

(a) With advanced control.

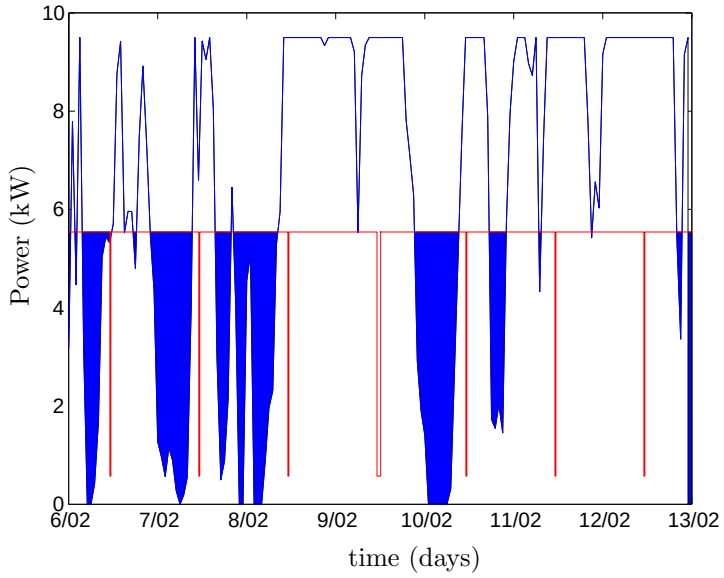

(b) Without advanced control.

Figure 4.18: The blue line is the availability of renewable power over one week, while the red line is the power consumption by the desalination plant. The blue area corresponds to the total non-renewable energy consumption.

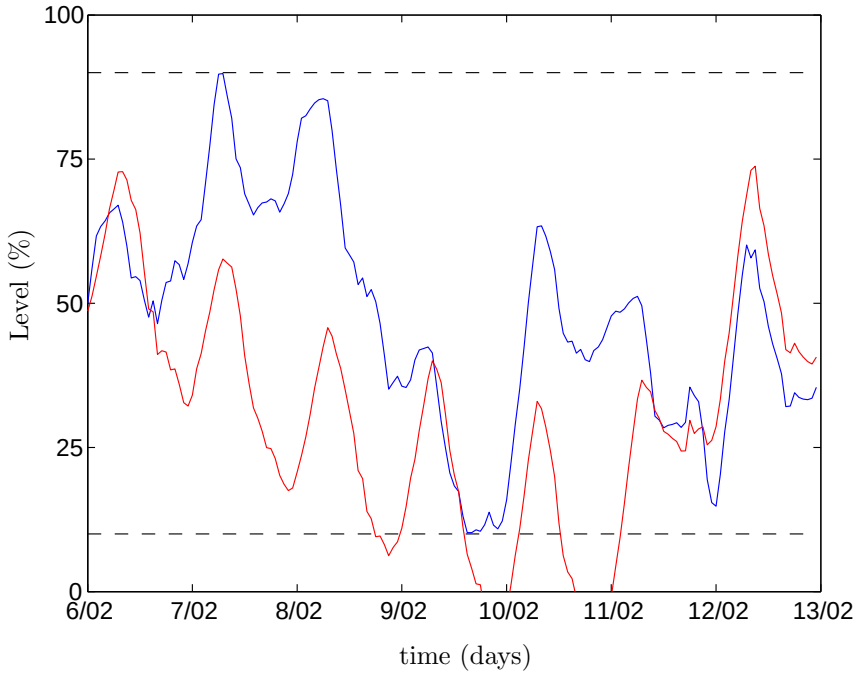

Figure 4.19: Evolution of the water level in the tank at the outlet of the production line ('T3') over one winter week. The blue line is the level profile with advanced control, while the red line is the level profile without advanced control.

4.2 Integrated Process and Control Design

This section presents an extension of the optimization of the control of the desalination plant. The proposal is to design the desalination pilot plant (see chapter 3) jointly with the advanced control (described in the previous section), using dynamic simulation. The key idea is to solve a dynamic optimization problem, which takes into account the size of the units of the pilot plant and penalizes the use of non-renewable energy, while still fulfilling the water demand. In particular, the objective is to minimize the size of the storage tanks by taking into account the available information on water demand, energy availability

and the control strategy. This work was presented in Palacín et al. (2009a,b).

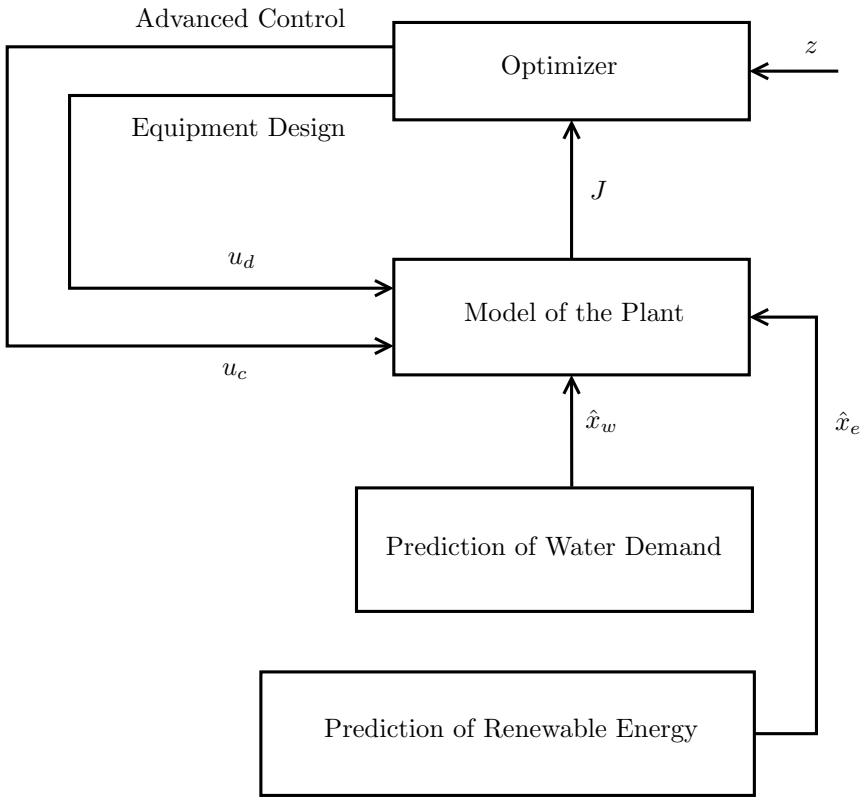

Figure 4.20: Flow diagram of the integrated process and control design.

Figure 4.20 represents the idea of the design proposal. $\hat{x}_w$ is the prediction of the water demand of the village, $\hat{x}_e$ is the prediction of the availability of renewable energy, J is the cost function of the optimization problem, z symbolizes the parameters (fixed by the user) and the constraints of the optimization problem, u_d symbolizes the main variables for the design of the units of the pilot plant (such as the operating point of the pumps, and the dimensions of the tanks), and u_c symbolizes the manipulated variables of the control system (such as the profiles of the feed and reject flows, and the time instant of the cleaning).

The dynamic predictions of water demand and renewable energy

are calculated using the mathematical models given in sections 4.1.3-4.1.5. The model of the desalination plant calculates the evolution of its variables (such as the level of the tanks, energy consumption, etc.) taking into account the profile of water demand, the size and characteristics of the units of the plant, and the profile of the variables manipulated by the control system. In the case of the advanced control described in section 4.1, the model of the desalination plant should be simple and fast because the optimization problem is solved on-line and the model is run several times per sample time. On the contrary, in the case of the integrated process and control design, the optimization is done off-line, and the calculation time required to solve the model of the plant is not crucial. So, in this case, instead of using a simplified modelling (seen in section 4.1.2), a more complex model of the desalination pilot plant is used (see the graphical modelling of the pilot plant shown in figure 3.13 at page 120, developed with the ROSIM library). Finally, the optimizer calculates the dynamic profile of the manipulated variables and the characteristic of the units of the desalination plant, taking into account the predictions of renewable energy and the estimated evolution of the plant, by minimizing an objective function which penalizes the operation cost and the installation expenses, taking into account several constraints.

4.2.1 Mathematical Formulation

The decision variables that are calculated by the optimizer are the manipulated variables of the control system, plus the characteristics of the units of the desalination plant, as seen below. Notice that the symbols correspond to the flow diagram of the RO pilot plant described in chapter 3 (see figures 3.2 and 3.13).

The manipulated variables of the control system (u_c) are:

- The feed flow (Q_f) pumped by the high-pressure pump ('P4').
- The reject flow (Q_p) manipulated by a control valve ('V1').
- The profile of the supply pump ('P1'), which pumps brackish water from the well to the input tank ('T1').
- The cleaning of the system.

The characteristics of the desalination plant to be optimized (u_d) are:

- The operating point of the system (pressure and feed flow).
- The dimensions (height and cross section) of the input and supply tanks ('T1' and 'T2').
- The dimensions (height and cross section) of the output tank ('T3').

The optimization problem may be formulated as follows:

$$\begin{cases} \min\limits_{u_c,u_d} \left(\kappa_{OP} \cdot \Phi \cdot \int_{t=0}^{t_H} E_{nr} \cdot dt + \dfrac{t_H \cdot \mathbb{C}_T}{\lambda_T} + \dfrac{t_H \cdot \mathbb{C}_P}{\lambda_P} + \dfrac{t_H \cdot \kappa_{RO} \cdot n_{RO}}{\lambda_{RO}} \right) \\ \text{taking into account the constraints (4.4-4.7).} \end{cases} \tag{4.35}$$

where u_c symbolizes all the manipulated variables of the control system, u_d symbolizes all the variables of the design of the units of the desalination plant, κ_{OP} is the energy cost (\$/kWh), t_H is the prediction horizon (h), E_{nr} is the energy consumption provided by the non-renewable energy sources (kW), $\mathbb{C}_T$ is the cost of one tank (\$), $\mathbb{C}_P$ is the cost of one pump (\$), κ_{RO} is the cost of one RO module (\$), λ_T, λ_P, and λ_{RO} are, respectively, the expected lifetime of the tanks, pumps and RO modules, and n_{RO} is the number of RO modules.

The energy consumption may be calculated by equation 4.9. The energy cost (κ_{OP}) and the cost of one RO module (κ_{RO}) are assumed constant, while the cost of the pumps and the tanks depends on the size of the corresponding unit and may be formulated by a polynomial function, as follows:

$$\mathbb{C}_P(i) = a_0 + a_{Q1} \cdot Q + a_{P1} \cdot P + a_2 \cdot Q \cdot P + a_{Q2} \cdot Q^2 + a_{P2} \cdot P^2 ... \tag{4.36}$$

where the parameters $a_0, a_{Q1}, a_{P1}, a_2 ...$ depend on the pump type.

$$\mathbb{C}_T(i) = b_0 + b_1 \cdot V + b_2 \cdot V^2 ... \tag{4.37}$$

where the parameters $b_0, b_1, b_2 ...$ depend on the characteristics of the tank.

The optimization problem formulated in equation (4.35) mixes continuous and discrete variables, which means the problem is of MINLP type. As commented in section 4.1, the problem may be transformed into a simple NLP, following the approach described in Sarabia et al. (2009). However, in order to do this, the number of switches of each discrete variable should be assumed. The number of switches of the variable which represents the cleaning of the desalination plant is known (one per day), while the number of switches for the supply pumps ('P1' and 'P2') is unknown. In addition, the number of RO modules is a variable calculated by the optimizer. As the number of alternatives is very limited, the alternative approach described here consists in repeating the solution of the optimization problem assuming different values for the discrete variables, and finally taking the best option.

4.2.2 Results

This section shows the evolution of the desalination pilot plant over two weeks, using the advanced control and the plant design described previously. Table 4.6 summarizes the parameters used in the minimization of equation 4.35. The control horizon is two days, the sample time is one hour, and the predictions are recalculated each hour. While the main nominal values of the desalination plant are summarized in table 4.7.

Next, figure 4.21 shows the behaviour of the availability of renewable energy. The renewable energy is estimated based on real data and it is recalculated by the control system each sample time. Next, figure 4.22 shows the profile of the water demand from the village. Since the pilot plant is not currently connected to any real village, the behaviour of the water demand is simulated. The advanced control calculates the evolution of the pump provided by the high-pressure pump ('P4'), the time instant of the cleaning of the desalination plant, and the switches of the on/off supply pump ('P1').

The manipulated variables of the control system may be seen in figures 4.23 and 4.24. Figure 4.23 shows the profile of the permeate water, as well as the time instant of the cleaning of the plant, which corresponds to the sudden peaks when this curve takes the value zero; while figure 4.24 shows the profile of the on/off input tank.

Parameters	
$t_H = 2$ days	$N = 24$ per day
$L_{min} = 10$ %	$L_{max} = 90\%$
$\xi_1 = 30$ min	$\xi_2 = 30$ min
$\xi_3 = 0.3$ m^3/h	$\Delta t_{CL} < 24$ h
$\lambda_T = 15$ years	$\lambda_P = 5$ years
$\lambda_{RO} = 5$ years	$A_0 = 7$ m^2
$\kappa_{OP} = 0.15$ \$/kWh	$\kappa_{RO} = 75$ \$
$a_1 = 4700$ \$	$a_{Q1} = 410$ \$/(m^3/h)
$a_{P1} = 44$ \$/bar	$b_0 = 6900$ \$
$b_1 =$ -62 \$/m^3	$b_2 = 6.8$ \$/(m^3)^2
$\Phi = 1.67$	

Table 4.6: Parameters of the optimization of the integrated process and control design: equations (4.35-4.37).

Nominal values	
$Q_f \sim$ 0.75-2.50 m^3/h	$Q_p \sim$ 0.50-1.25 m^3/h
$C_f \sim$ 15 000 ppm	$C_p \sim$ 200 ppm
pH $\sim$ 7.0	Temperature $\sim$ 10-30 ^{o}C.
Salt retention >99%	Recovery $\sim$ 60 %
Operating pressure $\sim$ 28-35 bar	
Boron concentration $\sim$ 5 ppm	
Suspended particles (larger than 10 μm) $\sim$ 10 g/m^3	
Suspended particles (between 1-10 μm) $\sim$ 2 g/m^3	
Suspended particles (between 0.1-1 μm) $\sim$ 2 g/m^3	
Suspended particles (between 10^{-2}-0.1 μm) $\sim$ 2 g/m^3	
Suspended particles (between 10^{-3}-10^{-2} μm) $\sim$ 0.1 g/m^3	
Number of RO modules = 1-10 per pressure vessel	
Number of pressure vessels = 2 in parallel	
Switches of the supply pumps = 0-2 per day	
Nominal flow of the supply pumps = 5 m^3/h	

Table 4.7: Nominal values of the integrated process and control design.

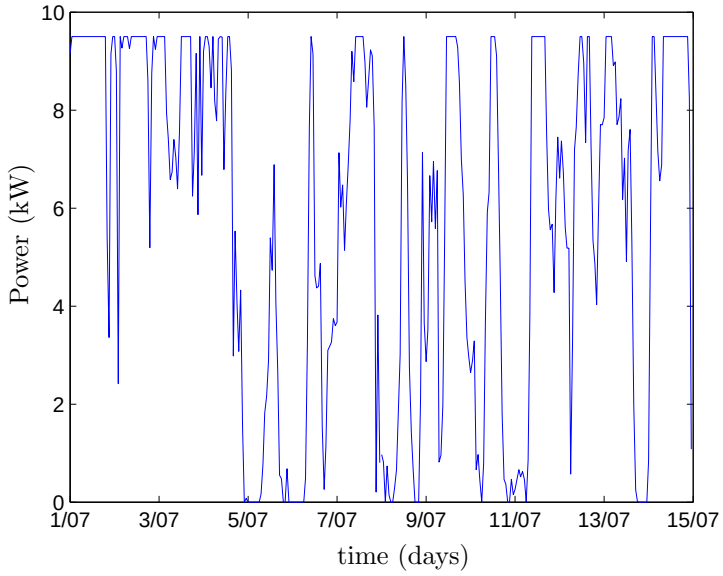

Figure 4.21: Availability of renewable energy.

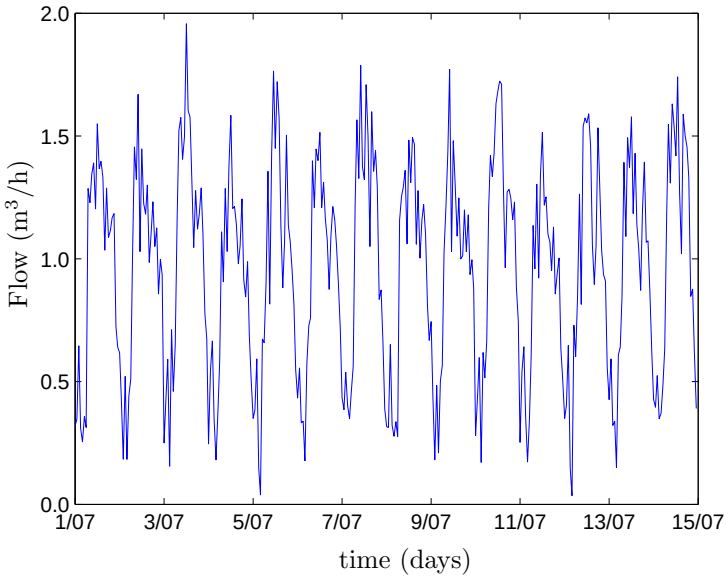

Figure 4.22: Profile of the water demand, over two weeks.

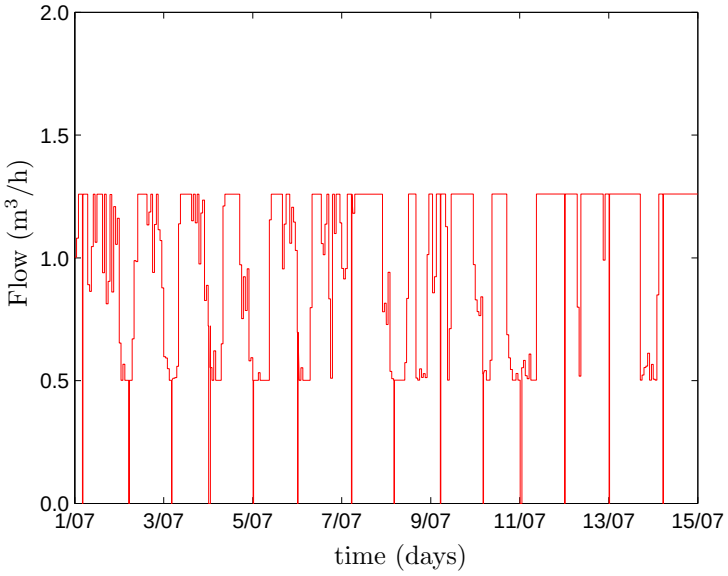

Figure 4.23: Profile of the permeate flow, over two weeks.

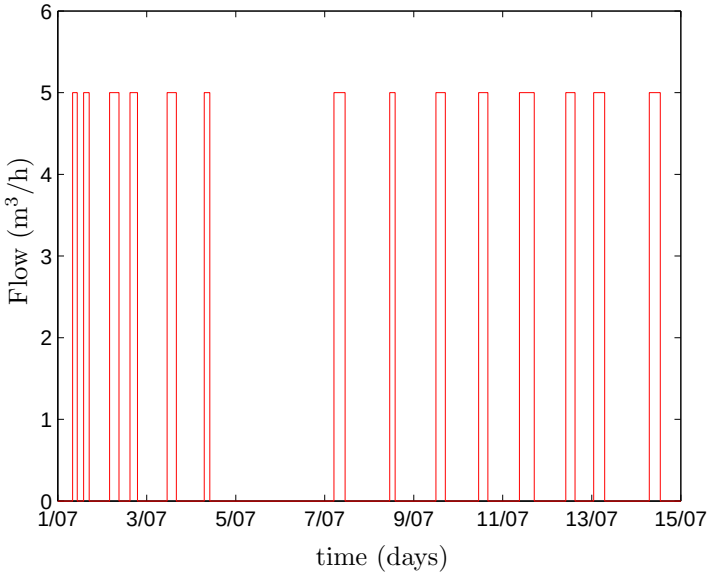

Figure 4.24: Profile of the on/off supply pump ('P1'), which sends feed water from the well to the input tank ('T1').

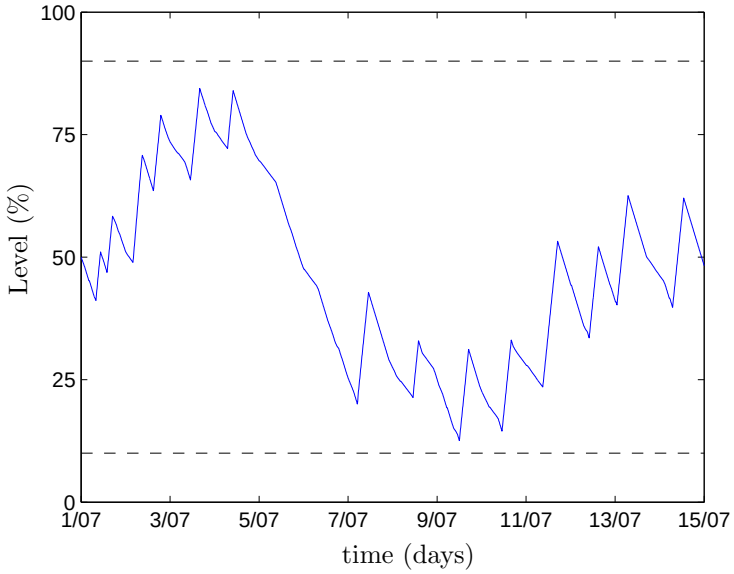

Figure 4.25: Evolution of the level of the input tank ('T1'), over two weeks.

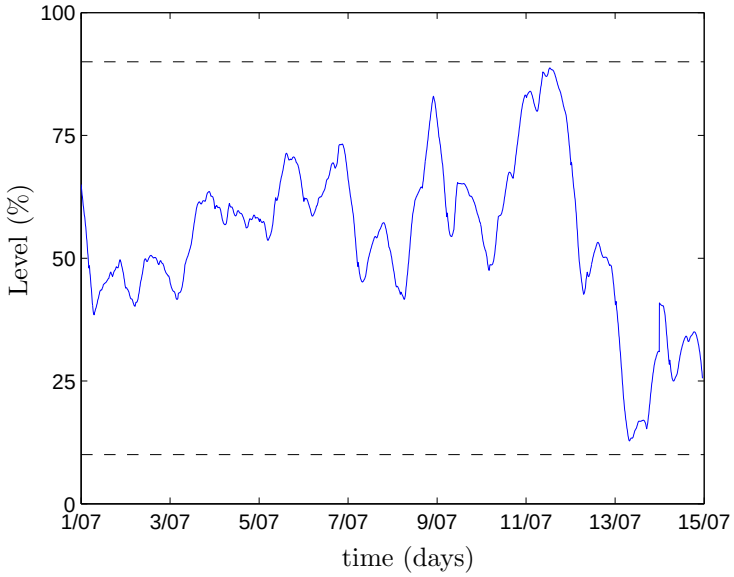

Figure 4.26: Evolution of the level of the output tank ('T3'), over two weeks.

Figures 4.25 and 4.26 show the evolution of the water level in the input tank ('T1') and the output tank ('T3'), respectively. The levels in the tanks are kept between a minimum and a maximum value by the advanced control, guaranteeing the water demand is fulfilled. Finally, the advanced control minimizes the consumption of energy by the desalination plant, linked with non-renewable sources, as seen in figure 4.27. The blue line is the availability of renewable power, while the red line is the power consumed by the plant. The use of non-renewable energy is carried out when the consumed power curve goes beyond the renewable power curve. The total energy provided by non-renewable energies corresponds to the blue-coloured areas.

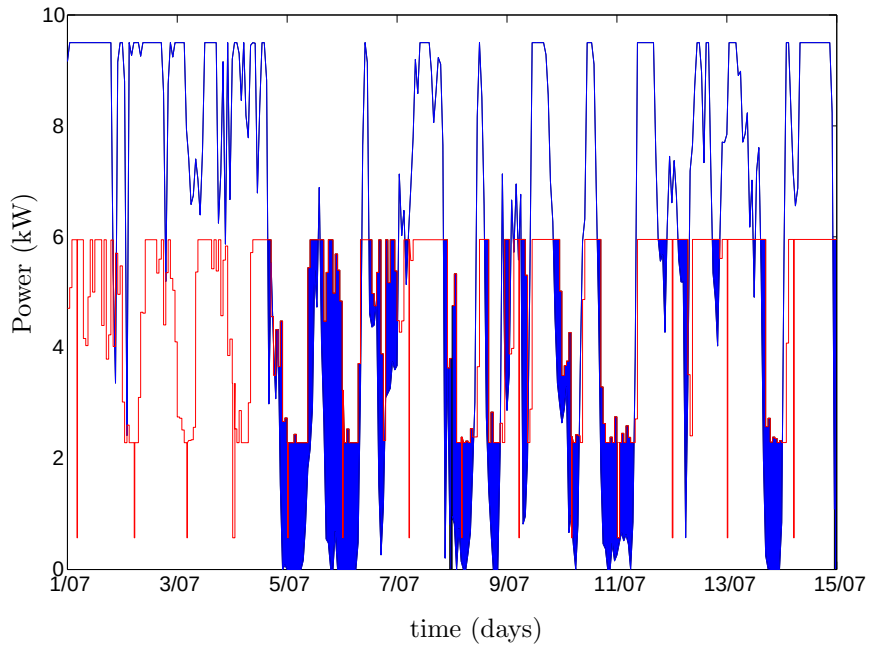

Figure 4.27: The blue line is the availability of renewable power, while the red line is the power consumption by the desalination plant. The blue area corresponds to the total non-renewable energy consumption.

In addition, the optimizer calculates the size of the main units of the desalination plant as follows:

– Input tank ('T1'): The height is 3.0 m, and the cross section is

35 m^2.

- Supply tank ('T2'): The height is 2.3 m, and the cross section is 3.0 m^2.
- Outlet tank ('T3'): The height is 2.8 m, and the cross section is 4.5 m^2.
- High-pressure pump: The calculated nominal flow is 1.7 m^3/h.
- Pressure vessels: The number of RO modules is 8.

The proposed integrated design of desalination plants uses a dynamic simulation of the system. This makes it possible to consider the effect of the control system and the prediction of water demand and available energy, reducing the installation and operation costs by using more realistic data than the usual worst-case approach, which only uses steady-state values for the variables. The optimization is based on a reformulation of the control problem in terms of continuous variables that avoids mixed-integer optimization and integrates the economic operation of the process. Hourly predictions of water demand are used to schedule the cleaning times and the operation of the pumps, taking into account the operational constraints. Preliminary results, based on the application to a model of a specific pilot plant powered by renewable energies, are promising in the sense that an adequate control of the system is achieved with small storage tanks, always fulfilling the control objectives and satisfying the water demand.

4.3 Scheduling of the Operation

This section deals with the optimization of the scheduling of an RO desalination plant on a long-term scale (several years), and takes into account: 1) the rotation of the RO modules; 2) the replacement of the RO modules; and 3) the chemical cleaning of the plant (see, for example, the works developed by Lu and Hu (2005), Lu et al. (2006) and Bhutani et al. (2013)). As commented in chapter 1, in an RO desalination plant, the osmosis is carried out in a train of pressure vessels. Each pressure vessel consists of several RO modules (between

1 to 14, but typically around 7) in series. The RO modules closer to the feed inlet are prone to be damaged by biofouling and solids, while the modules closer to the reject outlet are prone to be damaged by scaling due to increased salt concentration of the reject flow. In order to increase the life of the RO modules, it is a good practice to rotate the modules and change their position in the pressure vessel, thus spreading the different effects in each module. Typically, the rotation of the RO modules is carried out at the same time as the partial replacement of the RO modules, or during one long stop of the desalination plant.

Chemical cleaning is done once the fouling, the growth of microorganisms or the blocking of the pores, have being detected. The chemical cleaning is very aggressive to the RO membranes, and the life of the membranes is decreased after each chemical cleaning. Thus the chemical cleaning should be minimized as possible (one-two chemical cleanings per year).

Finally, the replacement of the RO modules is done according to their expected lifetime, or when the damage and breakage of the RO modules are detected. The replacement of the RO modules is not carried out for all the modules at the same time, but for a percentage of them. Typically, the ratio of replaced modules (r) is done proportionally to the number of replacements that will be done throughout the life of the modules, while the time instant of the replacements (t_{RP}) are scheduled at equal distances along the lifetime of the modules, as seen in equations (4.38-4.39). However, this is not necessarily the optimal solution:

$$r = \frac{1}{n_{RP}} \tag{4.38}$$

where n_{RP} is the number of replacements;

$$t_{RP} \propto \frac{\lambda_{RO}}{n_{RP}} \tag{4.39}$$

where λ_{RO} is the expected lifetime of the RO modules.

This work suggests a way to optimize the scheduling of the rotation and replacement of the RO modules, and the chemical cleaning of the desalination plant. The results were presented in Palacín et al. (2012a).

4.3.1 Mathematical Formulation

The objective of the optimization problem is to calculate the optimal scheduling for replacement, chemical cleaning and module rotation over a period of several years. The manipulated variables (u) are as follows:

- Number of chemical cleanings: n_{CL}
- Time instants of the chemical cleanings: $t_{CL}(1), t_{CL}(2), t_{CL}(3), ...t_{CL}(n_{CL})$
- Number of replacements: n_{RP}
- Time instants of the replacement: $t_{RP}(1), t_{RP}(2), t_{RP}(3), ...t_{RP}(n_{RP})$
- Percentage of each replacement: $r(1), r(2), r(3), ...r(n_{RP})$
- Number of module rotations: n_{ROT}
- Time instants of the module rotation: $t_{ROT}(1), t_{ROT}(2), t_{ROT}(3), ...t_{ROT}(n_{ROT})$

Mathematically, the problem can be formulated as a minimization of an objective function, which depends on the operation expenses, as follows:

$$\min_{u} \mathbb{C}_{CL} + \mathbb{C}_{RP} + \mathbb{C}_{ROT} + \mathbb{C}_{OP} \tag{4.40}$$

where u symbolizes all the manipulated variables, $\mathbb{C}_{CL}$ is the expense due to a chemical cleaning (\$), $\mathbb{C}_{RP}$ is the expense due to the partial replacement of RO modules (\$), $\mathbb{C}_{ROT}$ is the expense due to the rotation of RO modules (\$), and $\mathbb{C}_{OP}$ is the operation expense (\$).

The cost of chemical cleaning is assumed to be proportional to the total number of RO modules and the number of cleanings, as follows:

$$\mathbb{C}_{CL} = \kappa_{CL} \cdot n_{PV} \cdot n_m \cdot n_{CL} \tag{4.41}$$

where κ_{CL} is the cost of the chemical cleaning of one RO module (\$), n_{PV} is the number of pressure vessels, n_m is the number of RO

modules in each pressure vessel, and n_{CL} is the number of chemical cleanings.

While the cost of replacement of modules is assumed to be proportional to the number of modules replaced:

$$\mathbb{C}_{RP} = \sum_{i=1}^{n_{RP}} \kappa_{RO} \cdot n_{PV} \cdot n_m \cdot r(i) \tag{4.42}$$

where κ_{RO} is the cost of the replacement of one RO module ($), and n_{RP} is the number of module replacements.

The cost of the RO module rotation is assumed to be proportional to the number of pressure vessels and the number of rotations, as follows:

$$\mathbb{C}_{ROT} = \kappa_{ROT} \cdot n_{PV} \cdot n_{ROT} \tag{4.43}$$

where κ_{ROT} is the cost of the rotation of the RO modules of one pressure vessel, and n_{ROT} is the number of module rotations.

Finally, the operation cost is assumed to be proportional to the power consumed by the high-pressure pump:

$$\mathbb{C}_{OP} = \Phi \cdot \kappa_{OP} \cdot \int_{t=0}^{t_H} \frac{Q_f \cdot \Delta P}{\eta} \cdot dt \tag{4.44}$$

where Φ is the ratio between the power consumption of the plant and the power consumption from pumping, κ_{OP} is the cost of the energy ($/kWh), t_H is the simulated time (h), Q_f is the feed flow (m^3/h), ΔP is the pressure provided by the high-pressure pump (bar), and η is the pump efficiency and depends on the operating point, as seen below.

$$\eta = a_0 + a_1 \cdot Q_f + a_2 \cdot Q_f^2 + ... \tag{4.45}$$

The operating flow and pressure (Q_f, ΔP) are dynamic variables which depend on the state of the RO membranes and the scheduling of the plant (replacement and rotation of RO modules, chemical cleaning, etc.), as seen in section 2.1.2 at page 56.

Besides, several constraints should be taken into account. The operating pressure should not exceed a maximum value (P_{max}), for security reasons; while the concentration of the permeate flow should also not exceed a maximum value, ($C_{p\,max}$).

$$\Delta P \leq \Delta P_{max} \tag{4.46}$$

$$C_p \leq C_{p\,max} \tag{4.47}$$

This optimization problem consists of a mixed-integer nonlinear programming (MINLP) problem. Unlike the optimization problems of sections 4.1 and 4.2, this MINLP cannot be reformulated as an NLP because of the discrete variables of the number of chemical cleanings, rotations and replacements (n_{CL}, n_{ROT}, n_{RP}). Due to the complexity of this optimization problem, it may be approached using genetic algorithms or Monte Carlo optimization. See, for example, Gen and Cheng (2000), Pardalos and Romeijn (2002), and Rubinstein and Kroese (2011) for an in-depth description of this approach.

4.3.2 Results

This section shows the results of the scheduling of the operation described previously, applied to a simulated desalination plant (using the ROSIM library). The scheduling is calculated for 5 years (1800 days), which is, approximately, the expected lifetime of the RO membrane. Table 4.8 summarizes the parameters and constraints of the optimization problem.

Parameters	
Control horizon = 5 years (1800 days)	
Number of chemical cleanings (n_{CL}) $\sim$ 0-2 per year	
Number of chemical cleanings (n_{ROT}) $\sim$ 0-5 per year	
Number of chemical cleanings (n_{RP}) $\sim$ 0-5 per year	
κ_{CL} = 65 (\$)	κ_{ROT} = 1.30 (\$)
κ_{RO} = 75 (\$)	κ_{OP} = 0.15 (\$/kWh)
a_0 = -0.20	a_1 = 1.32 h/m^3
a_2 = -0.43 (h/m^3)^2	Φ = 1.67
ΔP_{max} = 40 bar	$C_{p\,max}$ = 300 ppm

Table 4.8: Parameters of the optimization of the scheduling of the operation: equations (4.40-4.47).

Parameters	
Number of pressure vessels (n_{PV}) = 50 in parallel	
Number of RO modules (n_m) = 8 per pressure vessel	
$A_w = 2.89 \cdot 10^{-7}$ m/(bar·s)	$B_s = 4.10 \cdot 10^{-8}$ m/s
Nominal values	
$Q_f \sim 1\,100$ m^3/h	$Q_p \sim 600$ m^3/h
$C_f \sim 20\,000$ ppm	$C_p \sim 150$ ppm
$\Delta P \sim$ 30-40 bar	Recovery ~ 55 %
Modelling of the ageing of the membranes	
$a_{\Psi_A} = 8.50 \cdot 10^{-4}$ days^{-1}	$b_{\Psi_A} = 0.64 \cdot 10^{-5}$ (days·m)$^{-1}$
$a_{\Psi_B} = 1.30 \cdot 10^{-3}$ days^{-1}	$b_{\Psi_B} = 3.23 \cdot 10^{-5}$ (days·m)$^{-1}$
$a_{\Gamma_A} = 840$ days	$b_{\Gamma_A} = 21$ days/m
$a_{\Gamma_B} = 310$ days	$b_{\Gamma_B} = 13$ days/m

Table 4.9: Characteristics of the desalination plant.

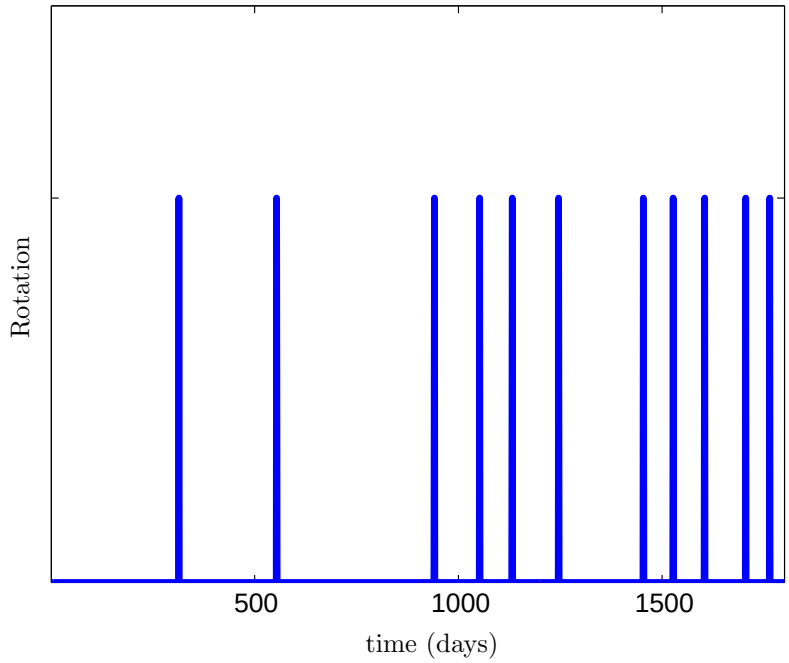

Figure 4.28: Scheduling of module rotation, over 5 years.

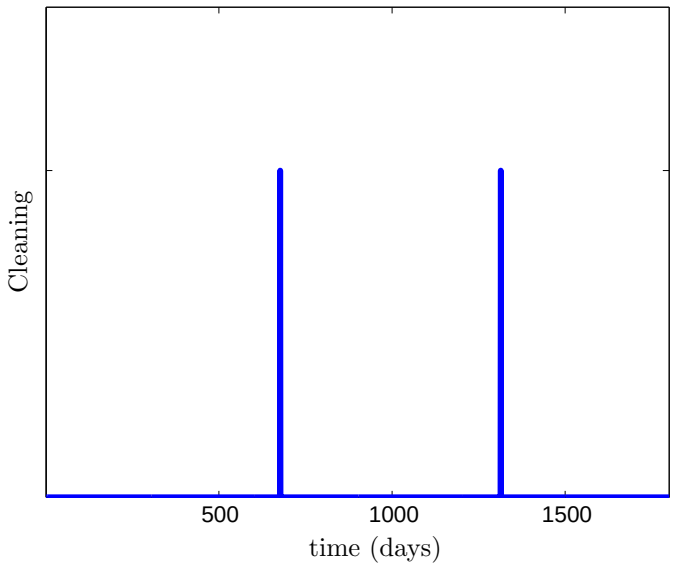

Figure 4.29: Scheduling of chemical cleaning, over 5 years.

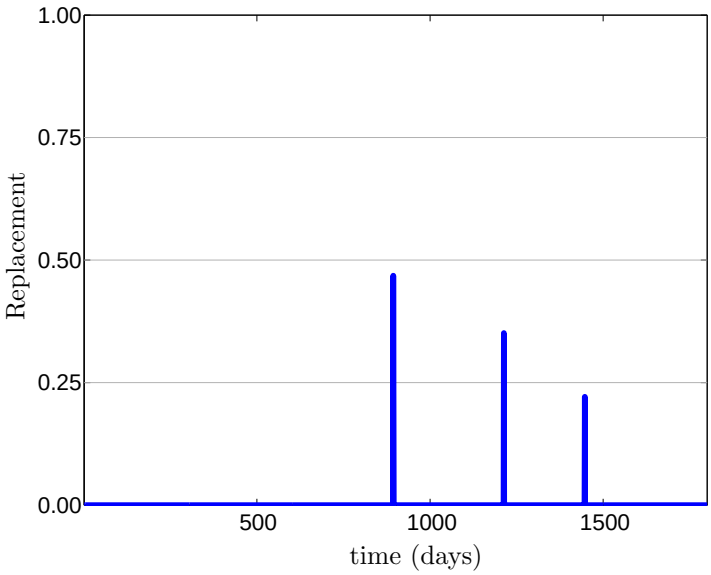

Figure 4.30: Scheduling of module replacement, over 5 years. The height of the peaks corresponds to the ratio of replaced modules (r).

In our case, the optimization problem was solved using genetic algorithms, developed in the mathematical software Matlab. Figures 4.28-4.30 show the proposed scheduling over 5 years. In particular, the time instant of the rotation of the RO modules is shown in figure 4.28, the chemical cleaning in figure 4.29, and the time instant of the replacement of the RO modules, as well as the percentage of replaced modules, is shown in figure 4.30.

The integration of equation (4.44) requires knowledge of several empirical parameters. These parameters should be estimated for each system, which is the major disadvantage of the proposed approach. However, this estimation may be easily done from historical data, after the corresponding plant has being operating over a long period. Table 4.9 summarizes the characteristics of the simulated desalination plant, the nominal values of the operating point, and the parameters of the modelling of the ageing of the membranes (section 2.1.2).

The results presented in this section are promising, in the sense that the scheduling of a desalination plant, over the long-term, may be optimized. The proposed approach uses a dynamic simulation of the desalination plant, while the optimization problem is solved using genetic algorithms, to avoid the formulation as an MINLP problem. The parameter estimation for the empirical parameters of the mathematical model may be easily done from historical data from the desalination plant.

Chapter 5

Two-Scale Modelling of the Concentration Polarization

Concentration polarization (CP) is the unwanted and inevitable effect of an increase of salt concentration in the boundary layer close to the RO membrane surface (see, for example, Chanukya et al. (2013)). Salt molecules accumulate in the boundary layer after being transported by the permeate flow (which crosses the membrane), where the majority are rejected by the membrane itself. CP is one of the most important factors influencing the performance of RO desalination plants (McCutcheon and Elimelech (2006)), due to the fact that the permeate flow and the scaling on the membrane surface are proportional to the osmotic pressure between both sides of the membrane, that is, to the salt concentration on the membrane surface. Several authors have proposed different approaches for the modelling of the CP, such as the Film Theory model (see Michaels (1968)) and the Retained Solute model (see Song and Elimelech (1995)). Every modelling approach has advantages, assumptions and disadvantages. This chapter proposes a new approach based on two-scale modelling, which aims to solve the main disadvantages of the previous models.

The two-scale approach organizes the mathematical modelling of the system in two layers: one microscopic and the other macroscopic. The microscopic layer deals with the modelling of the behaviour of the variables on a microscopic scale, that is, the behaviour of the salt molecules, their velocity, rejection by the RO membrane, etc. The macroscopic layer, on the other hand, deals with the modelling of

macroscopic variables, such as the permeate flow, the feed flow, the operating pressure, etc. The macroscopic model uses average parameters and properties (such as the diffusion, the reflection coefficient, the concentration polarization, etc.), which should be calculated for each system. The microscopic model is used for infer these properties for the macroscopic model.

Section 5.1 briefly describes the CP effect and the different approaches for its modelling. Next, section 5.2 presents the two-scale approach for the CP. Finally, section 5.3 shows the parameter estimation and the simulation of the proposed model.

This chapter summarizes the work which was developed during my stay in the School of Chemical Engineering and Analytical Science of the University of Manchester (UK), under the supervision of Constantinos Theodoropoulos, and with the help of Weiguo Xie. This work was presented in Palacín et al. (2012c).

5.1 Concentration Polarization

Figure 5.1 qualitatively symbolizes the concentration polarization (CP) effect that takes place in the boundary layer close to the membrane surface, in an RO desalination plant. The left and right hand sides of the figure symbolize, respectively, the feed side and the permeate side of a pressure vessel. The feed flows from bottom to top on the left hand side, and the permeate flux (J_w) flows from left to right, crossing the membrane. The salt concentration increases from the bulk in the feed side (C_f), to the membrane surface (C_m). Since the majority of the salt molecules are rejected by the membrane, the permeate concentration (C_p) in the permeate side is several times lower than in the feed. This inevitable increase of salt perpendicular to the feed flow is called the "concentration polarization", and is measured by the polarization module (ϕ) (Cath et al. (2013)):

$$\phi = \frac{C_m - C_p}{C_f - C_p} \tag{5.1}$$

As commented in chapter 2, the permeate flow produced in the desalination plant and the operating pressure depend on the salt concentration on the membrane surface (C_m). Thus, knowing the correct

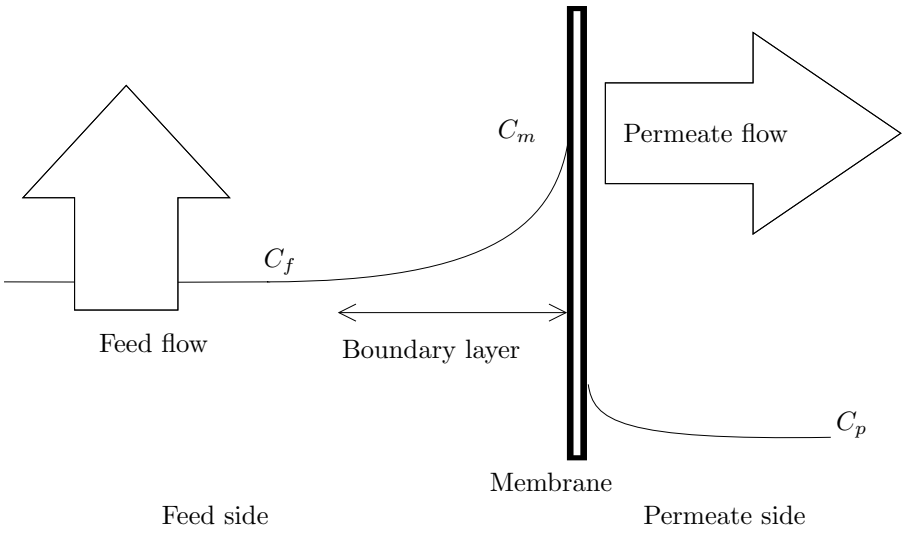

Figure 5.1: Increase of the salt concentration in the boundary layer close to the RO membrane surface.

value of C_m is essential for the design and operation of the plant. The concentrations of the feed, reject and permeate flows are easily measured with redox and conductivity sensors at the input and outputs of the racks of the pressure vessels. However, the concentration at the membrane cannot be measured, and should be estimated from the polarization module.

Several models have been proposed to calculate C_m, such as the Film Theory model (FT), proposed by Michaels (1968); the Retained Solute model (RS), proposed by Song and Elimelech (1995); and the Convection-Diffusion model (CD), proposed by Kim and Hoek (2005), which will be described next.

Notice that the salt concentration (C_f), the feed and permeate flows, the operating pressure, and the polarization module (ϕ), vary along the length of the pressure vessel, from the feed inlet to the reject outlet (x direction). So, as commented in chapter 2, the RO membrane and the pressure vessel should be discretized in a certain number of elements, and C_m calculated in each element. However, in several contexts, such as in optimization problems (see, for example, Lu et al. (2006)), when the simplicity of the model may be more important than its accuracy, it is possible that instead of discretizing the system,

working with average values ($\overline{C_f}$) may be enough, as follows:

$$\overline{C_f} = 0.5 \cdot (C_f|_{x=0} + C_f|_{x=L}) \tag{5.2}$$

where L is the length of the pressure vessel, $C_f|_{x=0}$ is the salt concentration at the input of the pressure vessel, and $C_f|_{x=L}$ is the salt concentration of the reject flow.

The distribution of the salt concentration along the RO modules, taking into account the CP, may be seen in Song and Liu (2012) and Rathore et al. (2013). The internal CP is described in Heo et al. (2012) and Tan and Yong (2013). Finally, the use of specific membranes for the minimization of the internal CP is described in Fang et al. (2012) and Emadzadeh et al. (2013).

5.1.1 Film Theory (FT) Model

The FT model was proposed by Michaels (1968) and upgraded by Porter (1986). It is by far the most popular and commonly used model for the calculation of ϕ. See, for example, the works developed by Marinas and Urama (1996), Bhattacharjee and Johnston (2002), Hoek and Elimelech (2003), Deon et al. (2013) and Suh and Lee (2013). It analytically integrates a local one-dimensional mass balance. Figure 5.2 shows the local control volume, while equation (5.3) shows the local one-dimensional mass balance for salt particles over this control volume.

$$\frac{\partial C_i}{\partial t} = J_w \cdot \frac{\partial C_i}{\partial z} - \mathcal{D} \cdot \frac{\partial {C_i}^2}{\partial z^2} \tag{5.3}$$

where C_i is the salt concentration of the control volume, $\mathcal{D}$ is the diffusion coefficient, and δ is the boundary layer thickness.

Assuming a steady state and taking into account that the total convective salt flow crossing the membrane is $J_w \cdot C_p$, equation (5.3) gives:

$$\mathcal{D} \cdot \frac{\partial C_i}{\partial z} - J_w \cdot (C_i(z) - C_m) = 0 \tag{5.4}$$

With the following boundary conditions:

$$\begin{cases} z = 0 & \rightarrow & C_i(0) = C_f \\ z = \delta & \rightarrow & C_i(\delta) = C_m \end{cases} \tag{5.5}$$

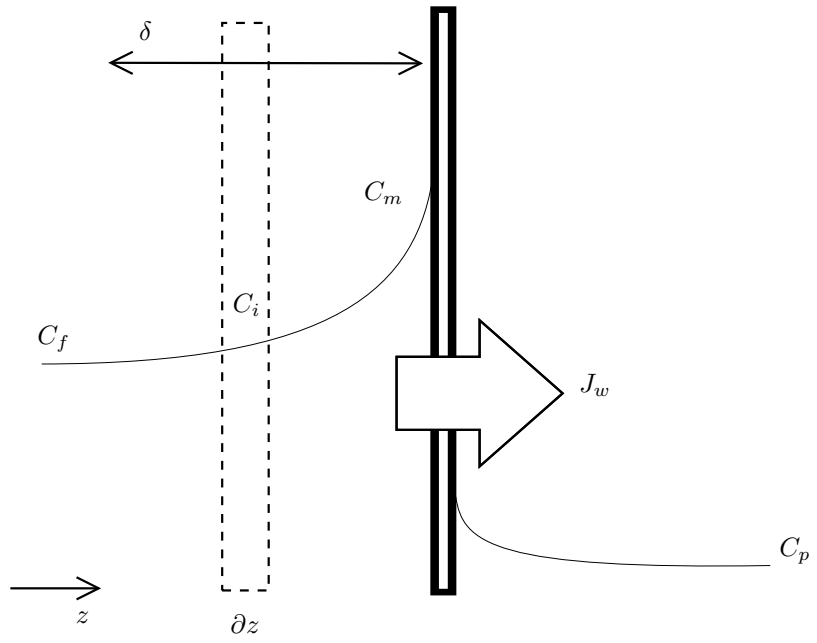

Figure 5.2: Control volume for the one-dimensional mass balance.

Assuming a constant diffusivity, the integration of equation (5.4) over the boundary layer (δ), gives:

$$\phi = \frac{C_m - C_p}{C_f - C_p} = \exp\left(\frac{J_w \cdot \delta}{\mathcal{D}}\right) \tag{5.6}$$

The previous equation may be written as follows:

$$\phi = \frac{C_m - C_p}{C_f - C_p} = \exp\left(\frac{J_w}{k_m}\right) \tag{5.7}$$

where k_m ($= \mathcal{D}/\delta$) is the mass-transfer coefficient from Fick's Law for molecular diffusion.

Since the FT model was proposed by Michaels, the major effort in CP modelling has been focused on the calculation of k_m. From then on, several empirical and theoretical equations have been proposed in the literature. However, most of them are available only under laboratory conditions. For example, Probstein (1994) proposed the calculation of the boundary layer (δ) for laminar flow in equation (5.8), while Blatt

et al. (1970) proposed the calculation of k_m for short pressure vessels in equation (5.9):

$$\frac{\delta(x)}{x} = 1.475 \cdot \left(\frac{h}{x}\right)^{2/3} \cdot \left(\frac{\mathcal{D}}{J_{w\ max} \cdot h}\right)^{1/3} \tag{5.8}$$

where h means the channel half height and $J_{w\ max}$ means the maximum permeate flux crossing the membrane;

$$k_m = 0.807 \cdot \left(\frac{\mathcal{D}^2 \cdot 3 \cdot \overline{J_w}}{L \cdot h}\right)^{1/3} \tag{5.9}$$

where L is the total pressure-vessel length, and $\overline{J_w}$ is the average permeate flux along the pressure vessel.

Equation (5.10) has been proposed by Evangelista (1986), while equation (5.11) has been proposed by Zydney and Colton (1986), and upgraded in Davis (1992).

$$k_m = 0.753 \cdot \left(\frac{\mathcal{K}}{2-\mathcal{K}}\right)^{1/2} \cdot \left(\frac{\mathcal{D}}{h_f}\right) \cdot Sc^{-1/6} \cdot \left(\frac{Pe \cdot h_b}{\mathcal{L}}\right)^{1/2} \tag{5.10}$$

where Pe is the Peclet number ($Pe = (u_f \cdot h_f)/\mathcal{D}$), Sc is the Schmidt number ($Sc = \mu/(\rho \cdot \mathcal{D})$), $\mathcal{K}$ and $\mathcal{L}$ are experimental parameters which quantify the blending efficiency and should be estimated for each type of RO membrane, h_f is the height of the feed side, and u_f, μ and ρ are, respectively, the velocity, viscosity and density of the feed flow.

$$k_m = \frac{1}{1.475} \cdot \left(\frac{h}{z}\right)^{2/3} \cdot \left(\frac{\mathcal{D}}{J_{w\,\max} \cdot h}\right)^{1/3} \tag{5.11}$$

Nowadays, the typical way to calculate k_m is to assume an empirical dependence between k_m and J_w as shown in equation (5.13) or (5.12):

$$k_m = a_1 \cdot u_p^{b_1} \tag{5.12}$$

where a_1 and b_1 are parameters that should be estimated for each particular system.

$$Sh = a_2 \cdot Re^{b_2} \cdot Sc^{b_3} \tag{5.13}$$

where Sh is the Sherwood number ($Sh = (k_m \cdot h_f)/\mathcal{D}$), Re is the Reynolds number ($Re = (\rho \cdot u_f \cdot h_f)/\mu$), and a_2, b_2 and b_3 are parameters that depend on the characteristics of the system.

There are several limitations to the FT model, such as the assumption that the boundary layer thickness (δ) does not depend on the permeate flux, the use of average parameters over the total pressure vessel, the use of empirical equations for the calculation of k_m, and the assumption of time equilibrium (Murthy and Gupta (1997), Goosen et al. (2002), Rathore et al. (2013)). However, owing to its simplicity and that it gives reasonable predictions, especially for low permeate flux and low operating pressure, it is the most widely used model for concentration polarization. See, for example, Jamal et al. (2004), Senthilmurugan et al. (2005), and Bhutani et al. (2013).

5.1.2 Retained Solute (RS) Model

The RS model was proposed in Song and Elimelech (1995) and upgraded in Song and Yu (1999). As in the case of the FT model, the RS model solves the CP problem by analytically integrating the mass balance for salt particles, but in this case, over two directions: in the direction of the permeate flux, as in the FT model (z axis), and in the direction of the feed flow (x axis). Figure 5.3 shows the two-dimension discretization which is used in the RS model.

The retained solute (C^*) means the difference of salt concentration between the membrane surface and the bulk of the feed flow, as shown in equation (5.14).

$$C^*(x) = C_m(x) - C_b(x) \tag{5.14}$$

Applying a mass balance for C^* over each element of figure 5.3, assuming a steady state and neglecting axial transport in the boundary layer, gives:

$$J_w(x) \cdot C^*(x) + \mathcal{D}\frac{\partial C^*}{\partial x} = 0 \tag{5.15}$$

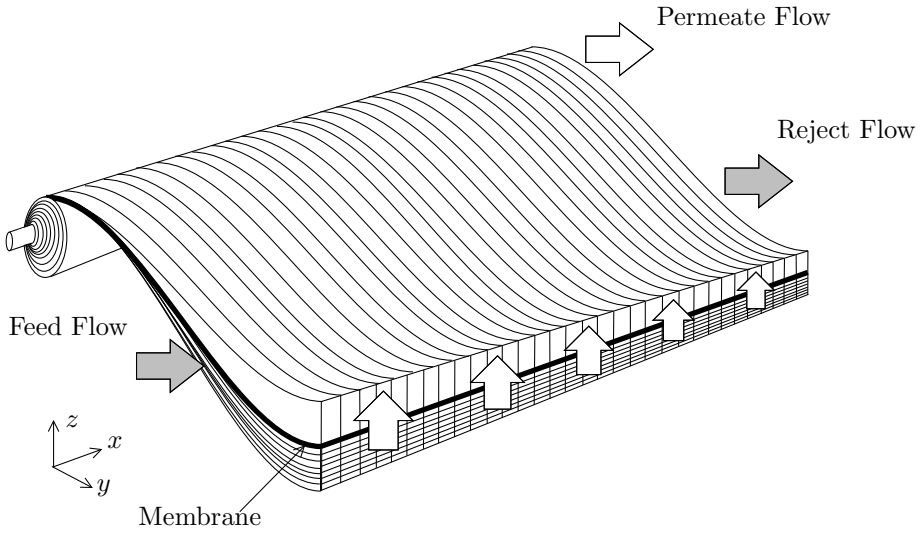

Figure 5.3: Two-dimension discretization of the RO module for the RS model.

where $J_w(x)$ can be calculated from the difference between the operating pressure and the osmotic pressure (as commented in chapter 2):

$$J_w(x) = A \cdot (\Delta P(x) - \Delta\pi(x)) \tag{5.16}$$

The major limitation of this model is that it requires a known profile of the operating pressure over the pressure vessel for it to be analytically integrated. In addition, this model assumes a steady state.

5.1.3 Convenction-Diffusion (CD) Model

The CD model was proposed in Kim and Hoek (2005) and solves the same two-dimensional mass balance as the RS model, now coupled with the Navier-Stokes equations. This model should be integrated numerically, owing to the complexity of the equation system. The CD model improves the prediction on permeate flow and CP for conditions of high pressure and flux, and is attractive due to the correct calculation of flows for realistic ranges in RO desalination plants. However, its major limitations are that a steady state is assumed, and its high number of unknown parameters.

5.2 Two-Scale Modelling

This section presents a new dynamic model for the calculation of the concentration polarization and the salt distribution along the pressure vessel. This model aims to solve the main disadvantages of the previous models, such as the constant size of the boundary layer (δ), the assumption of a known profile of pressure along the pressure vessels, and the assumption of a steady state.

The approach of this model is based on two-scale modelling. The RO module is modelled in two scales: a macroscopic scale and a microscopic scale. The macroscopic part of the model deals with the calculation of the pressure , and the salt concentration of the bulk of the feed side (C_f). While the microscopic part deals with the calculation of the salt concentration of the membrane surface (C_m) and the concentration polarization (ϕ).

5.2.1 Macroscopic Model

The macroscopic model is based on the mathematical modelling described in chapter 2. The RO module is discretized in three dimensions: in the axial direction, parallel to the feed flow (x axis), and in the radial direction (y axis), as seen in figure 5.4.

In each element of the discretization, the permeate flux crossing the membrane (J_w) is calculated by the equation (5.17):

$$J_w = A_w \cdot (P_f - P_p - \sigma \cdot i \cdot \frac{R \cdot T}{PM} \cdot (C_m - C_p)) \tag{5.17}$$

where A_w is the water permeability, P_f is the pressure at the feed side, P_p is the pressure at the permeate side, σ is the reflection coefficient, i is the van't Hoff coefficient, R is the gas constant, T is the temperature, and PM is the molar weight.

The pressure at the feed and permeate sides may be calculated, respectively, by equations (5.18) and (5.19):

$$\frac{\partial P_f}{\partial x} = a_f \cdot \mu \cdot u_f^{b_f} \tag{5.18}$$

where u_f is the water velocity of the feed flow, and a_f and b_f are proportional factors that depend on each system.

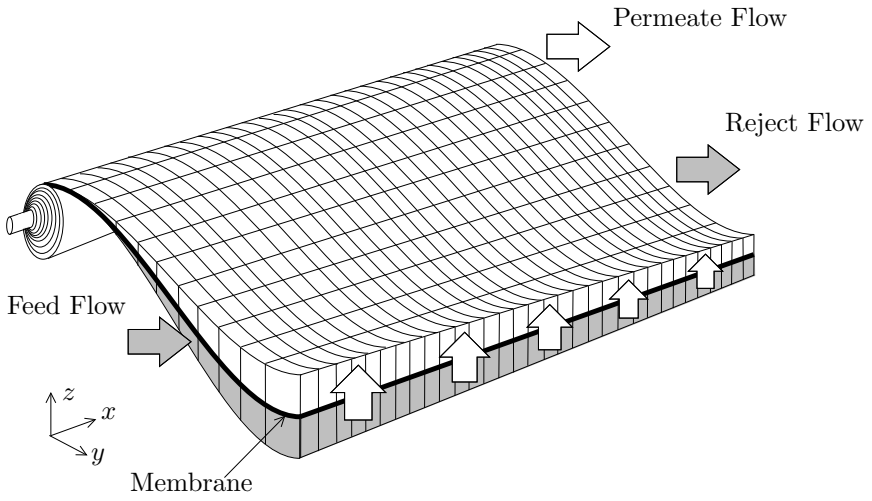

Figure 5.4: Two-dimension discretization of the RO module for the macroscopic scale.

$$\frac{\partial P_p}{\partial y} = a_p \cdot \mu \cdot u_p^{b_p} \tag{5.19}$$

where u_p is the water velocity of the permeate flow, and a_p and b_p are proportional factors that depend on each system.

The salt concentration of the bulk of the feed flow (C_f) in each element of the discretization is calculated as follows:

$$\frac{\partial C_f}{\partial t} = \frac{\partial (u_f \cdot C_f)}{\partial x} - \frac{J_s}{h_f} \tag{5.20}$$

where h_f is the size of the feed spacer and J_s is the salt flux that crosses the membrane.

The salt flux is calculated as a function of the salt difference between both sides of the membrane, as follows:

$$J_s = B_s \cdot (C_f - C_p) \tag{5.21}$$

Finally, the salt concentration of the permeate may be calculated as follows:

$$\frac{\partial C_p}{\partial t} = \frac{\partial (u_p \cdot C_p)}{\partial y} + \frac{J_s}{h_p} \tag{5.22}$$

where h_p is the size of the permeate spacer.

The mathematical system formed by equations (5.17-5.22) has one independent variable (per each element of the discretization): the salt concentration on the surface of the membrane (C_m), which will be calculated by the microscopic part of the two-scale model.

5.2.2 Microscopic Model

The microscopic model calculates the salt concentration on the surface of the membrane (for each element of the discretization of the macroscopic model). This model is applied in the boundary layer close to the RO surface, and is based on Monte Carlo methods and the Langevin equation. The Langevin equation is basically the Newton's second law and describes Brownian motion. An in-depth description of this equation may be seen in Biagini et al. (2009) and Huang (2009); while several examples of Monte Carlo-based simulations, such as the simulation of colloidal systems, may be seen in Chena and Kimb (2004), Cecconi et al. (2005) and Jacobs (2009). Finally, an in-depth description of the molecular dynamic simulation in an RO membrane, may be seen in, for example, Baker (2004), Hu et al. (2011), Aragonés et al. (2012) and Ebro et al. (2013).

The position of one salt particle is modelled by a Langevin equation, as follows:

$$m_j \cdot x_j'' = F_j(x_j) - b_j \cdot x_j' + e_j \tag{5.23}$$

where m_j is a parameter linked with the mass of the particle, x_j is the position of the particle along the boundary layer, $F_j(x_j)$ is the convective flow that pushes the particle in the membrane surface direction and is linked with the permeate flux (J_w), b_j is a parameter that depends on the opposition of the particle to be moved (by Stokes Law), and e_j is a stochastic parameter that simulates the Brownian motion. Typically, e_j may be calculated by a Gaussian distribution with zero mean and variance σ_j^2, as seen in Biagini et al. (2009).

In the model proposed, the mean of the Gaussian distribution is not zero, but proportional to the salt concentration gradient, as shown in equation (5.24).

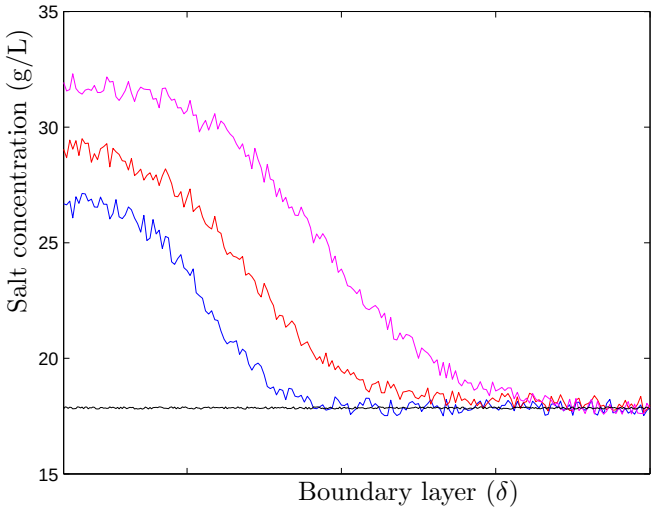

Figure 5.5: Profile of the concentration polarization in one element. The black line is the initial profile, while the blue, red and magenta lines are the profiles at 5, 10 and 20 seconds, respectively.

$$\mu_j = k_j \cdot \frac{\partial C_i}{\partial z} \tag{5.24}$$

with the following boundary values:

$$\begin{cases} z = 0 & \rightarrow & C_i(0) = C_f \\ z = \delta & \rightarrow & C_i(\delta) = C_m \end{cases} \tag{5.25}$$

where k_j is a parameter which depends on the system, and $\dfrac{\partial C_i}{\partial z}$ is the salt concentration difference in the boundary layer (z axis).

The mathematical system formed by equations (5.23-5.25) has two independent variables: the salt concentration of the bulk of the feed flow (C_f) and the permeate flux (J_w). These two variables will be calculated by the macroscopic part of the two-scale model.

The calculation of the position of one single particle does not produce any useful result. However, by repeating the calculations for a high number of particles, the average result is able to predict the concentration polarization. The number of particles is chosen by the user.

In the present case, the same simulation was repeated several times, increasing the number of particles in each simulation. In the cases with low number of particles, the results are different and depends on the number of particles. However, from a certain point, the results are approximately the same, and independent of the number of particles. The number of particles selected is given by the simulation with the lower number of particles, which results are approximately the same. In this case, the number of particles was fixed to 1 million. However, this parameter is subjective and depends on the user.

Figure 5.5 shows the profile of salt concentration by the integration of the microscopic model in one element of (figure 5.4). The membrane is placed in the ordinate axis, while the permeate flux will cross the membrane from right to left. The salt concentration of the bulk is assumed to be equal to 18 g/L. Initially, the operating pressure and the feed flow is zero, there is no permeate flow and the salt particles are distributed uniformly along the boundary layer (black line). Then, the system is connected, and the high-pressure pump supplies enough pressure to produce the passing of water through the membrane. The salt particles are pushed against the membrane and rejected by the membrane itself, and the concentration polarization may be measured. The blue, red and magenta lines are, respectively, the profile of the concentration polarization after 5, 10 and 20 seconds.

5.2.3 Coupling both Models

As commented before, the macroscopic model calculates the operating pressure, the salt concentration of the bulk of the feed flow (C_f) and the permeate flux (J_w), as a function of the salt concentration on the membrane surface (C_m); while the microscopic model calculates the salt concentration on the membrane surface (C_m), as a function of the salt concentration of the bulk of the feed flow (C_f) and the permeate flux (J_w). Both models should be solved sequentially, as follows: macroscopic model - microscopic model - macroscopic model - etc. Besides, while the macroscopic model calculates the variables in all the RO module, the microscopic model calculates the variables in each element of the discretization. So, in each sample time, the microscopic model should be applied as many times as the number of elements of the discretization.

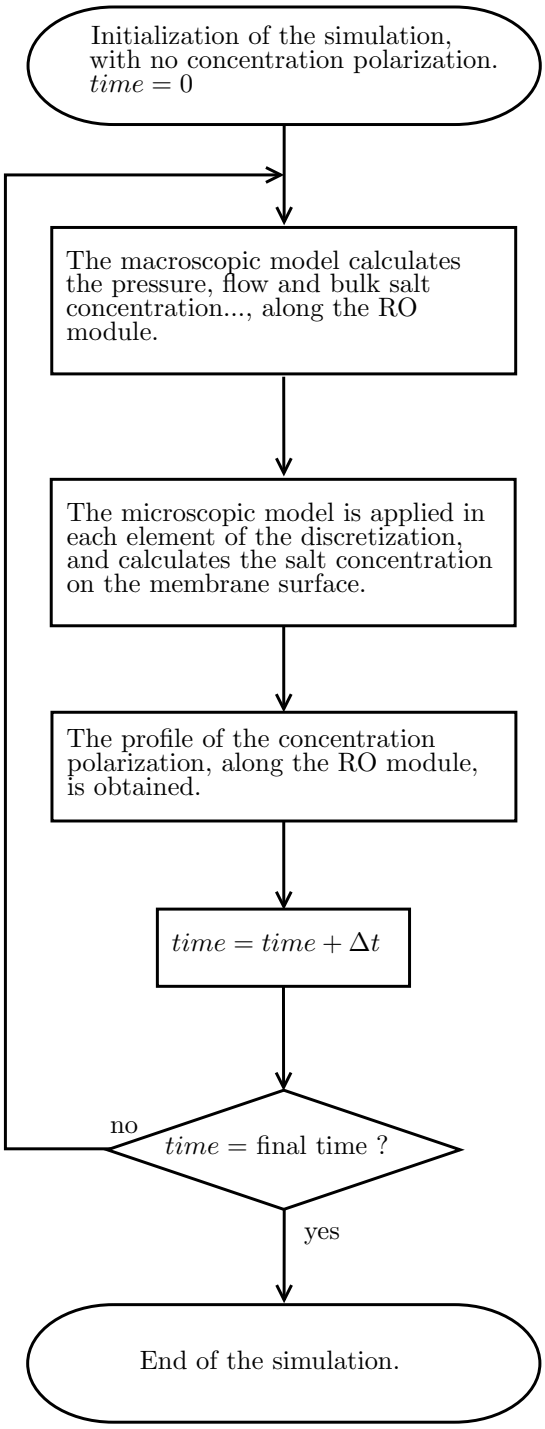

Figure 5.6: Algorithm to couple both models.

The algorithm that couples both models is symbolized in figure 5.6 and described now below:

1. The RO membrane is discretized in $n_1 \times n_2$ elements, along the axial and radial directions.

2. Initially, it is assumed that there is no concentration polarization along the RO membrane.

3. The macroscopic model calculates the operating pressure, the flow of the feed and the permeate, and the salt concentrations of the feed flow and of the permeate flow, along the RO module, taking into account the profile of concentration polarization.

4. The microscopic model is applied in each element of the discretization, and calculates the salt concentration on the membrane surface, taking into account the profile of pressure, salt concentration and permeate flux along the RO module.

5. Steps 2 and 3 are repeated sequentially, each sample time, until the system reaches the steady state.

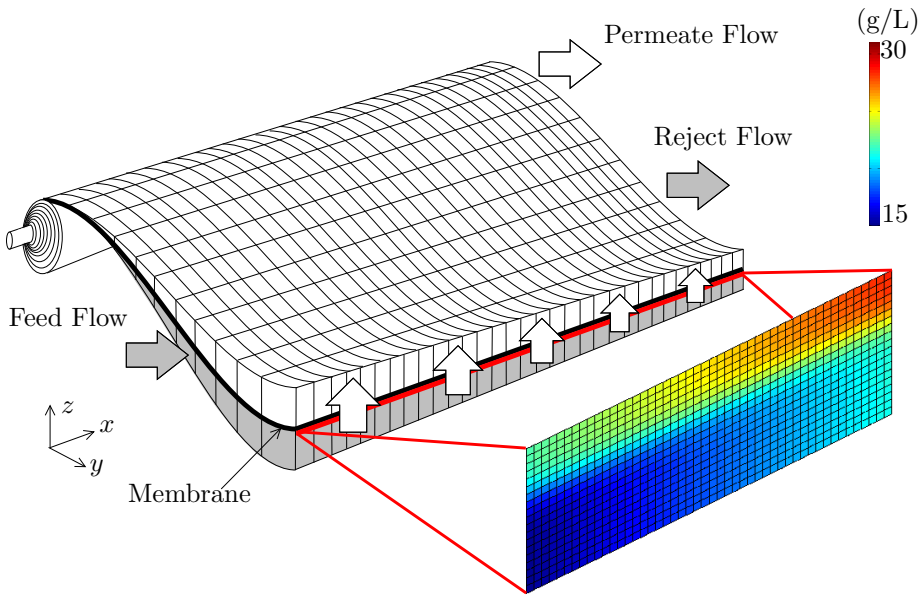

Figure 5.7: Profile of concentration polarization along the RO module.

Finally, figure 5.7 shows the concentration of polarization in the boundary layer, close to the RO membrane, obtained from the two-scale model. Notice the salt concentration on the membrane surface and in the bulk of the feed stream, increases along the RO module, due to a higher percentage of permeate crossing the membrane.

5.3 Simulation

Figure 5.8 shows the profile of concentration polarization along the RO module at six time instants (0, 2, 5, 10, 15, 30 seconds). Initially, it is assumed that there is no concentration polarization and the salt concentration is distributed uniformly along the boundary layer (figure a). When the plant is connected, and the passing of permeate through the membrane takes place, the salt concentration starts to increase (figures b-f). The salt concentration increases in the direction of the reject flow (right hand side of each figure) and increases over the time (compare the profile of figure f with the one of figure b). After 30 seconds, the system reaches the steady state (figure f).

The proposed model requires four parameters: m_j, b_j, k_j, σ_j^2, which depend on each system. These parameters are calculated for the RO modules of the pilot plant, described in section 3.1. The parameter estimation follows the same strategy shown in section 3.2, which is symbolized in figure 5.9.

The boundaries of the system are characteristic of the feed flow at the inlet of the pressure vessel (pressure supplied by the high-pressure pump, feed flow, salt concentration, and temperature). y are the variables measured at the outlet of the pressure vessel (flow and salt concentration of the permeate); while $\hat{y}$ are the same variables, but calculated using the two-scale model. *error* is the difference between y and $\hat{y}$.

The optimizer manipulates the unknown parameters, minimizing an objective function that embraces the errors between y and $\hat{y}$. This is a dynamic optimization problem as shown in equation (5.26):

$$\min_{m_j,b_j,k_j,\sigma_j^2} \sum_{i=1}^{K} \frac{(Q_p(i) - \hat{Q}_p(i))^2}{\overline{Q_p}} + \sum_{i=1}^{K} \frac{(C_p(i) - \hat{C}_p(i))^2}{\overline{C_p}} \tag{5.26}$$

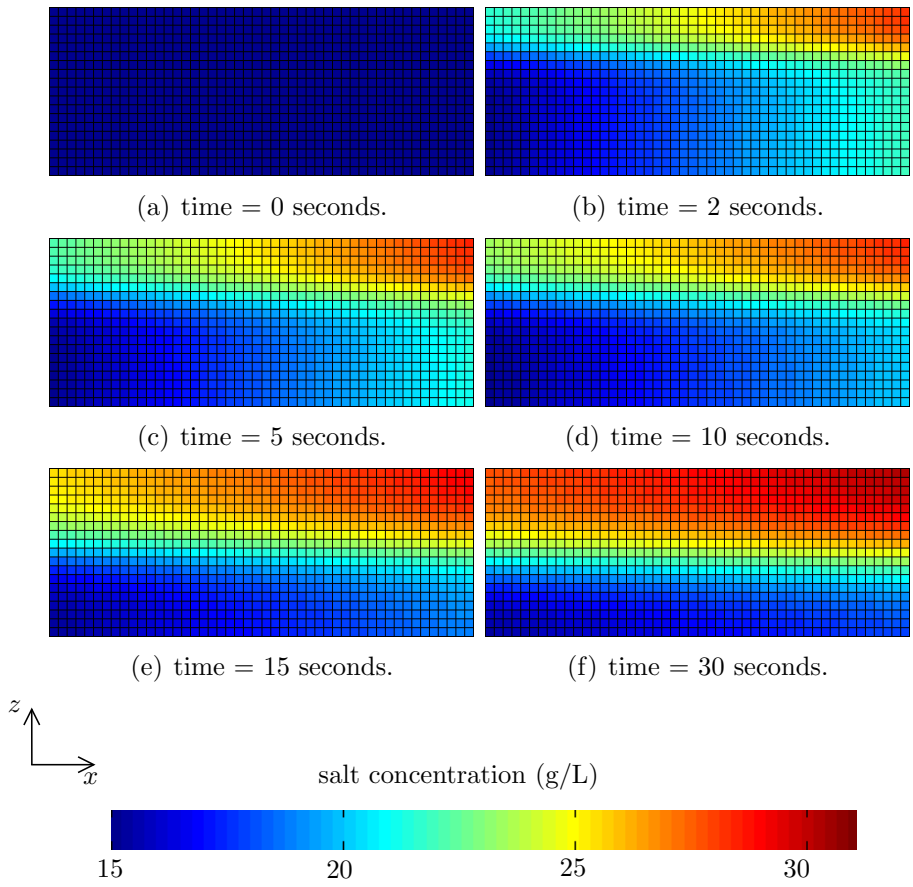

Figure 5.8: Profile of concentration polarization along the RO module over 30 seconds.

where K is the number of sample times, Q_p is the total permeate flow, $\overline{Q_p}$ is the average permeate flow, and $\overline{C_p}$ is the average salt concentration of the permeate.

The optimization problem was solved using the optimization packages provided by the software Matlab, the result of which is shown below:

$$\begin{cases} m_j &= 9.1 \cdot 10^{-4} \\ b_j &= 0.13 \\ k_j &= 0.33 \\ \sigma_j^2 &= 1.3 \cdot 10^{-2} \end{cases} \tag{5.27}$$

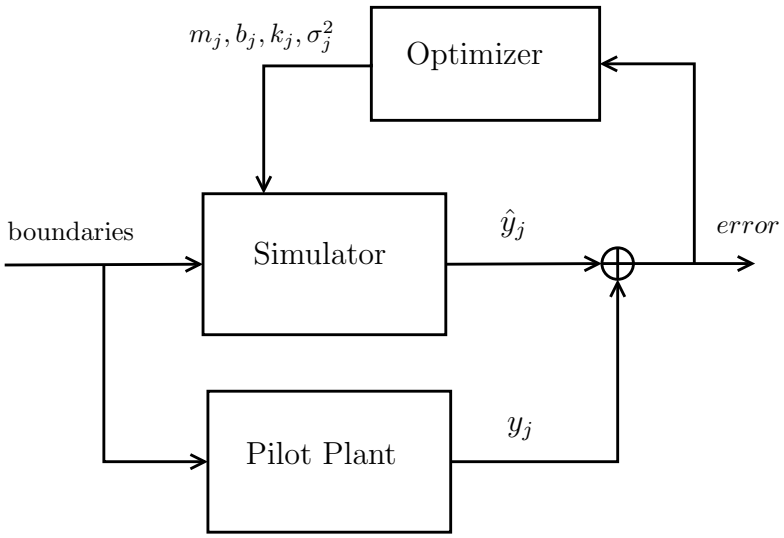

Figure 5.9: Parameter estimation for the two-scale model.

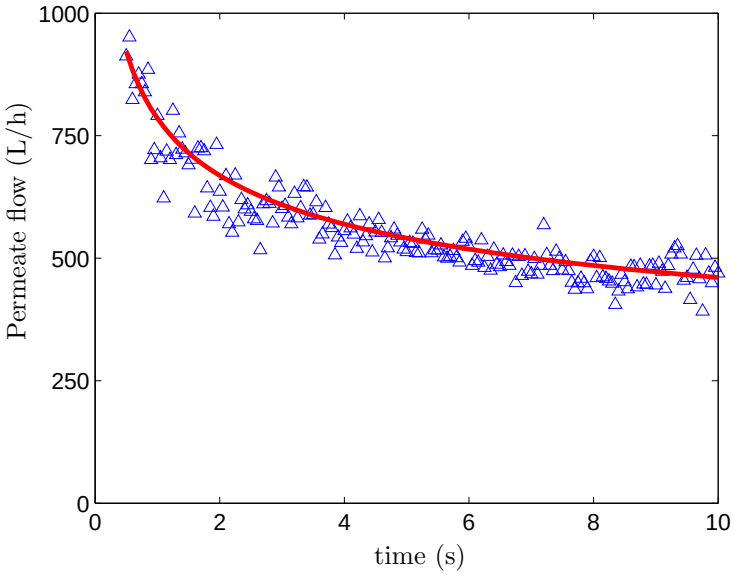

Figure 5.10: Behaviour of the permeate flow over 10 seconds. The red line is the calculated profile from the two-scale model, while the blue triangles are real data measured from the pilot plant.

The parameter estimation and the model validation should be done using the measurement of the salt concentration in the bulk of the feed flow, at different points along the pressure vessel. However, due to the limitiations of the pilot plant, the paramter estimation was done using data only at the outlet of the pressure vessel.

Figure 5.10 shows the behaviour of the permeate flow over 10 seconds, after a washing of the RO module. The red line is the calculated profile from the two-scale model, while the blue triangles are real data measured from the pilot plant.

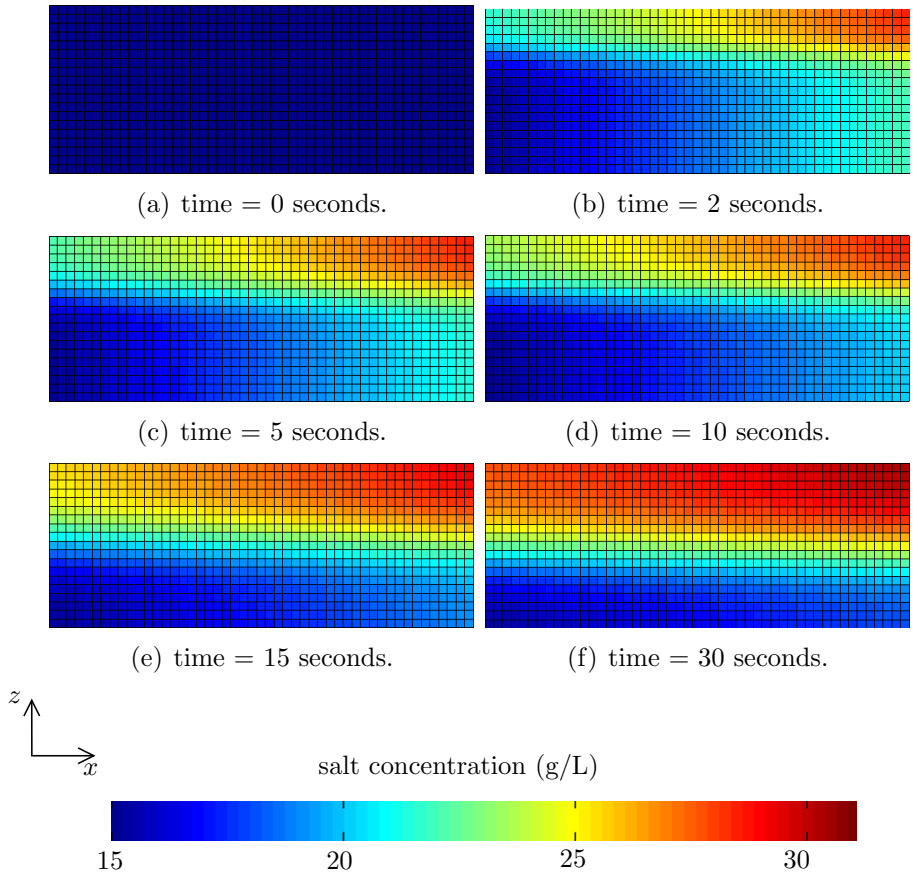

Figure 5.11: Profile of concentration polarization along the RO module over 30 seconds. The profile has been calculated using the model reduction-based technique proposed by Xie and Theodoropoulos (2010).

Due to the high number of equations and elements of the discretization, the computer time to solve the concentration polarization profile shown in figure 5.11 was slow (above 1 hour). However, this time may be drastically reduced using model reduction-based techniques, such as the algorithm proposed by Weiguo Xie and Constantinos Theodoropoulos (see Xie and Theodoropoulos (2010)), which is based on the training of special neural networks.

Figure 5.11 shows the same profile as figure 5.8, but using the model reduction proposed by Xie. The computer time for calculating this figure was less than 1 second. Notice that both figures are practically identical.

The use of the two-scale model presented here is promising, in the sense that this model is able to predict the profile of the concentration polarization along the RO module, which allows a better design of the RO modules and the pressure vessel. The major disadvantages of this model are the need for estimation of the unknown parameters, and the high computer time required.

Due to the goodness of the multi-scale approach applied to the concentration polarization, it would be possible to extend this approach to other effects that take place in a desalination plant and are difficult to model by classic approaches, such as the scaling of calcium carbonate in the metastable region, the blocking of the pores and the biofouling, that may be considered as future work.

Chapter 6

Conclusion and Future Work

Section 6.1 summarizes the main conclusions and completed tasks concerning this thesis. Next, section 6.2 includes the publications and presentations for conferences which have been developed arising from this thesis. Finally, section 6.3 gives general ideas for future work and open issues.

6.1 Conclusion

This thesis have presented several contributions on the modelling and control of RO desalination plants: the development of a new dynamic simulation library for RO desalination plants; the use of a two-scale approach for the modelling of the concentration polarization; and the study of the optimal operation of RO desalination plants, on a short and long-term scale; as follows:

1. We have developed a dynamic library for the design of RO desalination plants based on first principles, physical and chemical equations and correlations from the literature. This library is different to the commercial libraries, because is not focused on the nominal operating point, but on the dynamic behaviour of the system. This library takes into account the growth of microorganisms, the ageing of the membranes and the operation during cleanings and replacements. We have validated this library using real data from a pilot plant.

Thanks to the collaboration between the University of Valladolid and the company EA, this library has been successfully commercialised.

The mathematical modelling, which is in the core of the components of the library, was presented in Syafiie et al. (2008a,b, 2009, 2010) and Palacín et al. (2012a,b); while the library was presented in Palacín et al. (2008a), and upgraded in Palacín et al. (2009c, 2011b). Finally, the validation of the library was described in Palacín et al. (2010b,e).

2. In addition, we have tested different techniques of advanced control, in a small-scale desalination plant, powered by renewable energies (photovoltaic panels and wind turbines) and non-renewable energy (diesel generator). The results are promising, in the sense that we are able to decrease the operation costs, decrease the size of the tanks and equipments, and minimize the consumption of non-renewable energy, while still fulfilling the water demand.

   The idea is simple. Coupling the energy consumption with the control of the energy production, the plant operation may be improved. Operating the desalination plant as an active charge, and taking into account the prediction of renewable energy and water demand, it is possible to compensate the divergences between the availability of non-renewable energy and the energy consumption. This is done manipulating the operating point and selecting correctly the time instant for cleaning, in such way that a certain objective function is minimized, which takes into account the operating cost and penalize the use of non-renewable energy and the unfulfilment of the water demand.

   The advanced control of desalination plants have been presented in Palacín et al. (2009d, 2010d, 2011a); while the integrated process and control design was studied in Palacín et al. (2009a,b).

3. Next, we have presented a methodology to schedule the operation of a RO desalination plant, on a long-term scale (several years). The proposed approach is based on a dynamic optimization and uses a dynamic modelling of the plant. This work aims to calculate the time instant for chemical cleanings, replacement

and rotation of the RO modules, during the lifetime of the membranes. This work was presented in Palacín et al. (2012a).

4. Finally, we have proposed a new dynamic modelling of the concentration polarization effect, which takes place along the RO modules. The studied approach is based on a two-scale modelling and consists in dividing the system in two layers: one microscopic and the other macroscopic. The macroscopic layer calculates the macroscopic variables (such as the permeate flow and the operating pressure), while the microscopic layer infers the properties and parameters of the macroscopic model. This approach was described in Palacín et al. (2012c).

6.2 Publications Arising from the Thesis

The work arising from this thesis has been presented in several articles and conferences, which are summarized below.

The following journal articles were published during the development of this thesis:

- **Palacín, L. G.**, Tadeo, F., de Prada, C., and Salazar, J. (2012). Scheduling of the membrane module rotation in RO desalination plants. *Desalination and Water Treatment*, 48:1-8. IF: 0.852.

- **Palacín, L. G.**, Tadeo, F., de Prada, C., and Touati, K. (2012). Evaluation of the recovery of osmotic energy in desalination plants by using pressure retarded osmosis. *Desalination and Water Treatment*, 47:1-6. IF: 0.852.

- **Palacín, L. G.**, Tadeo, F., de Prada, C., and Salazar, J. (2011). Operation of desalination plants using hybrid control. *Desalination and Water Treatment*, 25:119-126. IF: 0.614.

- **Palacín, L. G.**, Tadeo, F., Elfil, H., de Prada, C., and Salazar, J. (2011). New dynamic library of reverse osmosis plants with fault simulation. *Desalination and Water Treatment*, 25:127-132. IF: 0.614.

- **Palacín, L. G.**, Tadeo, F., Salazar, J., and de Prada, C. (2011). Ósmosis inversa en instalaciones remotas con energías renovables. *InfoEnviro*, 65:42-45.

- Syafiie, S., Tadeo, F., **Palacín, L. G.**, de Prada, C., and Salazar, J. (2010). Modelling of the pretreatment section for dynamic simulation of water production using reverse osmosis. *International Journal of Management Science and Engineering Management*, 5:1-6.

The following presentations for international conferences were delivered during the development of this thesis:

- **Palacín, L. G.**, Theodoropoulos, C., Weiguo, X., Tadeo, F., and de Prada, C. (2012). Two-scale modelling of the concentration polarization in a reverse osmosis membrane. In *Chemical Process Control, CPC VIII, Savannah, USA*.

- **Palacín, L. G.**, Tadeo, F., Salazar, J., and de Prada, C. (2010). Operation of medium-size reverse osmosis plants with optimal energy consumption. In *9th International Symposium on Dynamics and Control of Process Systems, Leuven, Belgium*.

- **Palacín, L. G.**, Tadeo, F., Salazar, J., and de Prada, C. (2010). Initial validation of a reverse osmosis simulator. In *Emerging Technologies and Factory Automation, Bilbao, Spain*.

- **Palacín, L. G.**, Tadeo, F., Salazar, J., and de Prada, C. (2010). Validation of a reverse osmosis dynamic simulator. In *European Modeling and Simulation Symposium, EMSS, Fez, Morocco*.

- **Palacín, L. G.**, Tadeo, F., and de Prada, C. (2009). Integrated design using dynamic simulation of reverse osmosis plants. In *Industrial Engineering and Engineering Management, Hong Kong, China*.

- **Palacín, L. G.**, Tadeo, F., Elfil, H., and de Prada, C. (2009). New dynamic library of reverse osmosis plants with fault simulation. In *2nd Maghreb conference on desalination and water treatment, Hammamet, Tunisia*.

- **Palacín, L. G.**, Tadeo, F., Salazar, J., and de Prada, C. (2009). Operation of desalination plants using hybrid control. In *2nd Maghreb conference on desalination and water treatment, Hammamet, Tunisia*.

- **Palacín, L. G.**, de Prada, C., Syafiie, S., and Tadeo, F. (2008). Library for dynamic simulation of reverse osmosis plants. In *20th European Modeling and Simulation Symposium, EMSS, Calabria, Italy*.

- Tadeo, F., **Palacín, L. G.**, Salazar, J., and de Prada, C. (2011). Desalination in remote areas: A prediction-based approach. In *IDA World Congress, Perth, Australia*.

- García- Álvarez, D., **Palacín, L. G.**, de la Fuente, M. J., Tadeo, F., and de Prada, C. (2011). Control of a desalination plant, including U-PCA-based monitoring. In *the 12th International Conference on Environmental Science and Technology, Rhodes, Greece*.

- Tadeo, F., **Palacín, L. G.**, Syafiee, S., and de Prada, C. (2010). Improving the efficiency of small water production facilities. In *European Energy Conference, ESF, Barcelona, Spain*.

- Syafiie, S., **Palacín, L. G.**, de Prada, C., and Tadeo, F. (2008). Membrane modeling for simulation and control of reverse osmosis in desalination plants. In *Control, UKACC, Manchester, UK*.

- Cristea, S. P., Mazaeda, R., **Palacín, L. G.**, and de Prada, C. (2012). Reduced model of a beer microfiltration plant. In *8th IFAC Symposium on Advanced Control of Chemical Processes, Singapore*.

- García- Álvarez, D., de la Fuente, M. J., and **Palacín, L. G.** (2011). Monitoring and fault detection in a reverse osmosis plant using principal component analysis. In *the 50th IEEE Conference on Decision and Control and European Control Conference, CDC-ECC, Orlando, USA*.

- Tadeo, F., Val, R., **Palacín, L. G.**, Salazar, J., and de Prada, C. (2009). Control of reverse osmosis plants using renewable energies. In *International Conference on Control and Applications, Cambridge, UK*.

- Syafiie, S., Tadeo, F., **Palacín, L. G.**, de Prada, C., and Salazar, J. (2009). Modelling for dynamic simulation of pretreatment in reverse osmosis plants. In *Industrial Engineering and Engineering Management, Hong Kong, China*.

- Syafiie, S., Tadeo, F., **Palacín, L. G.**, and de Prada, C. (2008). Membrane modelling of desalination plants. In *International Conference on Industrial Engineering and Engineering Management, IEEM, Singapore*.

- Salazar, J., Tadeo, F., de Prada, C., and **Palacín, L. G.** (2010). Modelling and control of microgrids in island operation. In *International Renewable Energy Congress, IREC, Sousse, Tunisia*.

- Salazar, J., Tadeo, F., de Prada, C., and **Palacín, L. G.** (2010). Simulation and control of a wind turbine connected to a low voltage network. In *European Modeling and Simulation Symposium, EMSS, Fez, Morocco*.

The following presentations for national conferences were delivered during the development of this thesis:

- **Palacín, L. G.**, Tadeo, F., Salazar, J., and de Prada, C. (2010). Operación de plantas de desalinización mediante ósmosis inversa con consumo óptimo de la energía y detección de ensuciamiento por carbonato cálcico. In *XXXI Jornadas de Automática, CEA-IFAC, Jaén, Spain*.

- **Palacín, L. G.**, Merino, A., and de Prada, C. (2010). Estudio de la sensibilidad global y estimación de parámetros en un reactor SBR, con nitrificación desnitrificación, utilizando el modelo ASM1. In *XXXI Jornadas de Automática, CEA-IFAC, Jaén, Spain*. Award for Best Paper in Simulation.

- **Palacín, L. G.**, Tadeo, F., and de Prada, C. (2009). Diseño integrado y control usando simulación dinámica de una planta de

ósmosis inversa. In *XXX Jornadas de Automática, CEA-IFAC, Valladolid, Spain*. Award for Best Paper in Simulation.

- **Palacín, L. G.**, Tadeo, F., Syam, S., and de Prada, C. (2008). Librería dinámica de plantas de desalinización de ósmosis inversa. In *XXIX Jornadas de Automática, CEA-IFAC, Tarragona, Spain*.

- Tadeo, F., **Palacín, L. G.**, de Prada, C., and Salazar, J. (2010). Energías renovables para osmosis inversa en instalaciones aisladas: el proyecto OPEN-GAIN. In *III Congreso Nacional de la Asociación de Desalinización y Reutilización, Barcelona, Spain*.

- Salazar, J., Tadeo, F., de Prada, C., and **Palacín, L. G.** (2010). Simulation and control of a PV system connected to a low voltage network. In *XXXI Jornadas de Automática, CEA-IFAC, Jaén, Spain*.

6.3 Future Work

The work developed during this thesis may be continued in different ways, as shown below:

1. The upgrade of the ROSIM library is scheduled.

   In particular, different pre and post-treatment systems have been proposed to be added to the library, as follows:

   - **Dissolved air flotation (DAF):** This pretreatment system clarifies the feed water and removes suspended solids and oils. An air current is dissolved in the feed water in a pressurized tank. Then, the feed water is pumped to an open tank, where the air is desorbed. During this desorbtion, the air forms bubbles, which capture the suspended solids and oils causing them to float. Finally, the floating solids are easily skimmed.
   - **Lime saturator:** Part of the desalted water is pumped to a lime saturator, where calcium hydroxide ($Ca(OH)_2$) (also called "milk of lime") is produced. Next, the rest

of the desalted water is blended with the correct volume of calcium hydroxide, to adjust the pH before being consumed.

- **Calcite contactor:** This post-treatment system is similar to a lime saturator. Part of the desalted water is pumped to a calcite contactor, where calcium carbonate ($CaCO_3$) is produced. Next, the rest of the desalted water is blended with the correct volume of calcium carbonate, to adjust the pH before being consumed.

In addition, although the ROSIM library is focused on RO desalination plants, it has several components which simulate other desalination systems, such as MSF or MED. New components may be added to this library in order to extend the library to other desalination plants. In particular, the addition of components for the simulation of EDR, MD and HD is scheduled.

2. The advanced control techniques, which have been applied to small-scale RO desalination plants, may be extended to large-scale desalination plants, and to desalination plants based on other technologies, such as MSF, MED, EDR, MD or HD.

   In the same way, the proposed energy management of the RO plant, considered within the context of renewable energy supply systems, opens the door for other applications, integrating at the same time process design, control system and optimal operation of the plant.

3. Finally, the multi-scale modelling has been applied to the CP effect and may be extended to other effects. There are many open topics for the multi-scale modelling in a desalination system, such as the fouling of the membranes, the scaling in the metastable region of the calcium carbonate, the interaction of the different chemical species when the scaling takes place, the growth of microorganisms, and a long etcetera.

Appendix A

Extended Abstract in Spanish

A.1 Índice de Contenidos

A.2 Resumen

La desalinización de agua, tanto marina como salobre, es una técnica ampliamente utilizada para la producción de agua potable, en regiones en las que la disponibilidad de agua dulce es insuficiente, para abastecer a la comunidad. Desde los años noventa, la ósmosis inversa (conocida por sus siglas OI en español y RO en inglés) es, con mucho, la tecnología de desalinización más popular en el mundo, con la excepción de Oriente Medio, donde otras tecnologías como la evaporación multietapa (conocida por sus siglas en inglés, MSF), siguen siendo preferidas, a pesar de su menor eficacia energética. (Oriente Medio es una excepción, pero muy importante, ya que posee cerca de la mitad de la capacidad desaladora del mundo.)

Esta tesis está enfocada en el control de un tipo concreto de plantas de desalinización: plantas de pequeña capacidad (con una producción de varias decenas de metros cúbicos de agua potable al día), alimentadas por fuentes de energía renovable (placas fotovoltaicas y turbinas eólicas), y localizadas en zonas áridas y remotas. Este tipo de plantas es común en pequeños pueblos y asentamientos, situados en zonas de difícil acceso, como por ejemplo, en ciertas regiones del Magreb y del sur de Europa. En muchos de estos casos, existe una gran disponibilidad de energía renovable (radiación solar principalmente) con la que poder alimentar a la planta. Sin embargo, es necesario tener en cuenta otra serie de limitaciones, como puede ser el consumo de productos químicos (necesarios en el pre y postratamiento del agua), el recambio de elementos de la planta, o la imposibilidad de tener un operario supervisando la planta de manera continua.

Utilizando técnicas de control avanzado (tales como el control predictivo o el diseño integrado), se puede facilitar la operación y el diseño de la planta de desalinización: optimizar el tamaño de los depósitos y equipos, alargar la vida útil de los elementos de la planta, reducir el consumo de productos químicos, y en general, disminuir los gastos de operación e instalación, mientras se siguen cumpliendo las demandas de agua.

Para poder probar las técnicas de control avanzado estudiadas aquí, se ha desarrollado una librería dinámica de simulación de plantas de ósmosis inversa (llamada ROSIM, por sus siglas en inglés). En el mercado existen varias librerías de simulación para este tipo de plan-

tas, pero no son adecuadas para el diseño del sistema de control. Las librerías ya presentes en el mercado, se enfocan en el diseño del punto de operación y en la selección de los equipos de la planta. Mientras que la librería ROSIM se enfoca en la evolución dinámica de la planta de desalinización. En particular, dicha librería tiene en cuenta el ensuciamiento de las membranas, la precipitación de sales, la posible rotura de las membranas, el crecimiento de microorganismos, el envejecimiento de los componentes, el comportamiento de los lazos de control, la puesta en marcha de la planta, las paradas y limpiezas periódicas, etc. Gracias a una planta piloto de desalinización, se ha validado un simulador realizado con la librería ROSIM, y se han probado las técnicas de control avanzado.

A.3 Objetivos de la Tesis

El primer objetivo de esta tesis es el desarrollo de una librería dinámica de simulación de plantas de desalinización, basadas en ósmosis inversa. La librería está enfocada en el comportamiento dinámico de los distintos componentes, se basa en primeros principios y ecuaciones físico-químicas, y contiene los principales elementos presentes en una planta de desalinización, tales como filtros, membranas de ósmosis inversa, sistemas de recuperación de energía, bombas, sistemas de pre y postratamiento, etc. Por último, los componentes de dicha librería son validados en la medida de lo posible, utilizando datos reales de una planta piloto.

El segundo objetivo consiste en el estudio de diferentes técnicas de control avanzado, aplicadas a plantas de desalinización de pequeño tamaño, basadas en ósmosis inversa, y alimentadas con energías renovables; para tratar de mejorar el actual diseño y control de este tipo de plantas. Las técnicas estudiadas se aplican tanto a una planta simulada (utilizando la librería de simulación aquí desarrollada), como a una planta piloto real. Básicamente, el sistema de control propuesto trata de minimizar una cierta función objetivo, que penaliza los costes de operación, mientras cumple con una serie de restricciones (principalmente, satisfacer la demanda de agua). Para ello, el sistema de control manipula una serie de variables, tanto continuas (como el punto de operación, el flujo de las distintas corrientes y la presión de trabajo),

como discretas (como la realización o no de una limpieza de la planta, o el comportamiento de las bombas de tipo on/off).

El tercer y último objetivo de la tesis, consiste en la aplicación de las técnicas de modelado multi escala, al modelado de alguno de los efectos que tienen lugar en una planta de desalinización. El modelado multi escala es un método alternativo al modelado macroscópico (basado en primeros principios), que consiste en lo siguiente. El sistema estudiado se modela en varios niveles: por ejemplo, en un nivel microscópico y otro macroscópico. El modelo microscópico calcula los parámetros que utiliza el modelo macroscópico. Mientras que el modelo macroscópico calcula las variables macroscópicas del sistema. En particular, se realiza el modelado multi escala del efecto de la polarización de la concentración de sal, que tiene lugar en la capa límite junto a la superficie de las membranas de ósmosis inversa. Dicho efecto es fundamental en el diseño de las plantas de desalinización, pues está directamente ligado con la producción de agua potable en la planta.

A.4 Organización de la Tesis

Esta tesis está organizada de la siguiente manera.

Capítulo 1: En la primera parte de este capítulo, se describen las principales tecnologías de desalinización, que son utilizadas tanto de manera extensiva, en grandes plantas desalinizadoras, como aquellas utilizadas en pequeña escala, en plantas situadas en zonas aisladas. Se describe con mayor profundidad una planta de desalinización basada en ósmosis inversa, debido a que, en la actualidad, es la tecnología más popular. También se dan ideas sobre la situación mundial de la desalinización, la estimación para los próximos años, el impacto ambiental y el coste económico. En la segunda parte del capítulo, se describe el estado del arte del proceso de la desalinización, desde tres puntos de vista: control de la operación, modelado matemático, y herramientas de simulación para el diseño de plantas desalinizadoras. A continuación, se justifica la presente tesis, y se describen sus objetivos y principales aportaciones.

Capítulo 2: En la primera parte de este capítulo, se describe el modelado matemático de los principales elementos de una planta de

desalinización basada en ósmosis inversa, tales como los filtros, las membranas de ósmosis inversa, los sistemas de recuperación de energía o los sistemas de pre y postratamiento. Dicho modelado está basado en primeros principios, ecuaciones físico-químicas, y correlaciones bibliográficas. Las ecuaciones matemáticas utilizadas son función del tiempo, y en algunos casos, también de la posición. Es decir, las ecuaciones matemáticas están escritas en derivadas parciales. La segunda parte del capítulo está enfocada en la descripción de la librería ROSIM, que está basada en las anteriores ecuaciones matemáticas. Se describen los componentes más importantes de la librería, y se realizan varias simulaciones donde pueden observarse distintos procesos típicos de una planta de desalinización, como la limpieza de los filtros, el crecimiento de microorganismos o el envejecimiento de los componentes.

Capítulo 3: En este capítulo se describe la planta piloto de desalinización, que es utilizada para la validación tanto de los componentes de la librería ROSIM (descrita en el capítulo anterior), como de las estrategias de control avanzado (descritos en el capítulo siguiente). A continuación, se describe la validación cuantitativa y la estimación de parámetros, de algunos de los componentes de dicha librería.

Capítulo 4: Este capítulo muestra diferentes trabajos en los que se aplican técnicas de control avanzado a plantas de desalinización. Las distintas técnicas se prueban en la planta piloto descrita en el capítulo anterior. En particular se estudia la operación de una desaladora, para escalas de tiempo cortas (varios días) y largas (varios años). Se describe el control predictivo de la planta, la optimización de la planificación de las limpiezas de la planta, el diseño integrado de una desaladora de pequeño tamaño, y la optimización de los recambios y rotaciones de los módulos de ósmosis inversa.

Capítulo 5: En este capítulo se describe brevemente el modelado multi escala. En el que un sistema es modelado en varios niveles de detalle (por ejemplo, uno macroscópico y otro microscópico). El modelado multi escala se aplica al efecto de la polarizacion de

la concentración de sal, que consiste en el aumento de la concentración de sal cerca de las membranas de ósmosis inversa, debido al flujo de agua que cruza dichas membranas. El modelado multi escala es un enfoque alternativo al modelado de primeros principios descrito en el capítulo 2.

Capítulo 6: En este capítulo se resumen las conclusiones y el trabajo futuro de la tesis. Así como las publicaciones realizadas a partir de la tesis.

Apéndice A: Este apéndice contiene un resumen en español de la tesis: sus objetivos, conclusiones, trabajo futuro e índice de contenidos.

Apéndice B: Este apéndice contiene el manual de usuario de la librería de simulación ROSIM, donde se pueden consultar la metodología seguida, suposiciones y aplicaciones, así como una descripción de cada uno de los componentes de dicha librería.

Al final de la tesis se encuentran las listas con los símbolos y acrónimos utilizados, las páginas web correspondientes a las instituciones, empresas y proyectos mencionados en dicha tesis, las listas de las figuras y tablas que aparecen en la tesis, y por último, la bibliografía empleada.

A.5 Conclusiones

La presente tesis ha presentado varias contribuciones en el modelado, simulación y control de plantas de desalinización de ósmosis inversa. En particular, se ha desarrollado una librería dinámica para la simulación de plantas de desalinización, se ha presentado el modelado multi escala aplicado a la desalinización, y se ha estudiado la optimización de la operación de plantas de desalinización, tanto para escalas de tiempo cortas (días), como largas (años):

1. Se ha desarrollado una librería dinámica para el diseño de plantas de desalinización. Dicha librería está basada en primeros principios, ecuaciones físico-químicas y correlaciones bibliográficas.

La librería ha sido validada utilizando datos reales de una planta piloto y vendida a usuarios finales con éxito. La principal contribución de esta librería es que, mientras que las librerías de desalinización que se encuentran en el mercado están basadas en el cálculo del punto nominal de operación, esta se enfoca en el compartimiento dinámico de los distintos elementos. Por ejemplo, se ha modelado el envejecimiento de las membranas, el ensuciamiento causado por materia suspendida, la precipitación de sales, las operaciones de limpieza y reemplazamiento, y el crecimiento de microorganismos.

La librería ha sido presentada en Palacín et al. (2008a, 2009c, 2011b), mientras que su validación ha sido descrita en Palacín et al. (2010b,e). El modelado matemático, que se encuentra por debajo de cada uno de los componentes de la librería, está descrito en Syafiie et al. (2008a,b, 2009, 2010) y Palacín et al. (2012a,b).

2. A continuación, se han probado distintas técnicas de control avanzado (tales como el control predictivo y el diseño integrado), en una planta piloto de desalinización, cuya energía está suministrada por fuentes de energía renovable (placas fotovoltaicas y turbinas de viento) y no renovable (generador diésel). Los resultados son prometedores, en el sentido en que se ha conseguido disminuir el coste de operación e instalación, disminuir el tamaño de los equipos y minimizar los requerimientos de energía no renovable, mientras que se han seguido cumplimiento las demandas de agua.

   La idea es sencilla. Utilizando la planta de desalinización como una carga activa, y teniendo en cuenta las predicciones de energía renovable y demanda de agua, se puede operar la planta de manera que se compensen las diferencias entre la disponibilidad de energía renovable y evolución del consumo de energía por la planta. Esto se consigue variando el punto de operación y eligiendo correctamente los momentos para las limpiezas, de manera que se minimice una cierta función objetivo, que tenga en cuenta los costes de operación y penalice tanto el uso de energía no renovable como el incumplimiento de la demanda de agua.

   El control avanzado ha sido presentado en Palacín et al. (2009d,

2010d, 2011a), y el diseño integrado en Palacín et al. (2009a,b).

3. Además, se ha estudiado la optimización de la operación para largas escalas de tiempo (varios años). Proponiéndose estrategias para la toma de decisiones sobre cuándo realizar una limpieza química, o cuándo realizar el recambio y rotación de los módulos de ósmosis inversa.

   Este trabajo ha sido presentado en Palacín et al. (2012a).

4. Por último, se ha propuesto un nuevo modelo matemático, para el cálculo de la distribución de sal a lo largo de las membranas de ósmosis inversa, basado en modelado multi escala.

   Dicho modelado ha sido presentado en Palacín et al. (2012c).

A.6 Trabajo Futuro

Se pretende continuar el trabajo realizado a lo largo de esta tesis, a través de distintos caminos. En primer lugar, gracias a los acuerdos de colaboración entre la Universidad de Valladolid y la compañía EA, la librería ROSIM ha sido vendida a clientes finales. Por lo tanto, un trabajo de mantenimiento de la librería deberá ser realizado a lo largo de los próximos meses.

Se pretende ampliar la librería ROSIM, añadiendo nuevos componentes que simulen distintos sistemas de pre y postratamiento, como los que se muestran a continuación:

- **Sistema de flotación por aire:** Conocido por sus siglas en inglés DAF. Se trata de un sistema de pretratamiento que clarifica el agua de alimentación, eliminando los sólidos suspendidos, las espumas y aceites. Primero, el agua de alimentación se lleva a un depósito presurizado, donde se bombea aire que se absorbe por el agua. A continuación, la corriente de agua se lleva a un depósito abierto, donde se produce la desorción del aire. Durante dicho proceso se forman burbujas de aire, que atrapan la materia suspendida, y causan su flotación. Para, a continuación, ser fácilmente eliminada en la superficie del tanque.

- **Saturador de cal:** Parte del agua desalinizada, producida en la planta de desalinización, se lleva a un saturador de cal, donde se

produce hidróxido de calcio ($Ca(OH)_2$). Este hidróxido de calcio se mezcla en las proporciones adecuadas con el resto del agua desalinizada, para controlar el pH del agua producida.

- **Lecho de calcita:** Se trata de un sistema similar al saturador de sal. Parte del agua desalinizada se lleva al lecho de calcita, donde se forma carbonato cálcico ($CaCO_3$). A continuación, se mezcla con el resto de agua desalinizada en las proporciones adecuadas, para controlar el pH del agua producida.

La librería ROSIM está enfocada en plantas de desalinización de ósmosis inversa. Pero también tiene varios componentes para la desalinización por destilación. Se pretende ampliar dicha librería añadiendo nuevos componentes, que modelen otras técnicas populares de desalinización, tales como la electrodiálisis, los sistemas de humidificación-deshumidificación, o la destilación por membrana.

Por otro lado, las técnicas de control avanzado, que en esta tesis han sido aplicadas a desalinizadoras de ósmosis inversa de pequeño tamaño, pueden ser aplicadas a desalinizadoras de ósmosis inversa de gran tamaño, así como a otras técnicas de desalinización.

Finalmente, las técnicas de modelado multi escala, que en esta tesis han sido aplicadas al efecto de la polarización de sal, pueden ser aplicadas a muchos otros efectos que tienen lugar en una desalinizadora. De hecho, existen muchos efectos, difíciles de modelar mediante ecuaciones macroscópicas, que podrían abordarse desde el punto de vista del modelado multi escala. En particular, el ensuciamiento de membranas, el comportamiento del carbonato cálcico en la región metaestable, la interacción de distintas especies químicas durante la precipitación en las membranas, el crecimiento de microorganismos, y un largo etcétera.

Appendix B

User Manual of the ROSIM Library

This document is an adaptation of the user manual for the ROSIM library. This library is specific for the simulation of desalination plants, particularly those that operate with reverse osmosis (RO), and has been developed under the EcosimPro dynamic simulation platform. This library does not contain any experiments. It only includes the components that are typically found in a desalination plant, such as filters, RO membranes, pressure vessels, energy recovery systems, tanks, valves, pumps, etc. The ROSIM_EXAMPLES library was created to ease the training and familiarisation with the library, and it includes examples of the components in the ROSIM library.

B.1 Dependencies

The ROSIM library is independent. It does not require any other library to work. The ROSIM_EXAMPLES library requires the ROSIM library for its operation.

B.2 Methodology

The components of the ROSIM library can be divided into two groups: 1) Analogue components; and 2) Hydraulic components.

B.2.1 Analogue Components

The analogue components correspond to blocks that operate analogue signals. In general, they are used to configure the control system. The controllers, sensors, mathematical operators, etc., are examples of analogue blocks.

There are two types of analogue blocks: 1) blocks that operate with scalars; and 2) blocks that operate with vectors. Each type is linked to a type of port. The blocks that operate with scalars use port `p_1`, while the blocks that operate with vectors use port `p_n`. In addition, both types are identified with a colour. The blocks that operate with scalars are orange, while the blocks that operate with vectors are purple. Finally, there are specific components that can operate with both types of ports.

Whenever several analogue blocks, either of scalar or vector type, are connected, the calculation is done sequentially, in the direction of the connection. That is, each block calculates the variables of their output ports depending on the value of the variables of the input ports.

B.2.2 Hydraulic Components

The hydraulic blocks correspond to components that operate with hydraulic flows. In general, they correspond to the typical elements that can be found in a desalination plant. The hydraulic blocks include pumps, valves, tanks and reverse osmosis membranes.

The hydraulic blocks operate with the `p_osm` port, which comprises variables that have a direction in a liquid flow, such as pressure, flow, temperature, salt and boron concentration, etc. The sequence where these variables are calculated depends on each of the variables. The pressure is calculated in capacitive components that establish the pressure for both the input and output ports. The flow is calculated in resistive components, depending on the differential pressure between the input and output ports. Depending on the differential pressure, the flow will be direct (from the input port to the output port) or reverse (from the output port to the input port). The temperature and salt and boron concentration are calculated sequentially, in the direction of flow. If the flow is direct, the temperature and concentration of the output port will depend on the temperature and concentration of the input port. The opposite will apply for reverse flow. Bearing

this in mind, hydraulic components can be divided into three types: 1) capacitive components, which calculate pressure (such as a tank); 2) resistive components, which calculate flow (such as a valve); and 3) neutral components, which calculate neither flow nor pressure, but instead calculate temperature and concentration (such as a heat exchanger).

In order to prevent algebraic loops, which are generally a source of conflict and slow down the simulation, capacitive and resistive components must be connected alternately: Capacitive component - resistive component - capacitive component - resistive component - etc. Neutral components do not calculate the pressure or flow, so it is possible to connect as many as are necessary one after the other, between an capacitive and a resistive component.

For a easy component identification, the symbols of the capacitive components are shown in blue, the symbols of the resistive components are shown in green, and the symbols of the neutral components are shown in yellow.

B.3 Ports

As set out above, the ROSIM library operates with three types of ports: `p_1` for analogue scalar components, `p_n` for analogue vector components and `p_osm` for hydraulic connections.

B.3.1 Port `p_1`

This port corresponds to an analogue signal.

Variables:
u — Scalar.

B.3.2 Port `p_n`

This port corresponds to an analogue vector.

Construction parameters:
n — Vector length.

Variables:
$u[n]$ — Analogue vector.

B.3.3 Port `p_osm`

This port corresponds to a liquid flow.

Variables:
P — Pressure (bar).
Q — Flow (m^3/h). Flow may be positive or negative. Positive flow means that the direction of flow is direct, from the input port to the output port. Negative flow indicates that the direction of flow is in reverse, from the output port to the input port.
C — Salt concentration in the flow (ppm).
B — Boron concentration in the flow (ppm).
T — Temperature of the flow (°C).
pH — pH of the flow (-).
$x[mix]$ — Concentration of a different series of compounds that may be found in the flow. "mix" is an enumeration that includes the following species:

- X Microorganisms.
- S Substrate that serves as nourishment for the microorganisms.
- $p0$ Suspended particles larger than 10 μm.
- $p1$ Suspended particles of between 1 - 10 μm.
- $p2$ Suspended particles of between 0.1 - 1 μm.
- $p3$ Suspended particles of between 10^{-2} - 0.1 μm.
- $p4$ Suspended particles of between 10^{-3} - $10^{-2}\mu$m.

B.4 Simulation Time

The simulation time may vary from one experiment to another. On some occasions, users may want to simulate the behaviour of a desalination system in several minutes. On some other occasions, though, users may want to simulate the evolution of a plant over many days or even years. In this case, what work units should be used for the time variable? This question is not trivial. Some variables, such as the dynamics of a valve, operate with a timeframe of seconds. Other variables, such as the level in a tank, operate with a timeframe of minutes or hours. The fouling of a filter operates with a timeframe of days or months. The ageing of the reverse osmosis membranes operates with a timeframe of years. If seconds were selected are the time unit used by EcosimPro, the simulation of a system over several years would be done with a `TSTOP` of around 10^8 and a `CINT` of around 10^5. This would extend the simulation over several hours. If days or years were selected as the time unit used by EcosimPro, the simulation of a system over a few seconds would be done with a `TSTOP` of around 10^{-7} and a `CINT` of around 10^{-9}. This would cause huge numerical errors.

The ROSIM library was developed with a compromise solution. In general, seconds are the time unit used. However, when the plant simulation covers a longer period (days, months or years), users may decide to continue working with seconds (even if it lengthens the simulation time considerably) or changing the time unit to days or years. In this second case, the calculation time will be minimal, but the transient of some variables (but not the average value) may be distorted.

Users may change the time unit by modifying the *tsimulation* variable, which is found in the `simulation.el` file, as follows:

> $tsimulation = 1$ means that the `TSTOP` and `CINT` units are seconds.
>
> $tsimulation = 2$ means that the `TSTOP` and `CINT` units are days.
>
> $tsimulation = 3$ means that the `TSTOP` and `CINT` units are years.

The units of some of the variables of some components depend on the value of *tsimulation*. In the following sections, the use of the t symbol has to be understood as seconds, days or years if the value of the *tsimulation* variable is 1, 2 or 3, respectively.

B.5 Components

The following section describes the components that comprise the ROSIM library. The following philosophy has been applied for the component identification. The name of each component starts with a one- or two-letter code, which is used to codify the component, symbol "_", and the specific component name. This ensures that similar components are grouped in the same area of the library palette.

B.5.1 Analogue Components

B.5.1.1 bo_abs

This is an analogue component of scalar type. It calculates the absolute value of its input.

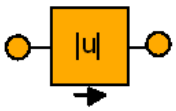

Figure B.1: `bo_abs` icon.

Ports:
s_in — Input scalar.
s_out — Output scalar.

B.5.1.2 bo_bound

This is an analogue component of scalar type. It limits the analogue signal between two values.

Ports:
s_in — Input scalar.
s_out — Output scalar.

Parameters:
umin — Minimum value.
umax — Maximum value.

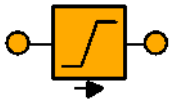

Figure B.2: `bo_bound` icon.

B.5.1.3 bo_boundv

This is an analogue component of vector type. It limits a vector between two values.

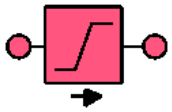

Figure B.3: `bo_boundv` icon.

Ports:
s_in — Input scalar.
s_out — Output scalar.

Construction parameters:
n — Vector size.

Parameters:
umin[*n*] — Vector with the minimum values for each element.
umax[*n*] — Vector with the maximum values for each element.

B.5.1.4 bo_delay

This is an analogue component of scalar type. It delays a variable by a given value.

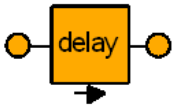

Figure B.4: `bo_delay` icon.

Ports:
s_in — Input scalar.
s_out — Output scalar.

Parameters:
dt — Delay (t).

B.5.1.5 bo_filter

This is an analogue component of scalar type. The input variable is filtered in accordance with a first-order derivative and a delay.

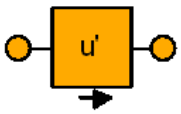

Figure B.5: `bo_filter` icon.

Ports:
s_in — Input scalar.
s_out — Output scalar.

Parameters:
k — Time constant (1/t).
*u*0 — Initial value of the filtered signal.

B.5.1.6 bo_gain

This is an analogue component of scalar type. The input variable is multiplied by a gain and increased by a certain value (bias).

Ports:
s_in — Input scalar.
s_out — Output scalar.

Parameters:
k — Gain.
b — Bias.

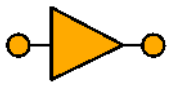

Figure B.6: `bo_gain` icon.

B.5.1.7 bo_gainv

This is an analogue component of vector type. Each element of the input vector is multiplied by a gain and increased by a certain value (bias).

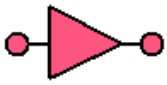

Figure B.7: `bo_gainv` icon.

Ports:
s_in — Input scalar.
s_out — Output vector.

Construction parameters:
n — Vector size.

Parameters:
$k[n]$ — Gain.
$b[n]$ — Bias.

B.5.1.8 bo_mux1

This is an analogue component that operates with scalar and vector ports. It forms a size 1 vector from one scalar.

Ports:
s_in — Input scalar.
s_out — Output scalar.

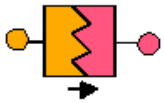

Figure B.8: `bo_mux1` icon.

B.5.1.9 bo_mux2

This is an analogue component that operates with scalar and vector ports. It forms a size 2 vector from two scalars.

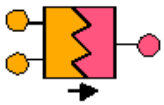

Figure B.9: `bo_mux2` icon.

Ports:

*s_in*1	—	First input scalar.
*s_in*2	—	Second input scalar.
s_out	—	Output scalar.

B.5.1.10 bo_mux3

This is an analogue component that operates with scalar and vector ports. It forms a size 3 vector from three scalars.

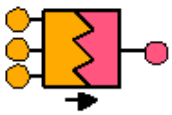

Figure B.10: `bo_mux3` icon.

Ports:

*s_in*1	—	First input scalar.
*s_in*2	—	Second input scalar.
*s_in*3	—	Third input scalar.

s_out — Output scalar.

B.5.1.11 bo_muxn

This is an analogue component of vector type. It blends two vectors of $n1$ and $n2$ size, respectively, into a single vector of size $n1 + n2$.

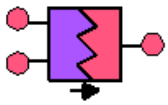

Figure B.11: `bo_muxn` icon.

Ports:
*s_in*1 — First input scalar.
*s_in*2 — Second input scalar.
s_out — Output scalar.

Construction parameters:
$n1$ — Size of the first input vector.
$n2$ — Size of the second input vector.

B.5.1.12 bo_operation

This is an analogue component of scalar type. It performs one of the following two mathematical operations, between two scalars. The user selects the mathematical operation with construction parameter x, as shown below:

$x = 1$ Performs the following sum:

$$u = k1 \cdot u1in + k2 \cdot u2in + k3 \tag{B.1}$$

$x = 2$ Performs the following multiplication:

$$u = k1 \cdot u1in \cdot k2 \cdot u2in + k3 \tag{B.2}$$

$x = 3$ Performs the following division:

$$u = \begin{cases} \text{if } u2in \neq 0 & u = \dfrac{u1in}{u2in} + k3 \\ \text{if } u2in = 0 & u = k1 + k3 \end{cases} \tag{B.3}$$

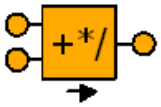

Figure B.12: `bo_operation` icon.

Ports:
*s_in*1 — First input scalar.
*s_in*2 — Second input scalar.
s_out — Output scalar.

Parameters:
*k*1 — Gain of the first scalar.
*k*2 — Gain of the second scalar.
*k*3 — Bias.

B.5.1.13 bo_sampling

This is an analogue component of scalar type. It is used to sample a continuous signal. Thus, the output variable evolves in increments.

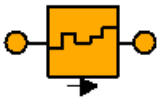

Figure B.13: `bo_sampling` icon.

Ports:
s_in — Input scalar.
s_out — Output scalar.

Parameters:
dt — Sampling frequency (t).
*u*0 — Initial value of the sampled signal.

B.5.1.14 bo_selector

This is an analogue component that operates with scalar and vector ports. This selects an element of a vector.

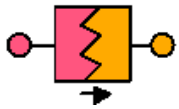

Figure B.14: `bo_selector` icon.

Ports:
s_in — Input vector.
s_out — Output scalar.

Construction parameters:
nin — Size of the input vector.
ne — Selected element.

B.5.1.15 bo_selectorv

This is an analogue component of vector type. A new vector is created based on the elements in an input vector. The size of the output vector may be smaller, equal to or larger than the size of the input vector.

Ports:
s_in — Input vector.
s_out — Output vector.

Construction parameters:
nin — Size of the input vector.
nout — Size of the output vector.

Parameters:

ne[*nout*] — Elements of the first vector, which then become part of the second vector. The values may be repeated.

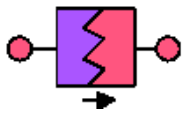

Figure B.15: `bo_selectorv` icon.

B.5.2 Addition of Chemicals

B.5.2.1 ch_chemical_addition

This is a hydraulic component of neutral type that simulates the addition of a chemical compound. The user defines its chemical species (bisulphite, antiscalant, etc.) and its concentration and flow. Furthermore, this component generates a pressure drop proportional to the flow of the main current.

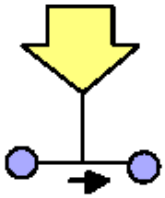

Figure B.16: `ch_chemical_addition` icon.

Ports:

f_in — Input flow.

f_out — Output flow.

Parameters:

a — Constant for calculating the pressure drop (-).

x — Species of added chemical: x = 1 means anticaling, x = 2 means sequestrant, x = 3 means sodium bisulfite, x = 4 means sodium hypochlorite.

k	—	Constant for calculating the pressure drop ($\text{bar}/(\text{m}^3/\text{h})^a$).
Q	—	Flow added (m^3/h).
c	—	Concentration of chemical species added (ppm).
C	—	Salt concentration added in the current (ppm).

B.5.2.2 ch_chemical_addition_pH

This is a hydraulic component of neutral type that simulates the addition of an acid or a base. The user defines the pH and flow of the added dose. Furthermore, the component generates a pressure drop proportional to the flow of the main stream.

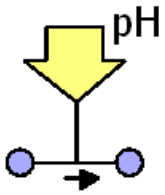

Figure B.17: `ch_chemical_addition_pH` icon.

Ports:

f_in	—	Input flow.
f_out	—	Output flow.

Parameters:

a	—	Constant for calculating the pressure drop (-).
k	—	Constant for calculating the pressure drop ($\text{bar}/(\text{m}^3/\text{h})^a$).
Q	—	Flow added (m^3/h).
pH	—	pH of the added dose (-).
C	—	Salt concentration added in the current (ppm).

B.5.2.3 ch_chemical_addition_pump

This is a hydraulic component of neutral type that simulates the addition of a chemical compound. The user defines its chemical species

(bisulphite, antiscaling, etc.) and its concentration. The added flow is set by means of an analogue input port. Furthermore, the component generates a pressure drop proportional to the flow of the main current.

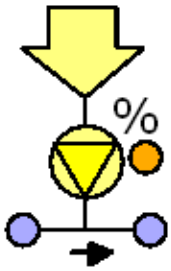

Figure B.18: `ch_chemical_addition_pump` icon.

Ports:

f_in	—	Input flow.
f_out	—	Output flow.
s_in	—	Analogue port that sets the added flow (%)

Parameters:

a	—	Constant for calculating the pressure drop (-).
x	—	Species of added chemical: x = 1 means anticaling, x = 2 means sequestrant, x = 3 means sodium bisulfite, x = 4 means sodium hypochlorite.
k	—	Filter of dosed fluid (1/t)..
kP	—	Constant for calculating the pressure drop (bar/(m^3/h)^a).
$Qmax$	—	Maximum added flow (m^3/h).
c	—	Concentration of chemical species added (ppm).
C	—	Salt concentration added in the current (ppm).

B.5.2.4 ch_chemical_addition_pump_pH

This is a hydraulic component of neutral type that simulates the addition of an acid or a base. The pH of the added dose is set by means of a parameter, and the flow rate of the dose is set through an analogue port. Furthermore, the component generates a pressure drop

proportional to the flow of the main current.

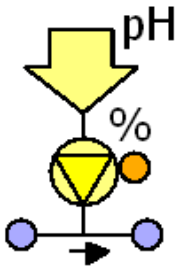

Figure B.19: `ch_chemical_addition_pump_pH` icon.

Ports:

f_in	—	Input flow.
f_out	—	Output flow.
s_in	—	Analogue port that sets the added flow (%)

Parameters:

a	—	Constant for calculating the pressure drop (-).
k	—	Filter of dosed fluid (1/t)..
kP	—	Constant for calculating the pressure drop (bar/(m^3/h)^a).
Qmax	—	Maximum added flow (m^3/h).
pH	—	pH of the added dose (-).
C	—	Salt concentration added in the current (ppm).

B.5.3 Controllers

B.5.3.1 c_diffcontrollersp

This is an analogue component of scalar type. It corresponds to a controller of incremental type. For each sampling period (*dt*), the controller checks the error between the process variable and the reference. If the difference is greater than a certain value (*gap*), the output variable increases or drops by a certain increment (*du*). The output variable will increase or drop, depending on the sign of the error and the type of response (reverse or direct). This component is similar to

`c_diffcontroller`, but the reference is defined externally.

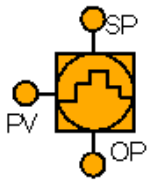

Figure B.20: `c_diffcontrollersp` icon.

Ports:

sSP	—	Reference.
sPV	—	Process variable.
sOP	—	Controller output.

Construction parameters:

$t1$	—	Direct or reverse response from the controller.

Parameters:

OPo	—	Initial output variable.
$OPmin$	—	Lower limit of the controller output.
$OPmax$	—	Upper limit of the controller output.
$PVmin$	—	Lower limit of the process variable.
$PVmax$	—	Lower limit of the process variable.
gap	—	Gap (in %) of the span of the process variable.
du	—	Increase in the controller output variable, (in %) of its span.
dt	—	Sampling frequency.
$switch\_autm$	—	Controller on manual (`FALSE`) or automatic (`TRUE`).

Variables that can be modified by the user:

$OPman$	—	Controller output when the controller is on manual.

B.5.3.2 c_diffcontroller

This is an analogue component of scalar type. It corresponds to a controller of incremental type. For each sampling period (dt), the controller checks the error between the process variable and the reference. If the difference is greater than a certain value (gap), the output variable increases or drops by a certain increment (du). The output variable will increase or drop, depending on the sign of the error and the type of response (reverse or direct). This component is similar to `c_diffcontroller`, but the reference is defined internally.

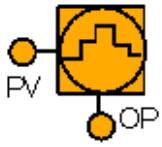

Figure B.21: `c_diffcontroller` icon.

Ports:

sPV	—	Process variable.
sOP	—	Controller output.

Construction parameters:

$t1$	—	Direct or reverse response from the controller.

Parameters:

OPo	—	Initial output variable.
$OPmin$	—	Lower limit of the controller output.
$OPmax$	—	Upper limit of the controller output.
$PVmin$	—	Lower limit of the process variable.
$PVmax$	—	Lower limit of the process variable.
gap	—	Gap (in %) of the span of the process variable.
du	—	Increase in the controller output variable, (in %) of its span.
dt	—	Sampling frequency.
$switch\_autm$	—	Controller on manual (`FALSE`) or automatic (`TRUE`).

Variables that can be modified by the user:

$OPman$	—	Controller output when the controller is on manual.
SP	—	Reference.

B.5.3.3 c_PID

This is an analogue component of scalar type. This corresponds to a PID-type controller. The proportional and integral part actuate on the error and the derivative part actuates on the process variable. For a given error between the reference and the process variable, the controller output will increase or drop depending on the type of response (reverse or direct). This component is similar to `c_PIDsp`, but the reference is defined internally.

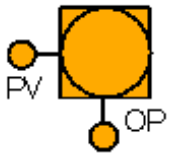

Figure B.22: `c_PID` icon.

Ports:

sPV	—	Process variable.
sOP	—	Controller output.

Construction parameters:

$t1$	—	Direct or reverse response from the controller.

Parameters:

Kp	—	Gain.
Ti	—	Integral time (t).
Td	—	Derivative time (t).
SPo	—	Initial reference.
$OPmin$	—	Lower limit of the controller output.
$OPmax$	—	Upper limit of the controller output.
$PVmin$	—	Lower limit of the process variable.

$PVmax$	—	Upper limit of the process variable.
$OPio$	—	Initial value of the integral term.
$switch\_atum$	—	Controller on manual (`FALSE`) or automatic (`TRUE`).

Variables that can be modified by the user:

$OPman$	—	Controller output when the controller is on manual.
SP	—	Reference.

B.5.3.4 c_PIDsp

This is an analogue component of scalar type. This corresponds to a PID-type controller. The proportional and integral part actuate on the error and the derivative part actuates on the process variable. For a given error between the reference and the process variable, the controller output will increase or drop depending on the type of response (reverse or direct). This component is similar to `c_PID`, but the reference is defined externally.

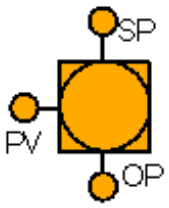

Figure B.23: `c_PIDsp` icon.

Ports:

sSP	—	Reference.
sPV	—	Process variable.
sOP	—	Controller output.

Construction parameters:

$t1$	—	Direct or reverse response from the controller.

Parameters:

Kp	—	Gain.
Ti	—	Integral time (t).
Td	—	Derivative time (t).
SPo	—	Initial reference.
$OPmin$	—	Lower limit of the controller output.
$OPmax$	—	Upper limit of the controller output.
$PVmin$	—	Lower limit of the process variable.
$PVmax$	—	Upper limit of the process variable.
$OPio$	—	Initial value of the integral term.
$switch\_atum$	—	Controller on manual (`FALSE`) or automatic (`TRUE`).

Variables that can be modified by the user:

$OPman$	—	Controller output when the controller is on manual.

B.5.4 Desalination Systems

B.5.4.1 de_MED

This is a hydraulic component of resistive type. It models a Multi Effect Desalination (MED) system. Supply flow is sprayed in the different effects, where part of the feed flow is evaporated. The required heat flow for the evaporation in the first effect is supplied by a steam stream. The required heat flow for the ith effect is supplied by the evaporated flow from the previous effect (i-1). In order to do this, a pressure drop between the different effects is required.

Ports:

$f \in$	—	Feed flow.
f_oute	—	Evaporated flow.
f_outb	—	Brine flow.
s_bin	—	Analogue variable with the supply flow valve (%).
s_sin	—	Analogue variable with the steam valve (%).

Construction parameters:

n	—	Number of effects.

Parameters:

$Qmax$	—	Maximum supply flow (m^3/h).
$Qsmax$	—	Maximum steam flow supplied to the system (m^3/h).
$Psteam$	—	Steam pressure (bar).
$P1$	—	Pressure drop in the first effect (bar).
$P2$	—	Pressure drop in the last effect (bar).
V	—	Volume of each effect (m^3).
Co	—	Initial salt concentration (ppm).
$Qevpo$	—	Initial evaporation flow in each effect (m^3/h).
kQ	—	Filter for the calculation of the flow (1/t).

Variables:

$Qbi[n]$	—	Feed flow which is supplied to each effect (m^3/h).
Qb	—	Supply flow (m^3/h).
Qs	—	Steam flow (m^3/h).
$Qri[n]$	—	Brine flow in each effect (m^3/h).
$Qevpi[n]$	—	Evaporated flow which is supplied to each effect (m^3/h).
$P[n]$	—	Pressure in each effect (bar).
$T[n]$	—	Temperature in each effect (°C).
$C[n]$	—	Salt concentration in each effect (ppm).

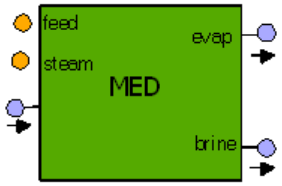

Figure B.24: `c_MED` icon.

B.5.4.2 de_MSF

This is a hydraulic component of resistive type. It models a Multi-Stages Flashes Desalination (MSF) system. Feed flow is pumped through different stages, where the partial evaporation is produced, thanks to the partial vacuum in each stage. Besides, previously to the first stage, feed flow temperature is increased thanks to a steam stream.

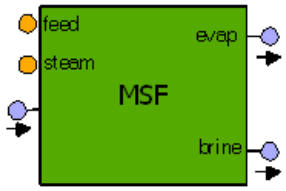

Figure B.25: `c_MSF` icon.

Ports:

$f \in$	—	Feed flow.
f_oute	—	Evaporated flow.
f_outb	—	Brine flow.
s_bin	—	Analogue variable with the supply flow valve (%).
s_sin	—	Analogue variable with the steam valve (%).

Construction parameters:

n	—	Number of stages.

Parameters:

$Qmax$	—	Maximum supply flow (m^3/h).
$Qsmax$	—	Maximum steam flow supplied to the system (m^3/h).
$Psteam$	—	Steam pressure (bar).
V	—	Volume of each effect (m^3).
Co	—	Initial salt concentration (ppm).
$Qevpo$	—	Initial evaporation flow in each stage (m^3/h).
kQ	—	Filter for the calculation of the flow (1/t).

Variables:

Qb	—	Supply flow (m^3/h).
Qs	—	Steam flow (m^3/h).
$Qri[n]$	—	Brine flow in each stage (m^3/h).
$Qevpi[n]$	—	Evaporated flow which is supplied to each stage (m^3/h).
$P[n]$	—	Pressure in each stage (bar).
$T[n]$	—	Temperature in each stage (°C).
$C[n]$	—	Salt concentration in each stage (ppm).

B.5.5 Energy Recovery Systems

B.5.5.1 er_DWEER

This is a hydraulic component of neutral type. This component simulates a Dual Work Exchange Energy Recovery system (DWEER). Here, a HP flow, typically the rejection current from a reverse osmosis system, comes in contact with a LP current, typically the fresh water flow. Given the structure of the component, the HP current gives up some of its pressure. Furthermore, due to the phase separation seals, the currents do not mix, and the concentrations are the same at the outlet as at the inlet.

Figure B.26: `er_DWEER` icon.

Ports:

f_in1	—	Low pressure inlet current.
f_out1	—	Outlet current, which has increased its pressure.
f_in2	—	High pressure inlet current.
f_out2	—	utlet current, which has released its pressure.
s_eff	—	Analogue port that shows the efficiency of the pressure recovery.

Parameters:

$DPudes$	—	Design pressure differential, between port f_in2 and f_out2 (bar).
$DPddes$	—	Design pressure differential, between port f_in1 and f_out1 (bar).
$Qfindes$	—	Design flow of the LP current (m^3/h).
$Qbindes$	—	Design flow of the HP current (m^3/h).
au	—	Parameter for calculating the pressure drop of the HP current (-).

ad	—	Parameter for calculating the pressure drop of the LP current (-).
$DPuo$	—	Initial differential pressure between port f_in2 and f_out2 (bar).
$DPdo$	—	Initial differential pressure between port f_in1 and f_out1 (bar).
kDP	—	Filter for calculating the differential pressure (1/t).

Variables:

DPd	—	Increase in pressure of the LP flow (bar).
DPu	—	Load drop of the HP flow (bar).
Qd	—	Inlet flow of the LP current (m^3/h).
Qu	—	Inlet flow of the HP current (m^3/h).
eff	—	Efficiency of the pressure recovery (-).

B.5.5.2 er_ERD

This component simulates an Energy Recovery Device (ERD). Here, a HP current (typically, the rejection from a reverse osmosis system) and the LP current (typically, the fresh water current) come into contact through a swivel cartridge. Differential pressure makes the cartridge swivel automatically. Not all the fresh water that enters through port f_in1 goes out along with the rejection flow through port f_out2. That loss of fresh water is called "lubrication flow" (lub). Thus:

$$\begin{aligned} Q(f\_in1) &= Q(f\_out1) + lub \\ Q(f\_out2) &= Q(f\_in2) + lub \end{aligned} \tag{B.4}$$

Assuming that the lubrication flow is proportional to the rejection inlet pressure and to the flow of fresh water, the calculation is done using the following equation:

$$\begin{aligned} lub = \; & a_0 + a_{P1} \cdot P(f\_in2) + a_{P2} \cdot P(f\_in2)^2 + ... \\ & + a_{Q1} \cdot Q(f\_in1) + a_{Q2} \cdot Q(f\_in1)^2 + ... \end{aligned} \tag{B.5}$$

Because there is no physical separation between the two currents, they mix together. This way, the concentration of salt (and of boron, temperature, pH etc.) of the outgoing fluid is not the same as the

concentration of salt in the fresh water inlet flow. In general, the concentration at the output can be calculated using the *mixt* parameter (which measures the percentage of mixture), as seen in the following equation:

$$c(f\_fout1) = mixt \cdot C(f\_in2) - mixt \cdot C(f\_in1) + C(f\_in1) \quad \text{(B.6)}$$

where the mixture can be calculated as a function of the lubrication flow:

$$mixt = a_{lubo} + a_{lub1} \cdot lub + a_{lub2} \cdot lub^2 + ... \quad \text{(B.7)}$$

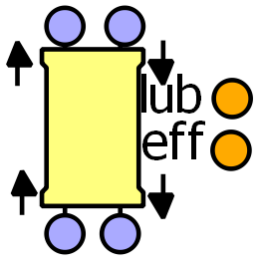

Figure B.27: `er_ERD` icon.

Ports:

f_in1	—	Low pressure inlet current.
f_out1	—	Outlet current, which has increased its pressure.
f_in2	—	High pressure inlet current.
f_out2	—	Outlet current, which has released its pressure.
s_eff	—	Analogue port that shows the efficiency of the pressure recovery.
s_lub	—	Analogue port indicating the lubrication flow.

Construction parameters:

nP	—	Degree of the polynomial for calculating the lubrication as a function of the rejection pressure.
nQ	—	Degree of the polynomial for calculating the lubrication as a function of the flow of fresh water.

$nmix$	—	Degree of the polynomial for calculating the mixture as a function of the flow of lubricant.

Parameters:

$DPudes$	—	Design pressure differential, between port f_in2 and f_out2 (bar).
$DPddes$	—	Design pressure differential, between port f_in1 and f_out1 (bar).
$Qfindes$	—	Design flow of the LP current (m^3/h).
$Qbindes$	—	Design flow of the HP current (m^3/h).
$aP[nP]$	—	Parameters for calculating the flow of lubricant.
$aQ[nQ]$	—	Parameters for calculating the flow of lubricant.
$DPuo$	—	Initial differential pressure between port f_in2 and f_out2 (bar).
$DPdo$	—	Initial differential pressure between port f_in1 and f_out1 (bar).
kDP	—	Filter for calculating the differential pressure (1/t).
ao	—	Parameter for calculating the flow of lubricant.
$am[nmix]$	—	Parameters for calculating the mixture
amo	—	Parameter for calculating the mixture.

Variables:

DPd	—	Increase in pressure of the LP flow (bar).
DPu	—	Load drop of the HP flow (bar).
Qd	—	Inlet flow of the LP current (m^3/h).
Qu	—	Inlet flow of the HP current (m^3/h).
eff	—	Efficiency of the pressure recovery (-).
lub	—	Flow of lubrication (m^3/h).
$mixt$	—	Percentage of mixture (-).

B.5.5.3 er_PRO

This is a hydraulic component of neutral type. This component simulates a Pressure Retarded Osmosis (PRO) energy recovery system. Where a high-concentration, low-pressure current (typically, the outlet rejection current from an energy recovery system) comes into contact with a low-concentration current (typically, the current of fresh water) through a semi-permeable membrane. This produces conventional os-

mosis. That is, the opposite of reverse osmosis, which is what occurs in the RO modules. Reverse osmosis generates the increase in pressure in the rejection current, which will then be able to be recovered with, for example, a turbine (`er_turbine` component).

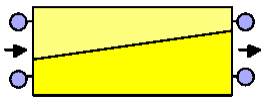

Figure B.28: `er_PRO` icon.

Ports:
*f_in*1 — Inlet current of fresh water.
*f_out*1 — Outlet current of fresh water.
*f_in*2 — High-concentration inlet current.
*f_out*2 — High-concentration outlet current.

Construction parameters:
npv — Number of pressure vessels in parallel.
nmo — Number of reverse osmosis modules within each pressure vessel.

Parameters:
DP — Design differential pressure (bar).
*Q*1*d* — Design flow of the fresh water current (m^3/h)
*Q*2*d* — Design flow of the high concentration current (m^3/h).
A — Hydraulic permeability (m^3/$foot^2$·h·bar).
area — Surface area of a reverse osmosis module ($foot^2$).

B.5.5.4 er_turbine

This is a hydraulic component of resistive type. This corresponds to a Pelton-type turbine. A high-pressure current is run through the turbine so that part of its pressure energy is recovered. The recovered energy is indicated through the analogue port *s_out*.

Ports:
f_in — Input flow.

f_out	—	Output flow.
s_out	—	Analogue variable with the energy recovery (kW).

Parameters:

$file$	—	Path of the file where the efficiency - flow curve is found.
$Qcolumn$	—	Column with the flow values.
$effcolumn$	—	Column with the efficiency values.
$Qmax$	—	Maximum flow (m^3/h).
K	—	Constant to calculate the flow ($m^3/h \cdot bar$)
dto	—	Parameter that needs to be close to zero and that is used to prevent problems with the integration when the `RESTORE_STATE` command is used.

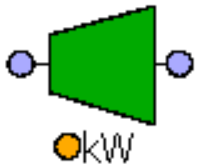

Figure B.29: `er_turbine` icon.

B.5.6 Filters

B.5.6.1 fis_pressurizedsandfilter

This is a hydraulic component of neutral type. It simulates a pressurized sand filter that eliminates particles larger than 10 μm. As time goes by, and as the system filters the feeder current, the sand filter becomes dirty and begins losing pressure between the inlet and outlet. The user defines cleaning of the sand filter either when the difference in pressure reaches a particular value or after a particular number of days. The cleaning strategy is defined using the construction parameter $t1$.

Ports:

f_in	—	Input flow.
f_out	—	Output flow.

Construction parameters:

$t1$	—	Strategy for cleaning . Whenever the pressure drop exceeds a given value ($DPmax$) or every dt number of days.

Parameters:

dt	—	Frequency of cleaning or replacing the filter (days).
$DPmax$	—	Maximum pressure drop before the filter is cleaned/replaced.
$DP0$	—	Pressure drop that the filter causes initially (bar).
$DP100$	—	Pressure drop that the filter causes when it is completely fouled (bar).
A	—	Area of the tank base (m^2).
H	—	Tank height (m).
$T0$	—	Initial temperature (°C).
$C0$	—	Initial salt concentration (ppm).
$B0$	—	Initial boron concentration (ppm).
$pH0$	—	Initial pH (-).
$x0[mix]$	—	Initial concentration of the rest of chemical types.

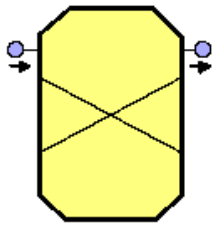

Figure B.30: `fis_pressurizedsandfilter` icon.

B.5.6.2 fis_pressurizedsandfilter_sin

This is a hydraulic component of neutral type. It simulates a pressurized sand filter that eliminates particles larger than 10 μm. As time goes by, and as the system filters the feeder current, the sand filter becomes dirty and begins losing pressure between the inlet and outlet. The moments of the cleanings are indicated by through an analogue port.

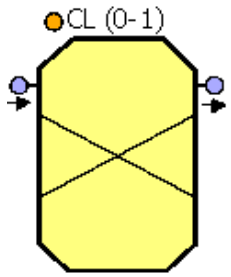

Figure B.31: `fis_pressurizedsandfilter_sin` icon.

Ports:

f_in	—	Input flow.
f_out	—	Output flow.
s_in	—	Analogue port that marks the instances of the cleanings.

Parameters:

dt	—	Frequency of cleaning or replacing the filter (days).
$DPmax$	—	Maximum pressure drop before the filter is cleaned/replaced.
$DP0$	—	Pressure drop that the filter causes initially (bar).
$DP100$	—	Pressure drop that the filter causes when it is completely fouled (bar).
A	—	Area of the tank base (m^2).
H	—	Tank height (m).
$T0$	—	Initial temperature (^oC).
$C0$	—	Initial salt concentration (ppm).
$B0$	—	Initial boron concentration (ppm).
$pH0$	—	Initial pH (-).
$x0[mix]$	—	Initial concentration of the rest of chemical types.

B.5.6.3 fis_sandfilter

This is a hydraulic component of accumulative type. It simulates an open sand filter. It encompasses the same equations as an open tank (`ta_tank` component), but also, where the sand filler eliminates particles whose size is >10 μm. As time goes by, and as the system

filters the feeder current, the sand filter becomes fouled and begins losing its filtering ability until a cleaning is performed. The user sets how much time passes between cleanings.

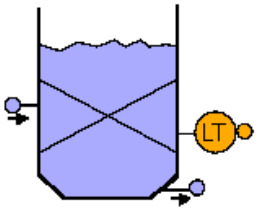

Figure B.32: `fis_sandfilter` icon.

Ports:

f_in	—	Input flow.
f_out	—	Output flow.
s_h100	—	Level sensor (%).

Parameters:

$dtCL$	—	Days every two cleanings (days).
$h100\_in$	—	Height of the input connection (%).
$h100\_out$	—	Height of the output connection (%).
$h100o$	—	Initial liquid level (%).
kh	—	Filter for the level sensor (1/t)
dth	—	Delay for the level sensor (t).
$kover$	—	Parameter to calculate the overflow.
A	—	Area of the tank base (m^2).
H	—	Tank height (m).
$T0$	—	Initial temperature (ºC).
$C0$	—	Initial salt concentration (ppm).
$B0$	—	Initial boron concentration (ppm).
$pH0$	—	Initial pH (-).
$x0[mix]$	—	Initial concentration of the rest of chemical types.
$kover$	—	Parameter to calculate the overflow.

B.5.6.4 fis_sandfilter_sin

This is a hydraulic component of accumulative type. It simulates an open sand filter. It encompasses the same equations as an open tank (`ta_tank` component), but also, where the sand filler eliminates particles whose size is >10 μm. As time goes by, and as the system filters the feeder current, the sand filter becomes fouled and begins losing its filtering ability until a cleaning is performed. Cleanings are indicated by means of an analogue port.

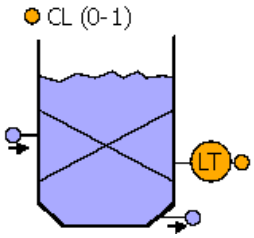

Figure B.33: `fis_sandfilter_sin` icon.

Ports:

f_in	—	Input flow.
f_out	—	Output flow.
s_h100	—	Level sensor (%).
s_in	—	Analogue port that marks the instances of the cleanings.

Parameters:

$dtCL$	—	Days every two cleanings (days).
$h100\_in$	—	Height of the input connection (%).
$h100\_out$	—	Height of the output connection (%).
$h100o$	—	Initial liquid level (%).
kh	—	Filter for the level sensor (1/t)
dth	—	Delay for the level sensor (t).
$kover$	—	Parameter to calculate the overflow.
A	—	Area of the tank base (m^2).
H	—	Tank height (m).
$T0$	—	Initial temperature (°C).
$C0$	—	Initial salt concentration (ppm).

$B0$	—	Initial boron concentration (ppm).
$pH0$	—	Initial pH (-).
$x0[mix]$	—	Initial concentration of the rest of chemical types.
$kover$	—	Parameter to calculate the overflow.

B.5.6.5 fi_filtration

This is a hydraulic component of neutral type. It corresponds to a filter. This filter eliminates particles larger than 1 μm. As time goes on, and as the system filters the flow of liquid, the filter becomes fouled and causes a greater pressure drop. Users can use construction parameter $t1$ to define the strategy to decide when to clean/replace the filter: 1) whenever the pressure drop exceeds a certain value ($DPmax$); 2) every given number of days (dt).

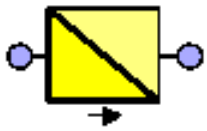

Figure B.34: `fi_filtration` icon.

Ports:

f_in	—	Input flow.
f_out	—	Output flow.

Construction parameters:

$t1$	—	Strategy for the cleaning/replacement of the filter. Whenever the pressure drop exceeds a given value ($DPmax$) or every dt number of days.

Parameters:

dt	—	Frequency for the cleaning/replacement of the filter (days).
$DPmax$	—	Maximum pressure drop before the filter is cleaned/replaced.
$DP0$	—	Pressure drop that the filter causes initially (bar).
$DP100$	—	Pressure drop that the filter causes when it is completely fouled (bar).

k — Parameter to calculate the pressure drop.

B.5.6.6 fi_microfiltration

This is a hydraulic component of neutral type. It corresponds to a microfiltering system. This system eliminates particles larger than 0.1 μm. As time goes on, and as the system filters the flow of liquid, the system becomes fouled and causes a greater pressure drop. Users can use construction parameter $t1$ to define the strategy to decide when to clean/replace the filter: 1) whenever the pressure drop exceeds a certain value ($DPmax$); 2) every given number of days (dt). Particles greater than 1 μm cause a premature fouling of the system.

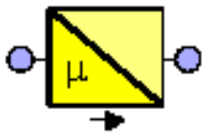

Figure B.35: `fi_microfiltration` icon.

Ports:
f_in — Input flow.
f_out — Output flow.

Construction parameters:
$t1$ — Strategy for the cleaning/replacement of the filter. Whenever the pressure drop exceeds a given value ($DPmax$) or every dt number of days.

Parameters:
dt — Frequency for the cleaning/replacement of the filter (days).
$DPmax$ — Maximum pressure drop before the filter is cleaned/replaced.
$DP0$ — Pressure drop that the filter causes initially (bar).
$DP100$ — Pressure drop that the filter causes when it is completely fouled (bar).
k — Parameter to calculate the pressure drop.

B.5.6.7 fi_ultrafiltration

This is a hydraulic component of neutral type. It corresponds to an ultrafiltration system. This system eliminates particles larger than 10^{-2} μm. As time goes on, and as the system filters the flow of liquid, the system becomes fouled and causes a greater pressure drop. Users can use construction parameter $t1$ to define the strategy to decide when to clean/replace the filter: 1) whenever the pressure drop exceeds a certain value ($DPmax$); 2) every given number of days (dt). Particles larger than 10^{-1} μm cause a premature fouling of the system.

Figure B.36: `fi_ultrafiltration` icon.

Ports:

f_in	—	Input flow.
f_out	—	Output flow.

Construction parameters:

$t1$	—	Strategy for the cleaning/replacement of the filter. Whenever the pressure drop exceeds a given value ($DPmax$) or every dt number of days.

Parameters:

dt	—	Frequency for the cleaning/replacement of the filter (days).
$DPmax$	—	Maximum pressure drop before the filter is cleaned/replaced.
$DP0$	—	Pressure drop that the filter causes initially (bar).
$DP100$	—	Pressure drop that the filter causes when it is completely fouled (bar).
k	—	Parameter to calculate the pressure drop.

B.5.6.8 fi_znanofiltration

This is a hydraulic component of neutral type. It corresponds to a nanofiltration system. This system eliminates particles larger than 10^{-3} μm. As time goes on, and as the system filters the flow of liquid, the system becomes fouled and causes a greater pressure drop. Users can use construction parameter 't1' to define the strategy to decide when to clean/replace the filter: 1) whenever the pressure drop exceeds a certain value ($DPmax$); 2) every given number of days (dt). Particles larger than 10^{-2} μm cause a premature fouling of the system.

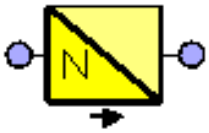

Figure B.37: `fi_znanofiltration` icon.

Ports:

f_in	—	Input flow.
f_out	—	Output flow.

Construction parameters:

$t1$	—	Strategy for the cleaning/replacement of the filter. Whenever the pressure drop exceeds a given value ($DPmax$) or every dt number of days.

Parameters:

dt	—	Frequency for the cleaning/replacement of the filter (days).
$DPmax$	—	Maximum pressure drop before the filter is cleaned/replaced.
$DP0$	—	Pressure drop that the filter causes initially (bar).
$DP100$	—	Pressure drop that the filter causes when it is completely fouled (bar).
k	—	Parameter to calculate the pressure drop.

B.5.7 Heat Exchangers

B.5.7.1 he_heater

This is a hydraulic component of neutral type that simulates a liquid-liquid heat exchanger. The user sets the inlet temperature of the secondary current, while the flow of that current is calculated based on the opening of the valve and the characteristic curve. In addition, this component generates a pressure drop in the main current. Lastly, this component contains a temperature sensor modelled with a filter plus a delay.

This component is discretized in nd finite volumes, to numerically resolve the energy balance:

$$V \cdot Cv \cdot \partial T = Q \cdot Cv \cdot \partial T/\partial z + U \cdot \Delta T/\partial z \tag{B.8}$$

where the heat transfer coefficient (U) is calculated as a polynomial of the temperature:

$$U = a_{U0} + a_{U1} \cdot T + a_{U2} \cdot T^2 + ... \tag{B.9}$$

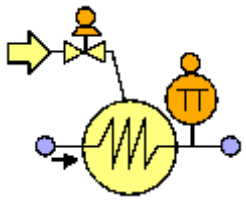

Figure B.38: `he_heater` icon.

Ports:

f_in	—	Input flow.
f_out	—	Output flow.
s_in	—	Electric current (%).
s_T	—	Temperature sensor (ºC).

Construction parameters:

$t1$	—	Valve characteristic curve: linear, of equal percentage and quick opening type or defined by means of a polynomial.

n	—	Order of the polynomial of the characteristic curve (if applicable).
nd	—	Number of elements in the mathematical discretization.
nU	—	Degree of the polynomial for calculating the heat transfer coefficient.

Parameters:

$T2in$	—	Inlet temperature of the secondary current (ºC).
DP	—	Differential pressure of the secondary current (bar).
K	—	Constant for flow calculation ($m^3/h \cdot bar^{0.5}$).
ku	—	Filter for the valve plug (1/t).
$rang$	—	Rangeability.
$u0$	—	Initial position of the valve plug (%).
$ai[n]$	—	Coefficients of the polynomial of the characteristic curve (if applicable).
aU	—	Coefficients of the polynomial for calculating the heat transfer coefficient.
L	—	Length of the exchanger (m).
$V1$	—	Volume occupied by the main liquid (m^3).
$V2$	—	Volume occupied by the secondary liquid (m^3).
KP	—	Parameter for the calculation of the pressure drop (bar).
aP	—	Parameter for the calculation of the pressure drop (-).
kp	—	Pressure filter (1/t).
Po	—	Initial pressure (bar).
Cv	—	Volumetric heat ($kW/(m^3 \cdot ºC)$).
$T1o$	—	Initial temperature of the main current (ºC).
$T2o$	—	Initial temperature of the secondary current (ºC).
pHo	—	Initial pH of the main current (-).
Co	—	Initial concentration of salt in the main current (ppm).
Bo	—	Initial concentration of boron in the main current (ppm).
$x0[mix]$	—	Initial concentration of all the other chemical species.
kh	—	Filter for the temperature sensor (1/t).
dtT	—	Delay of the temperature sensor (t).

Parameters:

$U[nd]$	—	Heat transfer coefficient at each discretization (kW/ºC).
$q[nd]$	—	Heat transferred at each discretization (kW).

$T[nd]$ — Temperature of the main current at each discretization (°C).

B.5.7.2 he_heaterr

This is a hydraulic component of neutral type that simulates a heater of a liquid current by means of an electrical resistance. In addition, this component generates a pressure drop in the main current. Lastly, this component contains a temperature sensor modelled with a filter plus a delay.

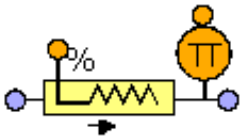

Figure B.39: `he_heaterr` icon.

Ports:
f_in — Input flow.
f_out — Output flow.
s_in — Electric current (%).
s_T — Temperature sensor (°C).

Parameters:
V — Volume occupied by the liquid (m^3).
$qmax$ — Maximum heat generated by the electric current (kW).
KP — Parameter for the calculation of the pressure drop (bar).
aP — Parameter for the calculation of the pressure drop (-).
kp — Pressure filter (1/t).
Po — Initial pressure (bar).
Cv — Volumetric heat (kW/(m^3·°C)).
To — Initial temperature of the liquid current (°C).
kh — Filter for the temperature sensor (1/t).
dtT — Delay of the temperature sensor (t).

Variables:
$qmax$ — Heat generated by the electric current (kW).

B.5.7.3 he_heaters

This is a hydraulic component of neutral type that simulates a heat exchanger by means of solar radiation. Said radiation is set by an analogue vector port. In addition, this component generates a pressure drop in the main current. Lastly, this component contains a temperature sensor modelled with a filter plus a delay.

This component is discretized in nd finite volumes, to numerically resolve the energy balance:

$$V \cdot Cv \cdot \partial T = Q \cdot Cv \cdot \partial T/\partial z + q/\partial z \tag{B.10}$$

Ports:

f_in	—	Input flow.
f_out	—	Output flow.
s_in	—	Analogue vector that collects the solar radiation and the ambient temperature.
s_T	—	Temperature sensor (ºC).

Construction parameters:

nd	—	Number of elements in the mathematical discretization.

Parameters:

$area$	—	Surface area (m^2).
V	—	Volume occupied by the liquid (m^3).
KP	—	Parameter for the calculation of the pressure drop (bar).
aP	—	Parameter for the calculation of the pressure drop (-).
kp	—	Pressure filter (1/t).
Po	—	Initial pressure (bar).
Cv	—	Volumetric heat ($kW/(m^3 \cdot ºC)$).
To	—	Initial temperature of the liquid current (ºC).
kh	—	Filter for the temperature sensor (1/t).
dtT	—	Delay of the temperature sensor (t).

Variables:

$q[nd]$	—	Heat gained by the liquid current due to solar radiation (kW).

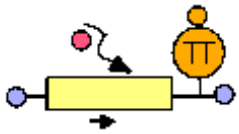

Figure B.40: `he_heaters` icon.

B.5.8 RO Membranes

B.5.8.1 me_membrane

This is a hydraulic component of resistive type. It models a rack of reverse osmosis pressure vessels. A supply flow with a high salt concentration is pumped up to the component. Part of the current is forced through the membrane (permeated). Most of the salt is retained by the membrane and the salt concentration of the permeation is several orders of magnitude lower than the concentration in the supply. The rest of the salt and water forms the rejection current.

The permeated flow is proportional to the surface area of the membrane, to the difference between the supply pressure and the pressure on the permeation side and to the difference in osmotic pressure due to the chemical potential from the salt concentration gradient on both sides of the membrane. As shown below:

$$Qp = A \cdot area \cdot (\Delta P - \Delta\pi) \tag{B.11}$$

where factor A corresponds to the hydraulic permeability. The fouling and aging of the membrane can be modelled as set out below:

$$A = A_o \cdot A_i \cdot A_r = A_o \cdot (1 - \Psi \cdot t) \exp(-t/\Gamma) \tag{B.12}$$

where A_i and A_r correspond to the irreversible fouling (only eliminated if the reverse osmosis module is replaced) and the reversible fouling (which can be eliminated with chemical cleaning), respectively, and the parameters Ψ and Γ depend on each particular system.

Users decide the strategy to perform the chemical cleaning: 1) Every given number of days ($dtCL$) or every time the reversible permeability exceeds a certain threshold. Users also decide the strategy for the partial replacement of the reverse osmosis modules: 1) every

given number of days ($dtRP$); 2) every time the irreversible permeability exceeds a certain threshold. In addition, the percentage of modules that are replaced is also decided.

The salt concentration in the permeating (Cp) is calculated as follows:

$$Cp = B \cdot \Delta C/Qp \tag{B.13}$$

where B corresponds to the permeability of salt. The aging of the membrane causes a greater salt concentration to be capable of crossing the membrane. As in the case of the hydraulic permeability, the salt permeability can be calculated as follows:

$$B = B_o \cdot B_i \cdot B_r = B_o \cdot (1 + \Psi \cdot t) \exp(t/\Gamma) \tag{B.14}$$

The boron behaviour and modelling is similar to the case of salt.

Finally, this component includes an analogue port that indicates the water recovery, that is, the ratio between the permeation flow and the supply flow.

Figure B.41: `me_membrane` icon.

Ports:

f_in	—	Supply flow.
f_outp	—	Permeate flow.
f_outr	—	Reject flow.
s_out	—	Analogue variable with the water recovery value (%).

Construction parameters:

t1	—	Strategy for the cleaning of the membranes. Whenever the term for reversible permeability exceeds a certain value ($Armin$) or every $dtCL$ number of days.

$t2$ — Strategy for the partial replacement of the reverse osmosis modules. Whenever the term for irreversible permeability exceeds a certain value ($Aimin$) or every $dtRP$ number of days.
npv — Number of pressure vessels in parallel.
nmo — Number of reverse osmosis modules within each pressure vessel.

Parameters:
$Armin$ — Value of reversible hydraulic permeability to perform the cleaning.
$dtCL$ — Frequency of the cleaning (days).
$Aimin$ — Irreversible hydraulic permeability strategy for the partial replacement of the reverse osmosis modules.
$dtRP$ — Frequency for the partial replacement of the reverse osmosis modules (days).
$area$ — Surface area of a reverse osmosis module (foot^2).
Ao — Initial hydraulic permeability (m^3/foot^2·h·bar).
Bo — Permeability of the initial salt (1/h).
BBo — Permeability of the initial boron (-).
RP — Replacement percentage (0-1).
PSIA, PSIB, PSIBB, GAMMAA, GAMMAB —
— Parameters for the modelling of the fouling.
Kr — Parameter for the calculation of the rejection flow (m^3/h·bar).
$Cravo$ — Average initial salt concenration on the supply side (ppm).
rpH — Ratio for the acidification of the permeation.
$foulingmax$ — Maximum fouling value caused by particles $> 10^{-4}$ μm
$Dpio$ — Initial value of the osmotic pressure (bar).
kQ — Filter for the calculation of the permeation and rejection flow (1/t).
Qpo — Initial value of the permeation flow (m^3/h).
Qro — Initial value of the rejection flow (m^3/h).

B.5.8.2 me_membrane_d

This is a hydraulic component of resistive type. It models a rack of reverse osmosis pressure vessels. A supply flow with a high salt concentration is pumped up to the component. Part of the current is forced through the membrane. Most of the salt is retained by the membrane and the salt concentration of the permeation is several orders of magnitude lower than the concentration in the supply. The rest of the salt and water forms the rejection current. This component is similar to `me_membrane`, except that said element is divided into *nd* elements along the pressure tube in order to resolve the material balance.

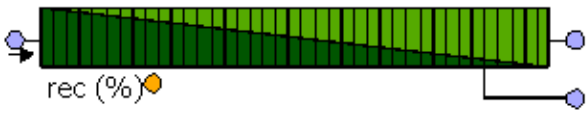

Figure B.42: `me_membrane_d` icon.

Ports:

f_in	—	Supply flow.
f_outp	—	Permeate flow.
f_outr	—	Reject flow.
s_out	—	Analogue variable with the water recovery value (%).

Construction parameters:

*t*1	—	Strategy for the cleaning of the membranes. Whenever the term for reversible permeability exceeds a certain value ($Armin$) or every $dtCL$ number of days.
*t*2	—	Strategy for the partial replacement of the reverse osmosis modules. Whenever the term for irreversible permeability exceeds a certain value ($Aimin$) or every $dtRP$ number of days.
npv	—	Number of pressure vessels in parallel.
nmo	—	Number of reverse osmosis modules within each pressure vessel.

nd	—	Number of finite volumes to resolve the material balance.

Parameters:

$Armin$	—	Value of reversible hydraulic permeability to perform the cleaning.
$dtCL$	—	Frequency of the cleaning (days).
$Aimin$	—	Irreversible hydraulic permeability strategy for the partial replacement of the reverse osmosis modules.
$dtRP$	—	Frequency for the partial replacement of the reverse osmosis modules (days).
$area$	—	Surface area of a reverse osmosis module (foot^2).
Ao	—	Initial hydraulic permeability (m^3/foot^2·h·bar).
Bo	—	Permeability of the initial salt (1/h).
BBo	—	Permeability of the initial boron (-).
RP	—	Replacement percentage (0-1).
PSIA, PSIB, PSIBB, GAMMAA, GAMMAB	—	Parameters for the modelling of the fouling.
Kr	—	Parameter for the calculation of the rejection flow (m^3/h·bar).
$Cravo$	—	Average initial salt concenration on the supply side (ppm).
rpH	—	Ratio for the acidification of the permeation.
$foulingmax$	—	Maximum fouling value caused by particles $> 10^{-4}$ μm
$Dpio$	—	Initial value of the osmotic pressure (bar).
kQ	—	Filter for the calculation of the permeation and rejection flow (1/t).
Qpo	—	Initial value of the permeation flow (m^3/h).
Qro	—	Initial value of the rejection flow (m^3/h).

B.5.8.3 me_membrane_sin

This is a hydraulic component of resistive type. It models a rack of reverse osmosis pressure vessels. A supply flow with a high salt concentration is pumped up to the component. Part of the current is forced through the membrane. Most of the salt is retained by the membrane

and the salt concentration of the permeation is several orders of magnitude lower than the concentration in the supply. The rest of the salt and water forms the rejection current. This component is similar to `me_membrane`, except that the instants of the chemical cleaning, the instants of the replacements and the percentages of the replacements are set by means of analogue ports.

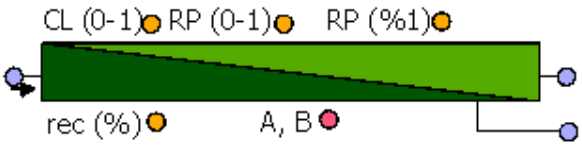

Figure B.43: `me_membrane_sin` icon.

Ports:

f_in	—	Supply flow.
f_outp	—	Permeate flow.
f_outr	—	Reject flow.
s_rec	—	Analogue variable with the water recovery value (%).
s_AB	—	Analogue vector with the hydraulic and salt permeability.
s_CL	—	Analogue port that sets the cleaning instants.
s_RP	—	Analogue port that sets the instants at which the modules are replaced.
s_RPp	—	Analogue port that sets the percentage of replacements.

Construction parameters:

npv	—	Number of pressure vessels in parallel.
nmo	—	Number of reverse osmosis modules within each pressure vessel.

Parameters:

area	—	Surface area of a reverse osmosis module (foot^2).
Ao	—	Initial hydraulic permeability (m^3/foot^2·h·bar).
Bo	—	Permeability of the initial salt (1/h).
BBo	—	Permeability of the initial boron (-).

RP	—	Replacement percentage (0-1).
PSIA, PSIB, PSIBB, GAMMAA, GAMMAB	—	
	—	Parameters for the modelling of the fouling.
Kr	—	Parameter for the calculation of the rejection flow (m^3/h·bar).
$Cravo$	—	Average initial salt concenration on the supply side (ppm).
rpH	—	Ratio for the acidification of the permeation.
$foulingmax$	—	Maximum fouling value caused by particles $> 10^{-4}$ μm
$Dpio$	—	Initial value of the osmotic pressure (bar).
kQ	—	Filter for the calculation of the permeation and rejection flow (1/t).
Qpo	—	Initial value of the permeation flow (m^3/h).
Qro	—	Initial value of the rejection flow (m^3/h).

B.5.8.4 me_membrane_2m

This is a hydraulic component of resistive type. It models a rack of reverse osmosis pressure vessels. A supply flow with a high salt concentration is pumped up to the component. Part of the current is forced through the membrane. Most of the salt is retained by the membrane and the salt concentration of the permeation is several orders of magnitude lower than the concentration in the supply. The rest of the salt and water forms the rejection current. This component is similar to `me_membrane`, except that the pressure tube has two different types of membranes. The membranes near the pressure tube inlet are specific so as to have a low flow density. The membranes near the pressure tube outlet are specific for high salinity conditions. In this way a more constant flow density is achieved along the pressure tube.

Figure B.44: `me_membrane_2m` icon.

Ports:

f_in	—	Supply flow.
f_outp	—	Permeate flow.
f_outr	—	Reject flow.
s_out	—	Analogue variable with the water recovery value (%).

Construction parameters:

$t1$	—	Strategy for the cleaning of the membranes. Whenever the term for reversible permeability exceeds a certain value ($Armin$) or every $dtCL$ number of days.
$t2$	—	Strategy for the partial replacement of the reverse osmosis modules. Whenever the term for irreversible permeability exceeds a certain value ($Aimin$) or every $dtRP$ number of days.
npv	—	Number of pressure vessels in parallel.
$nmo1$	—	Number of reverse osmosis modules of the first type of membrane, inside each pressure pressure vessel.
$nmo2$	—	Number of reverse osmosis modules of the second type of membrane, inside each pressure pressure vessel.

Parameters:

$Armin$	—	Value of reversible hydraulic permeability to perform the cleaning.
$dtCL$	—	Frequency of the cleaning (days).
$Aimin$	—	Irreversible hydraulic permeability strategy for the partial replacement of the reverse osmosis modules.
$dtRP$	—	Frequency for the partial replacement of the reverse osmosis modules (days).
$area$	—	Surface area of a reverse osmosis module ($foot^2$).
Ao	—	Initial hydraulic permeability ($m^3/foot^2 \cdot h \cdot bar$).
Bo	—	Permeability of the initial salt (1/h).
BBo	—	Permeability of the initial boron (-).
RP	—	Replacement percentage (0-1).

PSIA, PSIB, PSIBB, GAMMAA, GAMMAB —
— Parameters for the modelling of the fouling.

Kr — Parameter for the calculation of the rejection flow (m^3/h·bar).

Cravo — Average initial salt concenration on the supply side (ppm).

rpH — Ratio for the acidification of the permeation.

foulingmax — Maximum fouling value caused by particles $> 10^{-4}$ μm

Dpio — Initial value of the osmotic pressure (bar).

kQ — Filter for the calculation of the permeation and rejection flow (1/t).

Qpo — Initial value of the permeation flow (m^3/h).

Qro — Initial value of the rejection flow (m^3/h).

B.5.8.5 me_membrane_2out

This is a hydraulic component of resistive type. It models a rack of reverse osmosis pressure vessels. A supply flow with a high salt concentration is pumped up to the component. Part of the current is forced through the membrane. Most of the salt is retained by the membrane and the salt concentration of the permeation is several orders of magnitude lower than the concentration in the supply. The rest of the salt and water forms the rejection current. This component is similar to `me_membrane`, except that the permeate flow is extracted from two different zones of the pressure tube. The first outlet is near the supply inlet, with a low concentration of salt and boron. The second outlet is near the rejection outlet, with a high concentration of salt and boron, and which, depending on the requirements, may need to filtered again.

Ports:

f_in — Supply flow.

*f_outp*1 — First permeate flow.

*f_outp*2 — Second permeate flow.

f_outr — Reject flow.

s_out — Analogue variable with the water recovery value (%).

Construction parameters:

$t1$ — Strategy for the cleaning of the membranes. Whenever the term for reversible permeability exceeds a certain value ($Armin$) or every $dtCL$ number of days.

$t2$ — Strategy for the partial replacement of the reverse osmosis modules. Whenever the term for irreversible permeability exceeds a certain value ($Aimin$) or every $dtRP$ number of days.

npv — Number of pressure vessels in parallel.

nmo — Number of reverse osmosis modules within each pressure vessel.

Parameters:

$Armin$ — Value of reversible hydraulic permeability to perform the cleaning.

$dtCL$ — Frequency of the cleaning (days).

$Aimin$ — Irreversible hydraulic permeability strategy for the partial replacement of the reverse osmosis modules.

$dtRP$ — Frequency for the partial replacement of the reverse osmosis modules (days).

$area$ — Surface area of a reverse osmosis module (foot^2).

Ao — Initial hydraulic permeability (m^3/foot^2·h·bar).

Bo — Permeability of the initial salt (1/h).

BBo — Permeability of the initial boron (-).

RP — Replacement percentage (0-1).

PSIA, PSIB, PSIBB, GAMMAA, GAMMAB — — Parameters for the modelling of the fouling.

Kr — Parameter for the calculation of the rejection flow (m^3/h·bar).

$Cravo$ — Average initial salt concenration on the supply side (ppm).

rpH — Ratio for the acidification of the permeation.

$foulingmax$ — Maximum fouling value caused by particles $> 10^{-4}$ μm

$Dpio$ — Initial value of the osmotic pressure (bar).

kQ — Filter for the calculation of the permeation and rejection flow (1/t).

Qpo — Initial value of the permeation flow (m^3/h).
Qro — Initial value of the rejection flow (m^3/h).

Figure B.45: `me_membrane_2out` icon.

B.5.9 Pipes and Connectors

B.5.9.1 no_node11

This is a hydraulic component of accumulative type. It calculates the pressure (P) at a point on the hydraulic line so as to meet the mass balance between the input and output flow (Q_i), using the following equation:

$$P' = k \sum_{i=1}^{n} Q_i \tag{B.15}$$

This component is useful when two resistive components that are installed one after the other need to be connected.

Figure B.46: `no_node11` icon.

Ports:
f_in — Input flow.
f_out — Output flow.

Parameters:
k — Parameter to calculate the pressure (1/t).
Po — Initial pressure (bar).

B.5.9.2 no_node12

This is a hydraulic component of accumulative type. It calculates the pressure (P) at a point on the hydraulic line so as to meet the mass balance between the input and output flow (Q_i), using the following equation:

$$P' = k \sum_{i=1}^{n} Q_i \tag{B.16}$$

This component is useful to model a T-type joint in a pipe.

Figure B.47: `no_node12` icon.

Ports:

f_in	—	Input flow.
f_out1	—	First output flow.
f_out2	—	Second output flow.

Parameters:

k	—	Parameter to calculate the pressure (1/t).
Po	—	Initial pressure (bar).
ki	—	Filter for the rest of the variables of the analogue port (1/t).
To	—	Initial temperature (ºC).
Co	—	Initial salt concentration (ppm).
Bo	—	Initial boron concentration (ppm).
pHo	—	Initial pH (-).
$xo[mix]$	—	Initial concentration of the remaining variables.

B.5.9.3 no_node21

This is a hydraulic component of accumulative type. It calculates the pressure (P) at a point on the hydraulic line so as to meet the mass balance between the input and output flow (Q_i), using the following

equation:

$$P' = k \sum_{i=1}^{n} Q_i \tag{B.17}$$

This component is useful to model a T-type joint in a pipe.

Figure B.48: `no_node21` icon.

Ports:

f_in1	—	First input flow.
f_in2	—	Second input flow.
f_out	—	Output flow.

Parameters:

k	—	Parameter to calculate the pressure (1/t).
Po	—	Initial pressure (bar).
ki	—	Filter for the rest of the variables of the analogue port (1/t).
To	—	Initial temperature (ºC).
Co	—	Initial salt concentration (ppm).
Bo	—	Initial boron concentration (ppm).
pHo	—	Initial pH (-).
$xo[mix]$	—	Initial concentration of the remaining variables.

B.5.9.4 pi_pipe

This is a hydraulic component of resistive type, which simulates a pipe. The flow is calculated by assuming turbulent flow, applying the following equation:

$$Q = \frac{\Delta P^{0.5} \cdot D \cdot S^2}{f \cdot L \cdot density} \tag{B.18}$$

where the parameter f depends on the Reynolds number, as shown

below:

$$f = k \cdot Re^a \tag{B.19}$$

Figure B.49: `pi_pipe` icon.

Ports:

f_in	—	Input flow.
f_out	—	Output flow.

Parameters:

d	—	Internal pipe diameter (mm).
L	—	Pipe length (m).
$v0$	—	Initial flow speed (m/s).
kv	—	Filter to calculate speed (1/t).
kQ	—	Filter for the calculation of the rest of the variables (1/t).
To	—	Initial temperature (°C).
Co	—	Initial salt concentration (ppm).
Bo	—	Initial boron concentration (ppm).
pHo	—	Initial pH (-).
$xo[mix]$	—	Initial concentration of the remaining variables.

B.5.9.5 pi_pipevalve

This is a hydraulic component of resistive type. It corresponds to a pipe and a control valve, and it has been obtained by joining components `pi_pipe` and `v_controlvalve`.

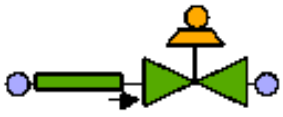

Figure B.50: `pi_pipevalve` icon.

Ports:
f_in — Input flow.
f_out — Output flow.
s_in — Opening of the valve (0-1).

Parameters:
The ones that correspond to the `pi_pipe` and `v_controlvalve` components.

B.5.10 Pumps

B.5.10.1 pu_centrifugalpump

This is a hydraulic component of resistive type. It corresponds to a centrifugal pump. The flow is calculated from the pump characteristic curve, which is set by users by means of a text file. In addition, this component has an analogue port that indicates the power consumption.

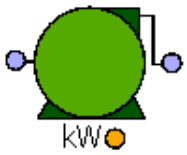

Figure B.51: `pu_centrifugalpump` icon.

Ports:
f_in — Input flow.
f_out — Output flow.
s_out — Pump power (kW).

Parameters:
$file$ — Path of the file where the pump characteristic curve is located.
$Qcolumn$ — Column with the flow values.
$DPcolumn$ — Column with the load values of the pump.
$effcolumn$ — Column with the efficiency values.
$Qmax$ — Maximum flow (m^3/h).

K	—	Constant to calculate the flow (m^3/h·bar)
$Pi0$	—	Initial pressure at the pump output (bar).
kPi	—	Filter in the calculation of the load supplied by the pump (1/t).
dto	—	Parameter that needs to be close to zero and that is used to prevent problems with the integration when the `RESTORE_STATE` command is used.

B.5.10.2 pu_centrifugalpumpvalve

This is a hydraulic component of resistive type. It corresponds to a centrifugal pump and a control valve, and has been obtained by joining the `pu_centrifugalpump` and `v_controlvalve` components.

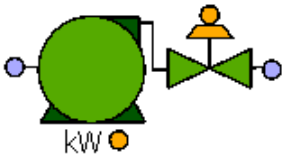

Figure B.52: `pu_centrifugalpumpvalve` icon.

Ports:

f_in	—	Input flow.
f_out	—	Output flow.
s_out	—	Pump power (kW).
s_in	—	Opening of the valve (0-1).

Parameters:
The ones that correspond to the `pu_centrifugalpump` and `v_controlvalve` components.

B.5.10.3 pu_centrifugalpumpvariator

This is a hydraulic component of resistive type. It corresponds to a centrifugal pump with a speed variator. The flow is calculated from the characteristic pump curve, established by means of a text file, and the variator speed, set by means of an analogue port. In addi-

tion, this component has an analogue port that indicates the power consumption.

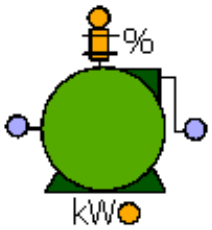

Figure B.53: `pu_centrifugalpumpvariator` icon.

Ports:

f_in	—	Input flow.
f_out	—	Output flow.
s_out	—	Pump power (kW).
s_in	—	Speed of the speed variator (%).

Parameters:

file	—	Path of the file where the pump characteristic curve is located.
*Qcolumn*0	—	Column with the flow values for the minimum speed.
DPcolumn	—	Column with the load values of the pump for the minimum speed.
*Qcolumn*0	—	Column with the efficiency values for the minimum speed.
*Qcolumn*100	—	Column with the flow values for the maximum speed.
*Qcolumn*0	—	Column with the load values of the pump for the maximum speed.
*Qcolumn*100	—	IColumn with the efficiency values for the maximum speed.
Qmax	—	Maximum flow (m^3/h).
K	—	Constant to calculate the flow ($m^3/h \cdot bar$).
*Pi*0	—	Initial pressure at the pump output (bar).
kPi	—	Filter in the calculation of the load supplied by the pump (1/t).

dto — Parameter that needs to be close to zero and that is used to prevent problems with the integration when the `RESTORE_STATE` command is used.

B.5.10.4 pu_positivepump

This is a hydraulic component of resistive type. It corresponds to a positive displacement pump. The flow is calculated from the variator speed, set through an analogue port. In addition, this component has an analogue port that indicates the power consumption.

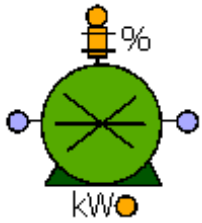

Figure B.54: `pu_positivepump` icon.

Ports:

f_in — Input flow.
f_out — Output flow.
s_out — Pump power (kW).
s_in — Speed of the speed variator (%).

Parameters:

file — Path of the file where the pump characteristic curve is located.
Qcolumn — Column with the speed values.
effcolumn — Column with the efficiency values.
Qmax — Maximum flow (m^3/h).
Qo — Initial flow (m^3/h).
kQ — Filter for the calculation of the rest of the flow (1/t).
dto — Parameter that needs to be close to zero and that is used to prevent problems with the integration when the `RESTORE_STATE` command is used.

B.5.11 RO Systems

B.5.11.1 ROsystem

This is a hydraulic component of resistive type. It models a system formed by a reverse osmosis pressure tube rack, with a high-pressure pump with a variable speed drive, an ERD-type energy recovery system, a control valve at the outlet of the rejection flow and a secondary pump. This is probably one of the most common type of desalination structures.

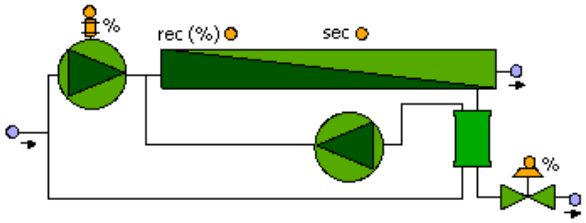

Figure B.55: `ROsystem` icon.

Ports:

f_in	—	Feed flow.
f_outp	—	Permeate flow.
s_outr	—	Reject flow.
s_rec	—	Analogue variable with the water recovery value (%).
s_sec	—	Analogue variable with the energy consumption variable (kW/m^3).
s_in	—	Analogue variable with the high-pressure pump speed (%).

Parameters:
These correspond to the components `pu_centrifugalpumpvariator`, `v_controlvalve`, `er_ERD`, and `me_membrane`.

B.5.11.2 ROsystem2

This is a hydraulic component of resistive type. It models a system formed by a reverse osmosis pressure tube rack, a high-pressure pump

with a variable speed drive and a control valve at the rejection flow outlet.

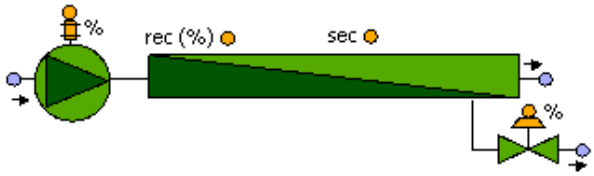

Figure B.56: `ROsystem2` icon.

Ports:

f_in	—	Feed flow.
f_outp	—	Permeate flow.
s_outr	—	Reject flow.
s_rec	—	Analogue variable with the water recovery value (%).
s_sec	—	Analogue variable with the energy consumption variable (kW/m^3).
s_in	—	Analogue variable with the high-pressure pump speed (%).

Parameters:
These correspond to the components `pu_centrifugalpumpvariator`, `v_controlvalve`, and `me_membrane`.

B.5.12 Sources and Sinks

B.5.12.1 sa_constant

This is an analogue component of scalar type. It sets the value of an analogue variable.

Ports:

s_out	—	Output scalar.

Parameters:

u	—	Output value.

k — Filter in the analogue value (1/t).

Figure B.57: `sa_constant` icon.

B.5.12.2 sa_constantv

This is an analogue component of vector type. It establishes the value of the elements of an analogue vector.

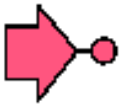

Figure B.58: `sa_constantv` icon.

Ports:
s_out — Output vector.

Construction parameters:
n — Vector size.

Parameters:
$u[n]$ — Vector elements.
$k[n]$ — Vector filter (1/t).

B.5.12.3 sa_file

This is an analogue component of scalar type. It establishes the value of an analogue variable using the data in a text file. The values of this text file repeat cyclically.

Ports:
s_out — Output scalar.

Parameters:

file	—	Path of the file where the output analogue signal is located.
Qcolumn	—	Column with the time values.
ycolumn	—	Column with the values of the analogue signal.
tmax	—	Maximum time of the file data (t).
k	—	Gain.
b	—	Bias.
dto	—	Parameter that needs to be close to zero and that is used to prevent problems with the integration when the `RESTORE_STATE` command is used.

Figure B.59: `sa_file` icon.

B.5.12.4 sa_function

This is an analogue component of scalar type. It establishes the value of an analogue variable as a time-dependent function. The type of function is set with construction parameter x, as set out below:

$x = 1$ constant value.

$x = 2$ step function.

$x = 3$ ramp function.

$x = 4$ sine function.

$x = 5$ pulse function.

$x = 6$ pulse train function.

$x = 7$ stair function.

$x = 8$ sawtooth function.

$x = 9$ trapezoid function (upwards only).

$x = 10$ trapezoid function (upwards and downwards).

Figure B.60: `sa_function` icon.

Ports:

s_out	—	Output scalar.

Parameters:

A	—	Amplitude.
T	—	Period (t).
$T1, T2, T3$	—	Parameters for the various functions (t).
b	—	Bias.

B.5.12.5 sa_sink

This is a hydraulic component of accumulative type. It calculates the pressure at the end of a hydraulic line. It also establishes the salt and boron concentrations, temperature, pH and concentration of the rest of the chemical types, in the event of reverse flow.

Ports:

f_in	—	Input flow.

Parameters:

P	—	Pressure (bar).
H	—	Height (m).
k	—	Filter to calculate the pressure (1/t).
T	—	Temperature of the reverse flow (ºC).
C	—	Salt concentration in the reverse flow (ppm).
B	—	Boron concentration in the reverse flow (ppm).
pH	—	pH of the reverse flow.

$x[mix]$ — Concentration of the rest of chemical types of the reverse flow.
$inverseflow$ — If this parameter is set to `TRUE`, reverse flow may occur. If it is set to `FALSE`, reverse flow may not occur.

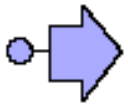

Figure B.61: `sa_sink` icon.

B.5.12.6 sa_source

This is a hydraulic component of accumulative type. It calculates the pressure at the start of a hydraulic line. It also establishes the salt and boron concentrations, temperature, pH and concentration of the rest of the chemical types.

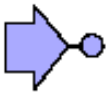

Figure B.62: `sa_source` icon.

Ports:
f_in — Input flow.

Parameters:
P — Pressure (bar).
H — Height (m).
k — Filter to calculate the pressure (1/t).
T — Temperature of the reverse flow (ºC).
C — Salt concentration in the reverse flow (ppm).
B — Boron concentration in the reverse flow (ppm).
pH — pH of the reverse flow.
$x[mix]$ — Concentration of the rest of chemical types of the reverse flow.

B.5.12.7 sa_sun

This is an analogue component of vector type. It generates an analogue vector whose first element is the solar radiation and whose second element is the ambient temperature. Both variables are read from a text file.

Figure B.63: `sa_sun` icon.

Ports:

s_out	—	Output vector with the solar radiation and the ambient temperature.

Parameters:

file	—	Path of the file that contains the radiation and the temperature
tcolumn	—	Column with the time values.
rcolumn	—	Column with the solar radiation values.
Tcolumn	—	Column with the ambient temperature values.
tmax	—	Maximum time of the file data (t).

Variables:

rad	—	Solar radiation.
T	—	Ambient temperature.

B.5.12.8 sa_table

This is an analogue component of scalar type. It establishes the value of an analogue variable as a table that repeats cyclically.

Ports:

s_out	—	Output scalar.

Construction parameters:

n — Number of elements in the table.

Parameters:
$dt[n]$ — Time increment between two points of the table (t).
$u[n]$ — Table output values.
k — Gain.
b — Bias.

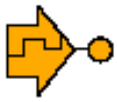

Figure B.64: `sa_table` icon.

B.5.12.9 sa_time

This is an analogue component of scalar type. It sets the value of an analogue variable as the simulation time value.

Figure B.65: `sa_time` icon.

Ports:
s_out — Output scalar.

B.5.13 Sensors

B.5.13.1 se_sensorQ

This is a hydraulic component of neutral type. It models a flow sensor with a first order filter and a delay.

Ports:
f_in — Input flow.
f_out — Output flow.

s_out — Sensor output.

Parameters:
k — Sensor filter (1/t).
dt — Sensor delay (t).
*u*0 — Initial value of the sensor.

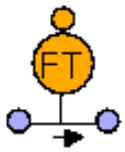

Figure B.66: `se_sensorQ` icon.

B.5.13.2 se_sensorB

This is a hydraulic component of neutral type. It models a boron concentration sensor with a first order filter and a delay.

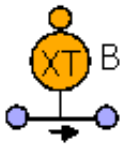

Figure B.67: `se_sensorB` icon.

Ports:
f_in — Input flow.
f_out — Output flow.
s_out — Sensor output.

Parameters:
k — Sensor filter (1/t).
dt — Sensor delay (t).
*u*0 — Initial value of the sensor.

B.5.13.3 se_sensorC

This is a hydraulic component of neutral type. It models a salt concentration sensor with a first order filter and a delay.

Figure B.68: `se_sensorC` icon.

Ports:
f_in — Input flow.
f_out — Output flow.
s_out — Sensor output.

Parameters:
k — Sensor filter (1/t).
dt — Sensor delay (t).
*u*0 — Initial value of the sensor.

B.5.13.4 se_sensorpH

This is a hydraulic component of neutral type. It models a pH sensor with a first order filter and a delay.

Ports:
f_in — Input flow.
f_out — Output flow.
s_out — Sensor output.

Parameters:
k — Sensor filter (1/t).
dt — Sensor delay (t).
*u*0 — Initial value of the sensor.

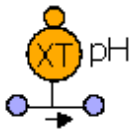

Figure B.69: `se_sensorpH` icon.

B.5.13.5 se_sensorT

This is a hydraulic component of neutral type. It models a temperature sensor with a first order filter and a delay.

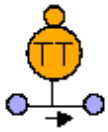

Figure B.70: `se_sensorT` icon.

Ports:

f_in	—	Input flow.
f_out	—	Output flow.
s_out	—	Sensor output.

Parameters:

k	—	Sensor filter (1/t).
dt	—	Sensor delay (t).
*u*0	—	Initial value of the sensor.

B.5.13.6 se_sensorx

This is a hydraulic component of neutral type. It models a concentration sensor with a first order filter and a delay. The chemical type is set by construction parameter x, as follows:

$x = 1$ Microorganisms

$x = 2$ Substrate that serves as nourishment for the microorganisms.

$x = 3$ Suspended particles of > 1 μm.

$x = 4$ Suspended particles of between 0.1 - 1 μm.

$x = 5$ Suspended particles of between 10^{-2} - 0.1 μm.

$x = 6$ Suspended particles of between 10^{-3} - 10^{-2} μm.

$x = 7$ Suspended particles of between 10^{-4} - 10^{-3} μm.

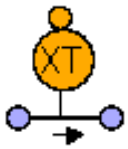

Figure B.71: `se_sensorx` icon.

Ports:
f_in — Input flow.
f_out — Output flow.
s_out — Sensor output.

Parameters:
k — Sensor filter (1/t).
dt — Sensor delay (t).
u0 — Initial value of the sensor.

B.5.14 Tanks

B.5.14.1 ta_pressurizedtank

This is a hydraulic component of accumulative type. It corresponds to a pressurized tank. There is also an analogue signal that marks the level of the liquid. This sensor is modelled with a first order filter and a delay.

Ports:
f_in — Input flow.
f_out — Output flow.

s_h100 — Level sensor (%).

Parameters:

A — Area of the tank base (m^2).
H — Tank height (m).
$h100\_in$ — Height of the input connection (%).
$h100\_out$ — Height of the output connection (%).
$h100o$ — Initial liquid head (%).
kh — Filter for the level sensor (1/t).
dth — Delay for the level sensor (1/t).
$T0$ — Initial temperature (ºC).
$C0$ — Initial salt concentration (ppm).
$B0$ — Initial boron concentration (ppm).
$pH0$ — Initial pH (-)
$x0[mix]$ — Initial concentration of the rest of chemical types.
$P0$ — Initial gas pressure (bar).

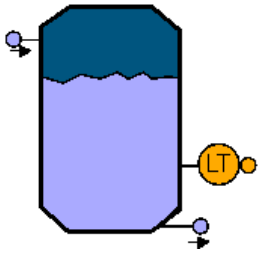

Figure B.72: `ta_pressurizedtank` icon.

B.5.14.2 ta_tank

This is a hydraulic component of accumulative type. It corresponds to an open tank. This component is modelled taking into account the potential draining or spillover of the tank. There is also an analogue signal that marks the level of the liquid. This sensor is modelled with a first order filter and a delay.

Ports:

f_in — Input flow.
f_out — Output flow.

s_h100 — Level sensor (%).

Parameters:

A — Area of the tank base (m^2).
H — Tank height (m).
$h100\_in$ — Height of the input connection (%).
$h100\_out$ — Height of the output connection (%).
$h100o$ — Initial liquid head (%).
kh — Filter for the level sensor (1/t).
dth — Delay for the level sensor (1/t).
$T0$ — Initial temperature (°C).
$C0$ — Initial salt concentration (ppm).
$B0$ — Initial boron concentration (ppm).
$pH0$ — Initial pH (-)
$x0[mix]$ — Initial concentration of the rest of chemical types.
$kover$ — Parameter to calculate the overflow.

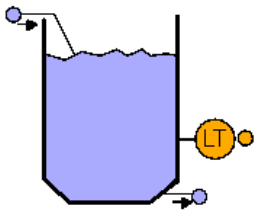

Figure B.73: `ta_tank` icon.

B.5.14.3 ta_tank2

This is a hydraulic component of accumulative type. It corresponds to an open tank. This component is modelled taking into account the potential draining or spillover of the tank. There is also an analogue signal that marks the level of the liquid. This sensor is modelled with a first order filter and a delay. This component is similar to component `ta_tank`, but with two input flows and two output flows.

Ports:

f_in1 — First input flow.
f_in2 — Second input flow.

f_out	—	Output flow.
s_h100	—	Level sensor (%).

Parameters:

A	—	Area of the tank base (m^2).
H	—	Tank height (m).
$h100\_in$	—	Height of the inputs connection (%).
$h100\_out$	—	Height of the output connection (%).
$h100o$	—	Initial liquid head (%).
kh	—	Filter for the level sensor (1/t).
dth	—	Delay for the level sensor (1/t).
$T0$	—	Initial temperature (ºC).
$C0$	—	Initial salt concentration (ppm).
$B0$	—	Initial boron concentration (ppm).
$pH0$	—	Initial pH (-)
$x0[mix]$	—	Initial concentration of the rest of chemical types.
$kover$	—	Parameter to calculate the overflow.

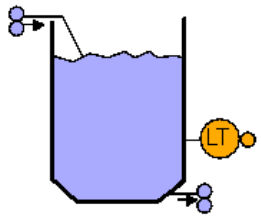

Figure B.74: `ta_tank2` icon.

B.5.14.4 ta_tanke

This is a hydraulic component of accumulative type. It simulates an open tank, from which the accumulated liquid evaporates, and heats up due to the solar radiation. This component is modelled taking into account the potential draining or spillover of the tank. In addition, there are two analogue signals that establish the liquid level and temperature. These sensors are modelled with a first order filter and a delay.

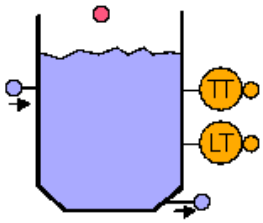

Figure B.75: `ta_tanke` icon.

Ports:

f_in	—	Input flow.
f_out	—	Output flow.
s_h100	—	Level sensor (%).
s_T	—	Temperature sensor (°C).
s_in	—	Analogue vector that collects the solar radiation and the ambient temperature.

Parameters:

A	—	Area of the tank base (m^2).
H	—	Tank height (m).
$h100\_in$	—	Height of the inputs connection (%).
$h100\_out$	—	Height of the output connection (%).
$h100o$	—	Initial liquid head (%).
kh	—	Filter for the level sensor (1/t).
dth	—	Delay for the level sensor (1/t).
kT	—	Filter for the temperature sensor (1/t).
dtT	—	Delay for the temperature sensor (1/t).
$T0$	—	Initial temperature (°C).
$C0$	—	Initial salt concentration (ppm).
$B0$	—	Initial boron concentration (ppm).
$pH0$	—	Initial pH (-)
$x0[mix]$	—	Initial concentration of the rest of chemical types.
$kover$	—	Parameter to calculate the overflow.
$kevap$	—	Parameter for the calculation of the evaporation.
$aevap$	—	Parameter for the calculation of the evaporation.
$Levap$	—	Latent heat of the evaporation (kW/kg).

B.5.14.5 ta_tankr

This is a hydraulic component of accumulative type. It corresponds to an open tank with a resistor. This component is modelled taking into account the potential draining or spillover of the tank. The heat generated by the resistor is established externally through an analogue port. In addition, there are two analogue signals that establish the liquid level and temperature. These sensors are modelled with a first order filter and a delay.

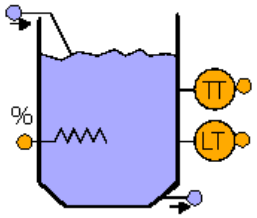

Figure B.76: `ta_tankr` icon.

Ports:

f_in	—	Input flow.
f_out	—	Output flow.
s_T	—	Temperature sensor (°C).
s_h100	—	Level sensor (%).
s_in	—	Resistor value (%).

Parameters:

A	—	Area of the tank base (m^2).
H	—	Tank height (m).
$h100\_in$	—	Height of the input connection (%).
$h100\_out$	—	Height of the output connection (%).
$h100o$	—	Initial liquid head (%).
kh	—	Filter for the level sensor (1/t).
dth	—	Delay for the level sensor (1/t).
$T0$	—	Initial temperature (°C).
$C0$	—	Initial salt concentration (ppm).
$B0$	—	Initial boron concentration (ppm).
$pH0$	—	Initial pH (-)
$x0[mix]$	—	Initial concentration of the rest of chemical types.

kover — Parameter to calculate the overflow.
qmax — Ratio between the generated heat and the specific heat (kg/°C·h)

B.5.15 Valves

B.5.15.1 v_ballvalve

This is a hydraulic component of resistive type. It corresponds to an on/off ball valve. It is similar to component `v_selenoidvalve`, but the valve position (open or closed) is defined internally.

Figure B.77: `v_ballvalve` icon.

Ports:
f_in — Input flow.
f_out — Output flow.

Parameters:
open — Variable that defines the valve position, either open (`TRUE`) or closed (`FALSE`).
k — Filter of the input (1/t).
K — Constant for flow calculation ($m^3/h \cdot bar^{0.5}$).

B.5.15.2 v_checkvalve

This is a hydraulic component of neutral type. It corresponds to a check valve, which prevents reverse flow in a hydraulic line.

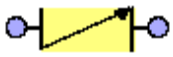

Figure B.78: `v_checkvalve` icon.

Ports:

f_in — Input flow.
f_out — Output flow.

B.5.15.3 v_controlvalve

This is a hydraulic component of resistive type. It corresponds to a control valve. The opening of the valve is set by means of an analogue port. The valve characteristic curve may be linear, equal percentage, quick opening or defined by means of a polynomial. This component is similar to `v_manualvalve`, but the valve position is defined externally.

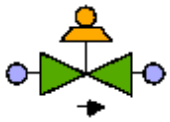

Figure B.79: `v_controlvalve` icon.

Ports:
f_in — Input flow.
f_out — Output flow.
s_in — Opening of the valve (0-1).

Construction parameters:
*t*1 — Valve characteristic curve: linear, of equal percentage and quick opening type or defined by means of a polynomial.
*t*2 — It allows or prevents reverse flow.
n — Order of the polynomial of the characteristic curve (if applicable).

Parameters:
K — Constant for flow calculation ($m^3/h \cdot bar^{0.5}$).
ku — Filter at the valve opening (1/t).
rang — Rangeability.
*u*0 — Initial position of the valve plug (%).
ai[*n*] — Coefficients of the polynomial of the characteristic curve (if applicable).

B.5.15.4 v_manualvalve

This is a hydraulic component of resistive type. It corresponds to a control valve. The valve characteristic curve may be linear, of equal percentage and quick opening type or correctly defined by means of a polynomial. This component is similar to `v_manualvalve`, but the valve position is defined internally.

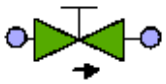

Figure B.80: `v_manualvalve` icon.

Ports:

f_in	—	Input flow.
f_out	—	Output flow.
s_in	—	Opening of the valve (0-1).

Construction parameters:

$t1$	—	Valve characteristic curve: linear, of equal percentage and quick opening type or defined by means of a polynomial.
$t2$	—	It allows or prevents reverse flow.
n	—	Order of the polynomial of the characteristic curve (if applicable).

Parameters:

K	—	Constant for flow calculation ($m^3/h \cdot bar^{0.5}$).
ku	—	Filter at the valve opening (1/t).
rang	—	Rangeability.
$u0$	—	Initial position of the valve plug (%).
$ai[n]$	—	Coefficients of the polynomial of the characteristic curve (if applicable).

B.5.15.5 v_solenoidvalve

This is a hydraulic component of resistive type. It corresponds to an on/off solenoid valve. It is similar to component `v_ballvalve`, but the valve position (open or closed) is defined externally by means of an analogue port.

Figure B.81: `v_solenoidvalve` icon.

Ports:
f_in — Input flow.
f_out — Output flow.
s_in — Opening of the valve (0-1).

Parameters:
K — Constant for flow calculation ($m^3/h \cdot bar^{0.5}$).
k — Filter of the valve opening (1/t).

B.5.15.6 v_threewaysvalve12

This is a hydraulic component of resistive type. It corresponds to a L-shaped three-way valve. It has one liquid input and two liquid outputs. The open path is defined by means of an analogue port (1-2). When value 1 is used, the flow runs between the input port and the first output port. When value 2 is used, the flow runs between the input port and the second output port.

Ports:
f_in — Input flow.
*f_out*1 — First output flow.
*f_out*2 — Second output flow.
s_in — Open path (1-2).

Parameters:

k	—	Filter of the valve opening (1/t).
K	—	Constant for flow calculation ($m^3/h \cdot bar^{0.5}$).
$P0$	—	Initial pressure (bar).

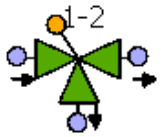

Figure B.82: `v_threewaysvalve12` icon.

B.5.15.7 v_threewaysvalve21

This is a hydraulic component of resistive type. It corresponds to a L-shaped three-way valve. It has two liquid inputs and one liquid output. The open path is defined by means of an analogue port (1-2). When value 1 is used, the flow runs between the first input port and the output port. When value 2 is used, the flow runs between the second input port and the output port.

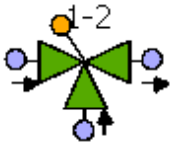

Figure B.83: `v_threewaysvalve21` icon.

Ports:

f_in1	—	First input flow.
f_in2	—	Second input flow.
f_out	—	Output flow.
s_in	—	Open path (1-2).

Parameters:

k	—	Filter of the valve opening (1/t).
K	—	Constant for flow calculation ($m^3/h \cdot bar^{0.5}$).
$P0$	—	Initial pressure (bar).

B.5.16 Miscellaneous Components

B.5.16.1 x_clock

This is a component without ports that is different to all the rest. This component calculates time in different units (seconds, minutes, hours, days, years) and may be used instead of the EcosimPro variable `TIME`, as the variable for the axis of abscissas of the charts.

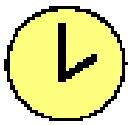

Figure B.84: `x_clock` icon.

Variables:

t_s	—	Time (s).
t_min	—	Time (min).
t_h	—	Time (h).
t_days	—	Time (days).
t_years	—	Time (years).

B.5.16.2 x_homogenizer

This is a hydraulic component of neutral type. It models a homogenizer, by means of a complete mixture volume. In addition, it generates a pressure drop proportional to the inlet flow.

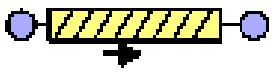

Figure B.85: `x_homogenizer` icon.

Ports:

f_in	—	Input flow.
f_out	—	Output flow.

Parameters:

kP — Parameter for the calculation of the pressure drop.
aP — Parameter for the calculation of the pressure drop.
Po — Initial pressure (bar).
To — Initial temperature (ºC).
Co — Initial salt concentration (ppm).
Bo — Initial boron concentration (ppm).
pHo — Initial pH (-).
$xo[mix]$ — Initial concentration of the remaining variables.
V — Volume (m^3).

List of Symbols

Capital letters:

A	—	Area (m^2)
A_w	—	Water permeability (m/(bar·s))
B_s	—	Salt permeability (m/s)
C	—	Salt concentration (g/m^3)
C_b	—	Average salt concentration at the bulk of the feed flow along an RO module (g/m^3)
C_f	—	Salt concentration at the bulk of the feed flow (g/m^3)
C_m	—	Salt concentration at the membrane surface (g/m^3)
C_p	—	Salt concentration at the bulk of the permeate (g/m^3)
$\mathbb{C}_{CL}$	—	Cost of the chemical cleaning ($)
$\mathbb{C}_{OP}$	—	Cost of the operation ($)
$\mathbb{C}_P$	—	Cost of the pumps ($)
$\mathbb{C}_{ROT}$	—	Cost of the rotation of the RO modules ($)
$\mathbb{C}_{RP}$	—	Cost of the replacement of the RO modules ($)
$\mathbb{C}_T$	—	Cost of the tanks ($)
$\mathcal{D}$	—	Diffusion coefficient (m^2/s)
F	—	Ratio of the permeate flux and the salt permeability (-)
F_j	—	Sum of forces over one particle in Brownian motion (N)
G	—	Maximum solar radiation (W/m^2)
G_s	—	Maximum solar radiation in a sunny day (W/m^2)
I	—	Solar radiation (W/m^2)
J	—	Cost function ($)
J_s	—	Salt permeate flux ($kg/(m^2 \cdot s)$)
J_w	—	Water permeate flux (m/s)
L	—	Water level (%)
P	—	Pressure (bar)

PM — Molar weight (kg/kmol)
Pe — Peclet number $Pe = (u_f \cdot h_f)/\mathcal{D}$ (-)
Q_f — Water flow of the feed (L/h) or (m^3/day)
Q_p — Water flow of the permeate (L/h) or (m^3/day)
Q_r — Water flow of the reject (L/h) or (m^3/day)
R — Gas constant ((Pa·m^3)/(mol·K))
R_m — Salt rejection on the membrane surface (-)
Re — Reynolds number $Re = (\rho \cdot u_f \cdot h_f)/\mu$ (-)
S — Conductivity (μS/cm)
S — Cross section (m^2)
Sc — Schmidt number $Sc = \mu/(\rho \cdot \mathcal{D})$ (-)
Sh — Sherwood number $Sh = (k_m \cdot h_f)/\mathcal{D})$ (-)
T — Temperature (°C)
T_l — Duration of the daylight (h)
W — Power (kW)
Wp — Watt-peak of a photovoltaic solar energy device (W/m^2)
X — Concentration of suspended solids in a stream (g/m^3)

Lower-case letters:

a_n — Proportional parameter
b_j — Parameter for Stokes Law in Brownian motion (-)
c — Degree of coverange (-)
e_j — Stochastic parameter for Brownian motion (-)
h — height (m)
h_f — height of the feed side of one RO module (m)
i — van't Hoff coefficient (-)
j_X — Mass flow of suspended solids captured in a sand filter (kg/(m^3·s))
k — Proportional parameter
k_m — Mass transfer coefficient (m/s)
m — Mass (kg)
mix — Mixture module (-)
n_{CL} — Number of chemical cleanings (-)
n_m — Number of RO modules in one pressure vessel (-)
n_{PV} — Number of pressure vessels (-)
r — Percentage of modules that are replaced (-)

u_f — Velocity of the feed flow (m/s)
u_p — Velocity of the permeate flow (m/s)
v — Wind velocity (m/s)
x_j — Particle position in Brownian motion (μm)

Greeks:

δ — Boundary layer thickness (m)
ε — Porosity (-)
η — Pump efficiency (-)
κ_{CL} — Cost of the chemical cleaning of one RO module ($)
κ_{OP} — Energy cost ($/kWh)
κ_{RO} — Cost of the replacement of one RO module ($)
κ_{ROT} — Cost of the rotation of the RO modules ($)
λ — Expected lifetime (years)
μ — Viscosity (kg/(m·s))
ξ — Constraint (-)
π — Osmotic pressure (bar)
π_{20} — Osmotic pressure at 20 °C (bar)
ρ — Density (kg/m^3)
σ — Reflection coefficient (-)
σ_j^2 — Variance in Brownian motion (-)
ϕ — Polarization module (-)
Φ — Ratio between the power consumption by pumping and the total consumption of a desalination plant (-)
Φ_w — Ratio between the nominal water demand and the average nominal value (-)

List of Acronyms

AEDyR: The Spanish Association of Desalination

CD: **C**onvenction-**D**iffusion (used in CP modelling)

CFD: **C**omputational **F**luid **D**ynamics

COAMBCV: The Spanish Association of Environmental Science

CP: **C**oncentration **P**olarization

CRTEn: The **R**esearch and **T**echnology **C**enter of **En**ergy

CSI: **C**alcium **S**aturation **I**ndex

CSP: The Process Control and Supervision Research Group

DAE: **D**ifferential **A**lgebraic **E**quations

DAF: **D**issolved **A**ir **F**lotation

DMC: **D**ynamic **M**atrix **C**ontrol

DWEER: **D**ual **W**ork **E**xchange **E**nergy **R**ecovery system

EDR: **E**lectro**d**ialysis **R**eversal

ERD: **E**nergy **R**ecovery **D**evice

FT: **F**ilm **T**heory (used in CP modelling)

HD: **H**umidification-**D**ehumidification

IDA: The **I**nternational **D**esalination **A**ssociation

KK: **K**edem-**K**atchalsky model

LSI: **L**angelier **S**aturation **I**ndex

MPC: **M**odel-based **P**redictive **C**ontrol

MD: **M**embrane **D**istillation

MED: **M**ultiple **E**ffect **D**istillation

MINLP: **M**ixed-**I**nteger **N**onlinear **P**rogramming

MIQP: **M**ixed-**I**nteger **Q**uadratic **P**rogramming

MSF: **M**ulti-**S**tage **F**lash

MVC: **M**echanical **V**apour **C**ompression

NLP: **N**on**l**inear **P**rogramming

OPEN-GAIN: **Op**timal **En**gineering Design for Dependable Water and Power **G**eneration in Remote **A**reas using Renewable Energies and **In**telligent Automation (6th Framework Programme of the EU, contract number 032535)

PID: **P**roportional-**I**ntegral-**D**erivative Controller

PLC: **P**rogrammable **L**ogic **C**ontroller

PRO: **P**ressure **R**etarded **O**smosis

PRODES: **Pro**motion of Renewable Energy for Water Production through **Des**alination Project

PSI: **P**uckorius **S**caling **I**ndex

RM: **R**isk **M**anagement

RO: **R**everse **O**smosis

ROSIM: **R**everse **O**smosis **Sim**ulation Library (the dynamic library arising with this thesis)

RS: **R**etained **S**olute (used in CP modelling)

RSI: **R**yznar **S**tability **I**ndex

SDI: **S**ilt **D**ensity **I**ndex

SEC: **S**pecific **E**nergy **C**onsumption

SK: **S**piegler-**K**edem model

SWRO: **S**ea**w**ater **R**everse **O**smosis

S&DSI: **S**tiff **&** **D**avis **S**tability **I**ndex

TBT: **T**op **B**rine **T**emperature

TDS: **T**otal **D**issolved **S**olids (ppm = g/m^3)

TVC: **T**hermal **V**apour **C**ompression

UVa: The **U**niversity of **Va**lladolid

VC: **V**apour **C**ompression

List of Websites

AEDyR: http://www.aedyr.eu/

Agbar: http://www.agbar.es/

ATLL: http://www.atll.cat/es/

COAMBCV: http://www.coambcv.com/

CRTEn: http://www.crten.rnrt.tn/

CSM: http://www.csmfilter.com/

CSP: http://csp.isa.cie.uva.es/index.php/en

Dosim: http://www.dosim.com/

DOW: http://www.dowwaterandprocess.com/

EA: http://www.empre.es/

EcosimPro: http://www.ecosimpro.com/

ERI: http://www.energyrecovery.com/

Flowserve: http://www.flowserve.com/

Grundfos: http://uk.grundfos.com/

Hydranautics: http://www.membranes.com/

IDA: http://www.idadesal.org/

KSB: http://www.ksb.com/

MathWorks: http://www.mathworks.com/

OMRON: http://omron.co.uk/

OPEN-GAIN: http://www.open-gain.org/

Pevasa: http://www.spe.co.id/

PRODES: http://www.prodes-project.org

SETA: http://www.gruposeta.com/

SMA: http://www.sma-uk.com/

TORAY: http://www.toraywater.com/

University of Manchester: http://www.cpi.umist.ac.uk/

University of Valladolid: http://www.isa.cie.uva.es/

List of Figures

List of Tables

Bibliography

Abbas, A. (2006). Model predictive control of a reverse osmosis desalination unit. *Desalination*, 194:268–280.

Abbas, A. and Al-Bastaki, N. (2005). Modeling of an RO water desalination unit using neural networks. *Chemical Engineering Journal*, 114:139–143.

Acebes, L. F., Merino, A., Palacín, L. G., Alves, R., Mazaeda, R., and Acedo, J. (2013). Educational simulators for industrial process control. *Advances in Intelligent Systems and Computing*, 197:151–163.

Achilli, A., Cath, T. Y., and Childress, A. E. (2009). Power generation with pressure retarded osmosis: An experimental and theoretical investigation. *Journal of Membrane Science*, 343:42–52.

Al-Ahmad, M. and Aleem, F. A. (1993). Scale formation and fouling problems effect on the performance of MSF and RO desalination plants in Saudi Arabia. *Desalination*, 93:287–310.

Al-Amoudi, A. S. (2010). Factors affecting natural organic matter (NOM) and scaling fouling in NF membranes: A review. *Desalination*, 259:1–10.

Al-Bastaki, N. M. and Abbas, A. (1999). Modeling an industrial reverse osmosis unit. *Desalination*, 126:33–39.

Al-Obaidani, S., Curcio, E., Macedonio, F., Profio, G. D., Al-Hinai, H., and Drioli, E. (2008). Potential of membrane distillation in seawater desalination: Thermal efficiency, sensitivity study and cost estimation. *Journal of Membrane Science*, 323:85–98.

Al-Sahlawi, M. A. (1999). Seawater desalination in Saudi Arabia: economic review and demand projections. *Desalination*, 123:143–147.

Al-Sharif, S., Albeirutty, M., Cipollina, A., and Micale, G. (2013). Modelling flow and heat transfer in spacer-filled membrane distillation channels using open source CFD code. *Desalination*, 311:103–112.

Al-Weshahi, M. A., Anderson, A., and Tian, G. (2013). Exergy efficiency enhancement of MSF desalination by heat recovery from hot distillate water stages. *Applied Thermal Engineering*, 53:226–233.

Alatiqi, I., Ettouney, H., and El-Dessouky, H. (1999). Process control in water desalination industry: an overview. *Desalination*, 126:15–32.

Ali, E., Alhumaizi, K., and Ajbar, A. (1999). Model reduction and robust control of multi-stage flash (MSF) desalination plants. *Desalination*, 121:65–85.

Aljohani, M. S. (2004). Nuclear desalination competitiveness in the western region of the Kingdom of Saudi Arabia. *Desalination*, 164:213–223.

Alklaibi, A. M. and Lior, N. (2005). Membrane-distillation desalination: Status and potential. *Desalination*, 171:111–131.

Allison, R. P. (1995). Electrodialysis reversal in water reuse applications. *Desalination*, 103:11–18.

Alves, R., Normey-Rico, J. E., Merino, A., Acebes, L. F., and de Prada, C. (2005). OPC based distributed real time simulation of complex continuous processes. *Simulation Modelling Practice and Theory*, 13:525–549.

Alves, R., Normey-Rico, J. E., Merino, A., Acebes, L. F., and de Prada, C. (2008). Distributed continuous process simulation: An industrial case study. *Computers & Chemical Engineering*, 32:195–205.

Alvisi, S., Franchini, M., and Marinelli, A. (2007). A short-term, pattern-based model for water-demand forecasting. *Journal of Hydroinformatics*, 9:39–50.

Aragonés, J. L., Sanz, E., and Vega, C. (2012). Solubility of NaCl in water by molecular simulation revisited. *The Journal of Chemical Physics*, 136:508–524.

Assef, J. Z., Watters, J. C., Deshpande, P. B., and Alatiqi, I. M. (1997). Advanced control of a reverse osmosis desalination unit. *Journal of Process Control*, 7:283–289.

Bacchin, P., Marty, A., Duru, P., Meireles, M., and Aimar, P. (2011). Colloidal surface interactions and membrane fouling: Investigations at pore scale. *Advances in Colloid and Interface Science*, 164:2–11.

Baker, R. (2004). *Membrane Technology and Applications*. Wiley.

Bartels, C. R. and Andes, K. (2013). Consideration of energy savings in SWRO. *Desalination and Water Treatment*, 51:717–725.

Bartman, A., Christofides, P. D., and Cohen, Y. (2009a). Nonlinear model-based control of an experimental reverse osmosis water desalination system. *Industrial & Engineering Chemistry Research*, 48:6126–6136.

Bartman, A., McFall, C., Christofides, P. D., and Cohen, Y. (2009b). Model predictive control of feed flow reversal in a reverse osmosis desalination process. *Journal of Process Control*, 19:433–442.

Bartman, A., Zhu, A., Christofides, P. D., and Cohen, Y. (2010). Minimizing energy consumption in reverse osmosis membrane desalination using optimization-based control. *Journal of Process Control*, 20:1261–1269.

Bhattacharjee, S. and Johnston, G. M. (2002). A model of membrane fouling by salt precipitation from multi-component ionic mixtures in crossflow nanofiltration. *Enviromental Engineering Science*, 19:399–412.

Bhutani, N., Purohit, A., Mantravadi, V. K., Mekapati, S., and Senthilmurugan, S. (2013). Energy efficiency solutions for RO desalination plant. *Desalination and Water Treatment*, 51:5049–5055.

Biagini, F., Oksendal, B., Sulem, A., and Wallner, N. (2009). An introduction to white-noise theory and malliavin calculus for fractional brownian motion. *Mathematical, Physical and Engineering Sciences*, 460:347–374.

Blatt, W., Dravid, A., Michaels, A., and Nelsen, L. (1970). Solute polarization and cake formation in membrane ultrafiltration: Causes, consequences, and control techniques. *Membrane Science and Technology*, 26:47–97.

Boo, C., Lee, S., Elimelech, M., Meng, Z., and Hong, S. (2012). Colloidal fouling in forward osmosis: Role of reverse salt diffusion. *Journal of Membrane Science*, 390:277–284.

Borsani, R. and Rebagliati, S. (2005). Fundamentals and costing of MSF desalination plants and comparison with other technologies. *Desalination*, 182:29–37.

Boudinar, M. B., Hanbury, W. T., and Avlonitis, S. (1992). Numerical simulation and optimization of spiral-wound modules. *Desalination*, 86:227–233.

Bourouni, K., Chaibi, M. T., and Tadrist, L. (2001). Water desalination by humidification and dehumidification of air: State of the art. *Desalination*, 137:167–176.

Browen, W. R., Welfoot, J. S., and Williams, P. M. (2002). Linearzed transport model for nanofiltration: development and assessment. *AIChE Journal*, 48:760–773.

Cameron, I. B. and Clemente, R. B. (2008). SWRO with ERIs PX pressure exchanger device - a global survey. *Desalination*, 221:136–142.

Cath, T. Y., Elimelech, M., McCutcheon, J. R., and McGinnis, R. L. (2013). Standard methodology for evaluating membrane performance in osmotically driven membrane processes. *Desalination*, 312:31–38.

Cecconi, F., Cencini, M., Falcioni, M., and Vulpiani, A. (2005). Brownian motion and diffusion: From stochastic processes to chaos and beyond. *CHAOS*, 15:26102–26111.

Chang, H., Lyu, S. G., Tsai, C. M., Chen, Y. H., Cheng, T. W., and Chou, Y. H. (2012). Experimental and simulation study of a solar thermal driven membrane distillation desalination process. *Desalination*, 286:400–411.

Chanukya, B. S., Patil, S., and Rastogi, N. K. (2013). Influence of concentration polarization on flux behavior in forward osmosis during desalination using ammonium bicarbonate. *Desalination*, 312:39–44.

Chao, Y. and Liang, T. M. (2008). A feasibility study of industrial wastewater recovery using electrodialysis reversal. *Desalination*, 221:433–439.

Chena, J. C. and Kimb, A. S. (2004). Brownian dynamics, molecular dynamics, and Monte Carlo modeling of colloidal systems. *Advances in Colloid and Interface Science*, 112:159–173.

Cheremisinoff, N. P. (2002). *Handbook of water and wastewater treatment and technologies*. Elsevier Science B.V.

Chiolle, A., Gianotti, G., Gramonod, M., and Parrini, G. (1978). Mathematical model of reverse osmosis in parallel-wall channels with turbulence promoting nets. *Desalination*, 26:3–16.

Chung, T. S., Zhang, S., Wang, K. Y., Su, J., and Ling, M. M. (2012). Forward osmosis processes: Yesterday, today and tomorrow. *Desalination*, 287:78–81.

Cristea, S. P., Mazaeda, R., Palacín, L. G., and de Prada, C. (2012). Reduced model of a beer microfiltration plant. In *8th IFAC Symposium on Advanced Control of Chemical Processes, Singapore*.

Davis, R. H. (1992). Modeling of fouling of cross-flow microfiltration of particulate suspensions. *Separation and Purification Methods*, 21:75–88.

Deon, S., Dutournie, P., Fievet, P., Limousy, L., and Bourseau, P. (2013). Concentration polarization phenomenon during the nanofiltration of multi-ionic solutions: Influence of the filtrated solution and operating conditions. *Water Research*, 47:2260–2272.

Dickson, J. M., Spencer, J., and Costa, M. L. (1992). Dilute single and mixed solute systems in a spiral wound reserve osmosis module part I: Theoretical model development. *Desalination*, 89:63–88.

Ebro, H., Kim, Y. M., and Kim, J. H. (2013). Molecular dynamics simulations in membrane-based water treatment processes: A systematic overview. *Journal of Membrane Science*, 438:112–125.

El-Bourawi, M. S., Ding, Z., Ma, R., and Khayet, M. (2006). A framework for better understanding membrane distillation separation process. *Journal of Membrane Science*, 285:4–29.

El-Dessouky, H. T. and Ettouney, H. M. (2002). *Fundamentals of Salt Water Desalination*. Elsevier Science B.V.

El-Dessouky, H. T., Ettouney, H. M., and Al-Juwayhel, F. (2000). Multiple effect evaporation - vapour compression desalination processes. *Chemical Engineering Research and Design*, 78:662–676.

El-Dessouky, H. T., Ettouney, H. M., and Al-Roumi, Y. (1999). Multistage flash desalination: present and future outlook. *Chemical Engineering Journal*, 73:173–190.

Elfil, H. and Hannachi, A. (2006). Reconsidering water scaling tendency assessment. *AIChE Journal*, 52:3583–3591.

Elfil, H. and Roques, H. (2004). Prediction of the limit of the metastable zone in the $CaCO_3$-CO_2-H_2O system. *AIChE Journal*, 50:1908–1916.

Emadzadeh, D., Lau, W. J., Matsuura, T., Ismail, A. F., and Sisakht, M. R. (2013). Synthesis and characterization of thin film nanocomposite forward osmosis membrane with hydrophilic nanocomposite support to reduce internal concentration polarization. *Journal of Membrane Science*, 449:74–85.

Ettouney, H., El-Dessouky, H., and Al-Roumi, Y. (1999). Analysis of mechanical vapour compression desalination process. *International Journal of Energy Research*, 23:431–451.

Evangelista, F. (1986). Improved graphical-analytical method for the design of reverse-osmosis plants. *Industrial & Engineering Chemistry Research*, 25:366–375.

Evangelista, F. and Jonsson, G. (1988a). Optimal design and performance of spiral wound modules I: Numerical method. *Chemical Engineering Communications*, 72:69–81.

Evangelista, F. and Jonsson, G. (1988b). Optimal design and performance of spiral wound modules II: Analytical method. *Chemical Engineering Communications*, 72:83–94.

Fang, W., Wang, R., Chou, S., Setiawn, L., and Fane, A. G. (2012). Composite forward osmosis hollow fiber membranes: Integration of RO and NF like selective layers to enhance membrane properties of anti-scaling and anti-internal concentration polarization. *Journal of Membrane Science*, 394:140–150.

Farid, M. M., Parekh, S., Selmand, J. R., and Al-hallaj, S. (2003). Solar desalination with a humidification-dehumidification cycle: mathematical modeling of the unit. *Desalination*, 151:153–164.

Fiorini, P. and Sciubba, E. (2007). Modular simulation and thermoeconomic analysis of a multi-effect distillation desalination plant. *Energy*, 32:459–466.

Floudas, C. A. (1998). Nonlinear and mixed-integer optimization. fundamentals and applications. *Journal of global optimization.*, 12:108–110.

Gambier, A. and Badreddin, E. (2003). Application of hybrid modeling and control techniques to desalination plants. *Desalination*, 152:175–184.

Gambier, A. and Badreddin, E. (2004). Dynamic modelling of MSF plants for automatic control and simulation purposes: a survey. *Desalination*, 166:191–204.

García-Álvarez, D., de la Fuente, M. J., and Palacín, L. G. (2011a). Monitoring and fault detection in a reverse osmosis plant using principal component analysis. In *the 50th IEEE Conference on Decision and Control and European Control Conference, CDC-ECC, Orlando, USA*.

García-Álvarez, D., Palacín, L. G., de la Fuente, M. J., Tadeo, F., and de Prada, C. (2011b). Control of a desalination plant, including U-PCA-based monitoring. In *the 12th International Conference on Environmental Science and Technology, Rhodes, Greece*.

García-Rodríguez, L. (2002). Seawater desalination driven by renewable energies: a review. *Desalination*, 143:103–113.

Gasmi, A., Belgaieb, J., and Hajji, N. (2010). Technico-economic study of an industrial reverse osmosis desalination unit. *Desalination*, 261:175–180.

Gebel, J. and Yuce, S. (2008). *An Engineer's Guide to Desalination*. V.G.B. PowerTech Service GmbH.

Gen, M. and Cheng, R. (2000). *Genetic Algorithms & Engineering Optimization*. EDA.

Ghadiri, M., Fakhri, S., and Shirazian, S. (2013). Modeling and CFD simulation of water desalination using nanoporous membrane contactors. *Industrial & Engineering Chemistry Research*, 52:3490–3498.

Ghaffour, N., Missimer, T. M., and Amy, G. L. (2013). Technical review and evaluation of the economics of water desalination: Current and future challenges for better water supply sustainability. *Desalination*, 309:197–207.

Giebel, G. (2002). The state-of-the-art in shor-term prediction of wind power. In *Project ANEMOS ENK5-CT*.

Goosen, M. F. A., Sablani, S. S., Al-Maskari, S. S., Al-Belushi, R. H., and Wilf, M. (2002). Effect of feed temperature on permeate flux and mass transfer coefficient in spiral-wound reverse osmosis systems. *Desalination*, 144:367–372.

Grady, C. P., Daigger, G. T., Love, N. G., and Filipe, C. D. (2011). *Biological wastewater treatment.* IWA.

Gray, N. F. (2010). *Water technology: an introduction for environmental scientists and engineers.* IWA.

Gu, H., Bartman, A., Uchymiak, M., Christofides, P. D., and Cohen, Y. (2013). Self-adaptive feed flow reversal operation of reverse osmosis desalination. *Desalination*, 308:63–72.

Gupta, S. K. (1985). Analytical design equation for reverse osmosis system. *Ind*, 24:1022–1027.

Guria, C., Bhattacharya, P. K., and Gupta, S. K. (2005). Multi-objective optimization of reverse osmosis desalination units using different adaptations of the non-dominated sorting genetic algorithm (NSGA). *Computers and Chemical Engineering*, 29:1977–1995.

Henderson, P., Bedworth, D., and Wolfe, P. (1991). *Computer integrated design and manufacturing.* McGraw-Hill.

Heo, J., Boateng, L. K., Flora, H. R. V., Lee, H., Her, N., Park, Y. G., and Yoon, Y. (2012). Comparison of flux behavior and synthetic organic compound removal by forward osmosis and reverse osmosis membranes. *Journal of Membrane Science*, 443:69–82.

Hernández-Sancho, F., Senante, M. M., and Sala-Garrido, R. (2011). Cost modelling for wastewater treatment processes. *Desalination*, 268:1–5.

Hernández-Suárez, M. (2010). *Guideline for the remineralisation of desalinated waters.* Centro Canario del Agua.

Hickey, P. J. and Gooding, C. H. (1994). Mass transfer in spiral wound pervaporation modules. *Journal of Membrane Science*, 92:59–74.

Ho, C. D., Chang, H., Chang, C. L., and Huang, C. H. (2013). Theoretical and experimental studies of flux enhancement with roughened surface in direct contact membrane distillation desalination. *Journal of Membrane Science*, 433:160–166.

Hoek, E. M. V. and Elimelech, M. (2003). Cake-enhanced concentration polarization: A new fouling mechanism for salt-rejecting membranes. *Enviromental Science Technology*, 37:5581–5588.

Hou, H., Bi, Q., and Zhang, X. (2012). Numerical simulation and performance analysis of horizontal-tube falling-film evaporators in seawater desalination. *International Communications in Heat and Mass Transfer*, 39:46–51.

Hu, Y. D. and Lu, Y. Y. (2005). Cleaning strategy of the membrane modules in the reverse osmosis seawater desalination system. *Industrial & Engineering Chemistry Research*, 56:499–505.

Hu, Z., Chen, Y., and Jiang, J. (2011). Zeolitic imidazolate framework-8 as a reverse osmosis membrane for water desalination: Insight from molecular simulation. *The Journal of Chemical Physics*, 134:705–711.

Huang, C. (2009). Mathematical modeling for colloidal dispersion undergoing brownian motion. *Applied Mathematical Modelling*, 33:978–998.

Jacobs, K. (2009). A Monte Carlo method for modeling thermal damping: Beyond the brownian motion master equation. *EPL*, 85:4002–4008.

Jamal, K., Khan, M. A., and Kamil, M. (2004). Mathematical modeling of reverse osmosis systems. *Desalination*, 160:29–42.

Jin, X., She, Q., Ang, X., and Tang, C. Y. (2012). Removal of boron and arsenic by forward osmosis membrane: Influence of membrane orientation and organic fouling. *Journal of Membrane Science*, 389:182–187.

Kahraman, N. and Cengel, Y. A. (2005). Exergy analysis of a MSF distillation plant. *Energy Conversion and Management*, 46:2625–2636.

Kamalesh, K., Dang, P. T. S., and Rao, G. H. (1982). Approximate design equation for reverse osmosis desalination by spiral-wound modules. *Industrial & Engineering Chemistry Research*, 21:517–527.

Karajeh, F. and BenJemaa, F. (2011). *Encyclopedia of Water Science*. Taylor & Francis.

Kargol, A. (2000). Modified Kedem-Katchalsky equations and their applications. *Journal of Membrane Science*, 174:43–53.

Kargol, M. and Kargol, A. (2003). Mechanistic equations for membrane substance transport and their identity with Kedem-Katchalsky equations. *Biophysical Chemistry*, 103:117–127.

Karuppiah, R., Bury, S. J., Vázquez, A., and Poppe, G. (2012). Optimal design of reverse osmosis-based water treatment systems. *AIChE Journal*, 58:2758–2769.

Kedem, O. and Katchalsky, A. (1958). Thermodynamics analysis of the permeability of biological membranes to non-electrolytes. *Biochemistry and Biophysics*, 27:229–246.

Kedem, O. and Katchalsky, A. (1961). A physical interpretation of the phenomenological coecients of membrane permeability. *the Journal of General Physiology*, 45:143–179.

Kim, C., Lee, S., Shon, H. K., Elimelech, M., and Hong, S. (2012a). Boron transport in forward osmosis: Measurements, mechanisms, and comparison with reverse osmosis. *Journal of Membrane Science*, 419:42–48.

Kim, H., Choi, J. S., and Lee, S. (2012b). Pressure retarded osmosis for energy production: membrane materials and operating conditions. *Water Science & Technology*, 65:1789–1794.

Kim, S. and Hoek, E. M. V. (2005). Modeling concentration polarization in reverse osmosis processes. *Desalination*, 186:111–128.

Kim, Y., Kang, M. G., Lee, S., and Gyu, S. (2013). Reduction of energy consumption in seawater reverse osmosis desalination pilot plant by using energy recovery devices. *Desalination and Water Treatment*, 51:766–771.

Kim, Y. C. and Elimelech, M. (2013). Potential of osmotic power generation by pressure retarded osmosis using seawater as feed solution: Analysis and experiments. *Journal of Membrane Science*, 429:330–337.

Klaysom, C., Cath, T. Y., Depuydt, T., and Vankelecom, I. F. J. (2013). Forward and pressure retarded osmosis: potential solutions for global challenges in energy and water supply. *Chemical Society Reviews*, 42:6989–6989.

Kleinhans, F. W. (1998). Membrane permeability modeling: Kedem-Katchalsky vs a two-parameter formalism. *Cryobiology*, 37:271–289.

Kostoglou, M. and Karabelas, A. J. (2013a). Comprehensive simulation of flat-sheet membrane element performance in steady state desalination. *Desalination*, 316:91–102.

Kostoglou, M. and Karabelas, A. J. (2013b). Modeling scale formation in flat-sheet membrane modules during water desalination. *AIChE Journal*, 59:2917–2927.

Koter, S. (2005). The Kedem-Katchalsky equations and the sieve mechanism of membrane transport. *Journal of Membrane Science*, 246:109–111.

Koter, S. (2006). Determination of the parameters of the Spiegler-Kedem-Katchalsky model for nanofiltration of single electrolyte solutions. *Desalination*, 198:335–345.

Kouhikamali, R. (2010). Numerical simulation and parametric study of forced convective condensation in cylindrical vertical channels in multiple effect desalination systems. *Desalination*, 254:49–57.

Lagana, F., Barbieri, G., and Diroli, E. (2000). Direct contact membranedistillation: modelling and concentration experiments. *Journal of Membrane Science*, 166:1–11.

Lemes, R., Falcon, R., Arocha, R., Curbelo, J., Platas, V., and de Lorenzo, L. (2013). Different designs in energy savings of SWRO plant of Las Palmas III. *Desalination and Water Treatment*, 51:749–758.

Li, K. (2007). *Ceramic membrane for separation and reaction*. John Wiley & Sons.

Li, Y. L., Tung, K. L., Chen, Y. S., and Hwang, K. J. (2012). CFD analysis of the initial stages of particle deposition in spiral-wound membrane modules. *Desalination*, 287:200–208.

Liang, L., Han, D., Ma, R., and Peng, T. (2013). Treatment of high-concentration wastewater using double-effect mechanical vapor recompression. *Desalination*, 314:139–146.

Lim, A. and Bai, R. (2003). Membrane fouling and cleaning in microfiltration of activated sludge wastewater. *Journal of Membrane Science*, 219:279–290.

Lior, N. (2012). *Advances in Water Desalination*. Wiley.

Lu, Y. and Hu, Y. (2005). Optimum design of reverse osmosis seawater desalination system. *Desalination and Water Treatment*, 3:9–16.

Lu, Y., Hu., Y., Xu, D., and Wu, L. (2006). Optimum design of reverse osmosis seawater desalination system considering membrane cleaning and replacement. *Journal of Membrane Science*, 282:7–13.

Mabrouk, A. (2013). Techno-economic analysis of tube bundle orientation for high capacity brine recycle MSF desalination plants. *Desalination*, 320:23–32.

Mabrouk, A. and Fath, H. E. (2013). Techno-economic analysis of hybrid high performance MSF desalination plant with NF membrane. *Desalination and Water Treatment*, 51:844–856.

Malek, A., Hawlader, M. N. A., and Ho, J. C. (1996). Design and economics of RO seawater desalination. *Desalination*, 105:245–261.

Manth, T., Gabor, M., and Oklejas, E. (2003). Minimizing RO energy consumption under variable conditions of operation. *Desalination*, 157:9–21.

Marcovecchio, M. G., Scenna, N. J., and Aguirre, P. A. (2010). Improvements of a hollow fiber reverse osmosis desalination model: Analysis of numerical results. *Chemical Engineering Research and Design*, 88:789–802.

Mariall, A. P., Greenbergb, A. R., Krantza, W., and Bond, J. (1999). Real-time measurement of inorganic fouling of RO desalination membranes using ultrasonic time-domain reflectometry. *Journal of Membrane Science*, 159:185–196.

Marinas, B. J. and Selleck, R. E. (1992). Reverse osmosis treatment of multi-component electrolyte solutions. *Journal of Membrane Science*, 72:211–229.

Marinas, B. J. and Urama, R. I. (1996). Modeling concentration polarization in reverse osmosis spiral-wound elements. *Journal of Enviromental Engineering*, 122:292–298.

Martín-Villalba, C., Urquía, A., and Dormido, S. (2008). Object-oriented modelling of virtual-labs for education in chemical process control. *Computers & Chemical Engineering*, 32:3176–3186.

Mathioulakis, E., Belessiotis, V., and Delyannis, E. (2007). Desalination by using alternative energy: Review and state-of-the-art. *Desalination*, 203:346–365.

McCutcheon, J. R. and Elimelech, M. (2006). Influence of concentrative and dilutive internal concentration polarization on flux behavior in forward osmosis. *Journal of Desalination Science*, 284:237–247.

McFall, C., Bartman, A., Christofides, P., and Cohen, Y. (2008). Control and monitoring of a high-recovery reverse-osmosis desalination process. *Industrial & Engineering Chemistry Research*, 47:6698–6710.

McGowan, J. G. and Manweli, J. F. (1998). *Hybrid Wind - PV - Diesel System Experiences*. Renewable Energy Laboratory.

McGowan, J. G., Manweli, J. F., and Avelar, C. (1996). *Hybrid wind - PV - Diesel Hybrid Power Systems Modeling and South American Applications*. National Renewable Energy Laboratory.

Mei, C. C., Liu, Y. H., and Law, A. W. K. (2012). Theory of isobaric pressure exchanger for desalination. *Desalination and Water Treatment*, 39:112–122.

Merino, A. (2008). *Librería de Modelos del Cuarto de Remolacha de una Industria Azucarera para un Simulador de Entrenamiento de Operarios*. PhD thesis, University of Valladolid.

Metaiche, M. and Kettab, A. (2005). Water desalination price from recent performances: modelling, simulation and analysis. *International Journal of Nuclear Desalination*, 1:456–468.

Mi, B. and Elimelech, M. (2010a). Gypsum scaling and cleaning in forward osmosis: Measurements and mechanisms. *Enviromental Science Technology*, 44:2022–2028.

Mi, B. and Elimelech, M. (2010b). Organic fouling of forward osmosis membranes: Fouling reversibility and cleaning without chemical reagents. *Journal of Membrane Science*, 348:337–345.

Michaels, A. S. (1968). New separation techniques for the CPI. *Chemical Engineering Programming*, 64:31–43.

Misra, B. M. and Kupitz, J. (2004). The role of nuclear desalination in meeting the potable water needs in water scarce areas in the next decades. *Desalination*, 166:1–9.

Mistry, K. H., Hunter, H. A., and Lienhard, J. H. (2013). Effect of composition and nonideal solution behavior on desalination calculations for mixed electrolyte solutions with comparison to seawater. *Desalination*, 318:34–47.

Mizrahi, G., Wong, K., Lu, X., Kujundzic, E., Greenberg, A. R., and Gilron, J. (2012). Ultrasonic sensor control of flow reversal in RO desalination. part 2: Mitigation of calcium carbonate scaling. *Journal of Membrane Science*, 419:9–19.

Mohammad, A. W. and Takriff, M. S. (2003). Predicting flux and rejection of multicomponent salts mixture in nanofiltration membranes. *Desalination*, 157:106–111.

Murthy, Z. V. P. and Gupta, S. K. (1997). Estimation of mass transfer coefficient using a combined nonlinear membrane transport and film theory model. *Desalination*, 109:39–49.

Nakayama, A. and Sano, Y. (2013). An application of the Sano-Nakayama membrane transport model in hollow fiber reverse osmosis desalination systems. *Desalination*, 311:95–102.

Narayan, G. P., Chehayeb, K. M., McGovern, R. K., Thiel, G. P., Zubair, S. M., and Lienhard, J. H. (2013). Thermodynamic balancing of the humidification dehumidification desalination system by mass extraction and injection. *International Journal of Heat and Mass Transfer*, 57:756–770.

Navia, D., Martí, R., Sarabia, D., Gutiérrez, G., and de Prada, C. (2012). Handling infeasibilities in dual modifier-adaptation methodology for real-time optimization. In *8th IFAC Symposium on Advanced Control of Chemical Processes, Singapore*.

Nfah, E. M. and Ngundam, J. M. (2008). Modelling of wind - diesel - battery hybrid power systems for far North Cameroon. *Energy Conversion and Management*, 49:1295–1301.

Oh, H. J., Choung, Y. K., Lee, S., Choi, J. S., Hwang, T. M., and Kim, J. H. (2009). Scale formation in reverse osmosis desalination: model development. *Desalination*, 238:333–346.

Ophir, A. and Lokiec, F. (2005). Advanced MED process for most economical sea water desalination. *Desalination*, 182:187–198.

Palacín, L. G., de Prada, C., Syafiie, S., and Tadeo, F. (2008a). Library for dynamic simulation of reverse osmosis plants. In *20th European Modeling and Simulation Symposium, EMSS, Calabria, Italy*.

Palacín, L. G., Merino, A., and de Prada, C. (2010a). Estudio de la sensibilidad global y estimación de parámetros en un reactor SBR, con nitrificación desnitrificación, utilizando el modelo ASM1. In *XXXI Jornadas de Automática, CEA-IFAC, Jaén, Spain*.

Palacín, L. G., Tadeo, F., and de Prada, C. (2009a). Diseño integrado y control usando simulación dinámica de una planta de ósmosis inversa. In *XXX Jornadas de Automática, CEA-IFAC, Valladolid, Spain*.

Palacín, L. G., Tadeo, F., and de Prada, C. (2009b). Integrated design using dynamic simulation of reverse osmosis plants. In *Industrial Engineering and Engineering Management, Hong Kong, China*.

Palacín, L. G., Tadeo, F., de Prada, C., and Salazar, J. (2011a). Operation of desalination plants using hybrid control. *Desalination and Water Treatment*, 25:119–126.

Palacín, L. G., Tadeo, F., de Prada, C., and Salazar, J. (2012a). Scheduling of the membrane module rotation in RO desalination plants. *Desalination and Water Treatment*, 48:1–8.

Palacín, L. G., Tadeo, F., de Prada, C., and Touati, K. (2012b). Evaluation of the recovery of osmotic energy in desalination plants by using pressure retarded osmosis. *Desalination and Water Treatment*, 47:1–6.

Palacín, L. G., Tadeo, F., Elfil, H., and de Prada, C. (2009c). New dynamic library of reverse osmosis plants with fault simulation. In *2nd Maghreb conference on desalination and water treatment, Hammamet, Tunisia*.

Palacín, L. G., Tadeo, F., Elfil, H., de Prada, C., and Salazar, J. (2011b). New dynamic library of reverse osmosis plants with fault simulation. *Desalination and Water Treatment*, 25:127–132.

Palacín, L. G., Tadeo, F., Salazar, J., and de Prada, C. (2009d). Operation of desalination plants using hybrid control. In *2nd Maghreb conference on desalination and water treatment, Hammamet, Tunisia*.

Palacín, L. G., Tadeo, F., Salazar, J., and de Prada, C. (2010b). Initial validation of a reverse osmosis simulator. In *Emerging Technologies and Factory Automation, Bilbao, Spain*.

Palacín, L. G., Tadeo, F., Salazar, J., and de Prada, C. (2010c). Operación de plantas de desalinización mediante ósmosis inversa con consumo óptimo de la energía y detección de ensuciamiento por carbonato cálcico. In *XXXI Jornadas de Automática, CEA-IFAC, Jaén, Spain*.

Palacín, L. G., Tadeo, F., Salazar, J., and de Prada, C. (2010d). Operation of medium-size reverse osmosis plants with optimal energy consumption. In *9th International Symposium on Dynamics and Control of Process Systems, Leuven, Belgium*.

Palacín, L. G., Tadeo, F., Salazar, J., and de Prada, C. (2010e). Validation of a reverse osmosis dynamic simulator. In *European Modeling and Simulation Symposium, EMSS, Fez, Morocco*.

Palacín, L. G., Tadeo, F., Salazar, J., and de Prada, C. (2011c). Ósmosis inversa en instalaciones remotas con energías renovables. *InfoEnviro*, 65:42–45.

Palacín, L. G., Tadeo, F., Syam, S., and de Prada, C. (2008b). Librería dinámica de plantas de desalinización de osmosis inversa. In *XXIX Jornadas de Automática, CEA-IFAC, Tarragona, Spain*.

Palacín, L. G., Theodoropoulos, C., Weiguo, X., Tadeo, F., and de Prada, C. (2012c). Two-scale modelling of the concentration polarization in a reverse osmosis membrane. In *Chemical Process Control, CPC VIII, Savannah, USA*.

Palanki, S. and Gupta, S. K. (1987). Analytical design equation for multi-solute reverse osmosis systems. *Industrial & Engineering Chemistry Research*, 26:2449–2454.

Pardalos, P. M. and Romeijn, H. E. (2002). *Handbook of Global Optimization*. Kluwer Academic Publishers.

Parekha, S., Farid, M. M., Selman, J. R., and Al-hallaj, S. (2004). Solar desalination with a humidification-dehumidification technique - a comprehensive technical review. *Desalination*, 160:167–186.

Peñate, B., Círez, F., Domínguez, F. J., Subiela, V. J., and Vera, L. (2013). Design and testing of an isolated commercial EDR plant driven by solar photovoltaic energy. *Desalination and Water Treatment*, 51:1254–1264.

Peñate, B. and García-Rodríguez, L. (2011). Energy optimisation of existing SWRO (seawater reverse osmosis) plants with ERT (energy recovery turbines): Technical and thermoeconomic assessment. *Energy*, 36:613–626.

Peñate, B. and García-Rodríguez, L. (2012). Current trends and future prospects in the design of seawater reverse osmosis desalination technology. *Desalination*, 284:1–8.

Porrazzo, R., Cipollina, A., Galluzzo, M., and Micale, G. (2013). A neural network-based optimizing control system for a seawater-desalination solar-powered membrane distillation unit. *Computers & Chemical Engineering*, 54:79–96.

Porter, M. C. (1986). Concentration polarization in reverse osmosis and ultrafiltration. *Synthetic Membranes: Science, Engineering and Applications*, 181:367–388.

Prada, C. de, Gutiérrez, G., Sarabia, D., Gómez, E., Méndez, C. A., Sola, J. M., and González, R. (2012). Implementing optimal hydrogen networks management. In *IFAC Symposium on Advanced Control of Chemical Processes, Singapore.*

Prada, C. de, Rodríguez, M., and Sarabia, D. (2011). On-line scheduling and control of a mixed continuous-batch plant. *Industrial & Engineering Chemistry Research*, 50:5041–5049.

Prats, D., Chillon-Arias, M. F., and Rodriguez-Pastor, M. (2000). Analysis of the influence of pH and pressure on the elimination of boron in reverse osmosis. *Desalination*, 128:269–273.

Probstein, R. P. (1994). *Physicochemical Hydrodynamics: An Introduction*. John Wiley & Sons.

Qureshi, B. A., Zubair, S. M., Sheik, A. K., Bhujle, A., and Dubowsky, S. (2013). Design and performance evaluation of reverse osmosis desalination systems: An emphasis on fouling modeling. *Applied Thermal Engineering*, 60:208–217.

Rathore, N. S., Kundariya, N., Sadistap, S., and Narain, A. (2013). Mathematical modeling and simulation of concentration polarization layer in reverse osmosis process. In *Students Conference on Engineering and Systems (SCES), Uttar Pradesh, India*.

Riverol, C. and Pilipovik, V. (2004). Mathematical modeling of perfect decoupled control system and its application: A reverse osmosis

desalination industrial-scale unit. *Journal of Automated Methods and Management in Chemistry*, 2:50–54.

Robertson, M. W., Watters, J. C., Desphande, P. B., Assef, J. Z., and Alatiqi, I. M. (1996). Model based control for reverse osmosis desalination processes. *Desalination*, 104:59–68.

Rubinstein, R. Y. and Kroese, D. P. (2011). *Simulation and the Monte Carlo Method*. Wiley.

Sablani, S. S., Goosen, M. F. A., Al-Belushi, R., and Wilf, M. (2001). Concentration polarization in ultrafiltration and reverse osmosis: a critical review. *Desalination*, 141:269–289.

Saffarini, R. B., Summers, E. K., Arafat, H. A., and Lienhard, J. H. (2012). Economic evaluation of stand-alone solar powered membrane distillation systems. *Desalination*, 299:55–62.

Sagiv, A. and Semiat, R. (2005). Backwash of RO spiral wound membranes. *Desalination*, 179:1–9.

Sagle, A. C., Wagner, E. M. V., Ju, H., McCloskey, B. D., Freeman, B. D., and Sharma, M. M. (2009). PEG-coated reverse osmosis membranes: Desalination properties and fouling resistance. *Journal of Membrane Science*, 340:92–108.

Said, S. A., Emtir, M., and Mujtaba, I. M. (2013). Flexible design and operation of multi-stage flash (MSF) desalination process subject to variable fouling and variable freshwater demand. *Processes*, 3:279–295.

Salazar, J., Tadeo, F., de Prada, C., and Palacín, L. G. (2010a). Modelling and control of microgrids in island operation. In *International Renewable Energy Congress, IREC, Sousse, Tunisia*.

Salazar, J., Tadeo, F., de Prada, C., and Palacín, L. G. (2010b). Simulation and control of a PV system connected to a low voltage network. In *XXXI Jornadas de Automática, CEA-IFAC, Jaén, Spain*.

Salazar, J., Tadeo, F., de Prada, C., and Palacín, L. G. (2010c). Simulation and control of a wind turbine connected to a low voltage network. In *European Modeling and Simulation Symposium, EMSS, Fez, Morocco*.

Salazar, J., Tadeo, F., Witheephanich, K., Hayes, M., and de Prada, C. (2012). Control for a variable speed wind turbine equipped with a permanent magnet synchronous generator (PMSG). *Sustainability in Energy and Buildings*, 12:151–168.

Sanaye, S. and Asgari, S. (2013). Four E analysis and multi-objective optimization of combined cycle power plants integrated with multi-stage flash (MSF) desalination unit. *Desalination*, 320:105–117.

Sapienza, F. J., Gill, W. N., and Soltanieh, M. (1990). Separation of ternary salt/acid aqueous solutions using hollow fiber reverse osmosis. *Journal of Membrane Science*, 54:175–189.

Sarabia, D., Capraro, F., Larsen, L. F. S., and de Prada, C. (2009). Hybrid NMPC of supermarket display cases. *Control Engineering Practice*, 17:428–441.

Sarabia, D., de Prada, C., Cristea, S., and Mazaeda, R. (2006). Hybrid model predictive control of a sugar end section. *Computer Aided Chemical Engineering*, 21:1269–1274.

Sarabia, D., de Prada, C., Gómez, E., Gutiérrez, G., Sola, J. M., and González, R. (2012). Data reconciliation and optimal management of hydrogen networks in a petrol refinery. *Control Engineering Practice*, 20:343–354.

Sarkar, B. and De, S. (2012). A combined complete pore blocking and cake filtration model for steady-state electric field-assisted ultrafiltration. *AIChE Journal*, 58:1435–1446.

Sayyaadi, H. and Saffari, A. (2010). Thermoeconomic optimization of multi effect distillation desalination systems. *Applied Energy*, 87:1122–113.

Schock, G. and Miquel, A. (1987). Mass transfer and pressure loss in spiral wound modules. *Desalination*, 64:339–352.

Schofield, R. W., Fane, A. G., and Fell, C. J. D. (1987). Heat and mass transfer in membrane distillation. *Journal of Membrane Science*, 33:299–313.

Schwinge, J., Neal, P. R., Wiley, D. E., Fletcher, D. F., and Fane, A. G. (2004). Spiral wound modules and spacers: Review and analysis. *Journal of Membrane Science*, 242:129–153.

Selvaraj, R., Deshpande, P. B., Tambe, S. S., and Kulkarni, B. D. (1995). Neural networks for the identification of MSF desalination plants. *Desalination*, 101:185–193.

Senthilmurugan, S., Ahluwalia, A., and Gupta, S. K. (2005). Modeling of a spiral-wound module and estimation of model parameters using numerical techniques. *Desalination*, 173:269–286.

Senthilmurugan, S. and Gupta, S. K. (2006). Modeling of a radial flow hollow fiber module and estimation of model parameters for aqueos multi-component mixture using numerical techniques. *Membrane Science*, 279:466–478.

Shakaib, M., Hasani, S. M. F., Ahmed, I., and Yunus, R. M. (2012). A CFD study on the effect of spacer orientation on temperature polarization in membrane distillation modules. *Desalination*, 284:332–340.

Sharafa, M. A., Nafeya, A. S., and Garcia-Rodriguez, L. (2011). Thermo-economic analysis of solar thermal power cycles assisted MED-VC (multi effect distillation-vapor compression) desalination processes. *Energy*, 36:2753–2764.

Sheikholeslami, R. (2007). *Fouling of membrane and thermal units: a unified approach. Its principles, assesment, control and mitigation.* Balaban Publishers.

Slater, C., Zielinski, J., Wendel, R., and Uchrin, C. (1985). Modeling of a small scale reverse osmosis systems. *Desalination*, 52:267–284.

Slezak, A. and Turczynski, B. (1986). Modification of the Kedem-Katchalsky equations. *Biophysical Chemistry*, 24:173–178.

Soltanieh, M. and Sahebdelfar, S. (2001). Interaction effects in multicomponent separation by reverse osmosis. *Journal of Membrane Science*, 183:15–27.

Sondhi, R. and Bhave, R. (2001). Role of backpulsing in fouling minimization in crossflow filtration with ceramic membranes. *Journal of Membrane Science*, 186:41–52.

Song, L. and Liu, C. (2012). A total salt balance model for concentration polarization in crossflow reverse osmosis channels with shear flow. *Journal of Membrane Science*, 401:313–322.

Song, L. F. and Elimelech, M. (1995). Theory of concentration polarization in cross-flow filtration. *Chemical Society Faraday*, 91:3389–3398.

Song, L. F. and Ma, S. (2005). Numerical studies of the impact of spacer geometry on concentration polarization in spiral wound membrane modules. *Industrial & Engineering Chemistry Research*, 44:7638–7645.

Song, L. F. and Yu, S. C. (1999). Concentration polarization in crossflow reverse osmosis. *AIChE Journal*, 45:921–928.

Spiegler, K. S. and Kedem, O. (1966). Thermodynamics of hyperfiltration (reverse osmosis): criteria for efficient membranes. *Desalination*, 1:311–326.

Stover, R. L. (2007). Seawater reverse osmosis with isobaric energy recovery devices. *Desalination*, 203:168–175.

Stover, R. L. and Martin, J. (2009). Titan PX-1200 energy recovery device - test results from the Inima Los Cabos, Mexico, seawater RO facility. *Desalination and Water Treatment*, 3:179–182.

Strathmann, H. (2010). *Sustainable Water for the Future: Water Recycling versus Desalination*. IWA.

Suh, C. and Lee, S. (2013). Modeling reverse draw solute flux in forward osmosis with external concentration polarization in both sides of the draw and feed solution. *Journal of Membrane Science*, 427:365–374.

Syafiie, S., Palacín, L. G., de Prada, C., and Tadeo, F. (2008a). Membrane modeling for simulation and control of reverse osmosis in desalination plants. In *Control, UKACC, Manchester, UK*.

Syafiie, S., Tadeo, F., Palacín, L. G., and de Prada, C. (2008b). Membrane modelling of desalination plants. In *International Conference on Industrial Engineering and Engineering Management, IEEM, Singapore*.

Syafiie, S., Tadeo, F., Palacín, L. G., de Prada, C., and Salazar, J. (2009). Modelling for dynamic simulation of pretreatment in reverse osmosis plants. In *Industrial Engineering and Engineering Management, Hong Kong, China*.

Syafiie, S., Tadeo, F., Palacín, L. G., de Prada, C., and Salazar, J. (2010). Modelling of the pretreatment section for dynamic simulation of water production using reverse osmosis. *International Journal of Management Science and Engineering Management*, 5:1–6.

Tadeo, F., Palacín, L. G., de Prada, C., and Salazar, J. (2010a). Energías renovables para ósmosis inversa en instalaciones aisladas: el proyecto OPEN-GAIN. In *III Congreso Nacional de la Asociación de Desalinización y Reutilización, Barcelona, Spain*.

Tadeo, F., Palacín, L. G., Salazar, J., and de Prada, C. (2011). Desalination in remote areas: A prediction-based approach. In *IDA World Congress, Perth, Australia*.

Tadeo, F., Palacín, L. G., Syafiee, S., and de Prada, C. (2010b). Improving the efficiency of small water production facilities. In *European Energy Conference, ESF, Barcelona, Spain*.

Tadeo, F., Val, R., Palacín, L. G., Salazar, J., and de Prada, C. (2009). Control of reverse osmosis plants using renewable energies. In *International Conference on Control and Applications, Cambridge, UK*.

Tan, C. H. and Yong, H. (2013). Revised external and internal concentration polarization models to improve flux prediction in forward osmosis process. *Desalination*, 309:125–140.

Tanaka, Y. (2012). Ion-exchange membrane electrodialysis program and its application to multi-stage continuous saline water desalination. *Desalination*, 301:10–25.

Taniguchi, Y. (1978). An analysis of reverse osmosis characteristics of ROGA spiral-wound modules. *Desalination*, 71:71–88.

Thorsen, T. and Holt, T. (2009). The potential for power production from salinity gradients by pressure retarded osmosis. *Journal of Membrane Science*, 335:103–110.

Thu, K., Chakraborty, A., Kim, Y. D., Myat, A., Saha, B. B., and Choon, K. (2013). Numerical simulation and performance investigation of an advanced adsorption desalination cycle. *Desalination*, 308:209–218.

Tripler, E., Ben-Gal, A., and Shani, U. (2007). Consequence of salinity and excess boron on growth, evapotranspiration and ion uptake in date palm Phoenix Dactylifera. *Plant and Soil*, 297:147–155.

Tsuru, T., Urair, M., Nakao, S. I., and Kimuran, S. (1991). Negative rejection of anions in the loose reverse osmosis separation of mono and divalent ion mixtures. *Desalination*, 81:219–227.

Tzen, E. and Papapetrou, M. (2012). Promotion of renewable energy sources for water production through desalination. *Desalination and Water Treatment*, 39:302–307.

Uche, J., Serra, L., and Valero, A. (2001). Thermoeconomic optimization of a dual-purpose power and desalination plant. *Desalination*, 136:147–158.

Urquía, A. and Dormido, S. (2003). Object-oriented design of reusable model libraries of hybrid dynamic systems - part one: A design methodology. *Mathematical and Computer Modelling of Dynamical Systems*, 9:65–90.

Valero, F. and Arbos, R. (2010). Desalination of brackish river water using electrodialysis reversal (EDR): Control of the THMs formation in the Barcelona (NE Spain) area. *Desalination*, 253:170–174.

Vince, F., Marechal, F., Aoustin, E., and Breant, P. (2008). Multi-objective optimization of RO desalination plants. *Desalination*, 222:96–118.

Vonk, M. W. and Smit, J. A. M. (1983). Thermodynamics of ternary system in reverse osmosis. *Desalination*, 48:105–119.

Vrouwenvelder, J. S., Hinrichsa, C., der Meer, W. G. J. V., Loosdrecht, M. C. V., and Kruithof, J. C. (2009). Pressure drop increase by biofilm accumulation in spiral wound RO and NF membrane systems: role of substrate concentration, flow velocity, substrate load and flow direction. *Biofouling*, 25:543–555.

Vázquez, F., Jiménez, J., Garrido, J., and Belmonte, A. (2010). *Introduction to Modelling and Simulation with EcosimPro*. Pearson.

Wang, X., Duitsman, E., Rajagopalan, N., and Namboodiri, V. V. (2013). Chemical treatment of commercial reverse osmosis membranes for use in FO. *Desalination*, 319:66–72.

Weinrich, L., Haas, C. N., and LeChevallier, M. W. (2013). Recent advances in measuring and modeling reverse osmosis membrane fouling in seawater desalination: a review. *Journal of Water Reuse and Desalination*, 3:85–101.

Wilf, M. and Bartels, C. (2005). Optimization of seawater RO systems design. *Desalination*, 173:1–12.

Williams, M. E., Hestekin, J. A., Smothers, C. N., and Bhattacharyya, D. (1999). Separation of organic pollutants by reverse osmosis and nanofiltration membranes: Mathematical models and experimental verification. *Industrial & Engineering Chemistry Research*, 38:3683–3695.

Wilson, W., Gruendisch, A., and Calder-Potts, I. (1987). The use of Pelton wheel turbines for energy recovery in reverse osmosis systems. *Desalination*, 65:231–240.

Wong, M. C. Y., Martínez, K., Ramón, G. Z., and Hoek, E. M. V. (2012). Impacts of operating conditions and solution chemistry on osmotic membrane structure and performance. *Desalination*, 287:340–349.

Woodcock, D. J. and White, I. M. (1981). The application of Pelton type impulse turbines for energy recovery on sea water reverse osmosis systems. *Desalination*, 39:447–458.

Wu, S. and Zhang, Z. (2003). An approach to improve the economy of desalination plants with a nuclear heating reactor by coupling with hybrid technologies. *Desalination*, 155:179–185.

Xie, W. and Theodoropoulos, C. (2010). An off-line model reduction-based technique for on-line linear MPC applications for nonlinear large-scale distributed systems. *Computer Aided Chemical Engineering*, 28:409–414.

Xu, P., Bellona, C., and Drewes, J. E. (2010). Fouling of nanofiltration and reverse osmosis membranes during municipal wastewater reclamation: Membrane autopsy results from pilot-scale investigations. *Journal of Membrane Science*, 353:111–121.

Yermiyahu, U., Ben-Gal, A., Kern, R., and Reid, R. J. (2008). Combined effect of salinity and excess boron on plant growth and yield. *Plant and Soil*, 304:73–87.

Zafra-Cabeza, A., Ridao, M. A., and Camacho, E. F. (2011). A mixed integer quadratic programming formulation of risk management for reverse osmosis plants. *Desalination*, 268:46–54.

Zamen, M., Amidpour, M., and Soufari, S. M. (2009). Cost optimization of a solar humidification-dehumidification desalination unit using mathematical programming. *Desalination*, 239:92–99.

Zhang, J., Dow, N., Duke, M., Ostarcevic, E., and Li, J. (2010). Identification of material and physical features of membrane distillation membranes for high performance desalination. *Journal of Membrane Science*, 349:295–303.

Zhao, S., Zou, L., and Mulcahy, D. (2012). Brackish water desalination by a hybrid forward osmosis-nanofiltration system using divalent draw solute. *Desalination*, 284:175–181.

Zhou, W., Song, L., and Guan, T. K. (2006). A numerical study on concentration polarization and system performance of spiral wound RO membrane modules. *Journal of Membrane Science*, 271:38–46.

Zhu, A., Christofides, P. D., and Cohen, Y. (2009). Effect of thermodynamic restriction on energy cost optimization of RO membrane water desalination. *Industrial & Engineering Chemistry Research*, 48:6010–6021.

Zhu, A., Rahardianto, A., Christofides, P. D., and Cohen, Y. (2010). Reverse osmosis desalination with high permeability membranes - cost optimization and research needs. *Desalination and Water Treatment*, 15:1–3.

Zuo, G. and Wang, R. (2013). Novel membrane surface modification to enhance anti-oil fouling property for membrane distillation application. *Journal of Membrane Science*, 447:26–35.

Zydney, A. L. and Colton, C. K. (1986). A concentration polarization model for the filtrate flux in cross-flow microfiltration of particulate suspensions. *Chemical Engineering Communications*, 47:346–348.